EXPERIMENTAL STUDY OF A NOVEL VALVETRAIN SYSTEM ON SI ENGINE EFFICIENCY AND EMISSIONS

A thesis submitted for the degree of
Doctor of Philosophy

By

Anna Minasyan

Department of Mechanical and Aerospace Engineering
College of Engineering, Design and Physical Sciences
Brunel University London

February 2022

Abstract

Strict emissions legislations and continuous race for improvement of fuel economy urge to develop more efficient and cleaner IC engines for commercial and private use. Engine downsizing has been shown as an effective means to reduce the vehicle's fuel consumption but the full potential of engine downsizing is limited by the knocking combustion at boosted operations and the presence of pumping loss at part load conditions. A variable valve train system can be used to minimise the knocking combustion by implementing Miller and Atkinson cycles through alteration of the effective compression ratio (ECR) at high load via Early Intake Valve Closure (EIVC) or Late Intake Valve Closure (LIVC), as well as reducing the pumping loss at part load.

In this work, a single cylinder direct injection Spark Ignition (SI) gasoline engine equipped with an electro-mechanical valvetrain system named iVT (intelligent Valve Technology) by Camcon was set up and used to investigate the potential benefits of the iVT. Engine experiments were carried out at 1500 and 3000rpm with various valve profiles including EIVC and LIVC with single and two intake valve mode as well as early intake Maximum Opening Position (MOP) at 35% and 40% MOP. Their effects on engine performance and emissions were measured and analysed at 4, 6, 9 and 12.6bar net IMEP. Results showed that EIVC and LIVC profiles were successful in reducing the fuel consumption with two valve mode at low loads thanks to lower pumping loss and at high loads where spark timing was knock limited. Those profiles also resulted in lower emissions. In particular, the LIVC profile reduced the NO_X concentration by up to 20% at low loads due to lowest ECR. Single valve mode operations also provided improved fuel economy at 4bar and 12.6bar net IMEP when combined with EIVC profiles. However, the most significant reduction in ISFC was achieved with early MOP. With combination of LIVC and early MOP, ISFC was reduced by up to 5.4% at low load and by up to 7.1% at high load compared to the baseline profile at 1500rpm.

Acknowledgements

I would like to thank my supervisor Professor Hua Zhao for finding a research engine and organising this project. I am very grateful for his support and guidance throughout the project. I would like to express my gratitude to Camcon Automotive Ltd. for providing a novel valvetrain system and technical support for engine and valve control. I also would like to acknowledge my colleagues from the engine lab, technicians Eamon Wyse and Andrew Selway for their help and advice. Finally, I would like to thank my family and my husband Alexandru for providing support and encouragement throughout my studies.

Table of Contents

Nomenclature

A/R	Area to Radius ratio
AFR	Air Fuel Ratio
AM	Air Motor
APA	Air Power Assisted
BDC	Bottom Dead Centre
BIK	Benefit In Kind
BMEP	Brake Mean Effective Pressure
BSFC	Brake Specific Fuel Consumption
BSL	Baseline
BTDC	Before Top Dead Centre
BTE	Break Thermal Efficiency
C	Carbon
C_6H_6	Benzene
CA deg	Crank Angle degrees
CA10	Crank Angle at 10% Mass Fraction of Fuel Burnt
CA50	Crank Angle at 50% Mass Fraction of Fuel Burnt
CA90	Crank Angle at 90% Mass Fraction of Fuel Burnt
CAI	Controlled Auto Ignition
CB	Compression Braking
CFD	Computational Fluid Dynamics
CI	Compression Ignition
CO	Carbon Monoxide
CO_2	Carbon Dioxide
CPS	Cam Profile Switching
CR	Compression Ratio
CU	Conventional Unthrottled
DAQ	Data Acquisition
DI	Direct Injection
DOHC	Dual Overhead Camshaft
DPF	Diesel Particulate Filter
DVVT	Dual Variable Valve Timing
ECR	Effective Compression Ratio
ECU	Engine Control Unit
EGR	Exhaust Gas Re-circulation

EIVC	Early Intake Valve Closing
EVC	Exhaust Valve Closing
EVO	Exhaust Valve Opening
FHEV	Full Hybrid Electric Vehicle
FTP-75	Federal Test Procedure for light-duty vehicles
GPF	Gasoline Particulate Filter
H	Hydrogen
HC	Hydrocarbon
HCCI	Homogeneous Charge Compression Ignition
HEV	Hybrid Electric Vehicle
HRR	Heat Release Rate
IMEP	Indicated Mean Effective Pressure
ISCO	Indicated Specific Carbon Monoxide
ISFC	Indicated Specific Fuel Consumption
ISHC	Indicated Specific Hydrocarbon
$ISNO_X$	Indicated Specific Nitrogen Oxides
IVC	Intake Valve Closing
IVO	Intake Valve Opening
iVT	Intelligent Valve Technology
i-VTEC	Intelligent Variable Valve Timing and Lift Electronic Control
LIVC	Late Intake Valve Closing
LogP	Logarithm of Pressure
LogV	Logarithm of Volume
MBT	Maximum Break Torque
MCP	Mechanical Cam Phaser
MFB	Mass Fraction Burned
MOP	Maximum Opening Position
NA	Naturally Aspirated
NIMEP	Net Indicated Mean Effective Pressure
NO_X	Nitrogen Oxides
O	Oxygen
Pb	Lead
PFI	Port Fuel Injection
PH	high pressure fluid
PHEV	Plug-in Hybrid Electric Vehicle

PL	low pressure fluid
PM	Particulate Matter
Pmax	Peak Cylinder Pressure
PMEP	Pumping Mean Effective Pressure
PV diagram	Pressure Volume diagram
RON	Research Octane Number
rpm	Revolutions per Minute
SFILB	Stratified Flame Ignition Lean Burn
SI	Spark Ignition
SO_2	Sulphur Dioxide
SOI	Start of Injection
TDC	Top Dead Centre
uHC	unburned Hydrocarbon
ULEZ	Ultra Low Emission Zone
VCR	Variable Compression Ratio
VCU	Valve Control unit
VGT	Variable Geometry Turbocharger
VVA	Variable Valve Actuation
VVEL	Variable Valve Event and Lift
VVL	Variable Valve Lift
VVT	Variable Valve Timing
WLTP/C	World Harmonized Light Vehicle Test Procedure/Cycle

List of Figures

List of Tables

List of Equations

Chapter 1 Introduction

1.1 Preface

Since mid-20th century global warming was observed by scientists around the world. The by-products of everyday human activities such as burning of fossil fuels contributes to the amount of greenhouse gases that absorb heat from the Sun. It is then radiated within Earth's atmosphere, causing the planet's temperature to increase gradually over the decades, eventually leading to climate change that is not appropriate for life [1].

CO_2 is considered to be one of the main contributors to global warming, production of which was largely increased due to human activity. As demonstrated in Figure 1.1, since the industrial revolution CO_2 concentration increased by 50% with peak value of 417 ppm measured in March 2021 at Mauna Loa.

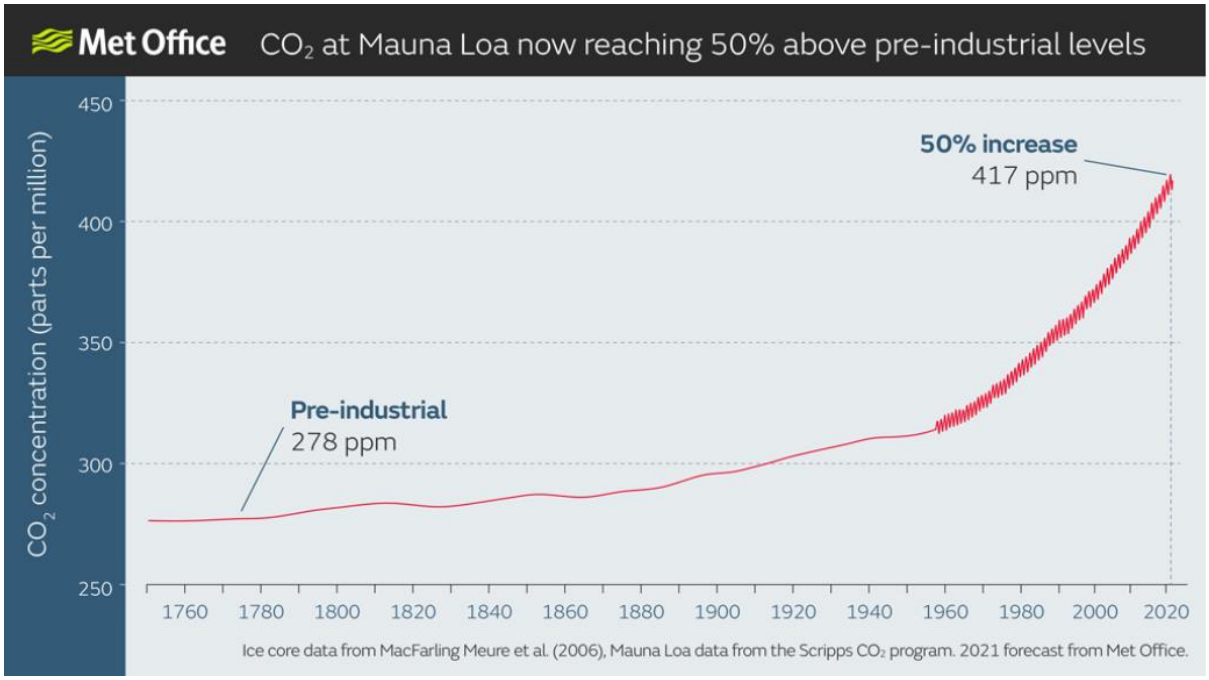

Figure 1.1 Atmospheric CO_2 levels, based on ice core data before 1958, the instrumental record at Mauna Loa and the 2021 forecast from the Met Office [2]

As mentioned previously burning of fussil fuels is the major cause of increasing CO_2 concentration in the planet's atmosphere. Figure 1.2 shows polution of CO_2 by sector on the left hand side, where 24.3% is produced by transport. On the right hand side, the transport sector is devided into transport modes. The light-duty vehicles such as passenger cars contributed to almost half of the trrasport sector and heavy-duty vehicles to over a quarter. Together, heavy and light-duty vehicles take 71.9% stake of CO_2 emissions in the transport

sector. Therefore, research should focus on emission reduction and fuel efficiency of powertains for vehicles. New engine operation strategies and technologies, as well as low carbon and zero carbon fuels, have the potential to drammaticaly reduce global grenhouse gas emissions either as a stand alone solution or as a combination with electrical powertrains.

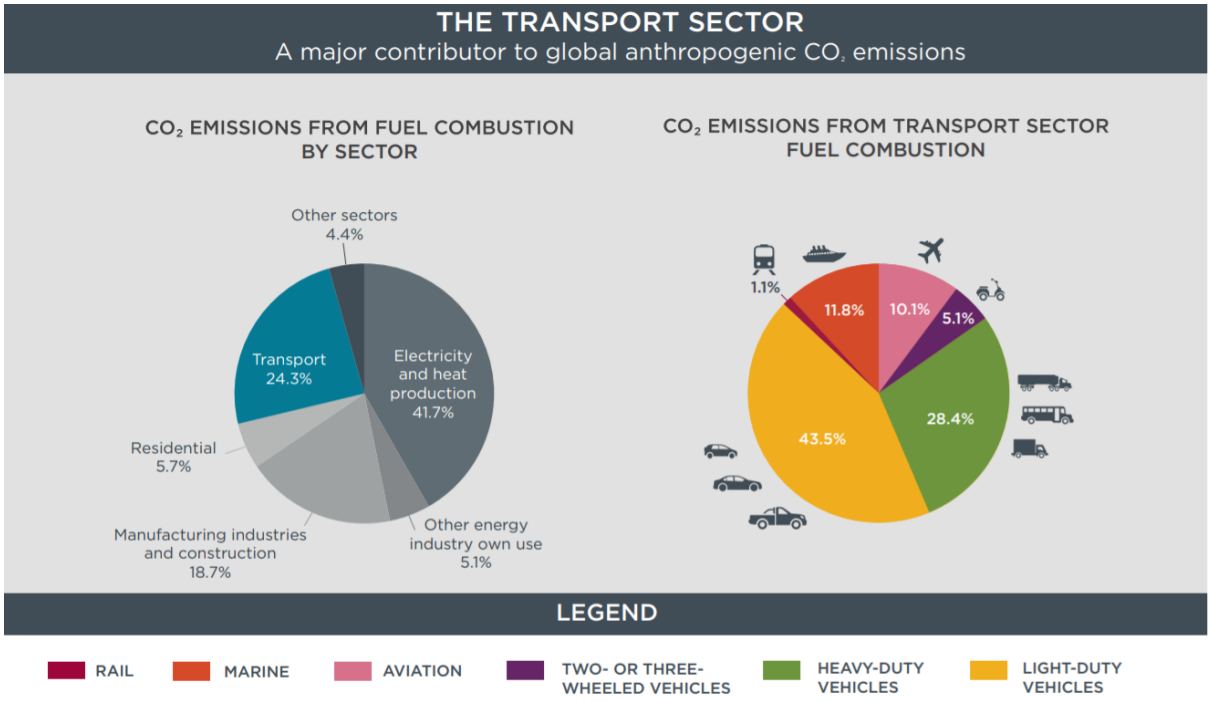

Figure 1.2 Worldwide CO_2 emissions by sectors and transport modes before the end of 2018 [3]

1.2 Thesis outline

This thesis comprises seven chapters. Chapter 1 introduces the topic of global warming associated with pollution from combustion engines to the reader including current challenges for automotive industry and their possible solutions

Chapter 2 provides more in-depth review of main challenges for automotive industry, principles of operation of conventional SI engines, and various engine and powertrain technologies which are used in order to meet the requirements set by the government. The chapter concludes with a summary of the major findings and the area of additional research required for further investigation, as well as the scope of the project and main objectives.

Chapter 3 describes the methodology and the experimental engine setup, and measurements systems used for the studies, as well as data acquisition and analysis. This chapter will also include a description of the iVT and its potential advantages for SI engines.

Chapter 4 focuses on a study of effects of valve profiles with various effective compression ratios on engine performance, fuel consumption and emissions in comparison to the baseline

profile with two intake valve operation. A description of test parameters such as engine load and speed together with valve profile parameters is presented, followed by discussion of experimental results

Chapter 5 presents the results of the single intake operation and compares them with those obtained with two intake valves of the same valve lift profiles. A description of test parameters and valve profiles together with discussion of the results is included in the chapter.

Chapter 6 provides a comparison of the best valve profiles used in Chapter 4 on the basis of lowest ISFC at specific engine load and speed to the same profiles with early maximum opening position (MOP) and to the baseline profile. A description of test parameters and valve profiles together with discussion of the results is also included in the chapter.

Chapter 7 summarises the main conclusions of the test results and suggestions for further work required for complete investigation of valve profiles with Miller and Atkinson cycle.

Chapter 2 Literature Review

2.1 Introduction

IC engines have been the main power plants for various transport on land, sea and air. Worldwide daily use of road vehicles with IC engines in the 20th century has led to the very stringent legislation on their pollutant emissions over the last few decades. Moreover, European Parliament and the Council set regulation for the maximum value of manufacturer's fleet average CO_2 emission level, targeting to 95g/km from 2020 followed by a reduction of 37.5% from 2030 in order to combat the global warming caused by increasing CO_2 concentration. If the average value exceeds the limit, the manufacturer has to pay monetary penalty for each registered car [4]. Another main issue associated with the use of IC engines is increasing fossil fuel consumption, which can lead to resource depletion as the amount of vehicles increases dramatically.

To fulfil the above requirements, automotive industry has been developing new technologies to improve the efficiency of modern IC engines. Downsizing is one of the successful methods of reducing fuel consumption and CO_2 emissions from a Spark Ignition (SI) engines. Engine downsizing can significantly reduce fuel consumption by operating the engine closer to its minimum fuel consumption region due to combination of reduced weight and friction as engine displacement reduces, and due to minimized pumping losses at part-load conditions thanks to boosting. In this way a smaller sized engine can achieve the same level of performance with improved fuel economy. However, downsized engines are more prone to knocking combustion at high boost.

In Otto cycle, some energy is lost after exhaust valve opening as contents of the combustion chamber is not allowed to expand fully before being released into the ambient. James Atkinson invented a gas engine with expansion stroke larger than compression stroke, allowing to utilise energy completely from the expanding gas and producing additional work (Figure 2.1). He was able to achieve this over-expanded cycle by modifying the crank mechanism. Later, Ralph Miller patented a method of achieving over-expanded cycle without crank mechanism alterations (Figure 2.2), however a supercharger was required to maintain the same power output of the engine [5].

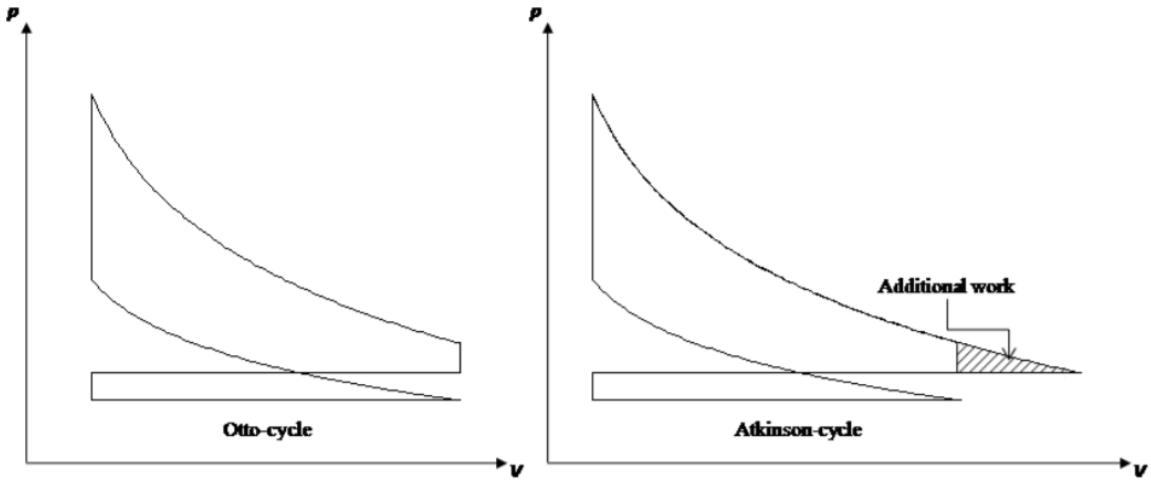

Figure 2.1 P-V diagrams of the ideal Otto and Atkinson cycles [5]

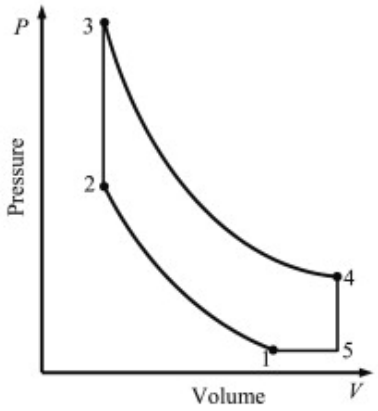

Figure 2.2 P-V diagram of the air standard Miller cycle [6]

Nowadays, Miller and Atkinson cycles can be realised by Variable Valve Actuation (VVA). Miller cycle is often referred as EIVC and Atkinson cycle as LIVC. Figure 2.3 illustrates PV diagrams and valve profiles of Miller and Atkinson cycles where effective compression ratio was reduced compared to the conventional. Clearly, profiles with reduced ECR provided lower peak cylinder pressures preventing knocking, moreover the pumping loops were significantly reduced compared to conventional profile.

The main challenge encountered with Miller cycle is its implementation for the whole range of engine operating conditions due to limitations of available VVA systems, which do not provide enough flexibility of valve control. Very limited investigations had been performed on modern direct injection SI engines with various combinations of valve profiles for Miller cycle and their effects on engine performance and emissions. Optimised VVA together with Miller cycle would allow for higher efficiency IC engines for hybrid powertrains, as hybridisation is the main route for meeting strict emissions regulations today.

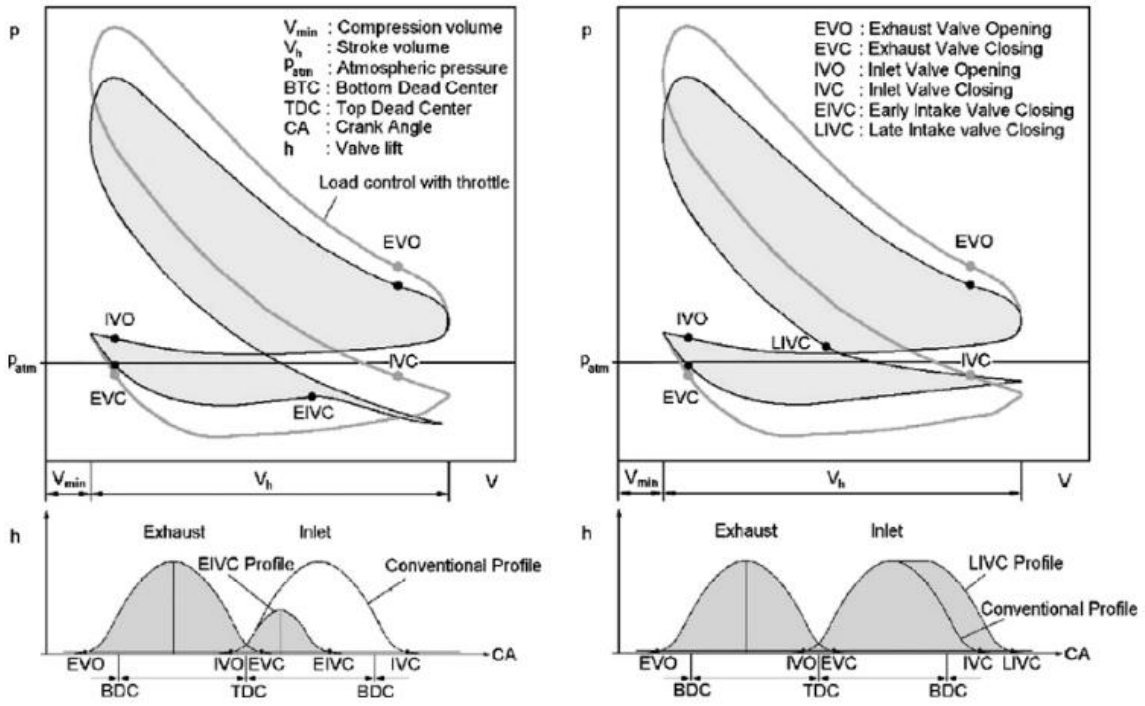

Figure 2.3 P-V diagrams and valve profiles of Miller (EIVC) / Atkinson (LIVC) cycles [7]

Camcon developed an electro-mechanical valvetrain system (iVT) capable of full control of the valve events at engine speeds up to 6000rpm. This system was installed on a single cylinder research engine for both intake and exhaust valves in order to investigate the effects of mentioned valve profiles on fuel economy and emissions by means of experimental testing.

2.2 Pollutant emission regulations

In everyday life people heavily use transport to get from one place to another, whether it is commute to work or shopping, visiting friends and family or going for a holiday. One of the most common types of transport is a passenger car.

In European Union 44.4% of total sales in 2017 were vehicles equipped with Compression Ignition diesel engines and 49.7% equipped with Spark Ignition gasoline engines. The remaining percentage was hybrid, electric and vehicles with alternative fuels [8]. Thus, 94% of vehicles sold in EU are using fossil fuels to produce power, emitting combustion pollutants into the atmosphere. These include Carbon Dioxide (CO_2), Carbon Monoxide (CO), Oxides of Nitrogen (NO_X), Sulphur Dioxide (SO_2), Hydrocarbons (HC), Benzene (C_6H_6) and Particulates (PM). Each of them has different negative effects; CO_2 is non-toxic gas but contributes towards global warming, CO will cause headaches, problems with breathing and even death (at high concentrations), long-term exposure of C_6H_6 might cause leukaemia. NO_X can cause acid rains, formation of particulate matter and asthma. HC reacts with NO_X and produces photochemical oxidants, causing breathing problems and increasing symptoms of asthma.

Particulate matter is mostly produced by diesel engines, however gasoline engines with direct injection also produce PM but in smaller quantities. It is usually filtered by DPF (Diesel Particulate Filter) or GPF (Gasoline Particulate Filter) in the exhaust system, however small particles can pass through into the atmosphere and cause respiratory problems [9].

Emission standards were introduced in order to reduce pollution from transport. This requires car manufacturers to produce cars with lower emission levels of CO, NO_X and PM. Figure 2.4 shows emission standards for passenger cars from Euro 1 to 6. European standards differentiate in emission requirements for gasoline and diesel vehicles. With implementation of Euro 6 emission limits didn't change much for gasoline vehicles, whereas NO_X emission limits were reduced by more than 50% for Diesel. The reason for that was rising concerns on health issues and even deaths related to exposure of NO_X and PM emissions, which are primarily produced by diesel vehicles. This led to diesel bans in major cities like Paris and Madrid, as well as introduction of schemes like ULEZ in London where a daily charge must be paid if certain emission standards are not met (Euro 4 for petrol and Euro 6 for diesel) [11]. Smaller cities also started to implement similar schemes and this resulted in sales reduction of almost 50% of new diesel cars in EU in 2020, while sales of petrol cars reduced by less than 3% compared to 2017 [8].

Stage	Date	CO	HC	HC+NOx	NOx	PM	PN
		g/km					*#/km*
Positive Ignition (Gasoline)							
Euro 1†	1992.07	2.72 (3.16)	-	0.97 (1.13)	-	-	-
Euro 2	1996.01	2.2	-	0.5	-	-	-
Euro 3	2000.01	2.30	0.20	-	0.15	-	-
Euro 4	2005.01	1.0	0.10	-	0.08	-	-
Euro 5	2009.09[b]	1.0	0.10[d]	-	0.06	0.005[e,f]	-
Euro 6	2014.09	1.0	0.10[d]	-	0.06	0.005[e,f]	6.0×10^{11} [e,g]
Compression Ignition (Diesel)							
Euro 1†	1992.07	2.72 (3.16)	-	0.97 (1.13)	-	0.14 (0.18)	-
Euro 2, IDI	1996.01	1.0	-	0.7	-	0.08	-
Euro 2, DI	1996.01[a]	1.0	-	0.9	-	0.10	-
Euro 3	2000.01	0.64	-	0.56	0.50	0.05	-
Euro 4	2005.01	0.50	-	0.30	0.25	0.025	-
Euro 5a	2009.09[b]	0.50	-	0.23	0.18	0.005[f]	-
Euro 5b	2011.09[c]	0.50	-	0.23	0.18	0.005[f]	6.0×10^{11}
Euro 6	2014.09	0.50	-	0.17	0.08	0.005[f]	6.0×10^{11}

* At the Euro 1..4 stages, passenger vehicles > 2,500 kg were type approved as Category N_1 vehicles
† Values in brackets are conformity of production (COP) limits
a. until 1999.09.30 (after that date DI engines must meet the IDI limits)
b. 2011.01 for all models
c. 2013.01 for all models
d. and NMHC = 0.068 g/km
e. applicable only to vehicles using DI engines
f. 0.0045 g/km using the PMP measurement procedure
g. 6.0×10^{12} 1/km within first three years from Euro 6 effective dates

Figure 2.4 European emission standards for passenger cars [10]

European Parliament and the Council introduced regulations for maximum CO_2. This regulation sets the maximum value for manufacturer's fleet average CO_2 emission level. The current target from 2020 is that the average CO_2 emission level to be less than 95g/km. From 2025 this value will be reduced by 15% and from 2030 the target will be set to 57g/km. If the average fleet's CO_2 limit is exceeded the manufacturer has to pay a penalty. From 2020 the penalty is calculated by multiplying excess emissions in g/km by €95 and number of vehicles registered in that calendar year. To reduce the average CO_2 emission level, manufacturers can produce low-emitting vehicles (CO_2 below 50 g/km) to earn super-credits, which have special weighting factor up to 2023 [12].

2.3 Fuel Economy and CO_2 emissions

Emission levels affect not only car manufacturers but also company car users in the UK, as the price for the lease is directly related to CO_2 emissions. Company cars have been provided to employees for personal and business travel. According to the company car scheme, employees must pay a fee for use of company cars. This is based on the original price of the car multiplied by company car tax and personal tax rates. Company car tax rate depends on the CO_2 emission levels of the car. Higher CO_2 level – higher fuel consumption and more tax employee has to pay for the use of a company car [13].

Company car tax rates change every year, for example: car that emits 70-74g/km of CO_2 will have 18% BIK (Benefit in Kind) rate for 2021-22 tax year, from the next year it will be increased to 19% until the end of 2024 tax year (Figure 2.5). This indicates that tax for company cars increases over years, which means that people will have to pay more for use of company cars or select cars with lower CO_2 emission levels. Even electric vehicles which don't emit CO_2 at the point of use have the same BIK rate as hybrid vehicles that emit up to 50g/km of CO_2 and have long range. Electric and hybrid vehicles are usually more expensive than petrol or diesel vehicles, meaning that company car tax in the end will be greater for an employee.

This motivates car manufacturers to produce vehicles with lower CO_2 emissions and competitive price as employees would prefer those in order to pay less tax for their company car.

WLTP BIK Rates April 2021 to March 2024

Table shows BIK rates for models registered from 6th April 2020, based on official WLTP CO2 figures.

Vehicle CO2 (g/km)	Electric range (miles)	FY 2021-22 %BIK Rate		FY 2022-23 %BIK Rate		FY 2023-24 %BIK Rate	
		Petrol, Electric, RDE2 Diesel**	Non-RDE2 Diesel**	Petrol, Electric, RDE2 Diesel**	Non-RDE2 Diesel**	Petrol, Electric, RDE2 Diesel**	Non-RDE2 Diesel**
0		1		2		2	
1-50	130+	1		2		2	
1-50	70-129	4		5		5	
1-50	40-69	7		8		8	
1-50	30-39	11		12		12	
1-50	<30	13		14		14	
51-54		14		15		15	
55-59		15		16		16	
60-64		16		17		17	
65-69		17		18		18	
70-74		18		19		19	
75-79		19	23	20	24	20	24
80-84		20	24	21	25	21	25
85-89		21	25	22	26	22	26
90-94		22	26	23	27	23	27
95-99		23	27	24	28	24	28
100-104		24	28	25	29	25	29
105-109		25	29	26	30	26	30
110-114		26	30	27	31	27	31

Figure 2.5 Company car tax rates 2021 to 2024. Adapted from [13]

2.4 Engine and powertrain technologies

2.4.1 Downsizing and boosting

Engine downsizing is a method of reducing size of an engine while maintaining or even increasing its power output. Smaller engines have less frictional, mechanical and heat losses, providing higher fuel efficiency and less emissions. Downsized engines are not very expensive as much less material is used, also there is an additional advantage in packaging which allows more space for passengers and other components in a vehicle.

Usually a turbocharger (one or more) is used to downsize an engine. The working principle of a turbocharger is to gain kinetic energy from high pressure and temperature exhaust gas and use that energy to compress air in the intake manifold (increasing air pressure and density). This provides the combustion chamber with a larger amount of air, which will be burned with increased quantity of fuel, leading to higher power output from a small engine. Moreover, increased pressure in the inlet manifold will reduce pumping losses during part load and idle conditions.

One of the main issues related to turbochargers is the low exhaust gas flow at low engine speeds, which leads to inefficient work of compressor as turbine wheel doesn't rotate fast

enough due to its moment of inertia. This low efficiency period is called “turbo lag”. During the turbo lag efficiency and performance of an engine is decreased and emissions are increased. To solve this issue a lot of various turbocharger types were designed to improve engine efficiency across the whole range of operating conditions.

A conventional turbocharger consists of two sections, a compressor and a turbine, which are connected by a common shaft as shown in Figure 2.6. At the turbine inlet high temperature and pressure exhaust gas enters turbine housing (volute) which leads to turbine wheel. Exhaust gas pushes the turbine wheel in order to exit, causing it to rotate.

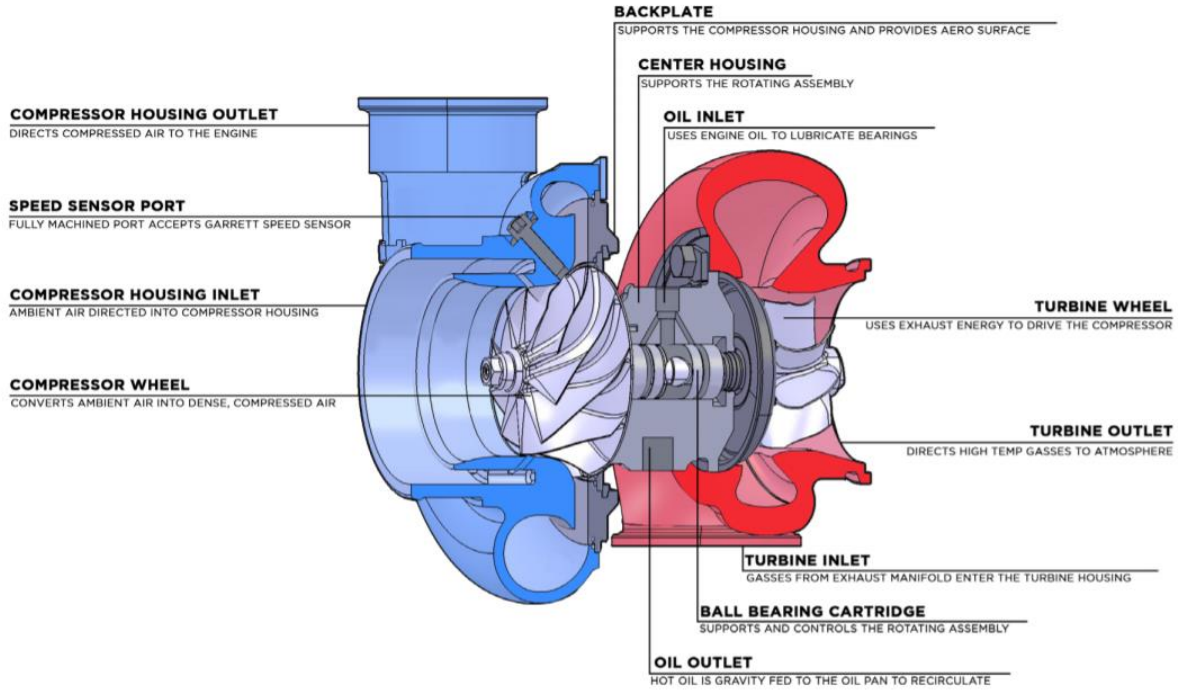

Figure 2.6 Schematic of a turbocharger [14]

This motion is transferred to compressor wheel, which sucks and compresses the air and passes it through compressor housing to the inlet manifold. Size of compressor and turbine wheels determines engine torque characteristics, for example large turbocharger would provide high power at high engine speed and small turbocharger would provide high torque at low engine speed as it spools faster. Conventional turbocharger is very cost effective and simple way of downsizing the engine, but it has a turbo lag caused by narrow effective engine speed range due to the fixed size of wheels [15].

Twin-scroll turbocharger has a different design of turbine housing compared to a conventional one, by having two intake channels – scrolls. Each scroll carries exhaust gas from a group of specific cylinders, in a 4-cylinder engine typically the first one is connected to exhaust pipe of cylinder 1 and 4 whereas the second one is connected to cylinder 2 and 3. In this way the

exhaust pulses are divided and interference in scavenging between cylinders is eliminated providing more pressure to the turbine. This type of turbocharger has wider effective engine speed range, which reduces the turbo lag. However, such design is complex and more expensive than a conventional turbocharger, it also requires even number of cylinders to split exhaust pipes evenly between the two scrolls [15].

One of the effective ways to reduce turbo lag is variable geometry turbocharger (VGT). Depending on the design, vanes or stator blades inside the housing alter area to radius ratio (A/R) to match the engine rpm. They act as nozzles (low A/R ratio) to increase the exhaust gas flow speed at low rpm, which leads to higher rotational speed of turbine wheel, thus more efficient work of compressor and turbocharger. When there is too much exhaust flow the A/R ratio increases to prevent turbocharger exceeding maximum rpm. Variable geometry allows for very wide effective engine speed range as well as reduces turbo lag. This type of turbocharger can be very expensive for gasoline engines due to vanes made of exotic metals in order to prevent damage from heat and to maintain reliability [15].

A combination of VGT and twin-scroll produces variable twin-scroll turbocharger concept by BorgWarner. Its volute has the same structure as twin scroll, however it has a valve at the inlet which replaces vanes or stator blades in VGT. The function of this valve is to redirect the exhaust gas into only one scroll reducing the A/R ratio for low rpm and to allow exhaust gas into both scrolls for high engine speeds (increasing A/R ratio). Moreover, it is possible to operate the valve in intermediate positions, which allows to alter A/R ratio at variable engine speeds. This provides very wide effective rpm range and reduced turbo lag. Due to the size and design of the valve, use of expensive materials can be avoided, therefore it is more cost effective and reliable than normal VGT [15].

Another novel type of turbocharger is called axial inflow. This concept reduces turbo lag by means of weight reduction of the turbine wheel or in other words reduction of turbine wheel's moment of inertia. This is achieved by replacement of the radial turbine wheel with an axial, which has lower moment or inertia. The original volute is also replaced as the exhaust gas enters turbine housing axially and leaves radially, whereas in conventional turbine it is other way round. Usually, axial inflow turbines have stator blades to direct the flow into the rotor blades to increase turbocharger efficiency. Some designs adopt mechanisms to rotate those stators accordingly to the exhaust flow, converting it into variable geometry axial turbocharger. This type of turbochargers has higher efficiency and reduced turbo lag, but the design is complex and requires expensive materials in order to maintain reliability of the blades [16].

The latest innovation in turbocharger technology was electric turbocharger. The turbine section is completely removed and replaced with a powerful electric motor. In this concept boost pressure does not depend on the exhaust gas anymore, instead it is achieved by use of electric charge from the batteries. The boost demand can be fulfilled at any rpm or engine load with a single electric turbocharger. The turbo lag is completely eliminated. However, batteries which carry electric charge for the motor are expensive, occupy significant amount of space and add more weight to the vehicle. Also, the motor requires cooling and additional control system. All these disadvantages make this concept not cost effective compared to VGT and twin-scroll turbochargers [15].

Downsizing is a good way of reducing fuel consumption and emissions while improving engine performance but there is always a trade-off between efficient and reliable turbocharger and its price.

2.4.2 Homogeneous and stratified charge combustion

In a conventional SI engine a mixture of air and fuel is drawn into the combustion chamber during the intake stroke, which is called a homogeneous charge, it is then ignited by a spark plug near TDC (Top Dead Centre). For a homogeneous mixture the air to fuel ratio is kept at stoichiometric value or close to it in order to achieve complete combustion. This provides stable combustion, but also limits engine's fuel economy. When attempting to operate engine with leaner homogeneous mixture the combustion becomes unstable, burning of fuel slows down and combustion will not be complete before the exhaust stroke. This reduces engine power and increases emissions, especially nitrogen oxides or NO_X [17].

When using a direct fuel injection for spark ignited engines the stratified combustion is possible. In stratified combustion the fuel is injected just before the ignition, air – fuel mixture is not mixed thoroughly, thus it is not homogeneous, the vaporization of fuel occurs during combustion. This allows to use higher compression ratios without knocking combustion, as it cannot occur when there is only compressed air in the cylinder, the fuel economy can also be improved as leaner mixture can be used [18].

The main advantage of stratified combustion is improved fuel efficiency during idling and low load conditions as well as the ability to run the engine un-throttled, which reduces pumping losses significantly. However, for peak power and high engine loads homogeneous combustion is necessary for complete combustion and higher power output due to stoichiometric mixture [18].

2.4.3 Controlled Auto Ignition (CAI) /Homogeneous Charge Compression Ignition (HCCI)

Significant reduction in fuel consumption and emissions in gasoline engines can be achieved with use of Controlled Auto Ignition (CAI) or HCCI during part load operation. CAI is when a homogeneous mixture ignites automatically once sufficiently high temperatures (1000-1100K for gasoline) and pressures are reached in the combustion chamber [19]. To achieve such conditions the intake air should be preheated, alternatively exhaust gas recirculation can be used. At the end of compression stroke the mixture ignites simultaneously in multiple locations of the combustion chamber once the temperature is high enough, unlike flame propagation in SI combustion. This provides even heat distribution across the chamber without relative high temperature regions, which prevents formation of NO_X emissions. However, there is a negative effect on CO emissions as its full oxidation to CO2 occurs at temperatures above 1400–1500 K [19].

Due to the multiple ignition sites with CAI the heat release occurs rapidly, thus combustion duration would be shorter than with homogeneous charge. The mixture for CAI has to be strongly diluted with fresh air and exhaust gas in order to reduce heat release rate to avoid excessive noise emission and reduce mechanical stress to the engine parts. Moreover, strong dilution can lead to engine de-throttling and improving fuel efficiency [20].

Lack of spark ignition in CAI introduces challenges with combustion timing control for performance optimisation. Instead of spark timing, combustion phasing is controlled by thermodynamic state of the charge inside the cylinder by means of fuel injection, valve timings and EGR depending on the engine design. For engines with port fuel injection PFI system VVA and EGR (external or internal) are used to control combustion [21][22].

For engines with DI system the combustion is controlled by late fuel injection just before the spark (stratified combustion) [23]. Stratification provides more effective control of the combustion timing and fast response compared to VVA and EGR, extending the limits of CAI combustion [24]. Sometimes dual fuel injection system is used to control CAI combustion. Such setup requires both PFI and DI injection systems to deliver fuels with different reactivity like diesel and gasoline, however higher efficiency can be achieved by using two DI injectors to deliver fuels directly into the cylinder [25]. In addition, to control combustion timing and to widen the CAI operational region some concepts use combination of VVA and DI systems [20].

CAI combustion has been extensively studied in four-stroke engines due to its promising potential in fuel economy and emission reduction, particularly NO_X emissions. The combustion temperature is lower which results in minimum heat losses improving the engine efficiency.

Moreover, CAI allows to use simple exhaust gas aftertreatment with a 3-way catalyst even during lean mode operation. CAI combustion produces similar level of uHC emissions as a conventional SI combustion process, but the exhaust temperature is too low for the oxidation of HC and CO [20].

2.4.4 Hybrid powertrains

2.4.4.1 Engine and electric hybrid configuration

A hybrid electric vehicle (HEV) is a motor vehicle that combines two different power sources. The most common combinations are petrol – electric and diesel – electric. These two power sources can be combined into a single powertrain, or they can be used as two separate propulsion systems. Figure 2.7 shows main combinations of engine and electrical motor in a hybrid vehicle [26].

In a series configuration IC engine produces electrical charge via a generator which is then either stored by the battery of supplied directly to the electrical motor. In this arrangement only electrical motor provides power and torque directly to the wheels.

With parallel configuration both IC engine and electrical motor are supplying power and torque to the wheels. IC engine does not contribute to battery charging or electrical supply.

Series-parallel configuration provides a combination of both configurations discussed earlier. The IC engine can charge the battery and provide electrical energy to the motor when its torque and power is not required for vehicle propulsion. However, the IC engine can stop battery charging and start providing power and torque to the wheels when required. This architecture is more complicated due to additional mechanisms and controls, but it ensures the battery charge and increased power output for the vehicle when needed.

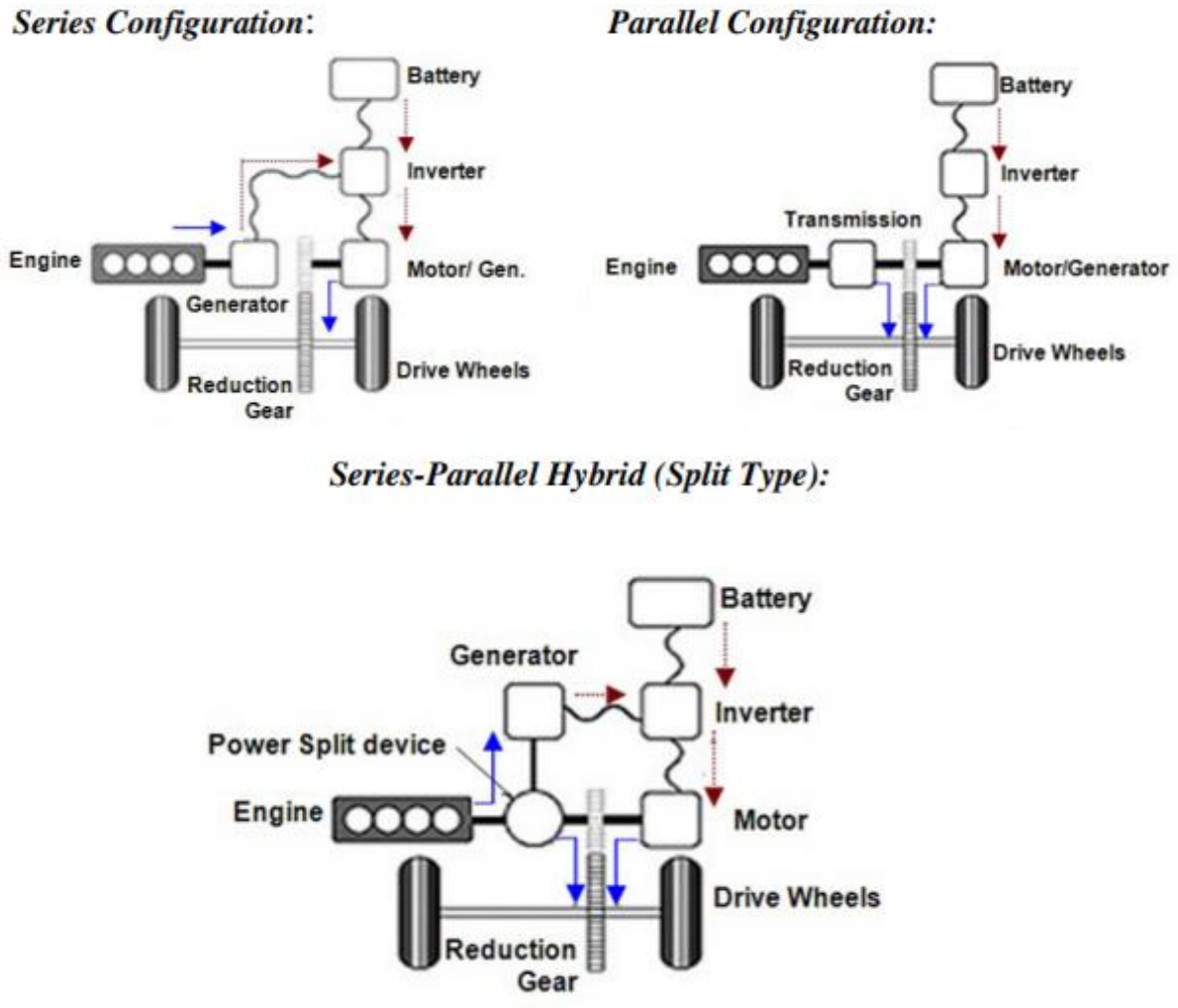

Figure 2.7 Architecture based HEV classification [26]

HEVs can be categorised by the degree of hybridisation i.e. by power supplied by IC engine and electrical motor calculated by Equation 2.1. Based on the percentage HEVs are split into three main classes - micro, mild and full hybrid (FHEV).

Equation 2.1

$$\text{Degree of hybridasation} = \frac{\text{Motor Power}}{\text{Motor Power} + \text{Engine Power}} * 100$$

A micro hybrid usually has less than 5% degree of hybridisation and features an electrical motor to start and stop IC engine during idling, this is a well-known start-stop system. The electrical motor in this case does not contribute to the vehicle as a propulsion system, whereas in a mild hybrid it provides up to 10% of the vehicle power to the wheels and works in parallel with IC engine. In a full hybrid electrical motor accounts for up to 75% of total vehicle power. FHEV can run on the combustion engine or electrical motor alone and even with combination

of both. Because electrical motor is more powerful the IC engine of a smaller power output can be selected [26][27].

FHEV also includes the plug-in hybrid (PHEV) which can be plugged into the grid to charge the battery. PHEV is essentially a full hybrid but with an option of fully electrical mode thanks to larger battery. This mode allows to save fuel on long distances when battery is charged. When it is low on charge the vehicle can switch to IC engine as main propulsion system or use it as a generator to recharge the battery as a normal full hybrid vehicle [26][27].

2.4.4.2 Engine for electric hybrid powertrain

Requirements for IC engine depend on the type of hybrid powertrain it will be integrated to. However, a DI turbocharged engine with high compression ratio, Miller cycle operation and high tumble would be a primary specification for a hybrid powertrain. As the IC engine and electrical motor are integrated together in HEV, engine speed range is reduced as electrical motor can compensate for vehicle's peak power demand. On top of that low speed torque can be delivered solely by the motor, thus a conventional single turbocharger would be an efficient and cost effective solution. Increased valve lift would benefit Miller cycle to maximise the efficiency. Due to the presence of heavy batteries and costly electrical powertrain the IC engine is targeted to reduce its weight and use low cost materials while reducing CO_2 emissions. Packaging must also be improved as future HEVs may implement underfloor installation of powertrain [28].

Table 2.1 shows main requirements for IC engine based on the application in HEV. A range extender would require the lowest power output, port fuel injection, conventional valve train and BTE of 35%. However, higher efficiency HEVs would require direct injection, variable valve actuation and Miller cycle (EIVC), a conventional turbocharger or VGT and TBE above 45%.

Table 2.1 IC engine requirements for hybrid powertrain [28]

Requirement	Range Extender	Value Parallel PHEV	Mid Parallel HEV/PHEV	High Efficiency Series HEV	Optimised BTE Series HEV
Power [kW]	32 to 64	80	80	70 to 80	60
Lambda	Stoichiometric			Lean	Ultra Lean
Fuel Injection	PFI	Dual PFI	Central DI 350bar		Active Pre-Chamber DI

Cam Timing	Fixed	DVVT	DVVT & EIVC		EIVC Optimised at Peak BTE
EGR System	No EGR		Cooled EGR		
Aspiration	NA		Conventional Turbocharger	VGT Turbocharger	Conventional Turbocharger Optimised at Peak BTE
Brake Thermal Efficiency (BTE)	~35%	~37%	39 to 41%	45%	Target 47 to 52%

2.4.4.3 Air hybrid engine

Pneumatic hybrid or air hybrid is a type of powertrain system, where IC engine is used as a pneumatic pump to convert kinetic energy into compressed air. During vehicle's deceleration, the fuel is not injected and combustion chamber is filled only with air, which is compressed by a piston during the compression stroke. This compressed air is then stored in high pressure air tank. During the intake stroke high pressure air can be injected into the cylinder, which will allow for boosting during turbo lag and reduce pumping losses at part load. Moreover, injected high pressure air will expand and propel the piston, which is known as pneumatic motor mode [29].

Usually, air hybrid system is installed on SI engine with an air tank. Some designs use an independently actuated valve for compressed air inside the cylinder, it could be one of the intake valves or a separate one, whereas others use camless valve actuation system to operate intake/exhaust valves for compressed air. Regardless of the design, principle of operation is the same. Air hybrid engine has four modes of operation: compression braking (CB) or pneumatic pump, air motor (AM) or pneumatic motor, air power assisted (APA) and a conventional mode, in case with camless engines this mode is conventional unthrottled (CU) as the load is controlled by valve lift and duration.

Figure 2.8 shows an example of CB mode with camless valve actuation. During the intake stroke fresh air is brought into the cylinder through unswitchable valve. This valve closes just before the compression stroke. The air trapped in the cylinder is compressed and transferred to the heat-insulated tank through switchable valve at the end of the compression stroke. This

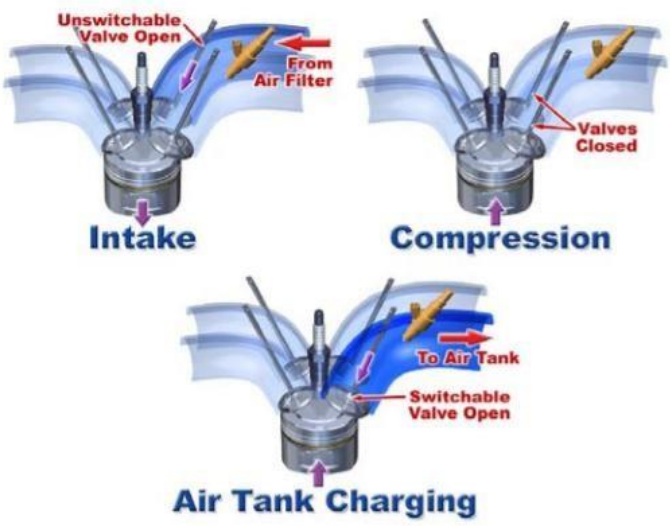

Figure 2.8 Compression braking mode [30]

mode is utilised to decelerate the vehicle when fuel is not injected (non-fired operation). The engine can work as 2-stroke or 4-stroke compressor [30].

During AM mode the air flows in opposite direction compared to CB mode (Figure 2.9). When the piston is near TDC the switchable valve opens and compressed air is charging the cylinder. Then air expands and pushes the piston down, using the energy saved during CB mode. When the piston starts to move up the unswitchable valve opens to release the expanded air from the cylinder. Air motor mode is used to accelerate the vehicle without using the fuel. The engine can be used as a 2-stroke or 4-stroke air motor with non-fired operation [30].

The Air Power Assist (APA) mode is similar to conventional SI combustion and demonstrated in Figure 2.10. During the intake stroke the switchable valve is opened and mixture of compressed air and fuel fills in the cylinder. Like in AM mode compressed air is allowed to expand, which produces part of the demanded power and less amount of fuel is needed to produce desired output. Following the compression stroke, mixture ignites and expands like in a conventional engine. The cycle is completed with exhaust stroke where exhaust valves operate normally. The APA mode uses only compressed air from the tank. This mode is used when AM mode cannot deliver required power or torque without fuel energy. However, fuel should be delivered by high pressure injectors (similar to injectors of DI systems) due to compressed air in the intake runners [30].

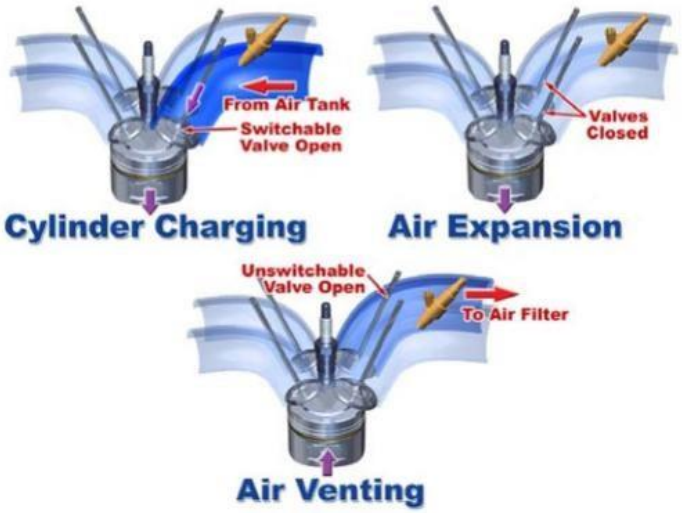

Figure 2.9 Air motor mode [30]

Once the air tank is empty the engine starts to run with conventional mode or with CU mode for camless engines. The switchable valve is used to deliver fresh charge and conventional

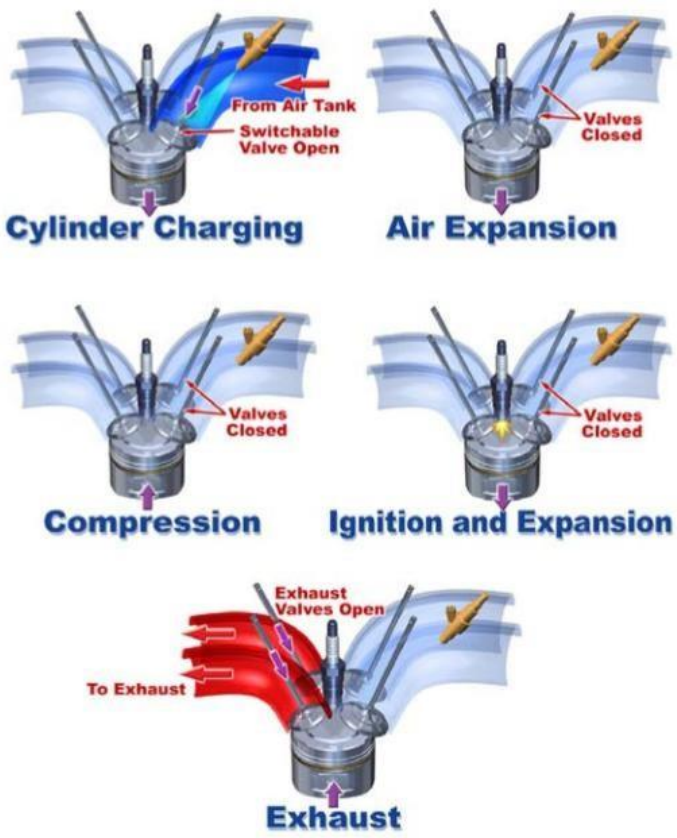

Figure 2.10 Air power assisted [30]

4-stroke cycle occurs. Camless engines have an advantage of almost zero pumping losses due to unthrottled operation during this mode [30].

The main principle of air hybrid is to absorb the energy during vehicle's deceleration (CB mode) and to reuse this energy during acceleration (AM and APA modes). Fuel is not used during CB and AM which allows to significantly reduce fuel consumption. The APA mode also reduces fuel consumption as part of the power demand is fulfilled by compressed air.

As mentioned before, there are few design variations of air hybrid system. For example, to eliminate the need for camless valves a separate camless valve was placed in the cylinder, connecting it with air tank without interfering with either intake or exhaust ports. According to Dönitz et al. simulations, downsized and supercharged engine with such air hybrid system allows to save up to 32% of fuel compared to same power rated NA engine [31]. Another example would be a system with cam profile switching (CPS) which controls an intake valve in order to operate engine in CB or AM mode, in conjunction with external air tank valve. Regenerative efficiency (ratio between positive and negative IMEP) for such design was 14.38-15.18% with air tank pressure of 10-15 bar [32]. Diesel engines are also compatible with air hybrid system, previous studies showed up to 33% maximum regenerative efficiency [33].

Air hybrid is very useful in city driving, where a lot of accelerations and decelerations are required. Rapid acceleration requires a lot of fuel and a lot of energy is wasted into heat in braking friction during deceleration. Air hybrid captures, stores and reuses this energy using the momentum of the crankshaft to compress the air, which is stored in a tank and then used to reduce fuel consumption and emissions. It is more advantageous than electric hybrid because it does not require additional propulsion source like electric motor. Also, it does not need very expensive and complex batteries to store the energy, which add more weight to the vehicle [30]. Air hybrid is very appealing for downsized and supercharged engines because of

the turbo lag which occurs at low exhaust gas flow rates. When boost pressure is insufficient, compressed air from the air tank can compensate it at idle and up to full load or until there is enough exhaust flow to generate required boost.

Not only passenger cars can benefit from air hybrid but also buses and commercial vehicles which require operation of pneumatic equipment such as bus doors or excavator arms on tractors. Normally, this equipment is operated by compressed air which is produced by engine driven compressor, which only increases fuel consumption, whereas air hybrid would use energy recovered from vehicle's braking leading to improved fuel efficiency and minimized emissions. Moreover, in diesel engines compressed air can be used in combination with high EGR percentage in order to reduce NO_X and smoke emissions. The air hybrid can enhance many aspects of engine and vehicle itself at a minimum cost and immediate availability [29].

2.4.5 Variable Valve Actuation (VVA) systems

Gas exchange process in conventional IC engine is controlled by opening and closing of intake and exhaust valves, which are operated by camshafts. The camshafts are driven by crankshaft via chain or belt, this provides constant (fixed) intake and exhaust valve timing for any engine speed and load.

To enhance gas exchange process IC engines feature valve overlap, where both exhaust and intake valves are open. Small overlap would prevent backflow losses (when exhaust gas flows into the intake port instead of exhaust port) and increase torque at low engine speeds, however volumetric efficiency would be reduced at higher speeds. On the other hand, large overlap would provide better scavenging of residual gas and more power output at high engine speeds, but this will lead to backflow losses and bad idle quality at low engine speeds. In conventional IC engines valve overlap is fixed for the whole range of engine speeds due to the geometry of camshafts, which

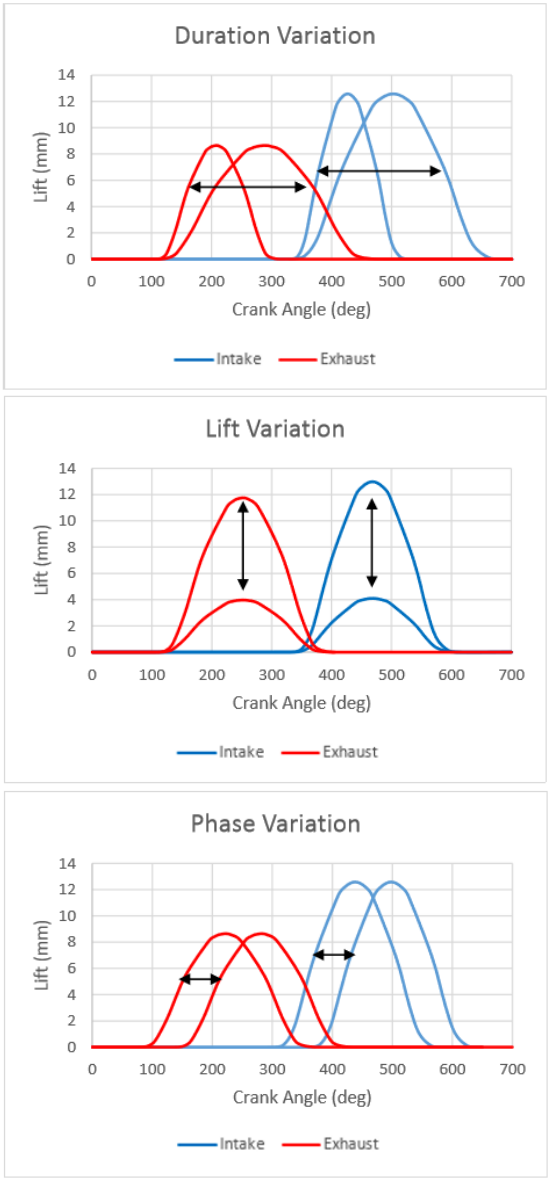

Figure 2.11 Three ways of altering valve profile

is a compromise between high power output, good idle quality and high torque at low engine speed [34].

VVA is used to optimise gas exchange process by altering valve timings and/or profiles. This can be done in different ways by altering: Intake valve opening (IVO) and closing (IVC) timing, Exhaust valve opening (EVO) and closing (EVC) timing, phase, duration of opening, valve overlap and lift (Figure 2.11).

VVA systems capable of full valve control would allow to eliminate the throttle and dramatically reduce pumping losses. Also, reduction of backflow losses and increased power output would be achieved by adjusting the valve overlap throughout the engine operating range.

There are many different types of VVA systems and some of them are already in production. Each system has different level of valve control, complexity, performance and cost.

2.4.5.1 Cam phasing

Phasing is achieved by a device called Mechanical Cam Phaser (MCP). Figure 2.12 illustrates main elements of this device. Crankshaft drives sprocket via chain. Sprocket is connected with exhaust flange and cam by two hexagonal bolts and this assembly rotates together, therefore exhaust valves have fixed timings. The drive flange is locked by D-slot and attached to the intake cam with centre bolt so that those parts rotate together as one unit. The sprocket and exhaust flange have two arc shaped apertures/slots, the drive flange has two straight slots. Drive pins are inserted through those slots in the sprocket, drive flange, fly weights (connected with extension springs with each other) and the exhaust flange. When engine is in operation, the MCP device rotates and the fly weights move out from the centre due to centrifugal force. Because drive pins have to follow different shapes of slots with fly weights' movement, the drive flange rotates relatively to the sprocket by angle θ (Figure 2.13). This delays opening and closure of the intake valves by the same cam angle. As a result, the continuous time

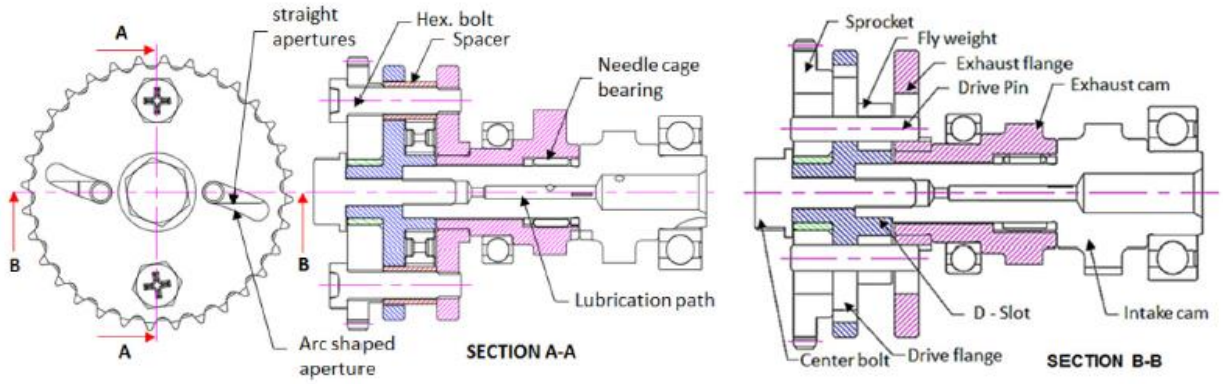

Figure 2.12 MCP structure [35]

phasing relative to engine speed is achieved (Figure 2.14). The speed at which phasing occurs can be adjusted by fly weights' masses and stiffness of springs.

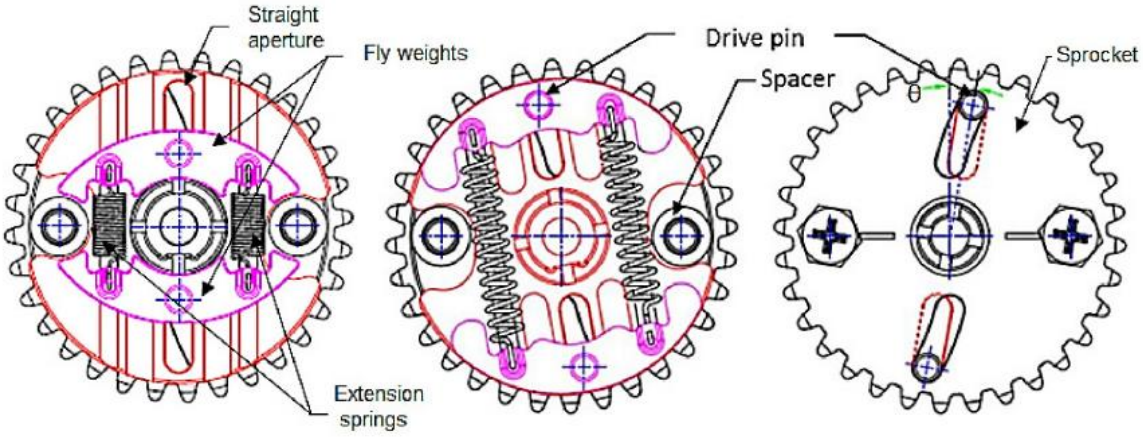

Figure 2.13 MCP working principle [35]

At low engine speeds the intake is advanced, which reduces the back flow significantly during the compression due to early closure of the intake valves, this increased BMEP (Brake Mean Effective Pressure) up to 8% for a particular engine. At high engine speeds the intake is retarded, which allows more air-fuel mixture in the cylinder due to inertia effects, but later opening of intake valve results in small valve overlap which causes poor scavenging of residual gases. The disadvantage of this system is that phasing depends only on the engine speed and adjustments in duration and lift of valve events are not possible [35].

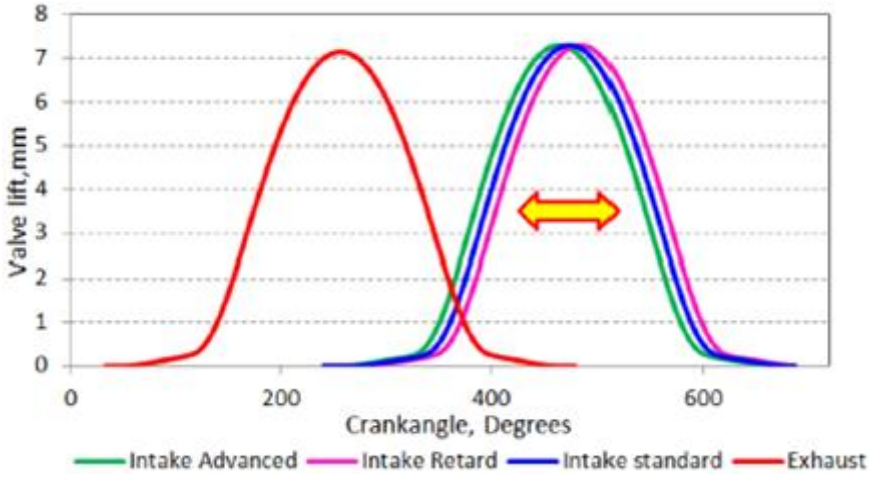

Figure 2.14 Effect of MCP on intake valve events [35]

2.4.5.2 Variable Valve Timing (VVT) and Variable Valve Lift (VVL)

Valvetronic is the intake valve actuation system designed by BMW. The aim of this system was to significantly reduce fuel consumption by eliminating the throttle mechanism, thus minimising pumping losses. This was achieved by changing continuously the lift of the intake valves according to the power demand. The result was a 10% reduction in fuel consumption.

However, this system does not benefit at WOT as it acts as a standard conventional valve train and pumping losses are minimised by fully open throttle, also additional components cause more friction losses which results in loss of power [36].

Valvetronic system consists of an electric motor, an eccentric shaft, an intermediate rocker arm and a standard camshaft. In this assembly the camshaft acts on the rocker arm through roller bearing and valve opens. When more power is needed, the electric motor turns the eccentric shaft, which changes the position of the intermediate rocker arm so that when the camshaft acts on the roller bearing, the valve opens further (larger valve lift). This is demonstrated in Figure 2.15 [36]. This system also allows for reduced valve opening time which means the intake closes earlier at idle. This avoids back-flow of the mixture at the start of the compression stroke, which ensures that engine will start at very low temperatures.

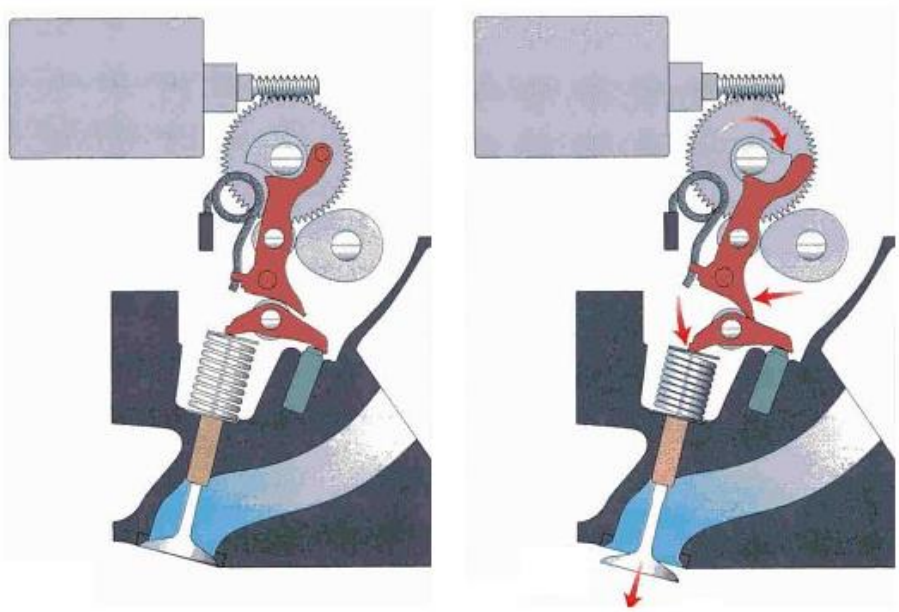

Figure 2.15 Valvetronic working principle [36]

The second generation of Valvetronic is capable of phasing each of the inlet valves independently. At idle the minimum valve lift is used for both intake valves, when engine load increases the lift of the inlet valve 1 increases while the lift of the inlet valve 2 remains unchanged. When more power is needed the lift of the valve 2 starts to increase. At part load conditions a significant lift difference is present (Figure 2.16). A subsequent increase in load, reduces the lift difference until both valves operate equally. Such configuration leads to the asymmetric distribution of the mixture flow and greater swirl motion which improves combustion stability and residual gas compatibility at part load [37].

This system reduced fuel consumption by 12% over cycle and up to 25% at idle [38]. However, there are disadvantages like increased size of the cylinder head and parasitic losses due to additional friction.

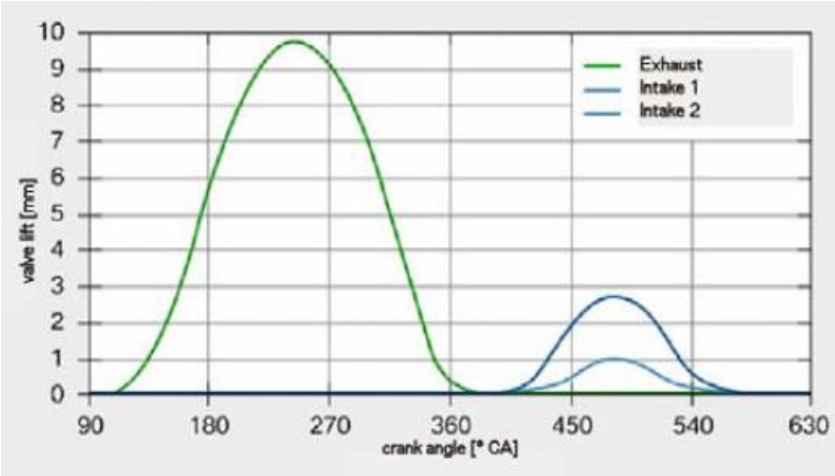

Figure 2.16 Valvetronic valve profiles [37]

Nissan VVEL is a Variable Valve Event and Lift actuation system. It is more compact compared to Valvetronic. Also it has less parts therefore less friction losses, what makes it suitable for high-performance engines [36]. Figure 2.17 demonstrates main components of the VVEL system, which can be divided into two subsystems: the mechanical, which opens and closes valves, and the actuator, which adjusts valve lift and event timing.

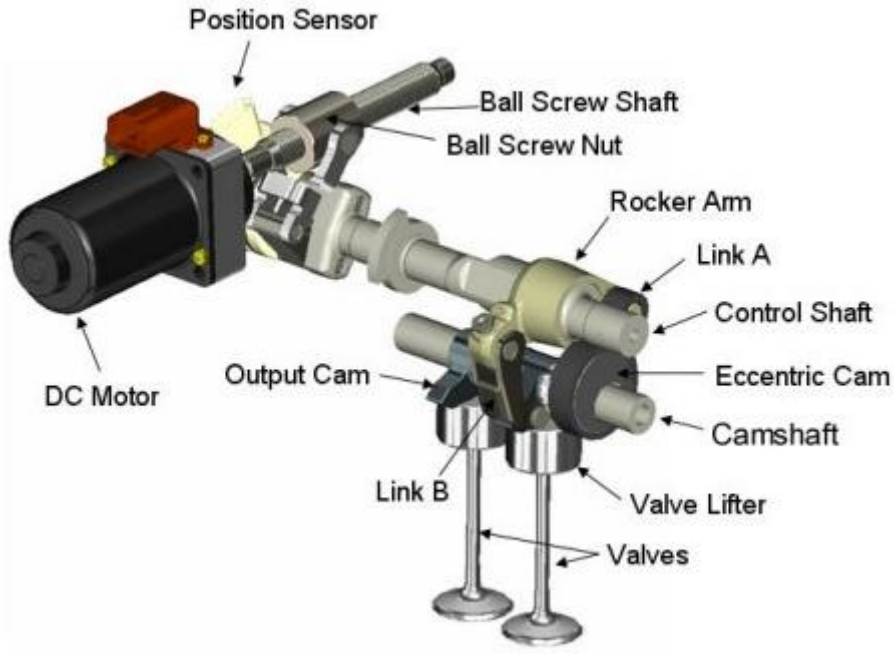

Figure 2.17 Nissan VVEL system [36]

Camshaft is driven by the crankshaft and has an eccentric cam which is connected to the output cam through link A and B and rocker arm, which is placed on the control shaft. When

eccentric cam rotates, the link A transfers movement through the rocker arm to the link B, which rotates output cam and valve opens. When different valve lift is needed the DC motor rotates the control shaft by a certain angle, this changes the position of the rocker arm so that the mechanical links make output cam move further down and open valve even more as well as changing the event timing (Figure 2.18). The angle is calculated by the engine control module based on the data from the crankshaft sensor. The position sensor, located at the control shaft, ensures high accuracy of rotation by the DC motor. Such system is compact, reliable, responsive and economic in terms of power consumption. It also allows to open throttle fully almost at all engine loads and increase fuel efficiency due to reduced pumping losses, but it does not eliminate throttle completely. Variable valve lift and timing improves performance and reduces emissions [39].

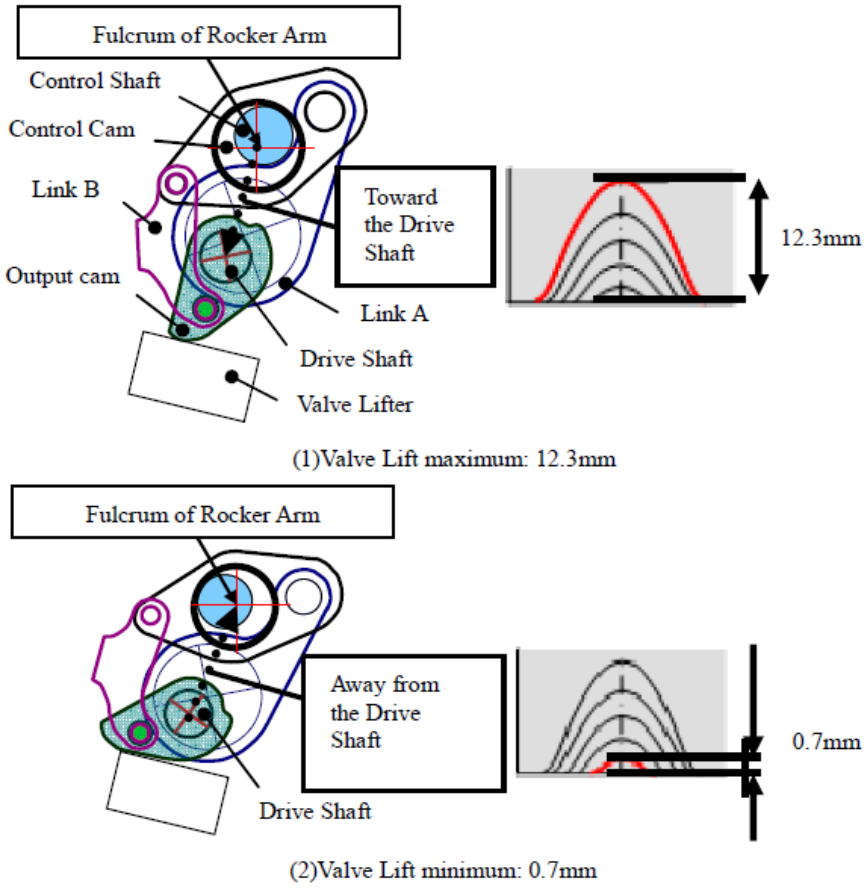

Figure 2.18 Nissan VVEL working principle [39]

Toyota Valvematic is another example of valve train with variable lift. Similarly to Valvetronic, it reduces the pumping loss at part load and improves fuel consumption by eliminating the throttle. Valvematic has simple and compact design, the friction losses from additional components are minimal compared to Nissan VVEL and BMW's Valvetronic systems. This provides improvement in power by 10% and reduction of fuel consumption by 5-10% in regular driving conditions [36]. The valves are actuated by the camshaft via roller and finger follower,

which are located on the intermediate shaft. The electric motor attached to the intermediate shaft rotates the finger followers via internal gear threads. The finger follower will move either away or toward the roller, the angle between them determines the lift of the valve. When the angle is narrow the low lift is achieved (Figure 2.19) and when the angle increases the lift is also increased (Figure 2.20). This allows to vary the lift continuously and eliminate throttle body, thus reducing fuel consumption at part load conditions, high lift configuration allows for greater top end power [40].

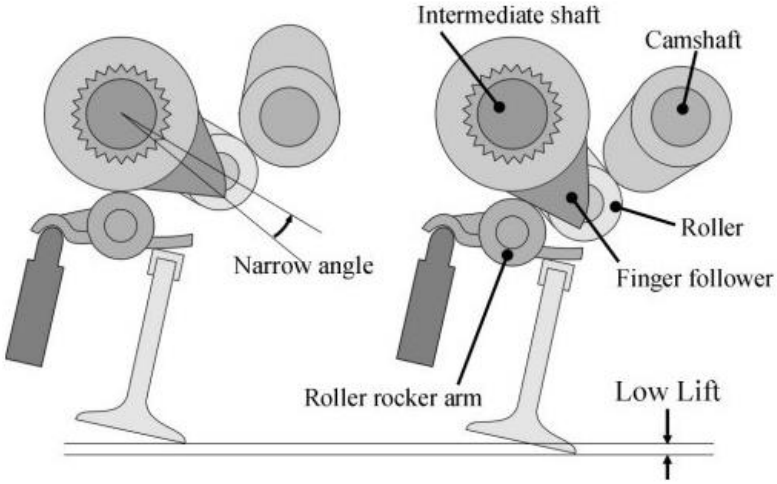

Figure 2.19 Valvematic working principle for low lift [36]

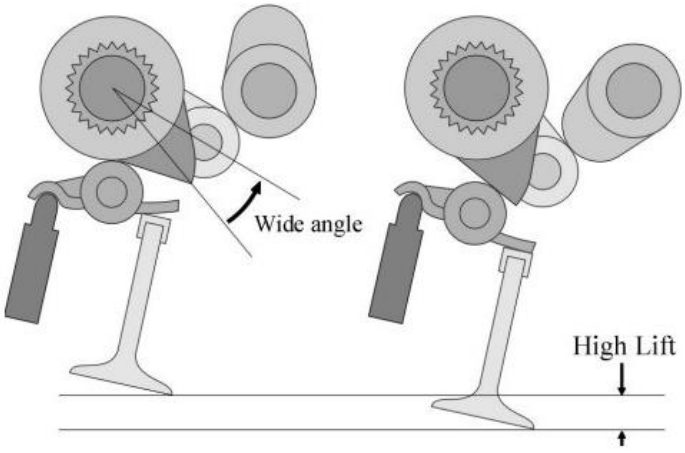

Figure 2.20 Valvematic working principle for high lift [36]

2.4.5.3 Cam switching

A cam switching system uses two cam profiles, one for fuel economy and another for performance. A good example of such system is Honda's i-VTEC which uses hydraulic switching mechanism to change cam profiles during engine operation. Rocker arms follow three different cam profiles: high output, delayed closure and fixed. When vehicle accelerates,

VTEC system is off and rocker arms for intake valves follow their default cam profiles: high output and fixed (one intake valve always follows this profile). When vehicle has reached the desired speed and starts cruising (low load) VTEC system switches on: hydraulic pressure is applied to synchro piston, which is built into the arms, the piston moves so that it connects two rocker arms together and one intake valve follows delayed closure cam profile (Figure 2.21). Simultaneously, electronically controlled throttle is fully opened, minimising pumping losses. Air-fuel mixture is sucked into the cylinder and pushed back to the intake port due to late intake valve closure, this ensures that exact amount of mixture is in the cylinder in order to continue cruising [42]. Cam switching allows variable valve timing, duration and lift depending on the selected cam profiles, however change of those parameters will be discrete rather than continuous as geometry of profiles is fixed.

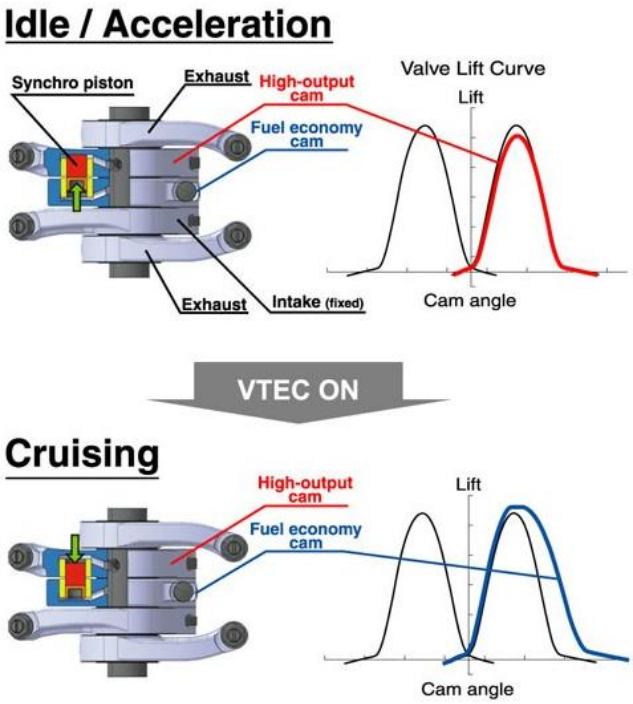

Figure 2.21 Working principle of i-VTEC system [41]

2.4.5.4 Fiat Multiair

Multiair is the VVT system that allows variable lift and control of IVO and IVC all together. It also allows multiple valve lift during one valve event. The system uses one camshaft that actuates exhaust valves directly and intake valves are controlled by electrohydraulic mechanism with intake cam lobes from the camshaft. The electrohydraulic mechanism includes roller rocker, hydraulic piston, hydraulic chamber with solenoid valve and hydraulic valve actuator (Figure 2.22).

When it is desired to run the engine with original valve profile (from camshaft) the solenoid valve is de-energised and closed. Intake cam lobe acts on the roller rocker and the oil from hydraulic piston cannot enter the chamber as valve is closed, so it flows directly to the hydraulic valve actuator and intake valve follows the profile of the cam lobe. The intake cam profile in this case is designed for high power output (high lift and long duration of valve event) and suitable for high engine speeds.

Once the solenoid valve is energised, the oil can flow into the hydraulic chamber, therefore hydraulic valve actuator will not have oil and the intake valve will close under the force of its

rebound spring. This enables to close the valve at any time when needed, thus changing the duration of the valve event.

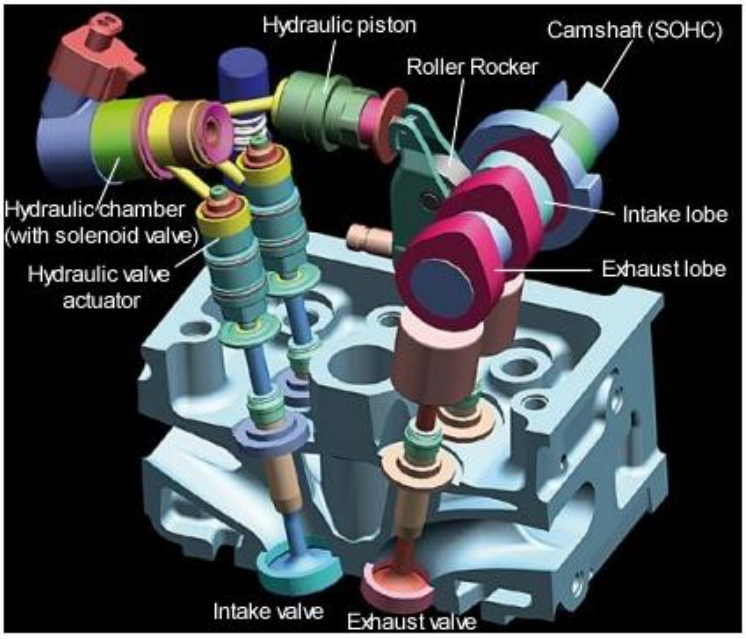

Figure 2.22 Fiat Multiair system [36]

When retard opening of the intake valve is needed the solenoid valve is energised and intake valve is not actuated. Then solenoid is de-energised and oil flows into the hydraulic valve actuator and the intake valve opens. However, part of the oil is flown into the chamber and there is not enough oil left to open valve at full lift. This determines the amount of valve lift, the later the solenoid de-energised – lower the valve lift.

Multiair has five different types of intake valve strategies to suit different engine conditions (Figure 2.23). The first one with high lift and long duration is suitable for high engine speeds. The second one has late valve opening and low valve lift which improves the air-fuel mixture leading to better fuel economy and emissions. Number three is suitable for a wide range of part-load conditions, the early closing of intake valves will vary depending on the power demand, this allows to eliminate throttle and reduce pumping losses. Number four is designed for enhanced acceleration at low engine speed, it allows sufficient amount of air into the cylinder and early valve closure ensures that there is no charge backflow. The last one is "Multilift" mode, it is designed for very low engine speeds, providing better fuel consumption and improved quality of air-fuel mixture. By

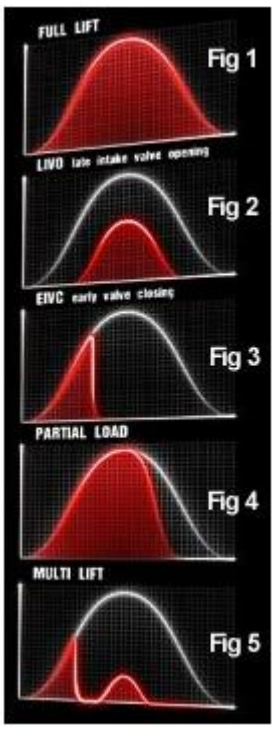

Figure 2.23 Multiair modes [36]

combining these modes Multiair system improves maximum power by 10%, low-rpm torque by 15% and fuel economy by 10% [36].

2.4.5.5 Electro-hydraulic camless VVA

This is one of the examples of camless VVA systems, where camshafts are replaced with valve actuators (one for each valve) which open and close valves. Figure 2.24 illustrates the valve actuator. When the top port is pressurised via an actuation valve (can be shared by pair of intake or exhaust valves), which is linked with low pressure fluid (PL) and high pressure fluid (PH), the engine valve is pushed down by the opening piston. When the top port is returned to its default low pressure state, the engine valve is pushed up by the return spring. The position of lift control sleeve determines the lift of engine valve. For the default position bottom port has enough pressure to keep lift control sleeve in the lower position so that the actuator will operate at the high lift (S2). In order to operate the actuator at low lift (S1) the lift port is pressurised via lift valve (can be shared by all engine valves), which is linked to the fluid tank and PH, the control sleeve moves up and prevents the opening piston to move further down. Due to the large surface area the control sleeve does not move down even when it is being hit by the opening piston during valve operation. The main advantage of such valve actuator is that the accuracy of lifts is mechanically guarantied, no displacement sensors needed which makes system reasonably priced. The system offers continuously variable timing, duration and two discrete lifts [43].

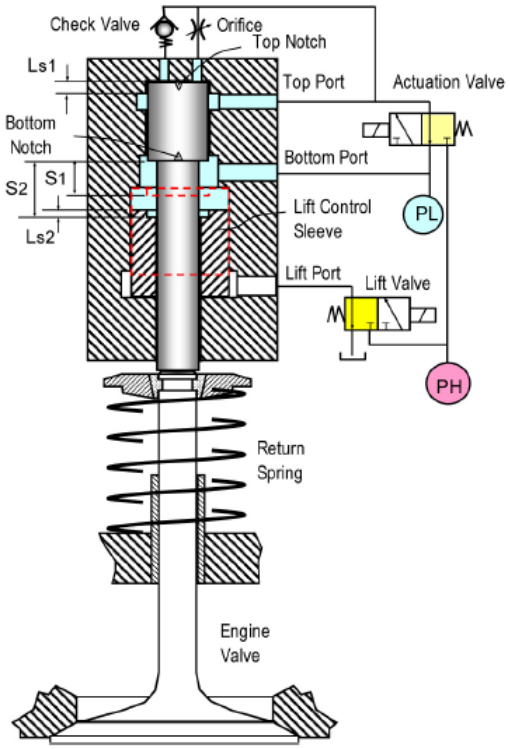

Figure 2.24 Electro-hydraulic valve actuator [43]

2.4.5.6 Electro-magnetic camless VVA

E-Valve was developed by VALEO Engine Management System. This actuation system was adopted for intake valve only. The intake camshaft was replaced with electromagnetic valve actuators (one for each cylinder) whereas the exhaust camshaft remained standard, therefore this system is classified as half camless. The main principle of this system is that valve actuators (Figure 2.25) open and close intake valves independantly at requested crankshaft angle timing, duration and lift of valve events. The Engine Control Unit (ECU) sends the

request to open or close intake valves to Valve Control Unit (VCU) via CAN bus. VCU drives the electromagnetic valve actuators and gives feedback to the ECU of what was applied through the CAN bus. E-Valve system has two modes of operation commutation and balistic.

Figure 2.25 Electro-magnetic valve actuator [44]

For the first mode ECU defines two crankshaft angles (at which valves opened and closed, inbetween those angles valves are maintained in the open possition) to the VCU. For the second mode ECU defines only one angle at which valves are opened, then a free flight of the valves due to mass-oscillator concept in the actuators is allowed to provide the minimum duration of valve event. This allows independant continuous controll of intake valve events which leads to reduced pumping losses by eliminating throttle, CO_2 emission reduction and increase in low end torque [44][45].

2.4.5.7 Pneumatic camless VVA

FreeValve is a fully variable valve actuation system, which offers programmable independent control of the intake and exhaust valves for any engine load. Based on driving conditions the system can offer maximized performance or minimized fuel consumption and emissions. FreeValve uses electro-hydraulic-pneumatic actuators combined with advanced sensor techniques. As a result it has overcome packaging disadvantages and high cost. It also achieved a reduction of 12-17% in fuel consumption and increase of 30 percent in volumetric efficiency [46]. Each actuator consists of an actuator piston, cylinder, two solenoids (timing and lift solenoid), two spool valves, two port valves and a hydraulic latch (Figure 2.26).

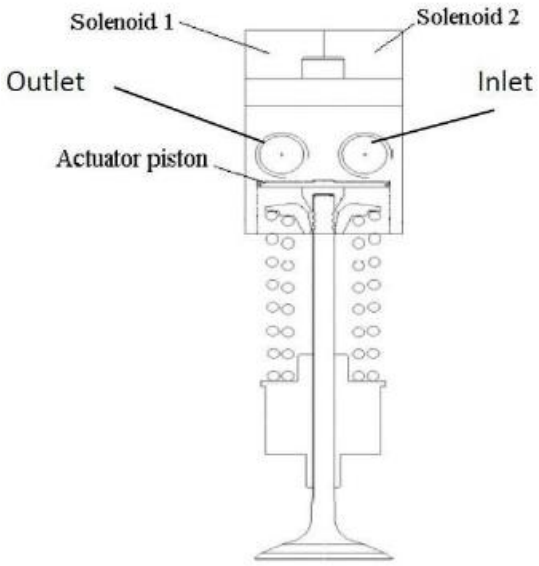

Figure 2.26 FreeValve actuator [47]

The dynamics of the system can be devided into three states: air charging, expansion and dwell, and air discharging. Air charging: timing solenoid energizes and opens spool valve 1, the compressed air is then sent into the actuator cylinder. Raised pressure pushes the actuator piston downwards and valve opens. Expansion and dwell: lift solenoid energizes and

opens spool valve 2, airflow is stopped. However, timing solenoid is not yet de-energized, the hydraulic latch still allows flow into the actuator and the air expands further until pressure force becomes equal to the spring force. The valve is secured in the maximum lift height. Air discharging: once timing solenoid is de-energized, spool valve 1 closes and the hydraulic latch is opened, air is released from the actuator cylinder. Actuator piston then moves back, closing the valve, and oil in the actuator is dampening the movement in order to prevent damage of the components [47].

FreeValve system provides full control of each valve (Figure 2.27). This enables an engine to achieve better fuel efficiency and lower emissions at increased torque and power. Implementation of this system results in reduced size of the engine and reduced weight, 50% and 30% respectively less than conventional valve train [48].

Figure 2.27 FreeValve system assembly [46]

2.4.5.8 Advantages and disadvantages of advanced VVA systems

Valve events determine the flow dynamics of charge mixture entering the engine and exhaust scavenging, which is one of the main factors affecting engine performance, fuel economy and emissions. Dual overhead cams or DOHC is a valve train system used in a conventional IC engines, where the shape of the valve profile is determined by the geometry of the cams and opening/closing timings of the valves are denoted by the rotation of crankshaft. These valve profiles are fixed throughout the engine's operation range, meaning that there is a compromise between low and high engine speed in terms of torque, fuel consumption and emissions.

A variable valve actuation system capable of full control of the valves can benefit the engine with optimum performance, fuel economy and emissions at any engine speed and load. Main advantages of VVA systems are highlighted below:

- Improved gas exchange via adjustment of the valve overlap for various engine speeds
- Increased torque at high and low engine speeds via delayed/advanced intake valve closing
- Improved charge mixing via uneven intake valve lifts
- Possibility of weight and friction reduction of valvetrain
- Reduction of pumping losses via replacement of throttle with valve load control

- Reduced fuel consumption and NO_X emissions at part load via adjustment of effective compression ratio

Along with many benefits VVA has some drawbacks compared to the conventional mechanical valvetrain:

- Higher cost
- More complex design
- Possible limitation of engine operating speeds to 5000rpm

Despite these drawbacks, a lot of research is focused on VVA systems as IC engines have to meet strict emission regulations and demands of consumers. This can be achieved with Miller and Atkinson cycle, which is implemented through variable valve actuation.

2.4.6 Miller and Atkinson cycle

2.4.6.1 History and working principle

Geometric compression ratio of an engine is defined by the maximum and minimum volume inside the cylinder, whereas effective compression ratio takes into account of the actual start of the compression process. In a conventional IC engine cycle, the effective compression and expansion ratios are equal, but if effective expansion ratio is larger, then it is referred to as over-expanded cycle.

In 1886 British engineer James Atkinson patented a four-stroke opposed piston engine with expansion stroke longer than compression, i.e. expansion ratio greater than compression ratio. This allowed to transmit more power from the combustion to the crankshaft rather than wasting it to the cooling water jackets. Also, the whole cycle of four strokes was completed in a single revolution of crankshaft [49]. A year later he patented another engine design with unequal expansion and compression strokes by utilising an unusual crank mechanism [50].

In 1954 American engineer Ralph Miller patented a new four-stroke cycle for boosted diesel engines, where charge temperature in the cylinder was reduced by advancing or retarding intake valve closure timing (EIVC or LIVC), or partial opening of exhaust or intake valves during compression stroke. This was done in order to achieve higher power output from an engine without causing material damage due to high temperatures. Miller described that the intake valve would close before piston reached BDC and the charge inside the cylinder would expand until the start of the compression stroke. During the expansion, pressure and temperature of the charge would decrease, thus in-cylinder pressure and temperature at the

beginning of the compression stroke will be lower than during the intake stroke (increasing the effective expansion ratio). This would result in lower pressure and temperature during compression and combustion, which allows to burn more fuel at higher loads, thus increasing mean effective pressure while maintaining the designed maximum combustion temperature. Similar results can be achieved by closing the intake valve part way during the compression stroke (reducing the effective compression ratio). As the piston moves toward TDC the charge will be expelled through the intake valve, reducing the in-cylinder pressure. At the end of compression stroke in-cylinder pressure and temperature will be the same as in the case with EIVC [51]. In 1956 Ralph Miller patented the over-expanded cycle with EIVC and LIVC specifically for SI engines in order to avoid pre-ignition of stoichiometric charge at full load while maintaining a high geometric compression ratio [52].

Atkinson was the first to show the benefits of over-expanded cycle, but Miller provided an idea of how effective compression ratio could be controlled via intake valves and achieving reduction of in-cylinder temperatures at the end of the compression stroke. Lower temperatures allow to use a higher CR without the risk of pre-ignition, thus improving engine's efficiency and performance.

2.4.6.2 Research and application in automotive industry

Since the invention of Miller and Atkinson cycle, over-expanded cycles have been intensively investigated by researchers in order to find a solution for improved fuel economy and emissions. Few examples of research on over-expanded cycles are discussed below:

Cleary and Silvas (2007) conducted an experimental investigation of unthrottled engine operation with EIVC on engine performance. Single cylinder engine was used to conduct experiments with ranges of IVO timings, intake valve durations and lifts at part load conditions. Optimisation of those three parameters led to 7% reduction in fuel consumption at 1300rpm and 330kPa NMEP due to reduced pumping work. On top of that NO_X emissions were reduced by 25%, but HC emissions were increased by 25% compared to throttled engine operation with conventional valve timings [53].

Constensou and Collee (2016) studied the effects of a range of geometric compression ratios coupled with Miller-Atkinson cycle on engine fuel consumption using experimental testing and 0D simulations. A single cylinder engine with 4 piston designs and maximum CRs was used to test EIVC and LIVC profiles and compare the results to a baseline. Up to 11% reduction in fuel consumption was achieved by coupling VCR (Variable Compression Ratio) and VVA [54].

Osborne et al. (2017) investigated Miller cycle intake valve closing strategies using high compression ratio, downsized, single cylinder DI gasoline engine (Magma engine concept). Miller cycle was mainly used to reduce knocking combustion while maintaining specific performance with geometric compression ratio of 13:1. The test results confirmed that EIVC reduces knock and fuel consumption by up to 9.4% at part-load conditions. Improvement in fuel economy of 12.5% and 16.4% was predicted for WLTC and FTP-75 cycles when a four cylinder baseline engine is replaced by three cylinder Magma concept with Miller cycle [55].

Garcia et al. (2020) studied the impact of Miller cycle on the engine performance of heavy-duty diesel engine. EIVC and LIVC profiles were compared to the baseline using single cylinder engine with hydraulic valvetrain. Test results showed that Miller cycle reduced peak cylinder pressure and increased exhaust temperature, while maintaining fuel consumption, NO_X and PM emissions similar to the baseline [56].

Miller and Atkinson cycles were proven to enhance fuel economy therefore some automotive companies started to implement them in engines for their passenger cars. As mentioned previously, Honda's i-VTEC with LIVC profile and Fiat's Multiair with EIVC profile are already used in production cars. From 2018 Volkswagen started sales of one of the car models with a new "B-cycle", which features EIVC profile for achieving better fuel economy at part-load [57].

2.5 Summary

This chapter highlighted challenges for automotive industry brought by global warming. In particular, strict emission regulations and legislation on CO_2 reduction drove vehicle manufacturers to focus on developing new engine and powertrain technologies and systems to overcome those challenges. Engine downsizing was proven to reduce fuel consumption and pumping loss, however knocking combustion imposes a limitation on further improvements. Miller and Atkinson cycles offer a solution to knock limitation when implemented with fully variable valve actuation system. However, previous research was limited in terms of flexibility of combinations of EIVC and various lifts which would produce a range of effective compression ratios (ECRs). On top of that the effects of varying lift with EIVC on pumping loss, flame speed and in-cylinder lambda were not studied. Therefore, effects on engine performance and emission of EIVC with various lifts and LIVC profiles should be thoroughly investigated in further research by means of experimental testing and then research focus should be directed to optimisation of Miller and Atkinson cycles for use in the spark ignition engines as the main powerplant or part of the powertrain system in HEVs.

2.5.1 Research objectives

The main goal of this project is to investigate the effects of valve profile combinations with different ECRs on the spark ignition (SI) engine efficiency and emissions at low to high load operations using a novel valvetrain system.

The specific objectives are:

- To implement Miller and Atkinson cycle with various valve profiles and investigate its effects at different operating engine conditions on engine's efficiency, combustion and emissions.
- To combine those valve profiles with single valve operation to further enhance fuel economy and lower emissions.
- To investigate the effect of new valve profiles such as early MOP on engine performance, emissions and fuel economy.

Chapter 3 Experimental Setup and Methodology

3.1 Introduction

This chapter highlights research methodology, experimental setup and working principles of novel valve actuation system used to obtain the experimental data. The aim of this study is to investigate the effect of Atkinson and Miller cycles on fuel economy and emissions of a gasoline DI engine. Testing was carried out on a single cylinder Ricardo Hydra engine with modified cylinder head and electromechanical valvetrain. The engine together with engine management and valve control was supplied by Camcon along with main systems like fuel and cooling. Some of the systems were adapted to the existing test bed, and some were modified according to the requirements of this research. Tests were executed on a dynamometer testbed with various instrumentation for data collection and post processing.

3.2 Experimental setup

All experiments were conducted in engine test cell and engine was operated from the control room. Figure 3.1 demonstrates main components and systems of the experimental setup. The main engine parts with exhaust pipe and air intake plenum are coloured in black, the dynamometer system in yellow, the intake system with Hasting HFM-200 laminar air flow meter in orange, the fuel supply system with Endress+Hauser Promass 83A Coriolis fuel flow meter in blue, the valve actuation system with its own coolant in purple, control and data acquisition in red, the lubrication system in green, the engine cooling system displayed in pink and the emission analyser in navy blue.

The engine was coupled to an AC dynamometer and installed on the test bed with closed loop control of oil and coolant circuits. The dynamometer allowed for motored and fired operation of the engine at set speeds. The spark timing, throttle angle and AFR were controlled via an engine control software. The air supplied to the engine was either at room temperature and pressure or at pre-set boost pressure from an external supercharger with closed loop control. The instantaneous intake and exhaust pressures were measured by a piezoresistive pressure transducer located just before the intake valves and another one in the exhaust port respectively. Heat release and combustion characteristics were calculated by a combustion analysis software based on the instantaneous cylinder pressure from a piezoelectric pressure transducer and crank angle from a crankshaft encoder. The emissions and lambda were measured by a Horiba 7170DEGR.

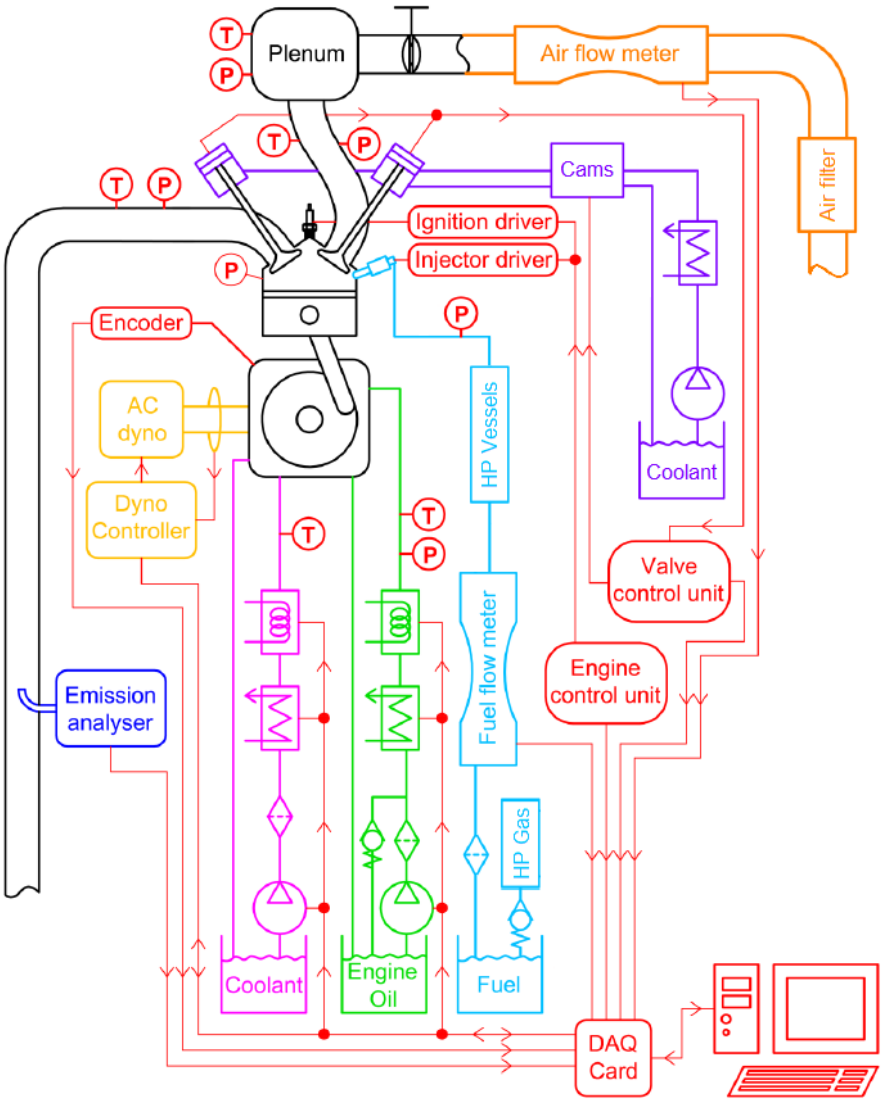

Figure 3.1 Schematic of the experimental setup (modified from [58])

3.2.1 Engine specification and iVT system

A single cylinder SI direct injection gasoline engine with 4 valves was used for this research and the specifications are given in Table 3.1. The engine block was Ricardo Hydra and the cylinder head with centrally mounted spark plug was re-designed by Camcon to accommodate new valvetrain.

IVT (intelligent Valve Technology) valvetrain system replaced conventional camshafts for each valve as shown in Figure 3.2. Each valve is actuated via an independent camshaft driven by an electrical motor. Full rotation of the cam produces a full lift event whereas partial rotation allows for lift control. Varying of the motor speed controls the start and duration of the valve opening [59]. Combination of cam rotation and motor speed allows for fully independent control of timings and lifts of each valve through the valve control software. On top of that the

profile shape can be altered, for example maximum opening position shifted etc. Variations of valve profiles produced by iVT are shown in Figure 3.3.

Table 3.1 Engine specifications

Engine Type	4-stroke, single cylinder, 2 intake and 2 exhaust valves
Bore x Stroke	81mm x 89mm
Connecting Rod length	155.5mm
Compression Ratio	10.8:1
Displacement Volume	458.6cc
Intake Valves Diameter (2)	29mm
Exhaust Valves Diameter (2)	26mm
Fuel Injection	Direct Injection

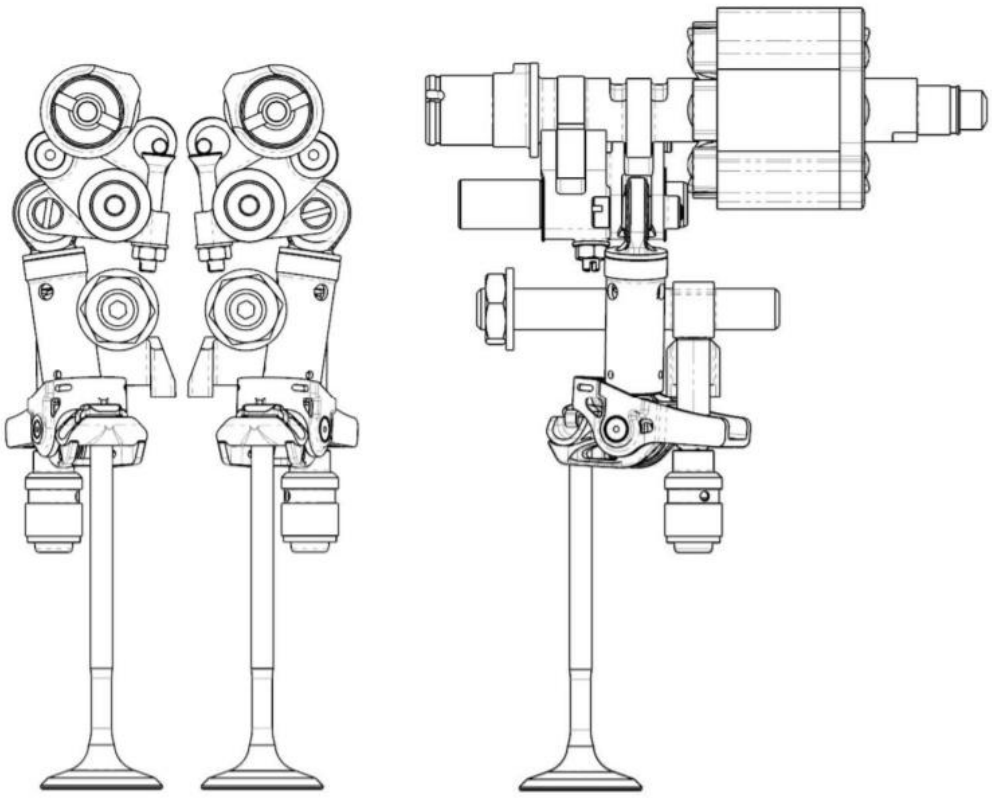

Figure 3.2 IVT valvetrain system [59]

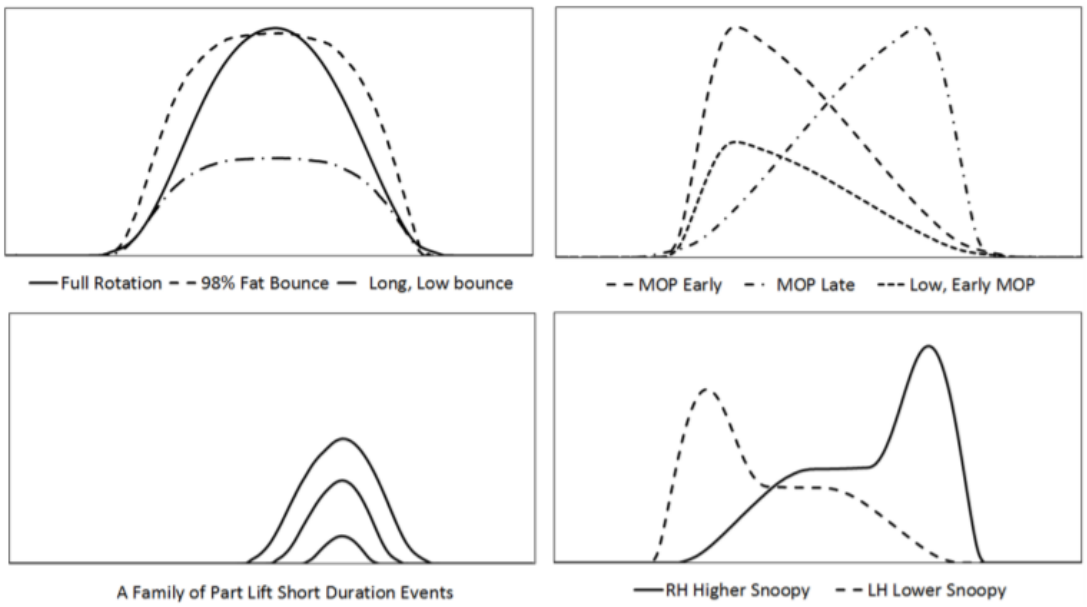

Figure 3.3 Examples of iVT valve profiles [59]

3.2.2 Fuel system and fuel properties

The engine was initially supplied with its own fuelling system, however when it was installed on the test bed the fuel flow meter was not capable of providing accurate measurements. The high pressure pump created pressure waves causing fuel flow rate to fluctuate so that the flow meter was unable to measure and was switching off. To solve this problem two large volume vessels were installed between the fuel pump and flow meter in order to dampen the pressure waves, but this was not enough. A decision was made to remove the fuel pump and replace it by a large pressure vessel (Figure 3.4). It was filled with fuel and connected to a high pressure gas bottle with pressure regulator. By adjusting the pressure regulator a desired constant pressure of fuel was achieved. The high pressure vessel was serving as a fuel tank and fuel pump at the same time, providing fuel with constant pressure without pulses which allowed for accurate flow rate measurements.

Figure 3.4 Fuel pressure vessel (tank)

The fuel used was EU VI 95 RON Gasoline (E10) with 10% Ethanol content by volume. Fuel specifications can be found in Table 3.2. All tests were conducted with a relative AFR (Lambda) of 1 and the fuel injection timing was fixed at 268deg CA BTDC at an injection pressure of 50bar.

Table 3.2 Fuel properties

Fuel	95 Ron Gasoline E10
Density at 15 ºC (kg/m^3)	746.1
Higher calorific value (kJ/kg)	44220
Lower calorific value (kJ/kg)	41420
Stoichiometric AFR	13.92:1

3.2.3 Emissions measurement

The exhaust gas emissions such as CO, CO_2, uHC, O_2 and NO_X were measured by Horiba MEXA 7170DEGR. The gas analyser was collecting exhaust gas at a sampling point via a heated line. The sampling point was located close to the engine to avoid water condensation which could lead to dilution of uHC.

Non-dispersive infrared AIA-72X series analyser was utilised for the analysis of CO and CO_2 emissions. Flame ionization analysis method was used to analyse uHC emissions by means of burning molecules in a hydrogen flame and measuring ion current produced. O_2 was measured by a magnetic pressure type oxygen detector which uses magnetic field to collect oxygen at the magnetic pole, this creates a pressure difference which is sensed by differential condensor microphone. NO_2 emissions were converted into NO by means of reaction with carbon in a converter (catalyst). Then all NO emissions get into chemical reaction with O_3 to emit light, this is called chemiluminescent analysis. The amount of light is proportional to NO_X emissions produced by the engine [60].

Due to E10 fuel AFR settings in the Horiba analyser were adjusted using H/C and O/C ratios recommended by the fuel supplier. Table 3.3 shows the original ratios for gasoline and E10 fuel used for testing.

Table 3.3 Horiba AFR settings

	Gasoline	**E10**
C	1	1
H	1.85	1.889
O	0.00	0.033

3.2.3 Engine management and data acquisition

Engine control was performed through an engine ECU connected to the laptop via LAN connection. SCM (Software Calibration Management for ECU) software was used for fuel mapping, spark and injection timing, closed loop throttle and AFR/lambda control as well as monitoring of the fuel and intake pressure. VCU (Valve Control Unit) was connected to the same laptop via USB connection. Vehicle Spy software was utilised to set and visualise desired valve profiles for VCU.

The engine was connected via prop shaft to an alternating current dynamometer from C&P Engineering. The dynamometer allowed for motored and fired engine operations up to 6000 rpm. PC with Cadet V12 software was used to control the speed of the dynamometer and switch between motored and fired modes, coolant and oil temperatures were also set and monitored there through closed loop control.

Data acquisition was performed by National Instrument (NI) USB-6353 high speed A/D card connected to another laptop via USB port. Signals from crankshaft encoder, cylinder pressure transducer, thermocouples and valve position sensors are sent to the high speed card. Intake and exhaust pressures as well as spark and injection timings were also recorded by the high speed card. The Horiba Emission analyser connected to the same laptop via LAN port provided data for instantaneous emissions and lambda. Data from high speed card and Horiba was displayed and recorded by transient combustion analysis software. The interface of this software is shown in Figure 3.5.

Combustion analysis software is processing some of the signals and displays calculated parameters such as heat release rate (HRR), mass fraction burned (MFB), IMEP, PMEP ISFC, indicated specific emissions of CO, HC and NO_X etc. for each engine cycle. A total of 100 cycles is recorded and average values are calculated for further analysis.

Due to the various IVC timings used in the experiments, some of the air and fuel could be expelled out of the cylinder into the intake manifold. This can cause differences between the measured exhaust lambda and the actual in-cylinder lambda. To mitigate this discrepancy the in-cylinder lambda was calculated based on the exhaust gas concentrations measured by Horiba gas analyser using Equation 3.4 [61].

Equation 3.1

$$\lambda_{in-cylinder} = \lambda_{exhaust} \frac{Trap_{eff(A)}}{Trap_{eff(F)}}$$

Where, $\lambda_{exhaust}$ is the exhaust lambda measured by Horiba gas analyser, $Trap_{eff(A)}$ is the air trapping efficiency (Equation 3.5), $Trap_{eff(F)}$ is the fuel trapping efficiency (Equation 3.6) [61].

Equation 3.2

$$Trap_{eff(A)} = \frac{0.5[CO] + [CO_2] + 0.25\left(\frac{yK[CO_2]}{[CO] + K[CO_2]}([CO] + [CO_2])\right) + 0.5[NO_X]}{0.5[CO] + [CO_2] + [O_2] + 0.25\left(\frac{yK[CO_2]}{[CO] + K[CO_2]}([CO] + [CO_2])\right) + 0.5[NO_X]}$$

Equation 3.3

$$Trap_{eff(F)} = \frac{[CO] + [CO_2]}{[CO] + [CO_2] + [uHC]}$$

Where, y is the ratio of hydrogen to carbon (1.889 for E10 gasoline was used in this research), K is the water-gas reaction constant (3.5 was used).

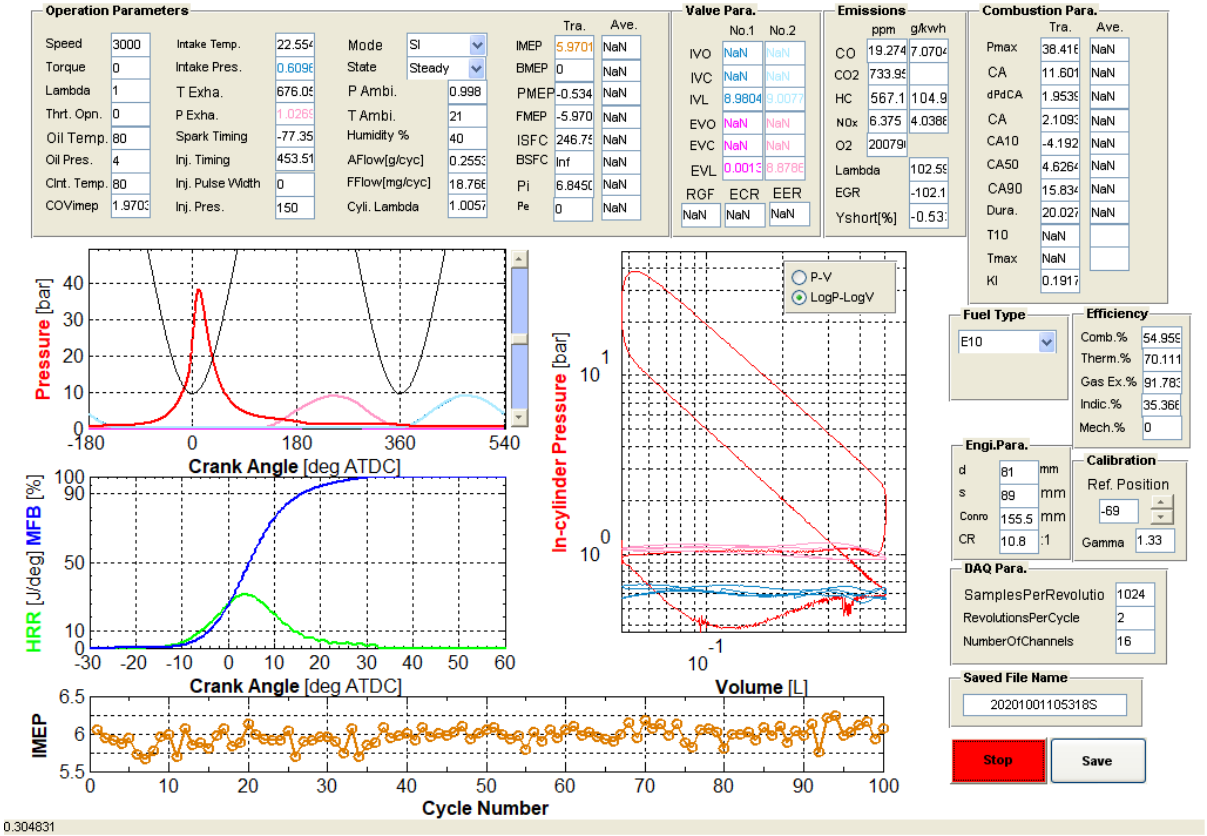

Figure 3.5 Combustion analysis software

3.3 Heat release analysis

As mentioned previously, the engine is equipped with in-cylinder pressure and crank position sensors, which allows to calculate heat release rate (HRR) and mass fraction burned (MFB)

from IC engine. Heat release rate is used to investigate combustion process when direct injection of fuel is used due to the fact that not all of the fuel is burned with sufficient air (e.g. SFILB combustion). The mass fraction burned is utilised for port fuel injection when the charge is premixed (e.g. HCCI combustion).

One-zone heat release analysis was applied in combustion analysis software to all experimental data for this study. In one-zone model the cylinder contents is considered as a single fluid - burned and unburned regions of gas in the combustion chamber were treated as one and modelled as homogeneous mixture, in-cylinder pressure variations were related to energy released from combustion of the fuel. This model allows to include heat transfer and gas flow phenomena in a simplified way. Moreover, one-zone heat release analysis is considered acceptable for engine combustion research [62][61].

First law of thermodynamics for an open system is utilised for heat release analysis, where U is the internal energy of the charge in the cylinder, Q is heat added to the system and W is work done by the piston pdV (Equation 3.4). Q consists of two variables: Qch - chemical energy from combustion and Qht - heat transferred out of the system as cylinder walls are not adiabatic (Equation 3.5). Also, mass flux term $\sum h_i dm_i$ was added to the Equation 3.5 due to the fact that part of the charge and burned gas could exit and enter the system through crevices in the combustion chamber, e.g. through piston rings $h' dm_{cr}$ and when fuel is directly injected $h_f dm_f$ (Equation 3.6) [62].

Equation 3.4

$$\Delta U = Q - W$$

Equation 3.5

$$dQ_{ch} = dU_s + dW + \sum h_i \, dm_i + dQ_{ht}$$

Equation 3.6

$$\sum h_i \, dm_i = (h' dm_{cr} - h_f dm_f)$$

Equation 3.7 represents the internal energy of the in-cylinder charge in terms of mean temperature of the charge, mass of the charge in the system and its specific heat at constant volume, the last term of the equation becomes $- udm_f$ as crevice flow effects are ignored when DI is used [62].

Equation 3.7

$$dU_s = mc_v(T)dT + u(T)dm$$

Assuming contents of the cylinder is an ideal gas and the enthalpy of the injected fuel $h_f \approx 0$ and is ignored, Equation 3.5 per increment of time becomes:

Equation 3.8

$$\frac{dQ_{ch}}{dt} - \frac{dQ_{ht}}{dt} = \frac{mc_v(T)dT}{dt} + \frac{pdV}{dt}$$

Chemical energy from combustion and heat transferred through cylinder walls can be combined into one term $\frac{dQ_n}{dt}$ called net heat release rate. Using the ideal gas law $pV = mRT$, assuming R is constant, then Equation 3.8 can be further simplified where γ is the ratio of specific heats and assumed to be constant from 1.3 to 1.35 (1.33 was used in this research) [62]:

Equation 3.9

$$\frac{dQ_n}{dt} = \frac{\gamma}{\gamma - 1} p \frac{dV}{dt} + \frac{1}{\gamma - 1} V \frac{dp}{dt}$$

The equation above can be used to calculate net heat release rate (HRR) using instantaneous in-cylinder pressure measurements and volume change when crevices flows are ignored. However, in-cylinder pressure is recorded by encoder in intervals of crank angle. To adopt this equation dt is replaced by $d\theta$ and all parameters are represented per crank angle degrees [62][61]:

Equation 3.10

$$\frac{dQ_n}{d\theta} = \frac{\gamma}{\gamma - 1} p \frac{dV}{d\theta} + \frac{1}{\gamma - 1} V \frac{dp}{d\theta}$$

Instantaneous cylinder volume can be calculated from the formula below based on its geometry at a certain crank angle:

Equation 3.11

$$V = V_c \left\{ 1 + \frac{1}{2}(r_v - 1) \left[R + 1 - cos\theta - (R^2 - sin^2\theta)^{1/2} \right] \right\}$$

Where V is the instantaneous volume, V_c is the clearance volume when the piston at TDC, r_v is the compression ratio, R is the ratio of connecting rod length to crank radius (half of stroke)

and θ is the crank angle. Thus, knowing engine's geometry only in-cylinder pressure at increment of crank angle needs to me measured in order to calculate heat release rate. Also, Equation 3.9 can be used to obtain fuel mass fraction burned (MFB). For this it is integrated and normalised to 100%. When MFB values are plotted on a graph relative to crank angle it is easy to understand duration of the initial flame development (up to 10% of MFB) and duration of the combustion (10 to 90% of MFB). This graph is also very useful for determining of spark timing based on combustion duration in order to prevent very late or early end of combustion [62].

3.4 In-cylinder pressure pegging

In this research, the in-cylinder pressure is measured by a piezoelectric transducer which provides a relative pressure at a given crank angle compared to a reference point in the cycle. Therefore, to obtain an absolute pressure the signal from the transducer has to be referenced or pegged to a known pressure during each cycle. Based on the previous research, where variable valve timings were utilised, it was decided to set the in-cylinder pressure equal to the intake pressure just before IVC for profiles with early valve closure and just before BDC for profiles with late valve closure (after BDC). This is due to the fact that the cylinder is completely filled with fresh charge at IVC. Examples of pegging for early and late IVC are demonstrated in Figure 3.6 and Figure 3.7. In-cylinder pressure was pegged for each test and individually for each profile.

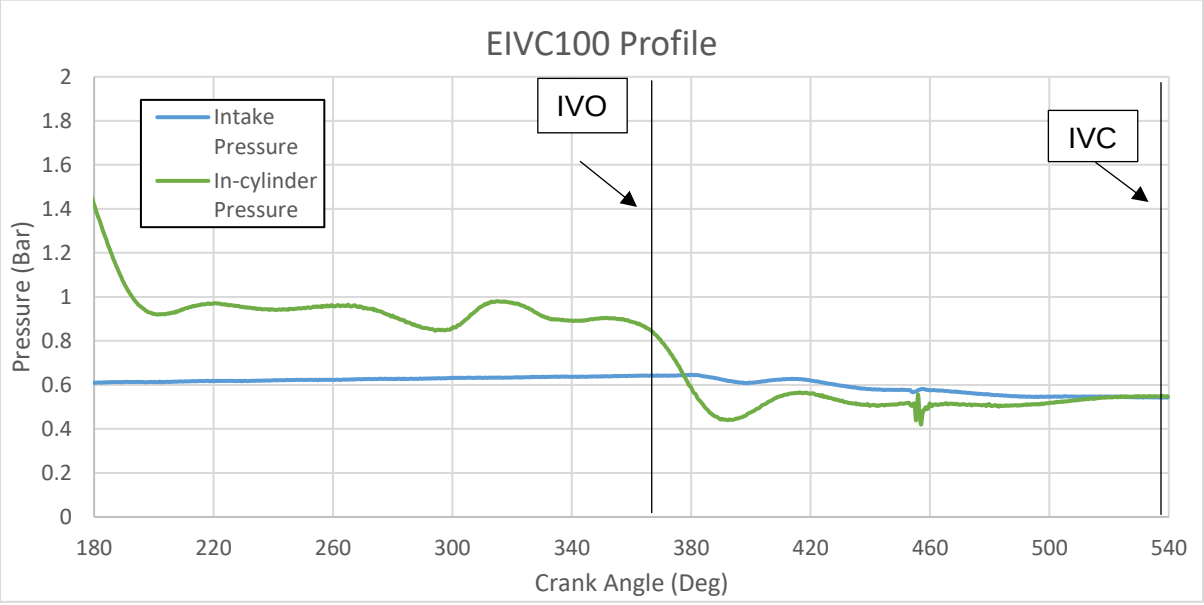

Figure 3.6 In-cylinder pressure pegging before IVC

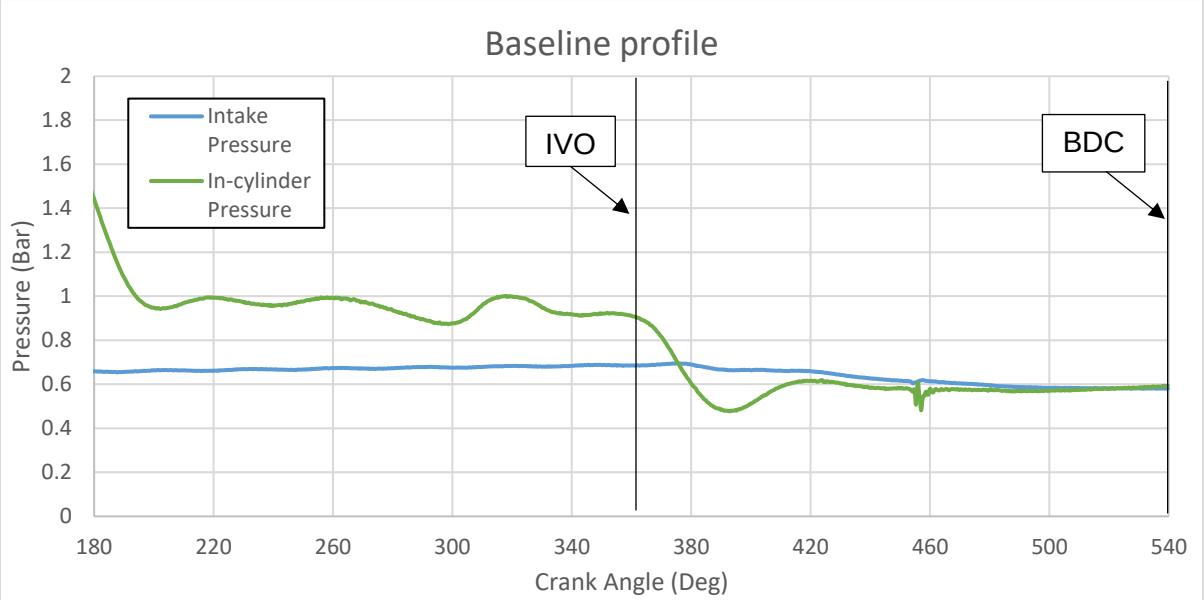

Figure 3.7 In-cylinder pressure pegging before BDC

3.5 Data validation and pre-test checks

To ensure consistency and accuracy of the test data two pre-test checks were done after the engine warmup prior the start of the tests:

- Engine motoring – engine motored by the dyno without fuel injection
- Engine firing – homogenous combustion at fixed operating conditions

Table 3.4 shows parameters used for engine motoring and firing checks, Figure 3.8 shows logs of pre-test checks.

Table 3.4 Parameters of pre-test checks

Parameter	Engine Motoring	Engine Firing
Speed (rpm)	1500	1500
Throttle position (%)	25	2.5
Oil temp. (C)	31.5+-1	31.5+-1
Coolant temp. (C)	58+-1.5	58+-1.5
Lambda	-	1
Spark timing (CAdeg BTDC)	-	36
SOI (CAdeg BTDC)	-	268
Inj. Pressure (bar)	-	50+-3

IVO/IVC (CA deg)	320/540	320/540
EVO/EVC (CA deg)	120/350	120/350

Due to variation of ambient temperature, humidity and ambient pressure, Pmax and net IMEP vary from day to day. The average value of Pmax is 23.7bar and day to day variation is not more than ±2%, whereas average net IMEP is 5.6bar with variation not more than ±4.4%.

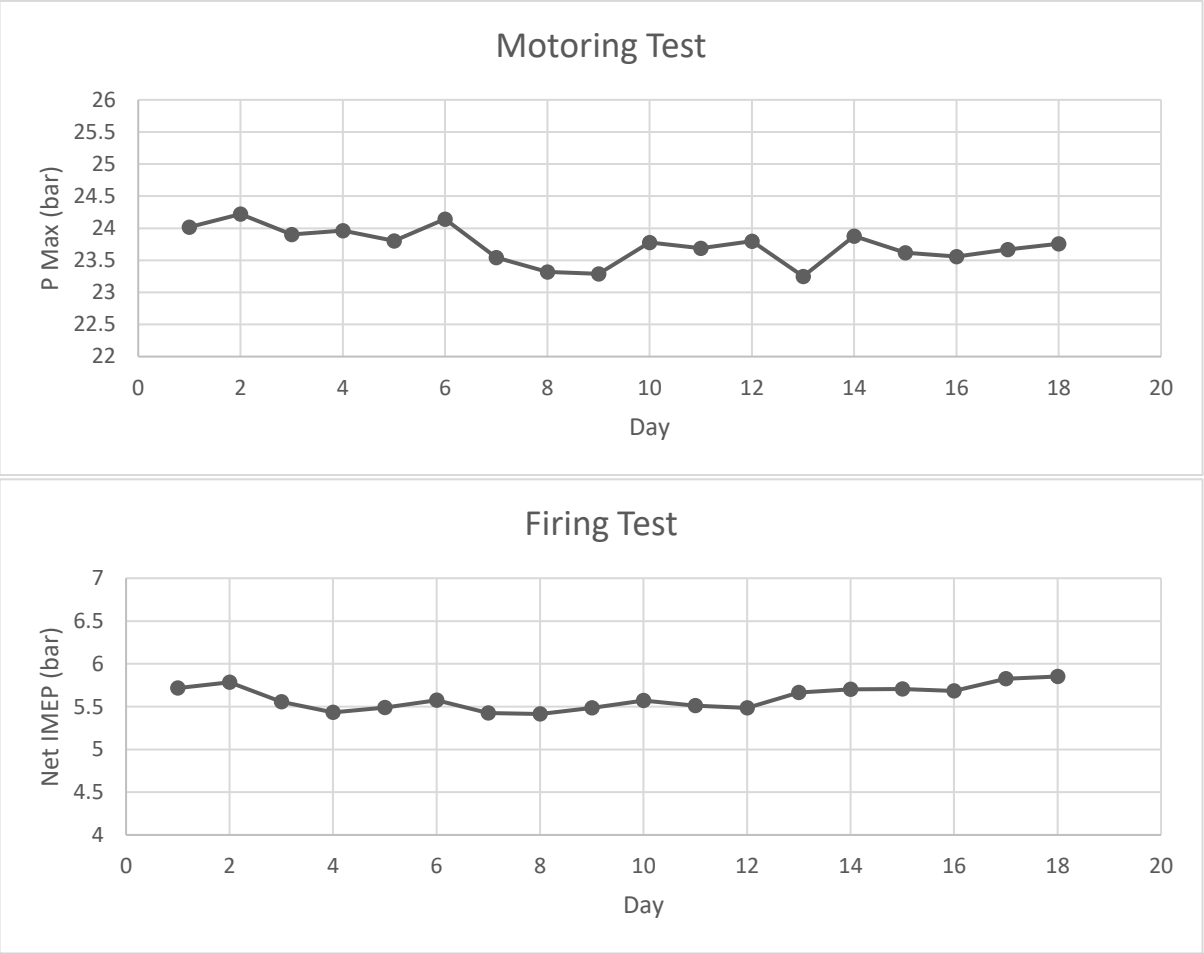

Figure 3.8 Daily logs of pre-test checks

3.6 Summary

In this chapter, the experimental setup and single cylinder engine with iVT system were presented. Engine specifications, iVT system and engine control were described in detail. The working principles of the main measurement devices were shown and explained. Essential changes to the fuel system were demonstrated. Also, data acquisition and post-processing software with equations for heat release calculation were discussed as well as cylinder pegging and pre-test checks.

Chapter 4 Miller Cycle and Atkinson Cycle Operations with Both Intake Valves

4.1 Introduction

Miller and Atkinson cycles feature effective compression ratio smaller than effective expansion ratio, which can be achieved by implementing EIVC or LIVC. Typically, Miller cycle would be associated with EIVC for boosted engines whereas Atkinson cycle is achieved by LIVC for oversized naturally aspirated engine.

This chapter presents the experimental results obtained with both intake valves in operation. Effects of EIVC and LIVC of five intake valve profiles are analysed on the engine's efficiency, combustion and emissions.

4.2 Test conditions

4.2.1 Valve profiles

Figure 4.1 shows the valve profiles which were used for the testing. There are five valve profiles: Baseline (BSL), Late Intake Valve Closing (LIVC) and Early Intake Valve Closing (EIVC) with three valve lift variations from 100% to 64%. The exhaust valve profile was unchanged for all the tests.

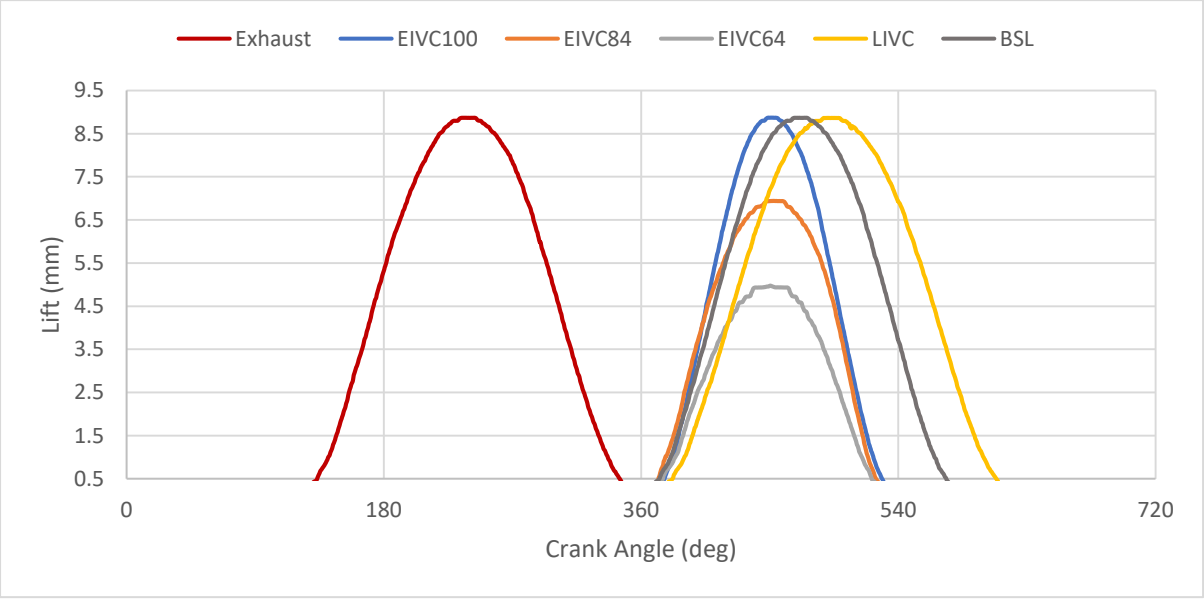

Figure 4.1 Valve profiles

EIVC and LIVC are used to reduce effective compression ratio of the engine in order to study the effects of Miller and Atkinson cycles on the efficiency, fuel economy and emissions of the experimental engine. Additionally, EIVC was set with three different valve lifts in order to investigate the effect on pumping losses, which could not be done in the previous studies by other researchers due to the limitations of the normal valve train systems. Table 4.1 shows valve timings measured at 0.5mm lift and durations of the five valve profiles.

Table 4.1 Valve timings and durations

Valve Profile	Lift (mm)	Duration (CA deg)	IVO/EVO (CA deg)	IVC/EVC (CA deg)
EIVC100	8.9	152	376	528
EIVC84	7	152	372	524
EIVC64	5	146	375	521
LIVC	8.9	226	382	608
Baseline	8.9	200	373	573
Exhaust	8.9	211	133	344

4.2.2 Operation points

Table 4.2 shows four operation points for engine testing with Miller and Atkinson cycles. These operation points can be split into two groups: low and high load. Low load tests will help to find fuel saving strategies for scenarios when a vehicle is cruising at constant speed either on motorway or on dual carriageway inside the city. High load tests will show full benefit of the Miller and Atkinson cycles as MBT spark timing will not be knock limited, which will provide additional fuel savings and CO_2 reduction.

Table 4.2 Testing points

Speed (rpm)	NIMEP (bar)			
1500	4	6	9	12.6
3000	4	6	9	12.6

However, at 12.6bar NIMEP at 3000rpm the in-cylinder pressure before EVO was higher than the advised pressure by Camcon for exhaust valve opening. In order to prevent damage to the iVT system it was decided to change the EVO timing for this particular test point so that the in-cylinder pressure would be lower than 6 bar at the time of exhaust valve opening. This was done in two ways for comparison: setting the EVO by 10 CA deg later which would lead

to shorter exhaust duration or by shifting the phase of exhaust event by 10 CA deg which would lead to later EVC and a small valve overlap as shown in Figure 4.2.

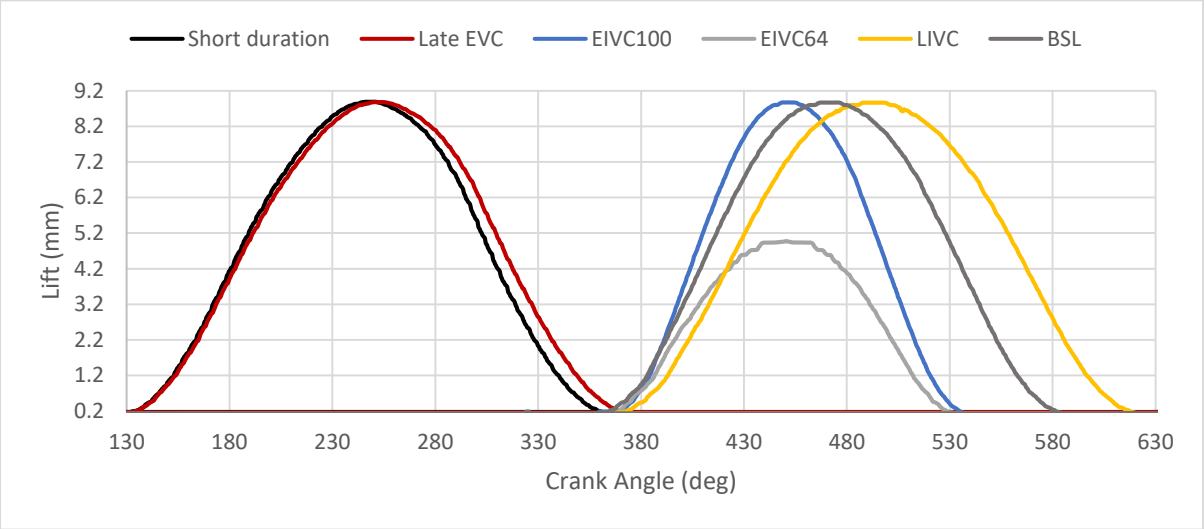

Figure 4.2 Exhaust valve profiles at 3000rpm 12.6bar NIMEP

4.3 Two intake valve mode

4.3.1 Test results at 1500rpm

To better understand experimental results the effective compression ratio (ECR) must be evaluated for each test as IVC timing and valve lift directly affecting it. ECR was calculated based on the in-cylinder pressure for each valve profile and for each load point rather than cylinder volume at IVC. This is due to the EIVC profiles which all have similar IVC timings but different valve lifts thus different ECRs. The start of the compression is defined at the crank angle when the polytropic compression line and intake manifold pressure are crossing on the logP-logV diagram (Figure 4.3). The cylinder volume at this crank angle is then divided by TDC volume to get the ECR.

As shown in Figure 4.4, the baseline profile has around 10.4 – 9.9 ECR from low to high load, whereas EIVC100 has the highest ECR throughout the whole load range, between 10.8 and 10.5. The difference in ECRs between the EIVC100 and the baseline case is due to the IVC timing, which is around 10 degrees before BDC for EIVC100 and is 30 degrees after BDC for baseline profile. As a result, a small amount of fresh charge is pushed back into the intake during the compression stroke before the compression starts, resulting in a lower effective compression ratio for BSL. With increasing load more charge is being expelled into the intake manifold, thus ECR is reduced further.

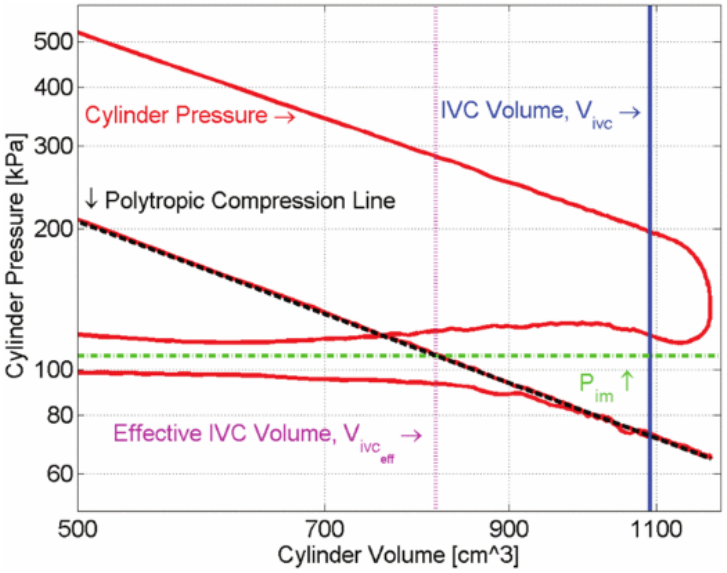

Figure 4.3 Pressure based method of ECR estimation [63][62]

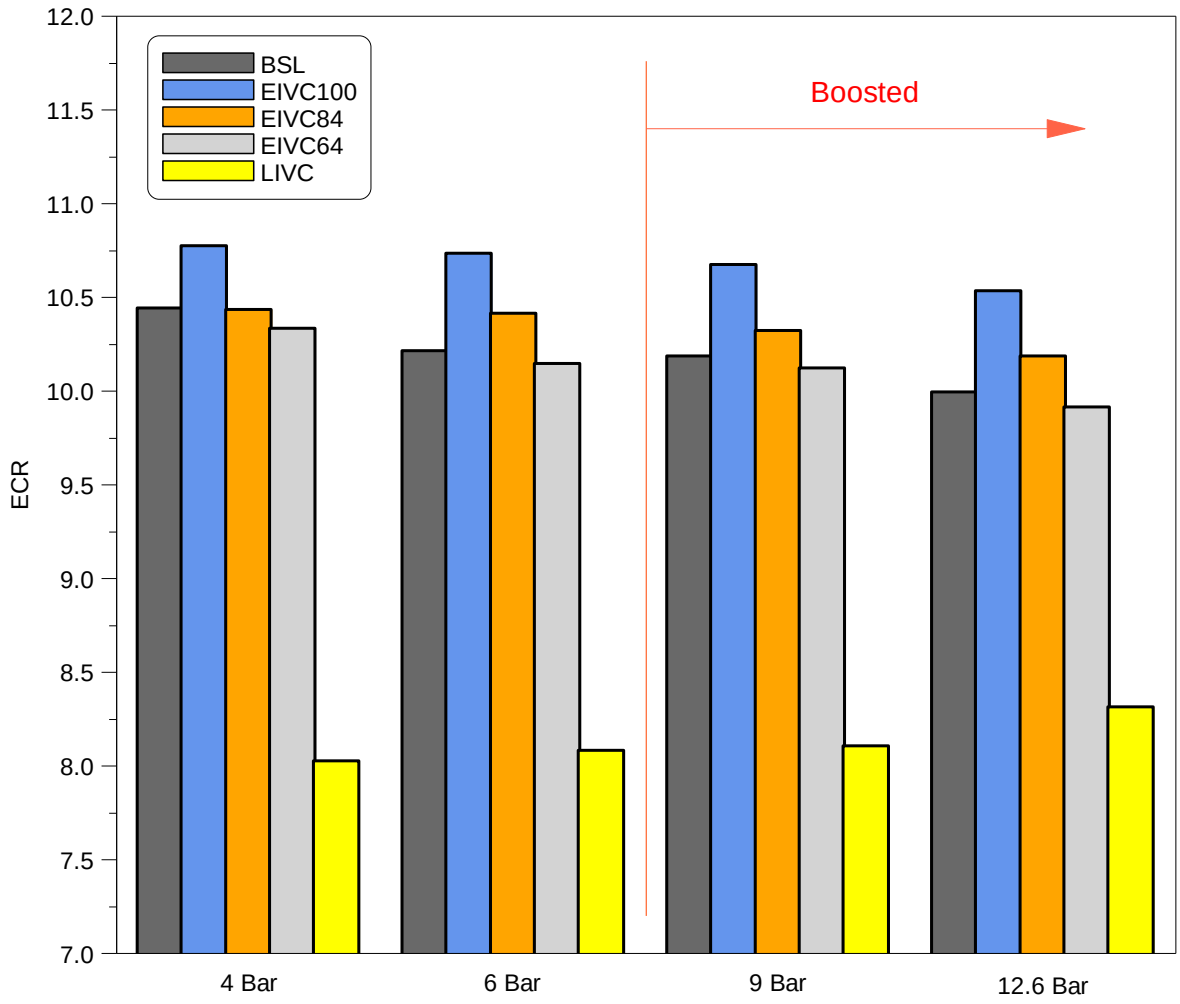

Figure 4.4 ECR comparison at various loads at 1500rpm

EIVC profiles have almost identical IVC timings, however the effective compression ratio is different for each of them. The reason for that is the variation of the valve lift. The smaller the lift the less fresh charge is sucked into the cylinder therefore lower effective compression ratio. This is clearly demonstrated by EIVC profiles across all the load points. Also, with increasing load the ECR decreases respectively as more charge is needed while a certain valve lift creates a constant flow restriction throughout the whole load range.

LIVC produced the lowest effective compression ratio (8 to 8.3) as a lot of fresh charge was expelled into the intake manifold due to very late IVC. Opposite to other profiles ECR is increasing with load for LIVC. This is due to higher pressure in the intake manifold as throttle opens more. When intake pressure is close to atmospheric the pressure difference between in-cylinder and manifold pressure becomes smaller and less percentage of the fresh charge is expelled into the intake.

At each load in most cases the throttle was opened more for those profiles with lower ECR as higher intake pressure (measured downstream of intake plenum as shown in Figure 3.1) was needed in order to achieve the same net IMEP as shown in Figure 4.5. However, there were some cases where throttle angle was the same but ECR was different, this was due to other factors which increased the intake pressure regardless of throttle angle. This will be explained in the next section.

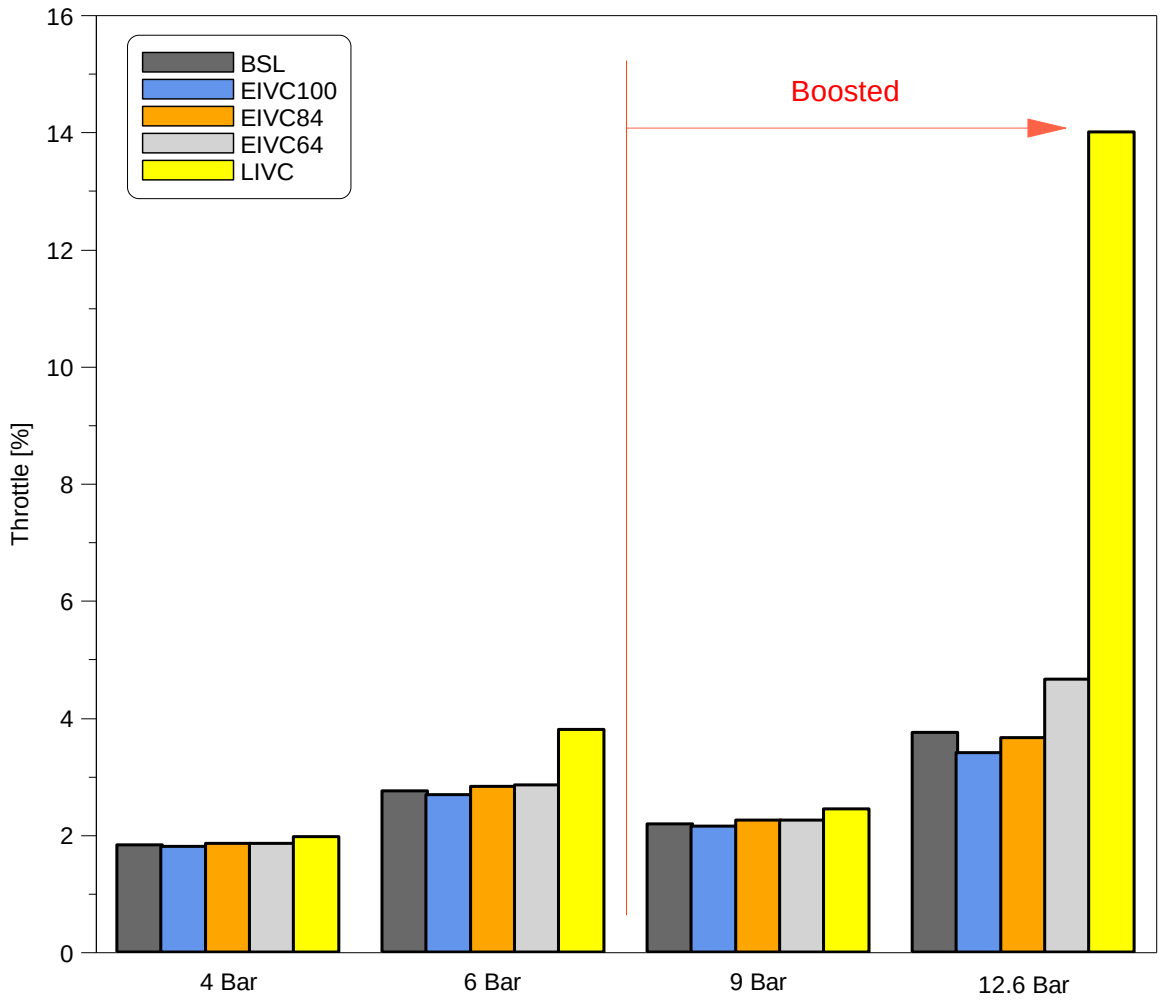

Figure 4.5 Throttle opening comparison at various loads at 1500rpm

In a conventional throttle controlled SI engine pumping loss is created due to the drop of manifold pressure below atmospheric pressure and it is one of the major causes of low engine efficiency at the low load. Comparison of Pumping Mean Effective Pressure (PMEP) for various valve profiles is shown in Figure 4.6.

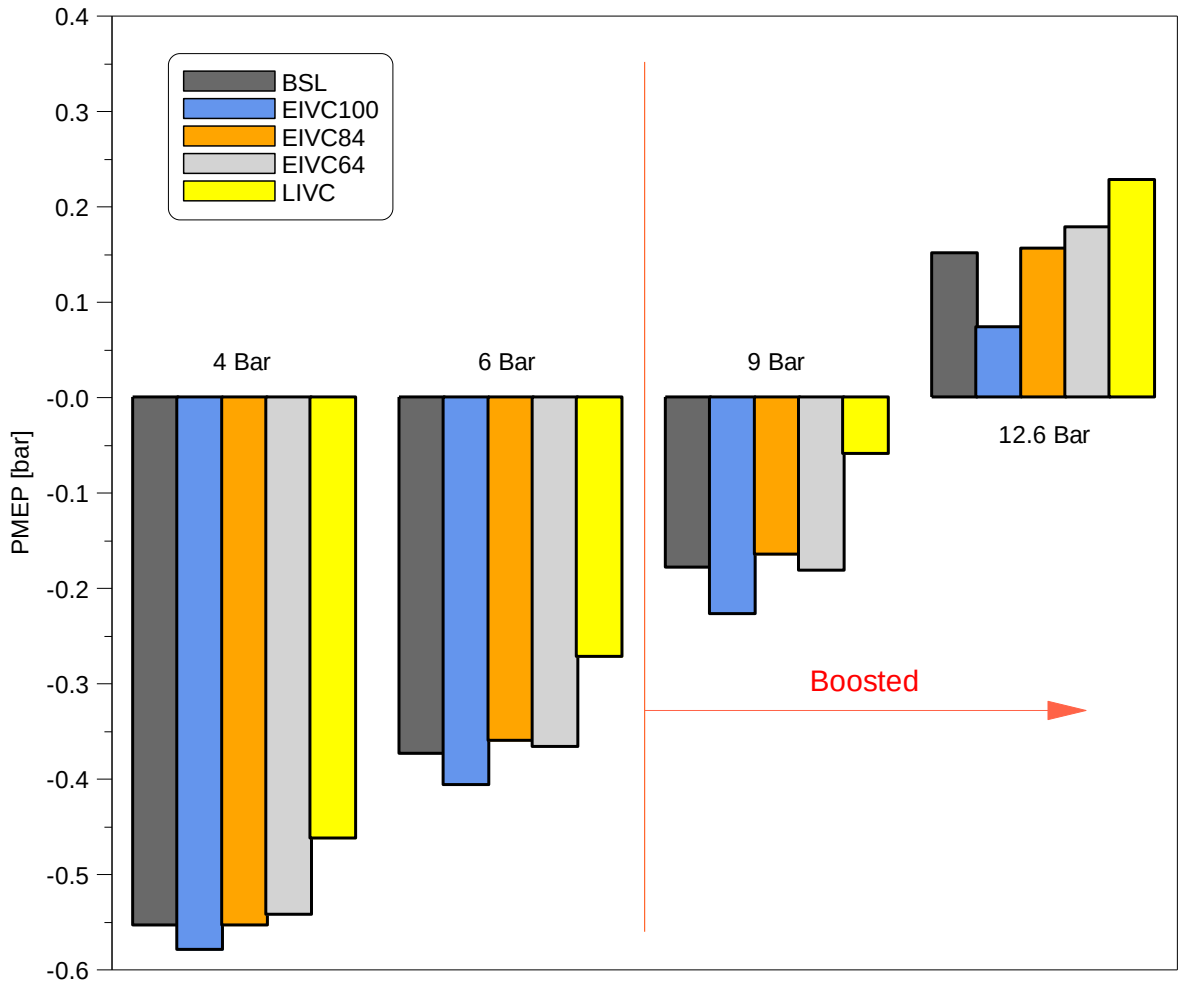

Figure 4.6 PMEP comparison at various loads at 1500rpm

At 4bar net IMEP, the LIVC valve profile produced the lowest negative PMEP due to larger throttle opening (0.13% more than STD) required to maintain the same IMEP with the lowest ECR. Also the charge was pushed out from the cylinder into the intake manifold during compression stroke, which increased the intake pressure for the subsequent intake strokes lowering pumping losses (Figure 4.7).

Amongst all EIVC profiles, EIVC100 produced the highest negative PMEP, whereas EIVC64 produced the least amount of pumping loss. For EIVC100 to achieve 4bar net IMEP, the throttle was closed by 0.05% more than for the lower lifts because of higher ECR, this resulted in increased pumping loss. For EIVC84 and EIVC64 valve profiles, the throttle position was identical, however intake manifold pressure was higher for the lower lift profile. A lower valve lift leads to lower flow area and hence a higher intake pressure is required to allow the same amount of air into the cylinder as the higher lift. This is usually achieved by larger throttle opening. However, in the case with EIVC64, it was noted that a bigger drop in the in-cylinder pressure at IVO caused an increase in the intake port pressure which was enough to trap the

required amount of air into the cylinder without altering throttle angle. Higher intake pressure led to lower pumping losses for EIVC64. Therefore, when operating an engine at low load with a small throttle opening, the lower intake valve lift increased the intake pressure and reduced pumping loss.

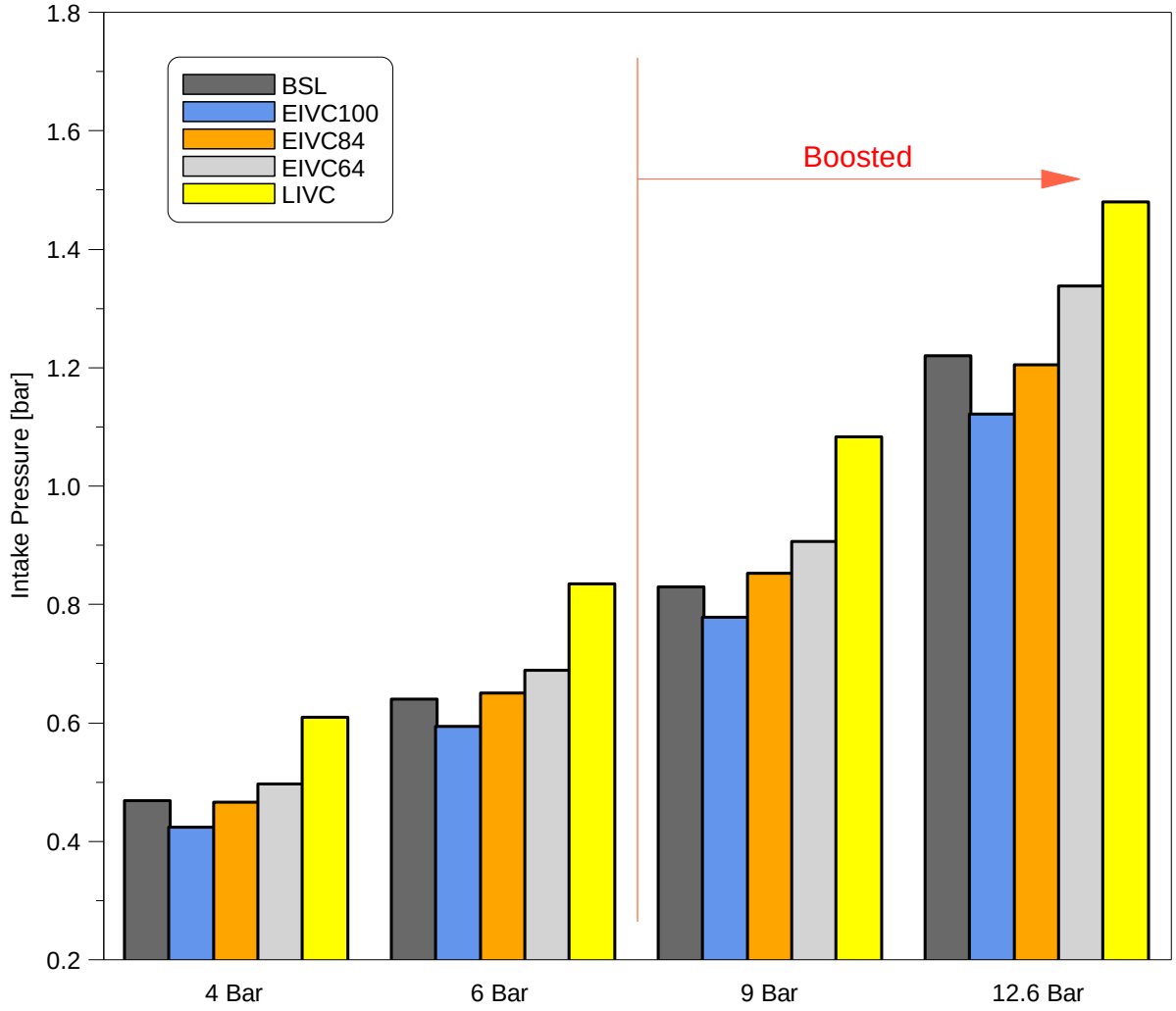

Figure 4.7 Intake pressure comparison at various loads at 1500rpm

However, an additional test with very short lift (EIVC44) produced the highest intake pressure but slightly larger pumping losses than EIVC64 (Table 4.3). According to J. B. Heywood this phenomenon could be explained by the relationship between valve lift and discharge coefficient [64][64]. Depending on the valve shape, at high lifts the flow separates and discharge coefficient decreases generating higher pumping losses. At lower lifts the flow speed across the intake valves increases and the flow remains attached to the valve providing high discharge coefficient, therefore reducing pumping losses. However, if the lift would be reduced further or flow speed would be increased, the flow might separate and cause an opposite effect, which was the case with EIVC44. The discharge coefficient at EIVC64 might have been higher than EIVC44 and this would reduce pumping losses, but this is purely

theoretical and to quantify the results a measurement of discharge coefficient via CFD simulations is required. In the case of this experiment 64% lift was the optimum for EIVC profiles in reduction of pumping losses, therefore EIVC44 was not considered in further analysis.

Table 4.3 Comparison of EIVC64 and 44 at 1500rpm

	EIVC64	EIVC44
Intake Pressure (bar)	0.495	0.601
PMEP (bar)	-0.54	-0.55

The intake pressure for baseline profile was higher than EIVC84 due the charge being expelled from the cylinder during compression strokes even though throttle was opened slightly less. However, negative PMEP was the same as EIVC84 due to lower effective flow area during the opening of the valve for BSL profile.

To summarise, EIVC100 got the highest pumping losses due to the lowest intake pressure. LIVC achieved major reduction in pumping losses due to increased intake pressure and the largest throttle opening.

At 6bar net IMEP a similar trend is present. LIVC had the lowest ECR and required a larger throttle angle, which increased the intake pressure, providing the lowest pumping losses among other profiles. EIVC100 had the highest pumping losses due to the lowest intake pressure followed by the baseline profile. EIVC64 had a higher intake pressure than EIVC84 but also higher negative PMEP. This indicates that EIVC84 might have higher discharge coefficient. A larger engine load requires larger volume of charge in the cylinder therefore flow velocity through the intake valves has to increase in order to accommodate for this. As discussed previously the discharge coefficient is affected by the change flow speed, due to this the discharge coefficient could be reduced at EIVC64 causing an increase in negative PMEP even though intake pressure was higher than at 84% lift.

For 9bar net IMEP tests, an external supercharger was used to provide the pressurised air. It was necessary to provide additional 0.6bar of boost pressure for the LIVC profile as it was not capable of achieving this load point with naturally aspirated mode, whereas other profiles didn't require boosting. Overall, the same trend was present as at 6bar. LIVC had the lowest negative PMEP due to the highest intake pressure. EIVC100 has the lowest intake pressure, thus the largest pumping losses. EIVC64 and 84 had the same throttle angle but intake pressure was increased for EIVC64 due to lower lift. EIVC84 achieved lower pumping losses potentially due to higher discharge coefficient as in the case with 6bar net IMEP. However,

further increased flow speed could have reduced discharge coefficient even more for EIVC64 resulting in a higher negative PMEP than the baseline valve profile, even though it had much lower intake pressure.

At 12.6bar net IMEP a positive pumping work was present due to additional boost (0.6bar). LIVC had the highest positive PMEP due to significantly higher intake pressure compared to the rest of valve profiles, followed by EIVC64. EIVC100 had the lowest positive PMEP due to lowest intake pressure which corresponds to the lowest throttle angle. EIVC84 had slightly higher positive pumping work compared to the baseline even though the intake pressure was slightly lower, this was caused by larger effective flow area during valve opening of EIVC84.

From the above results it is evident that intake port pressure has strong influence on the pumping losses. The intake port pressure can be increased via the throttle or valve lift. It is also possible that discharge coefficient can affect pumping losses. The discharge coefficient is influenced by the flow speed which can be altered either by intake pressure or valve lift or both. Where the difference between intake pressures is not significant the discharge coefficient is more dominant in reduction of pumping losses. Across all load cases LIVC reduced pumping loses significantly compared to the baseline profile due to significant increase in intake pressure. EIVC profiles with shorter lifts also were successful in reducing pumping losses due to higher intake pressure and possibly increased discharge coefficient.

Changes of the intake valve profile can also influence combustion duration, which is another factor affecting fuel economy. Comparison of combustion durations and spark timings can be seen in Figure 4.8.

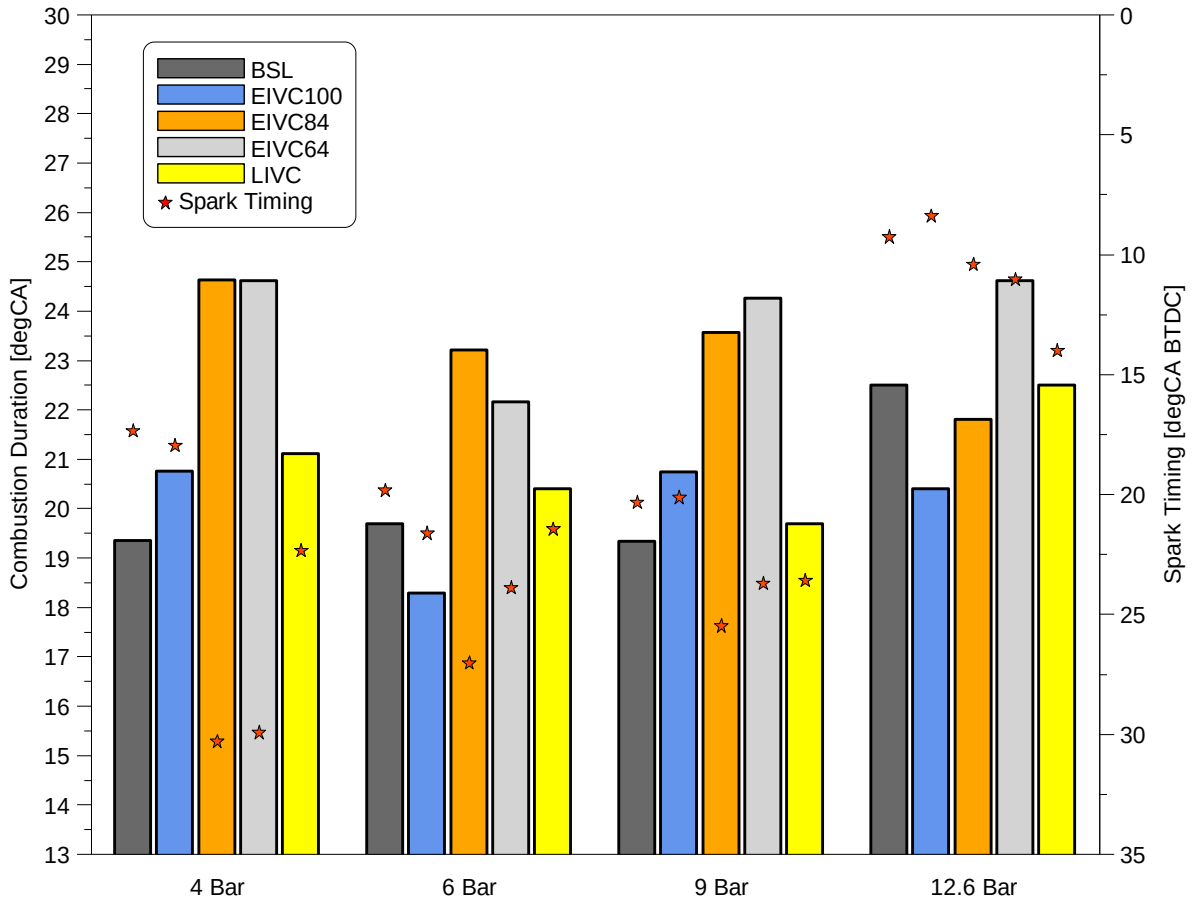

Figure 4.8 Combustion duration and spark timing comparison at various loads at 1500rpm

At 4bar net IMEP the baseline valve profile produced the shortest combustion duration (10-90% burn), whereas EIVC84 and 64 led to the longest duration indicating that flame speed was lower due to reduced tumble flow and hence turbulence intensity. EIVC100 and LIVC profiles had similar combustion durations which were slightly longer (less than 2 CA deg) than that of the baseline valve profile. The MBT spark timing was advanced accordingly to compensate for the longer combustion duration, however the flame development angle (angle between the spark timing and 10% burn in CA degrees) for short lift profiles was more than 30% longer than the baseline (Figure 4.9). LIVC also had slightly longer flame development angle indicating weaker in-cylinder turbulence than the baseline.

The trend for the first part of flame propagation period measured by 10-50% burn was similar to combustion duration for all profiles. However, the second half of flame propagation period indicated by the 50-90% burn was slightly different (Figure 4.10). The duration for CA50-90 was identical for EIVC100 and LIVC profiles and slightly longer than the baseline. EIVC profiles with short lifts also produced the identical duration for the second half of flame propagation period but longer than the baseline by almost 32%.

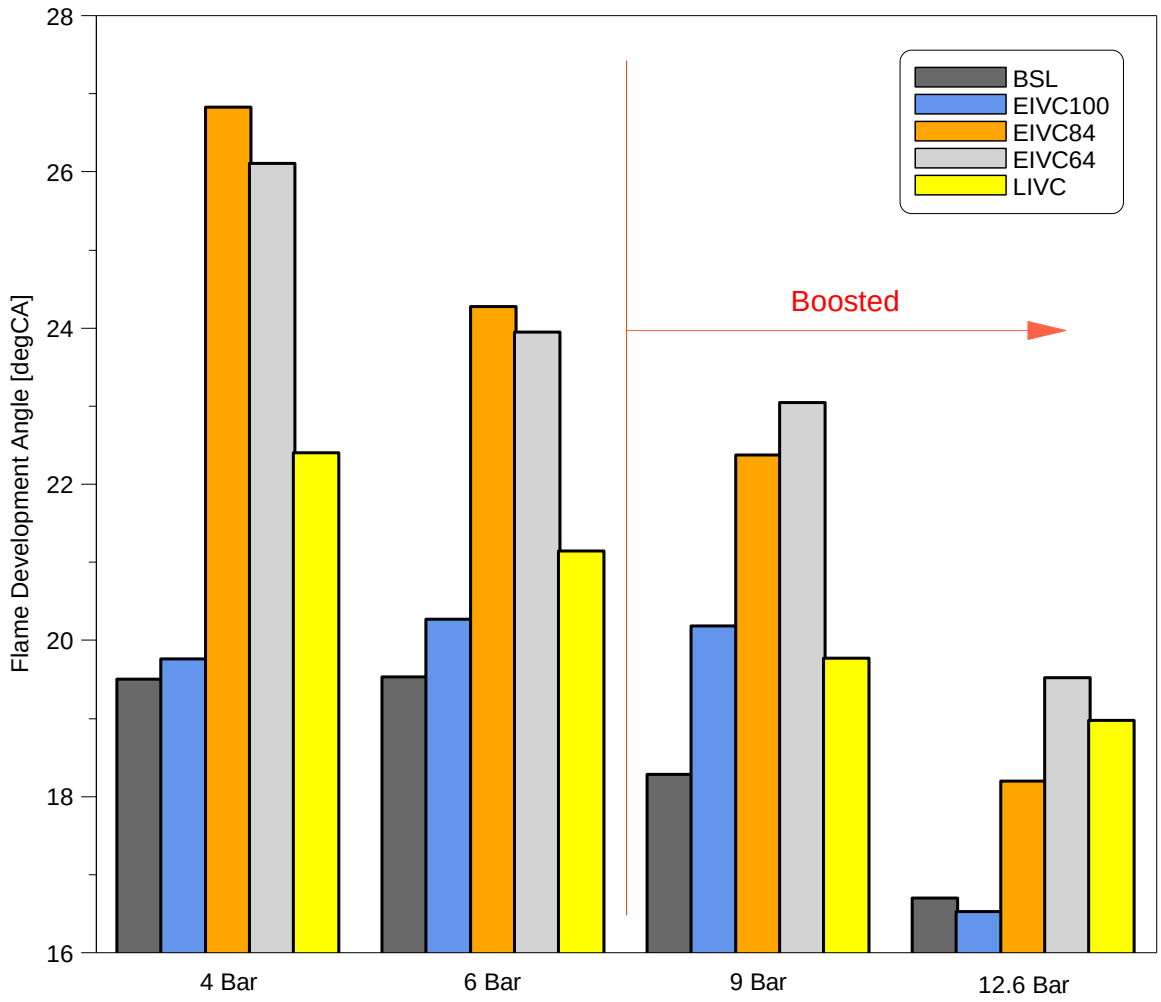

Figure 4.9 Flame development angle comparison at various loads at 1500rpm

At 6bar net IMEP combustion duration was reduced for all profiles except for the BSL profile with shortest being EIVC100 and longest EIVC84. The MBT spark timing was advanced respectively for profiles with longer flame development angle, longest being EIVC with shorter lifts followed by LIVC. EIVC100 had slightly longer flame development angle than the baseline. Therefore the spark timing was also slightly advanced. CA10-50 demonstrates the same trend as combustion duration, however CA50-90 was elongated more for BSL, EIVC84 and LIVC.

At 9bar net IMEP, the combustion duration was similar to 4bar but the advance in spark timing was limited by knocking combustion. LIVC spark timing was advanced by a few degrees compared to baseline profile due to lower in-cylinder temperature at the end of compression stroke thanks to lower effective compression ratio. This resulted in reduced knocking tendency and allowed to advance spark timing. EIVC84 and 64 spark timings were also more advanced than EIVC100 due to lower ECR. The longest flame development angle was found with EIVC64 and 84, followed by EIVC100 and LIVC. Both first and second half of flame propagation period had similar trend as combustion duration for all profiles.

At 12.6bar net IMEP knocking had more noticeable effect on spark timing. EIVC100 has the shortest combustion duration and the most retarded spark timing due to highest ECR. Whereas LIVC has the same combustion duration as the baseline but more advance spark timing due to lower knocking tendency. This was achieved because of reduced in-cylinder temperature as effective compression ratio was lowered. The same effect can be observed with EIVC84 and 64 spark timing compared to EIVC100. The longest flame development angle was produced by EIVC64 followed by LIVC and EIVC84. EIVC100 achieved shorter flame development angle and duration than BSL. Profiles with high lift produced identical duration of CA10-50, however BSL and LIVC got the longest CA50-90 except for EIVC64.

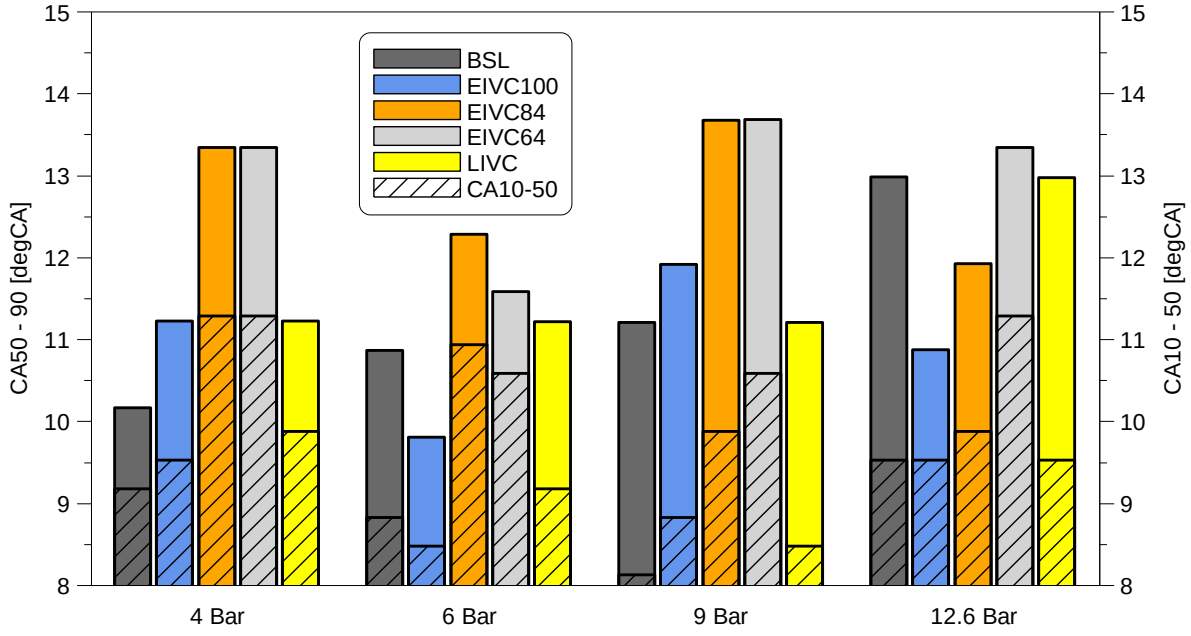

Figure 4.10 CA10-50 and CA50-90 comparison at various loads at 1500rpm

From the discussion above it can be concluded that lower ECR causes weaker in-cylinder flow motion leading to longer combustion duration and flame development angle. This effect is more prominent at lower load and very high load with knock limited combustion. On the other hand, a lower effective compression ratio allows to advance knock limited spark timing further. Shorter valve lifts lead to slower combustion except at the highest load case. This is evidenced by longer flame development angle and combustion duration of EIVC84 and 64. In almost all the load cases shorter lift had more noticeable effect on in-cylinder turbulence than the effect of lower ECR

Figure 4.11 demonstrates how valve profiles influence ISFC at various load points. At low load (4bar IMEP) LIVC valve profile reduced fuel consumption by 3.4g/kWh compared to the baseline due to reduced pumping losses. EIVC64 was also successful in reduction of ISFC, however due to very poor in-cylinder charge mixing and slow combustion it was less effective

than LIVC. EIVC100 and 84 lead to increased fuel consumption due to larger pumping losses and longer combustion duration.

At 6bar net IMEP the lowest fuel consumption was achieved by the baseline profile due to shorter combustion duration and medium pumping losses. EIVC64 was the second best followed by LIVC profile. The reason why LIVC achieved higher ISFC value than EIVC64 even though it has shorter combustion duration and lower pumping losses, is richer local in-cylinder charge (Figure 4.12). The probable cause of this can be due to some of the fuel being pushed out into the intake manifold and in the next cycle this fuel could be concentrated in one spot instead of homogeneously mixing. Whereas EIVC64 had in-cylinder AFR closest to stoichiometric. The worst fuel economy was achieved by EIVC100 due to the largest pumping loss.

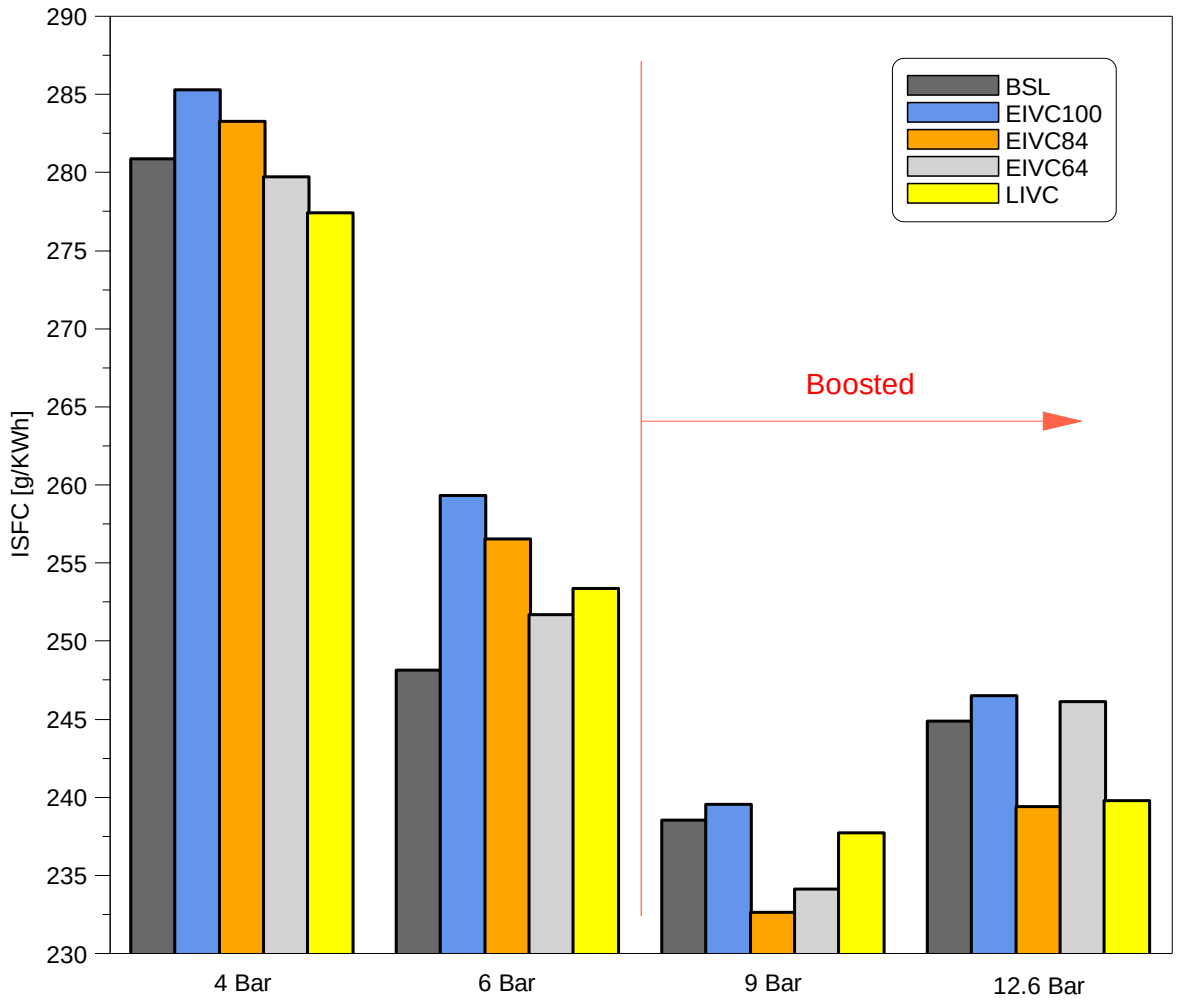

Figure 4.11 ISFC comparison at various loads at 1500rpm

A similar result for LIVC was achieved at 9bar net IMEP. Despite a shorter duration and the lowest pumping loss LIVC achieved higher fuel consumption than EIVC84 and 64 due to richer

in-cylinder mixture. Baseline profile also had higher fuel consumption due to lower in-cylinder lambda. EIVC100 has the largest ISFC due to larger pumping losses than the rest of the profiles and EIVC84 has the lowest fuel consumption due to stoichiometric in-cylinder AFR and lower pumping losses and shorter combustion duration than EIVC64.

At 12.6bar net IMEP in-cylinder lambda was slightly richer for EIVC84 than for LIVC, but EIVC84 had shorter combustion duration which led to lower ISFC. EIVC100 has highest fuel consuption due to smallest positive pumping work among other profiles. EIVC64 was the second worst due to longest combustion duration and richiest in-cylinder mixture.

From the above results it is evident that valve profiles influence pumping losses and combustion duration which in turn affects fuel consumption. Moreover, in-cylinder AFR is affected by valve profiles influencing ISFC. Overall Miller cylce was succefull in reducing fuel consumption at low loads thanks to lower pumping loss and at high loads where spark timing was knock limited.

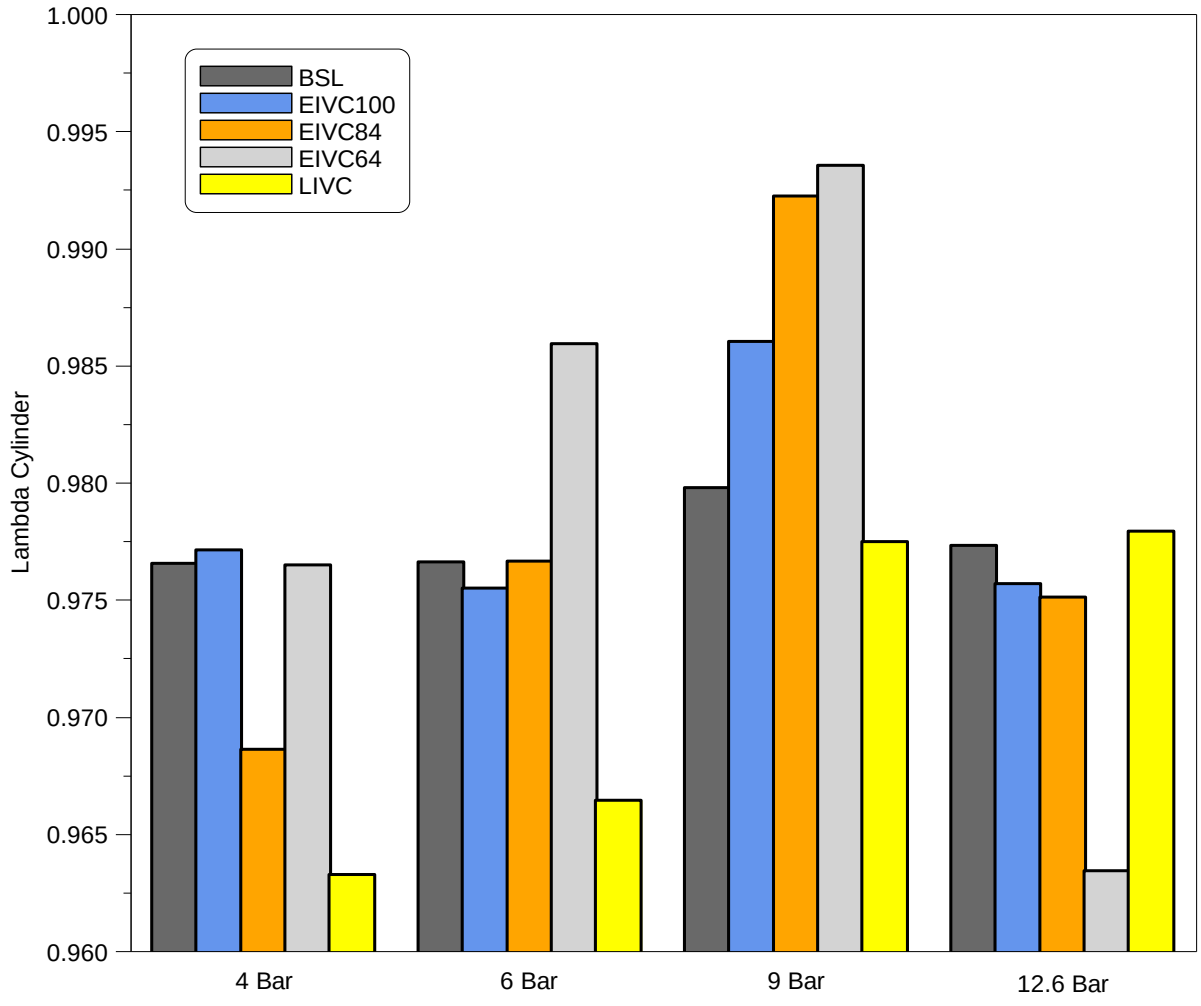

Figure 4.12 In-cylinder lambda comparison at various loads at 1500rpm

At 9 and 12.6bar net IMEP loads the net fuel consumption should also take into account of the compression work required where additional boost pressure was used. An external mechanical supercharger was used to provide the boost and was powered by electrical supply, in automotive application the supercharger would be driven by the engine crankshaft which would cause a power loss affecting ISFC. Due to this the compressor work was calculated and ISFC was then corrected taking into account supercharger work using the equations and variables below [65].

Equation 4.1

$$Wc = \frac{\dot{m}_{air} \times C_p \times T1}{\eta_C \times \eta_m} \times \left[(P2 \div P1)^{\gamma-1/\gamma} - 1 \right]$$

Equation 4.2

$$ISFC\ corrected = \frac{\dot{m}_{fuel}}{Pi - Wc}$$

Where,

$C_p = 1.012\ J/gK$

$\gamma = 1.4$

$\eta_c = 60\%$

$\eta_m = 90\%$

Figure 4.13 shows the values of ISFC when work required by the supercharger is taken into account. As mentioned before at 9bar net IMEP only LIVC profile required additional boost therefore the ISFC was corrected only for this profile. After correction LIVC achieved highest fuel consumption at 9bar due to the work required for the supercharger. At 12.6bar net IMEP all valve profiles had ISFCs corrected taking into account additional boost required for each profile. ISFC increased for all profiles proportional to the amount of required boost, for example EIVC100 had lowest increase in ISFC as it required the least boost whereas LIVC had the largest increase due to greatest amount of boost required. After correction EIVC84 still had the lowest ISFC among the rest of the profiles.

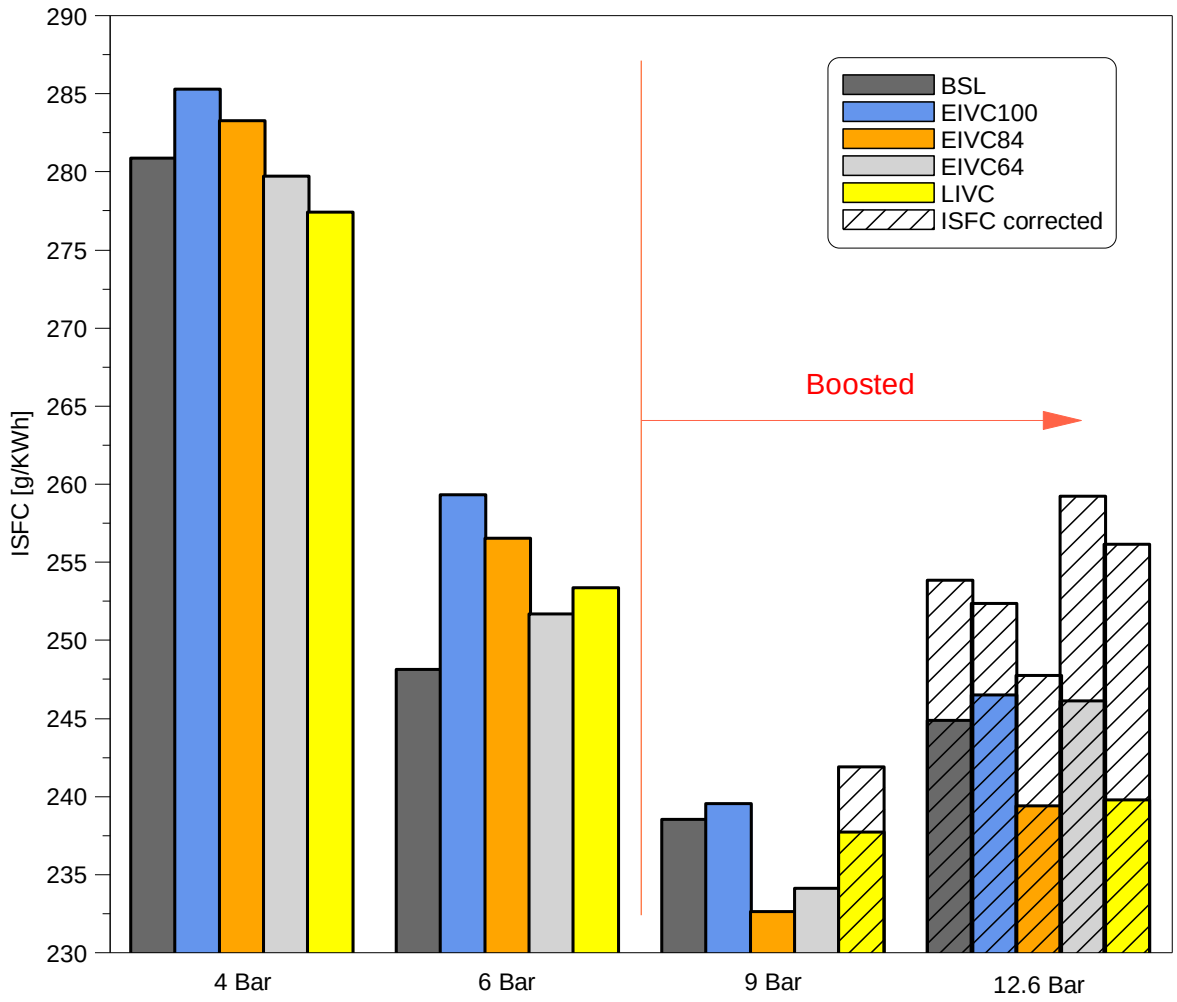

Figure 4.13 ISFC and ISFC corrected comparison at various loads at 1500rpm

Emissions results are shown in Figure 4.14, Figure 4.15 and Figure 4.16. Throughout all load cases higher concentration of ISCO was present with lower in-cylinder lambda i.e. combustion of fuel rich mixture. The lowest ISCO values were achieved when in-cylinder lambda was closer to 1 (stoichiometric combustion) with lowest value of 16 g/KWh at 9bar net IMEP with EIVC64 profile.

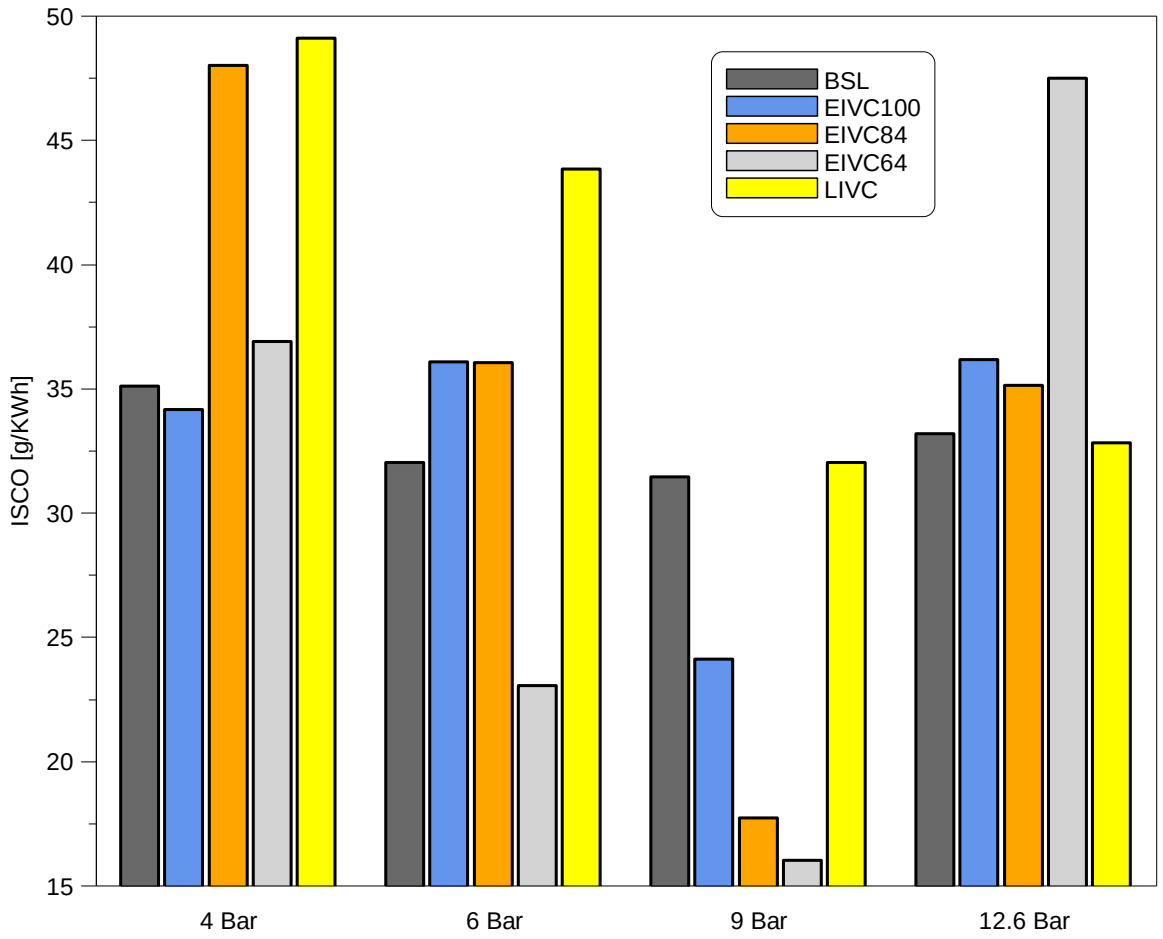

Figure 4.14 ISCO emission comparison at various loads at 1500rpm

At 4bar net IMEP the lowest level of HC emissions was achieved by LIVC profile due to the lowest in-cylinder pressure during compression stroke which prevented some of the mixture being forced into crevices and reasonably fast combustion which prevented bulk quenching of the flame next to the cylinder walls, leading to more complete combustion compared to the rest of the profiles. At 6bar net IMEP the lowest ISHC was achieved by EIVC84 due to lowered in-cylinder pressure and improved combustion speed which allowed to reduce bulk quenching at the cylinder wall. At 9bar net IMEP HC emissions were dramatically reduced for all profiles indicating more favourable conditions for complete combustion. EIVC100 achieved lowest ISHC of 5.38 g/KWh due to lower in-cylinder pressure during combustion stroke and relatively fast combustion, reducing bulk quenching at the cylinder wall. At 12.6bar net IMEP HC emissions increased overall indicating less complete combustion due to stronger knocking. Lowest ISHC value was achieved by EIVC84 due to low in-cylinder pressure during combustion and fast combustion due to advance spark timing, which allowed to reduce quenching at the cylinder wall.

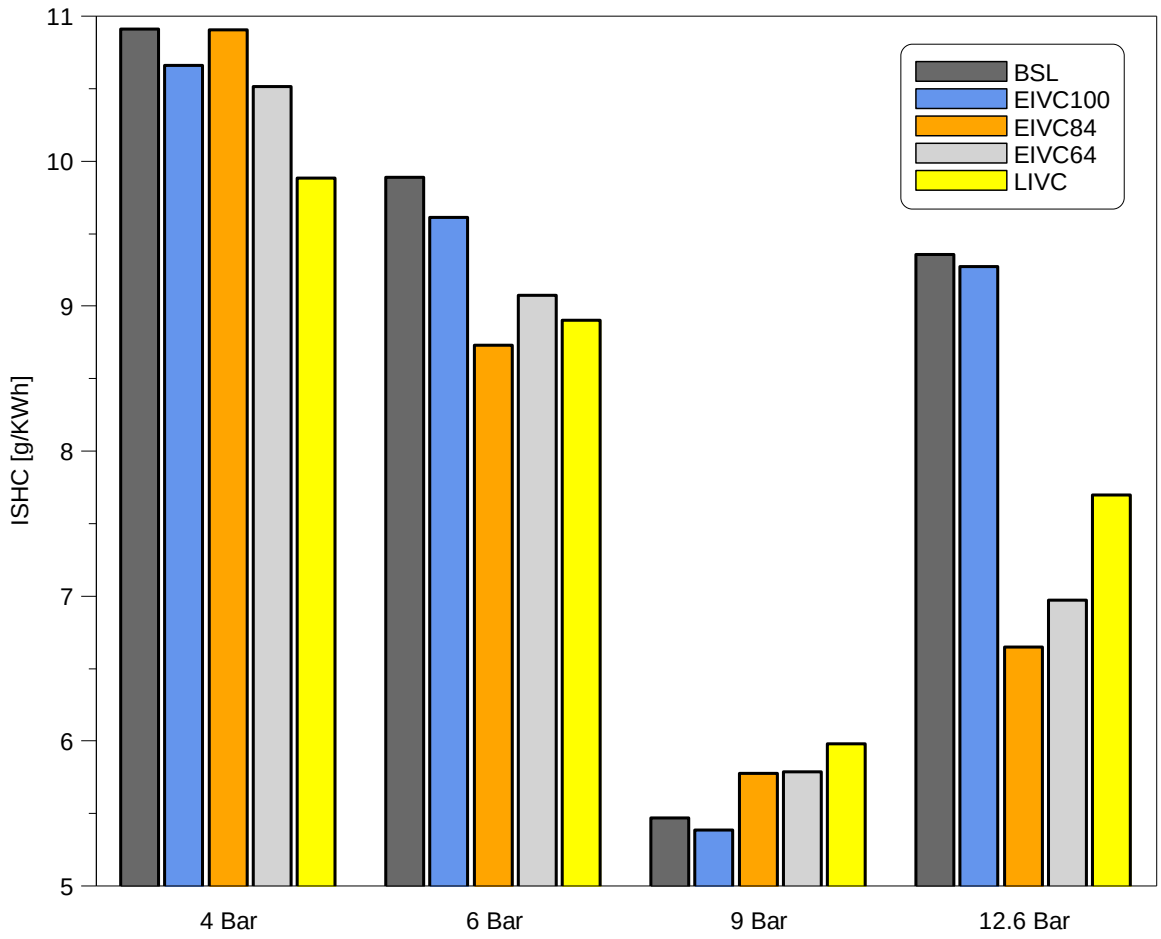

Figure 4.15 ISHC emission comparison at various loads at 1500rpm

Lowest NO_X level across all the load points was achieved with LIVC profile because of the lower effective compression ratio as indicated by the lower in-cylinder pressure during the compression stroke and lower peak temperature during combustion. As the load increases the $ISNO_X$ generally also increases due to increasing in-cylinder pressure during the compression stroke and peak temperature during combustion. EIVC profiles with shorter lifts generally produced higher NO_X emissions because of higher pressure at the end of the compression stroke and more advanced spark timing which provides higher rate of temperature increase, so that in-cylinder peak temperature would be greater than from other profiles.

Overall EIVC and LIVC profiles were successful in reduction of emissions. The major reduction was achieved by LIVC in NO_X emission across all the load cases.

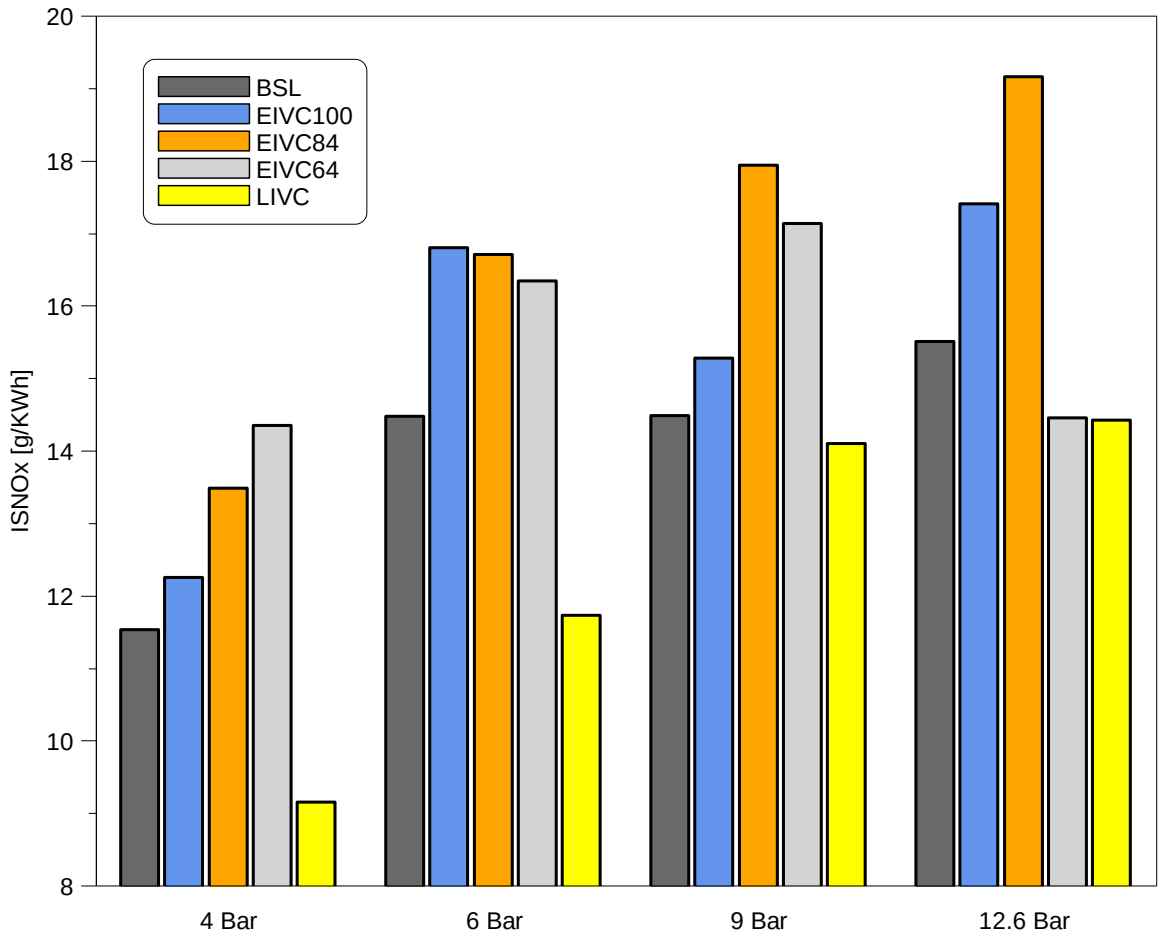

Figure 4.16 $ISNO_X$ emission comparison at various loads at 1500rpm

4.3.2 Test results at 3000rpm

Figure 4.17 shows a comparison of effective compression ratio at various loads. As can be noted EIVC84 was not included at 3000rpm test in order to avoid overheating of the electronic control of the iVT. EIVC100 has the highest ECR values throughout the whole load range due to IVC being just few degrees after BDC allowing for maximum amount of fresh charge being trapped inside the cylinder. The overall ECR value of baseline profile was lower by 3% than EIVC100 due to retarded IVC timing which allowed some of the fresh charge to escape into the intake manifold during the compression stroke. With increasing load effective compression ratio is reduced for BSL and EIVC100 as more charge is being expelled into the intake manifold due to increasing in-cylinder pressure.

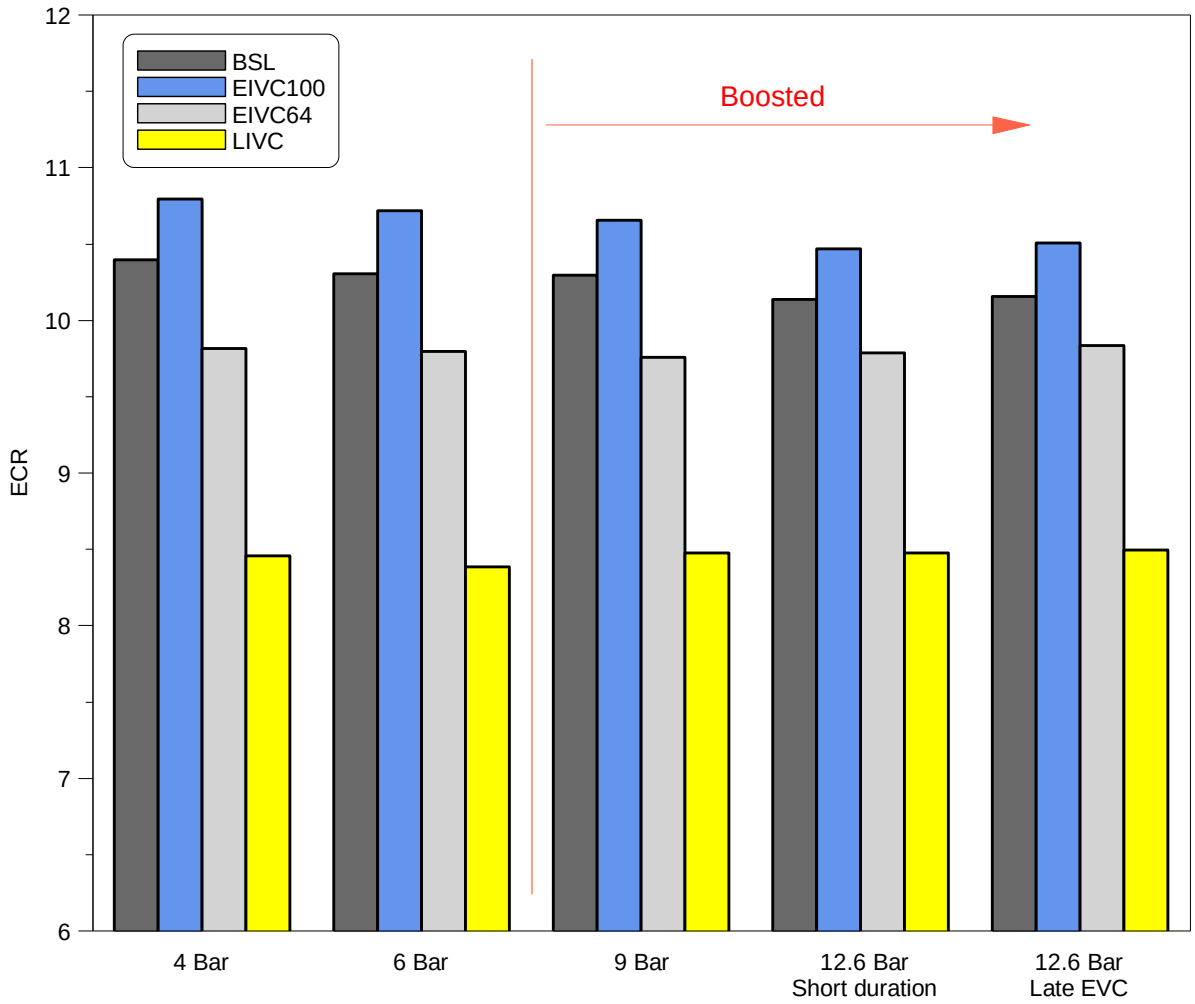

Figure 4.17 ECR comparison at various loads at 3000rpm

EIVC64 has significantly lower ECR than BSL and EIVC100 due to low lift as it allowed less fresh charge into the cylinder before compression could begin. Also with increasing load the LIVC produced the lowest effective compression ratio with average value of 8.45 due to very late IVC, allowing a significant amount of fresh charge to be expelled into the intake manifold during compression stroke. Both EIVC64 and LIVC had almost constant ECR level throughout the whole load range.

For each load case EIVC64 had the highest throttle opening, followed by LIVC and BSL as shown in Figure 4.18. EIVC100 had the lowest throttle opening due to the highest ECR except for load case at 4bar net IMEP where BSL profile had lower throttle opening. At 3000rpm

throttle angle was not always corresponding to the ECR and the reason for that will be discussed in the next section.

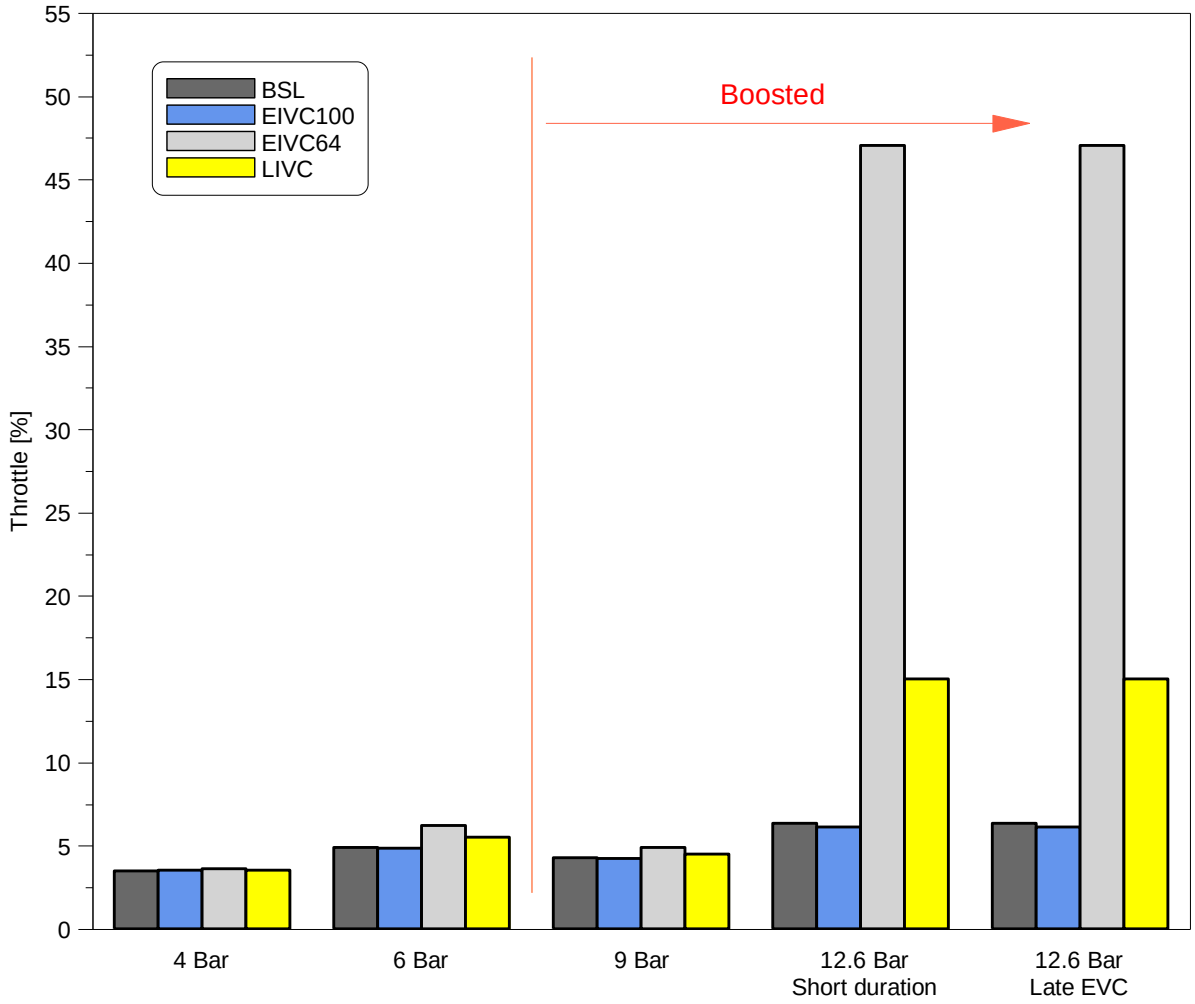

Figure 4.18 Throttle opening comparison at various loads at 3000rpm

Comparison of PMEP and intake pressure for various valve profiles is demonstrated in Figure 4.19 and Figure 4.20. At 4bar net IMEP EIVC64 valve profile achieved the lowest pumping loss due to the highest intake manifold pressure resulted from larger throttle opening and low valve lift. BSL profile had the largest negative PMEP due to low intake pressure and smaller effective flow area during valve opening compared to EIVC profiles. This explains why EIVC100 achieved slightly lower pumping losses with lower intake pressure than BSL. LIVC had relatively high intake pressure due to accumulating charge in the manifold during compression stroke before IVC. However, due to the lowest effective flow area during valve opening LIVC achieved larger pumping losses than EIVC64.

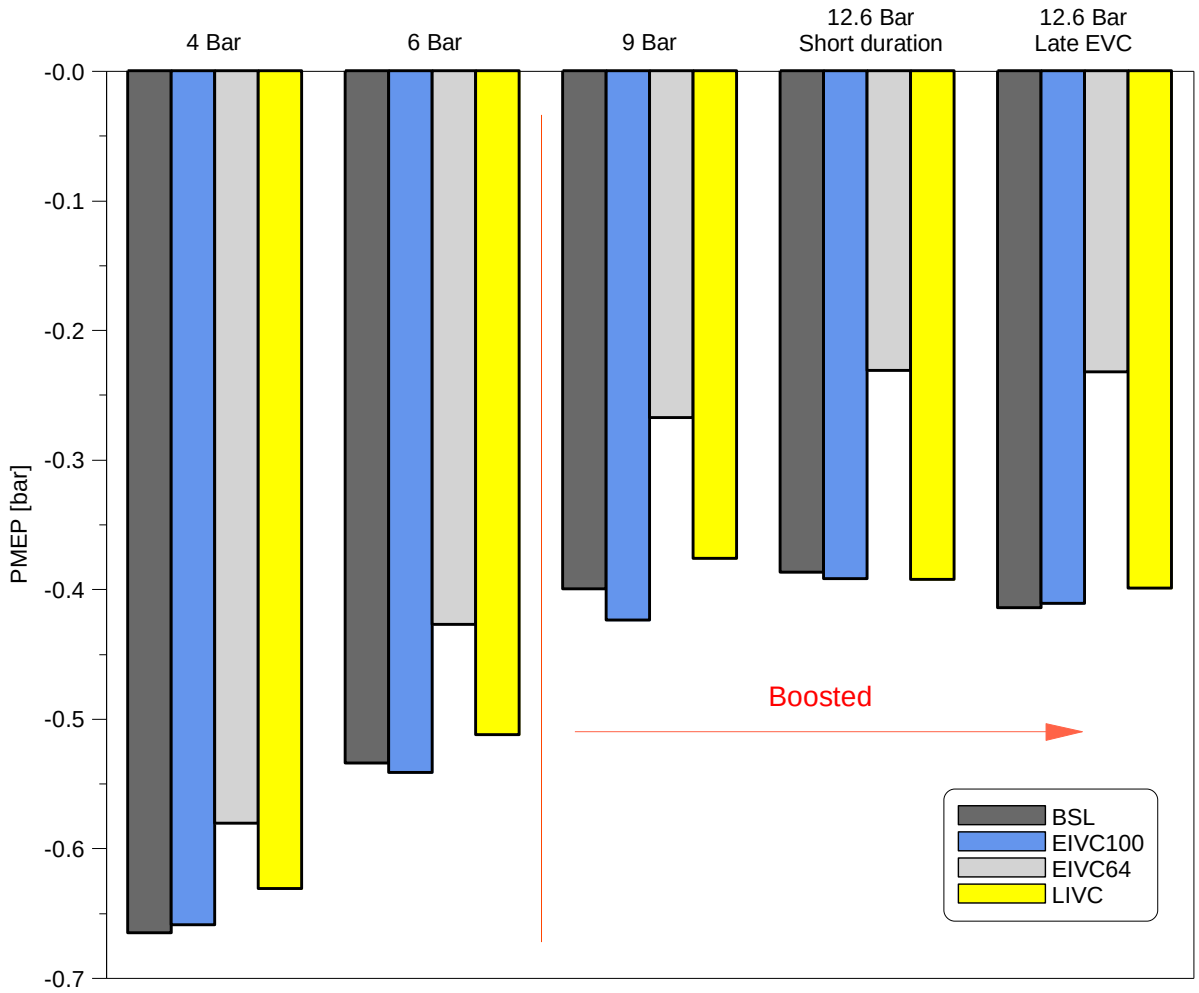

Figure 4.19 PMEP comparison at various loads at 3000rpm

At 6bar net IMEP the lowest negative PMEP was achieved by EIVC64 because of the highest intake manifold pressure. It was followed by LIVC profile where the lowest effective flow area during valve opening increased pumping losses significantly compared to EIVC64. The highest pumping loss was provided by EIVC100 due to the lowest intake pressure. BSL profile achieved slightly less pumping losses than EIVC100 due to higher intake pressure.

Similarly to 6bar, EIVC64 achieved the lowest pumping losses at 9bar net IMEP due to the highest intake pressure, followed by LIVC and BSL profiles. The largest negative PMEP was achieved by EIVC100 due to the lowest pressure in the intake manifold.

At 12.6bar net IMEP EIVC64 had the lowest pumping losses for both configurations of the exhaust profile, however with late EVO (small valve overlap) the intake pressure was increased due to lower in-cylinder pressure during the IVO. This allowed for increased inertia of the flow, thus higher pressure build up in the intake manifold after IVC. The change in the flow speed could have reduced discharge coefficient therefore pumping losses of EIVC64 with late EVO were almost the same as with short duration even though the intake pressure was

0.04bar higher. For the rest of the profiles the intake pressure was identical in both cases at 12.6bar net IMEP. In case with EIVC100 late EVO configuration of exhaust valve profile led to small valve overlap and internal EGR due to the pressure in the exhaust manifold being greater than in the cylinder. This led to higher pumping losses than with short duration. The same affect was is demonstrated by LIVC and BSL profiles with late EVO, however BSL experienced more significant increase in pumping losses due to larger valve overlap than other profiles. LIVC had the highest pumping losses with short duration due to the smallest effective flow area during the opening of the intake, which became more significant than the intake pressure at high load.

At 3000rpm EIVC64 was the best in reducing pumping losses across the whole range of engine loads due to the highest intake pressure. The minimum reduction in pumping losses was 15% compared to the baseline profile.

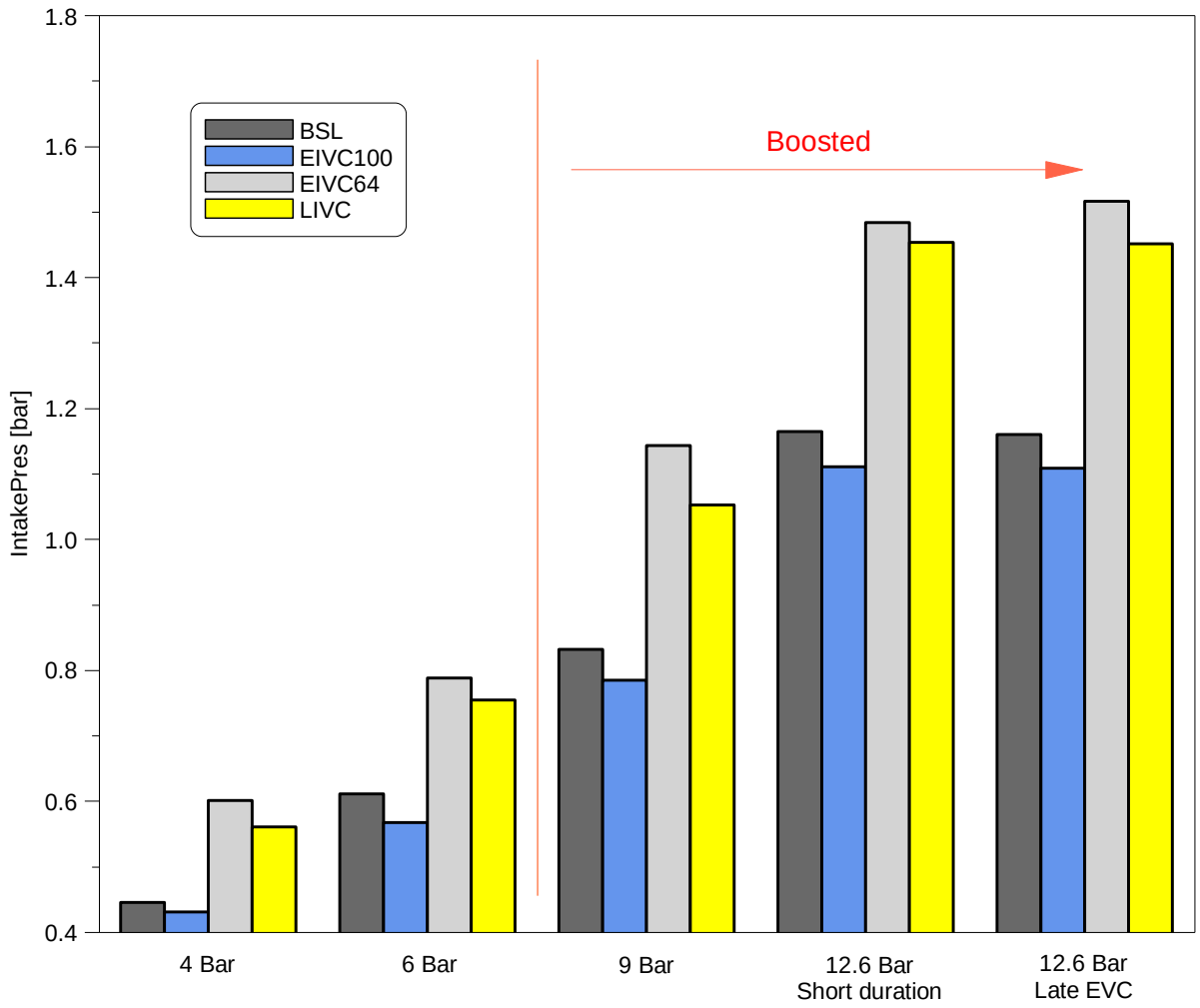

Figure 4.20 Intake pressure comparison at various loads at 3000rpm

Comparison of combustion durations and spark timings can be seen in Figure 4.21. At 4bar net IMEP the baseline valve profile produced the shortest combustion, whereas EIVC64 had 50% longer duration indicating that flame speed was significantly lower due to reduced tumble flow and hence turbulence intensity. EIVC100 and LIVC profiles had the same combustion duration which was only 1 crank angle degree longer than the baseline.

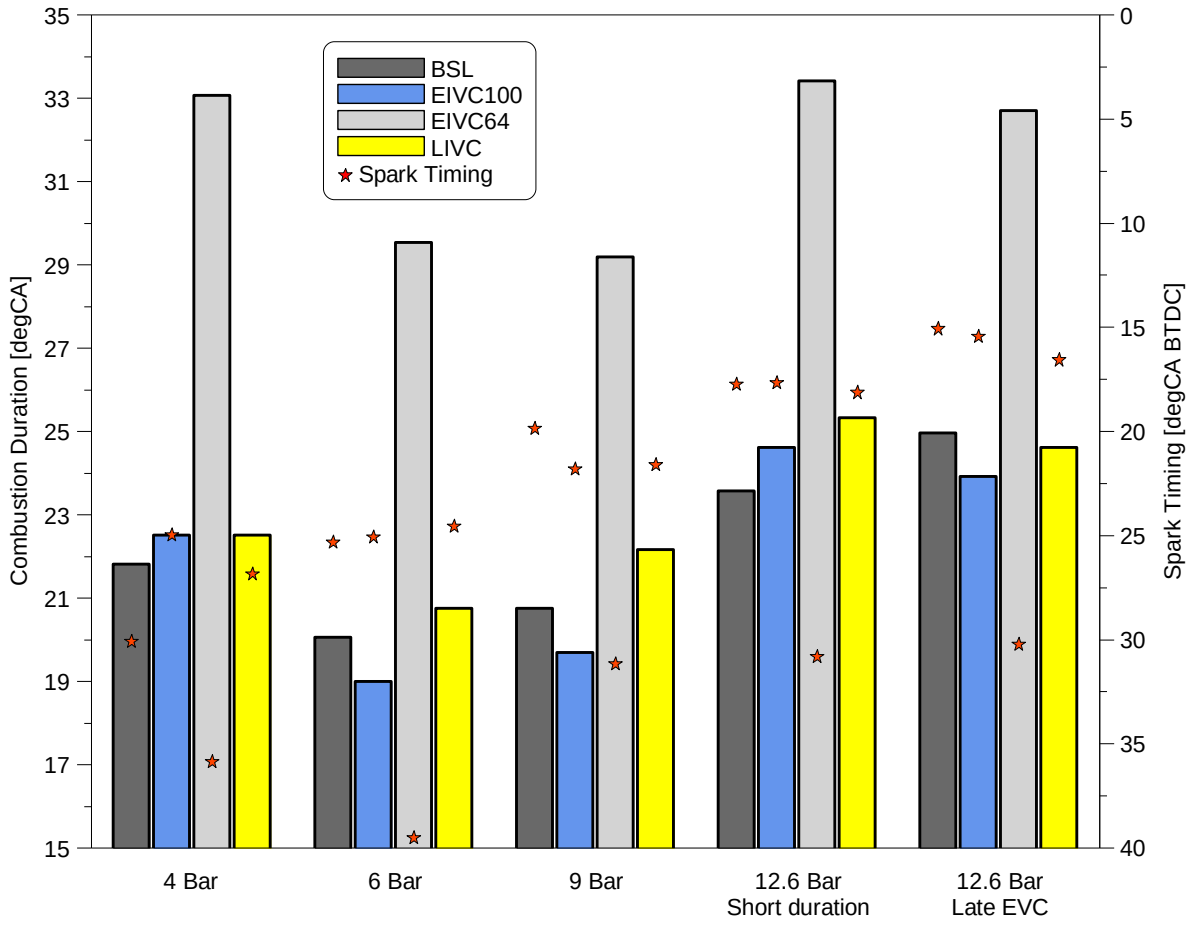

Figure 4.21 Combustion duration and spark timing comparison at various loads at 3000rpm

The MBT spark timing was advanced respectively to flame development angle (Figure 4.22) in order to compensate for slower combustion. EIVC64 had the largest flame development angle therefore the MBT spark timing was the most advance. The shortest flame development angle was achieved by EIVC100 and the MBT spark timing was the latest among the rest of the profiles for this load case.

At 6bar net IMEP combustion duration was noticeably reduced for all profiles with shortest being EIVC100 and longest EIVC64. The MBT spark timing was advanced respectively for profiles with longer flame development angle, except for LIVC with second longest flame development angle and the latest MBT timing.

At 9bar net IMEP combustion duration had the same trend and was slightly increased compared to 6bar except for EIVC64. The flame development angle was noticeably reduced for all profiles which was reflected in slightly retarded MBT spark timing.

The combustion duration was increased for all profiles at 12.6bar net IMEP with both exhaust configurations. Due to knocking combustion spark timing was retarded for all profiles except for EIVC64 due to lower knocking tendency. The flame development angle was almost the same as at 9bar net IMEP for most of the profiles. With late EVO spark timing was retarded further for BSL and EIVC100 due to higher EGR compared to other profiles which caused higher in-cylinder temperature, resulting in higher knocking tendency. LIVC spark timing was slightly retarded with late EVO due to shorter flame development angle, thus shorter combustion duration.

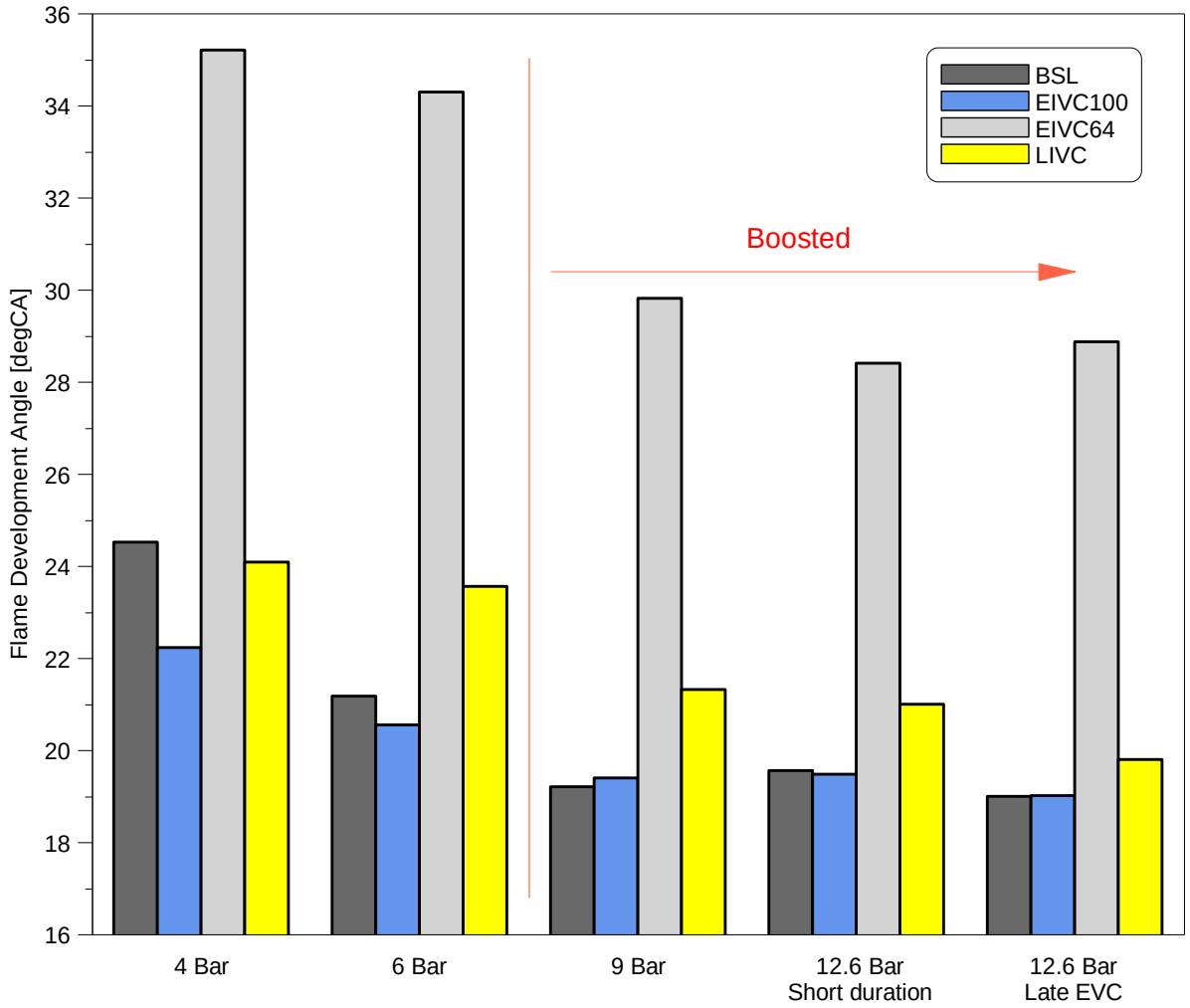

Figure 4.22 Flame development angle comparison at various loads at 3000rpm

Figure 4.23 demonstrates comparison of flame propagation between valve profiles at various loads. The trend for the first part of flame propagation period measured by 10-50% burn was

similar to combustion duration for all profiles throughout the whole load range. EIVC64 had longer 10-50% burn compared to other profiles due to slow combustion caused by low turbulence intensity. The second half of flame propagation period indicated by the 50-90% burn was similar to the first half, however at 12.6bar net IMEP it was increased due to late opening of the exhaust. In case with short exhaust duration not all of the burned gas may be expelled into the exhaust and in case with late EVC some of the exhaust gas could be recirculated into the cylinder due to valve overlap. Both of these cases may result in higher residual gas concertation in the cylinder which causes slower flame propagation. The second half of flame propagation period for EIVC64 was also longer than for other profiles due to lower tumble caused by low lift.

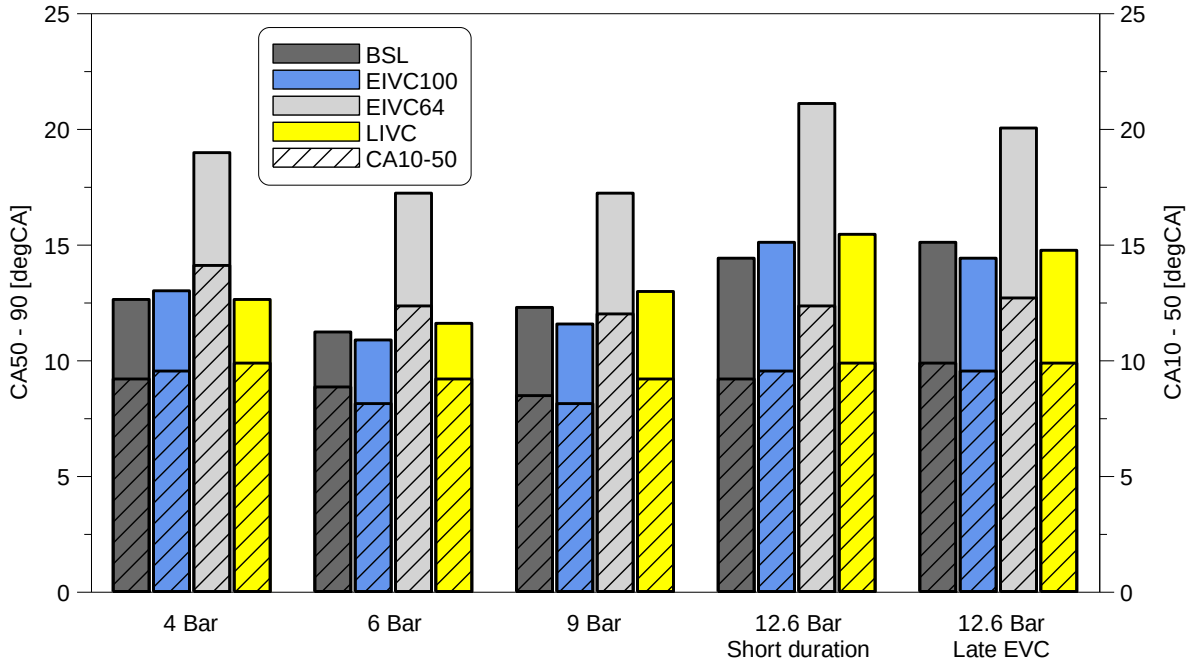

Figure 4.23 CA10-50 and CA50-90 comparison at various loads at 3000rpm

From the discussion above it can be concluded that low lift causes weaker in-cylinder flow motion leading to longer combustion duration and flame development angle like in case with EIVC64 at all load points. On the other hand, due to lower effective compression ratio EIVC64 was able to advance knock limited spark timing further than other profiles. However, LIVC with the lowest ECR didn't have such an impact on combustion duration and flame development angle, its results were similar to BSL and EIVC100 at various load cases. This indicates that at 3000rpm low lift has a stronger effect on in-cylinder tumble and flame speed than low ECR.

Figure 4.24 demonstrates how valve profiles influence ISFC at various load points, also taking into account of the compression work required for additional boost pressure at high load. At 4bar net IMEP LIVC valve profile reduced fuel consumption by 7g/kWh compared to the

baseline due to reduced pumping losses and cylinder lambda being closest to stoichiometric (Figure 4.25). EIVC64 also achieved reduction in ISFC compared to BSL profile, however due to very slow combustion and poor in-cylinder charge mixing it was less effective than LIVC. EIVC100 had the largest ISFC of 273.9g/KWh due to slightly longer combustion duration and the most fuel rich in-cylinder AFR.

At 6bar net IMEP BSL and EIVC100 achieved the same fuel consumption. EIVC64 and LIVC reduced ISFC by 7.5 and 8.5 g/KWh respectively. This was achieved thanks to reduced pumping losses and close to stoichiometric in-cylinder lambda. However, EIVC64 performed slightly worse than LIVC due to slow flame propagation caused by poor in-cylinder mixing.

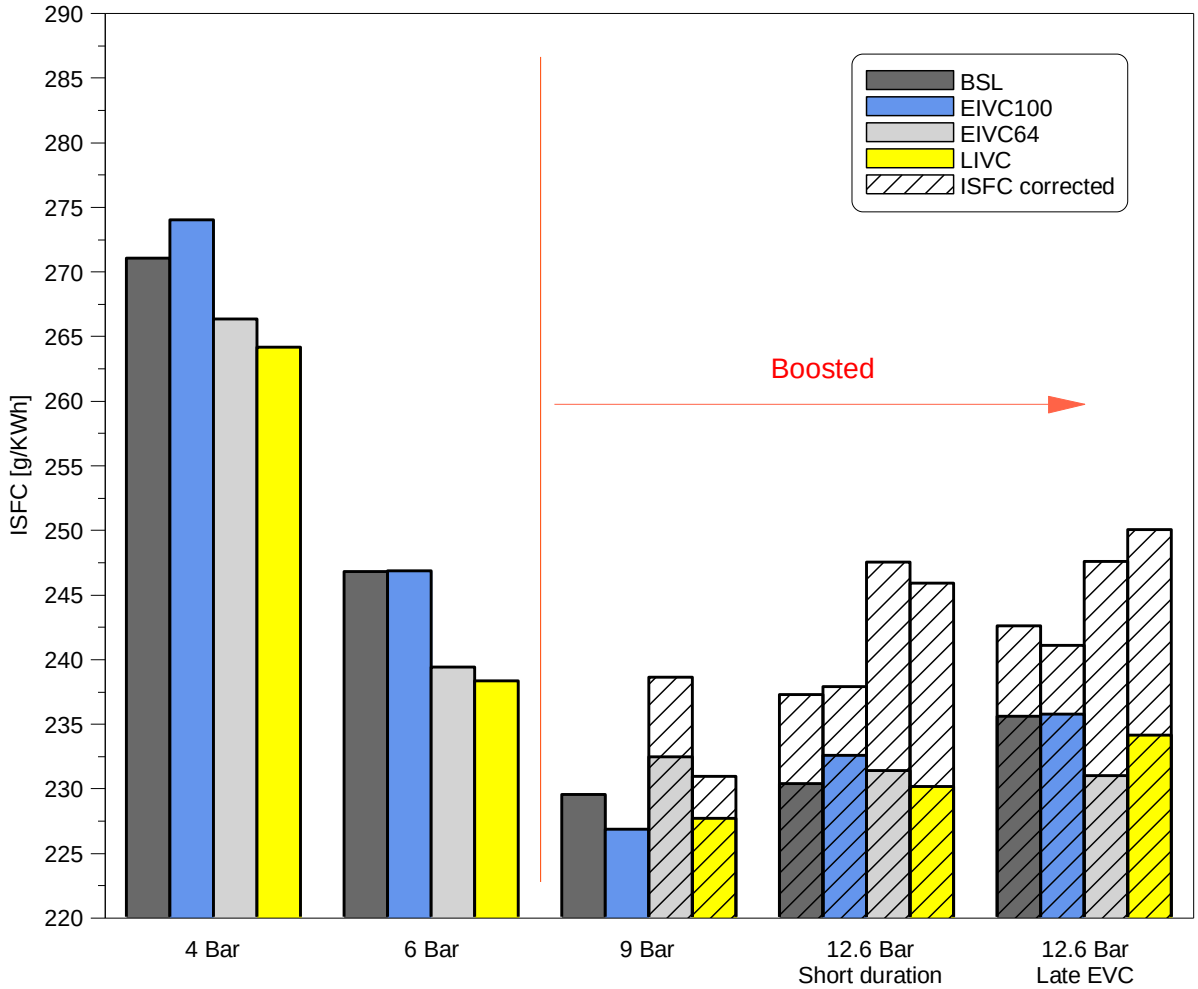

Figure 4.24 ISFC and ISFC corrected comparison at various loads at 3000rpm

At 9bar net IMEP EIVC100 achieved the lowest fuel consumption due to shortest combustion duration and near stoichiometric in-cylinder AFR. LIVC achieved a similar result thanks to reduced pumping losses, however this profile required additional boost pressure for this load case. When compression work of the supercharger is taken into account the fuel consumption is increased significantly for LIVC. Similarly fuel consumption was increased for EIVC64, on

top of that slow combustion and slightly richer in-cylinder lambda led to the highest ISFC among all the profiles.

At 12.6bar net IMEP all of the profiles required additional boost in order to achiev the desired load. With late EVC all profiles had increased ISFC compared to short duration of the exhaust profile. This is due to the presence of valve overlap and internal EGR. Sligthly richer in-cylinder lambda indicates the presence of residual gas in the cylinder for all valve profiles with late EVC. With short exhaust duration BSL profile achieved lowest ISFC due to the shortest combustion duration and relatively low additional boost required, whereas EIVC64 and LIVC profiles required significantly greater amount of boost which led to increased fuel consumption with supercharger work taken into account. EIVC100 was the second best due to least amount of boost required and relatively short combastion duration.

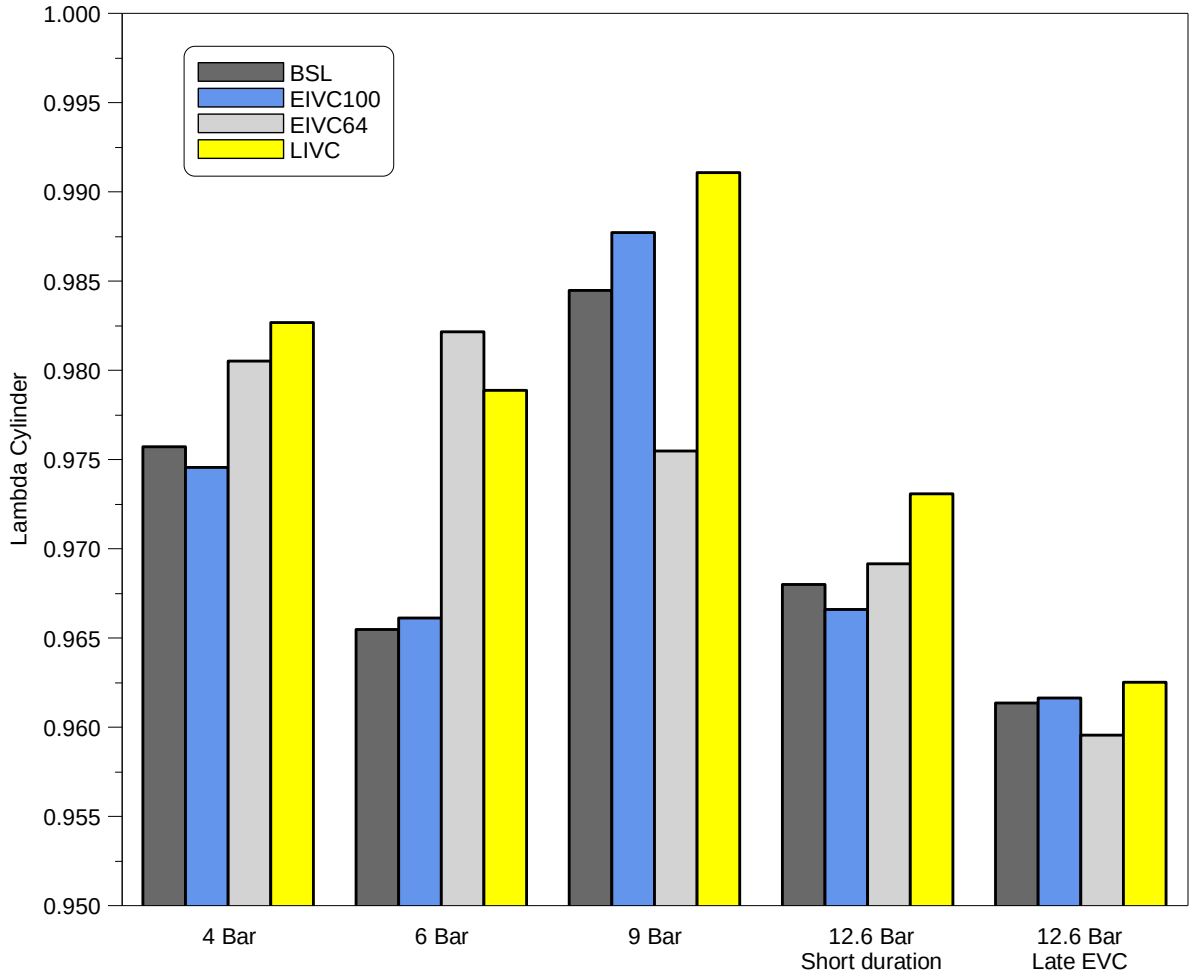

Figure 4.25 In-cylinder lambda comparison at various loads at 3000rpm

From the above results it is evident that lower ECR can improve fuel consumption significantly fow low load conditions thanks to reduced pumping losses and near stoichiometric in-cylinder

AFR. In case with high loads low ECR is not favourable as higher boost pressure is needed leading to higher overall fuel consumption.

Emissions results are shown in Figure 4.26, Figure 4.27 and Figure 4.28. Similarly, to 1500rpm tests, throughout all load cases higher concentration of ISCO was present with lower in-cylinder lambda i.e. combustion of fuel rich mixture. The lowest ISCO values were achieved when in-cylinder lambda was closer to 1 (stoichiometric combustion). Overall ISCO emissions were lower at 9bar with lowest value of 19.5 g/KWh with LIVC profile. At 12.6bar net IMEP with late EVC the highest amount of ISCO was produced overall due higher fraction of residual gas present in the cylinder leading to richer local AFR. EIVC64 and LIVC produced lower ISCO among other profiles throughout the whole load range.

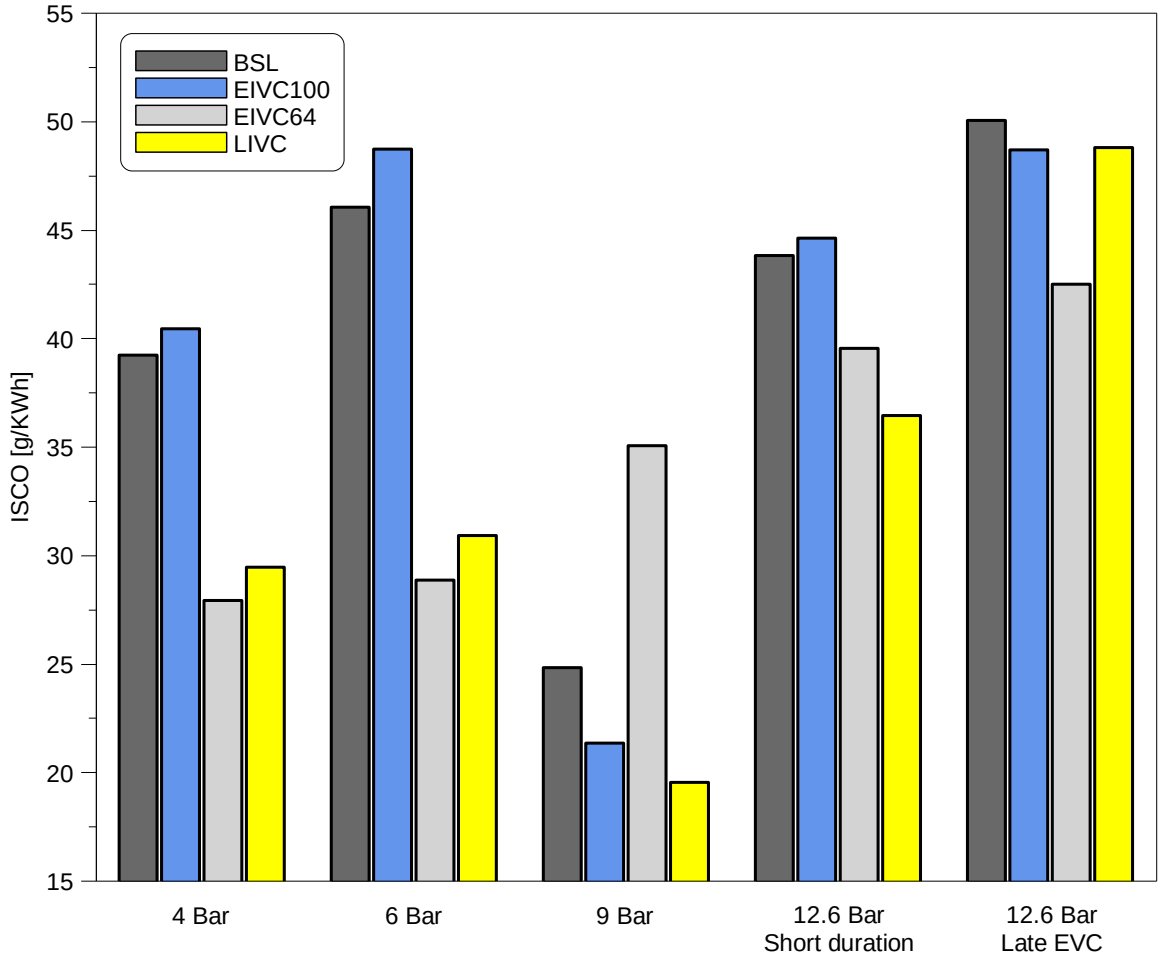

Figure 4.26 ISCO emission comparison at various loads at 3000rpm

At 4bar net IMEP the lowest level of HC emissions was achieved by EIVC64 profile due to the lowest in-cylinder pressure at the end of compression stroke and during combustion which prevented some of the mixture being forced into crevices. At 6bar net IMEP the lowest ISHC was achieved by EIVC64 due to low in-cylinder pressure during combustion, LIVC also had

low in-cylinder pressure but slightly richer local AFR caused higher HC emissions. At 9bar net IMEP EIVC100 achieved lowest ISHC of 3.4 g/KWh due to the fastest combustion which reduced bulk quenching at the cylinder wall allowing for more complete combustion. EIVC64 also achieved low HC emissions due to the lowest in-cylinder pressure during combustion, however slow combustion caused some of the quenching at the cylinder wall later in the expansion stroke leading to slightly higher HC level than EIVC100.

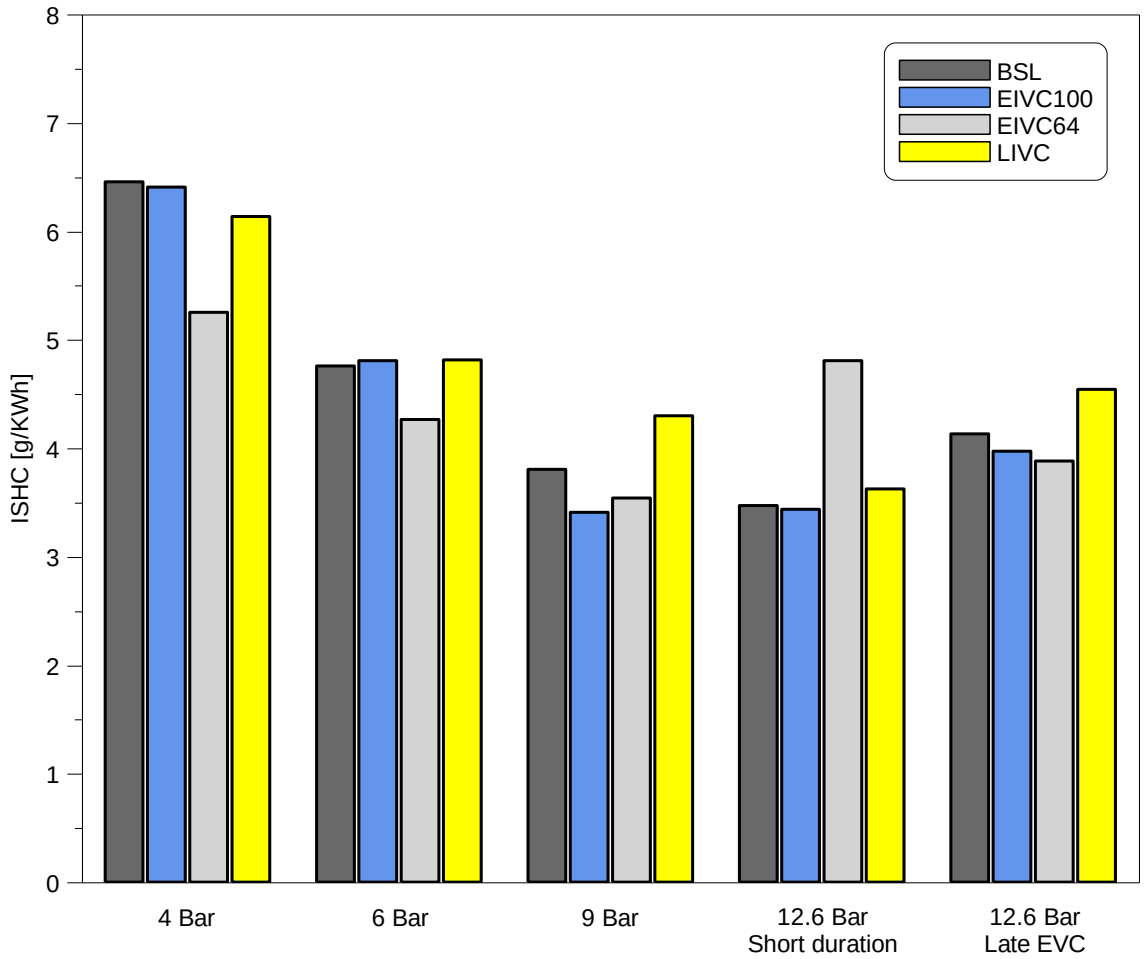

Figure 4.27 ISHC emission comparison at various loads at 3000rpm

At 12.6bar net IMEP with short exhaust duration lowest HC emissions were achieved by EIVC100 due to fast combustion and lower than BSL in-cylinder pressure during expansion stroke. EIVC64 had the highest ISHC due to very high in-cylinder pressure at the end of compression and beginning of expansion stroke which was caused by very advance spark timing compared to the rest of the profiles. With late EVC overall HC emissions were increased due to the presence of residual gas which led to richer local AFR and less complete combustion. Overall HC emissions were reducing with load except the case with late EVC where internal EGR is present.

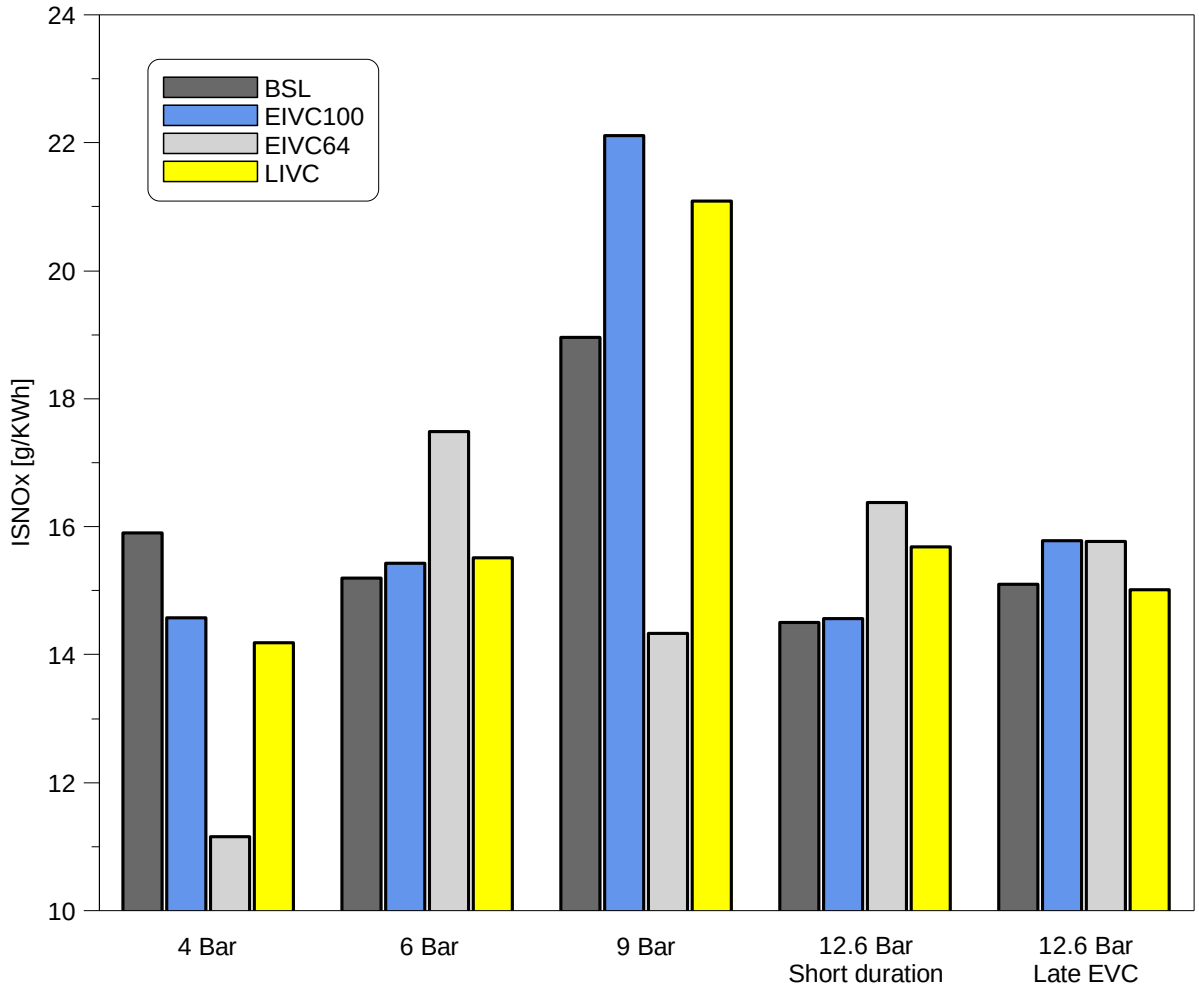

Figure 4.28 ISNO$_X$ emission comparison at various loads at 3000rpm

Lowest NO$_X$ level at 4bar net IMEP was produced by EIVC64 due to significantly lower in-cylinder pressure during combustion compared to the rest of the profiles, which led to the lowest peak combustion temperatures. At 6bar net IMEP EIVC64 achieved the highest ISNO$_X$ due to very advance spark timing, whereas baseline profile achieved lowest NO$_X$ due to moderate in-cylinder temperature and richer AFR. At 9bar net IMEP EIVC64 had the lowest in-cylinder pressure during combustion, richer local AFR and less advance spark timing than at 6bar. All of those factors led to very low ISNO$_X$ emissions compared to the other profiles. At 12.6bar net IMEP with short duration of exhaust BSL profile achieved the lowest NO$_X$ due to late spark timing and richer local AFR. With late EVC BSL and EIVC100 had NO$_X$ emissions increased due to higher fraction of the residual gas present which increases the overall temperature in the cylinder. EIVC64 and LIVC profiles had very small amount of the residual gas and thanks to slightly retarded spark timing NO$_X$ was reduced compared to results with short exhaust duration. LIVC performed better in this case due to more retarded spark timing than EIVC64 which allowed for lower peak cylinder temperature.

Overall EIVC64 and LIVC profiles were effective in reducing CO emissions in almost all load cases. EIVC64 was more effective in reduction of HC emissions and NO_X emissions in some load cases.

4.4 Summary

In this chapter, experimental results for five valve profiles with two valve operation were presented and discussed in terms of engine performance and emissions. The tests were performed at 1500rpm and 3000rpm engine speed with a range of loads from 4bar to 12.6bar. The main findings are summarised below:

- At 1500rpm at 4bar and 9bar NIMEP, EIVC64 had increased intake manifold pressure compared to EIVC84 even though throttle angle was identical.
- The discharge coefficient may influence PMEP when the difference in intake pressure is not significant.
- Overall LIVC and EIVC profiles with low lifts achieved lowest pumping losses at both 1500rpm and 3000rpm due to the highest intake pressures.
- Lower ECR allowed to advance spark timing when combustion was knock limited at high engine loads.
- Lower valve lift reduced flame speed more than low ECR.
- Valve profiles affected in-cylinder lambda even though exhaust lambda is kept at 1 as mixture in the cylinder was not always uniformly mixed due to the flow characteristics imposed by the shape of the profiles.
- Overall EIVC with short lifts and LIVC profiles were successful in reduction of fuel consumption.
- At 1500rpm LIVC reduced NO_X emissions but increased CO emissions whereas EIVC profiles lowered CO and HC emissions but increased NO_X almost at all load cases.
- At 3000rpm LIVC and EIVC64 achieved overall lower CO emissions whereas EIVC64 reduced HC emissions at part load.

Chapter 5 Miller Cycle and Atkinson Cycle Operations with Single Intake Valve

5.1 Test conditions

5.1.1 Valve profiles

In this experiment, the same set of valve profiles as the ones presented in Chapter 4 were used except one of the intake valves was kept closed to force the intake flow through the opened intake valve. Figure 5.1 and Table 5.1 shows the valve profiles and valve timings used. It was expected that the single valve operation may induce stronger tumble or swirl motion inside the cylinder in order to improve mixing of the fuel with air, which in turn could improve fuel efficiency and emissions. The exhaust valve profile had shorter duration for test point at 3000rpm 12.6bar NIMEP in order to avoid damage to the valvetrain system. The results from the single valve mode are compared to those of the two valve mode.

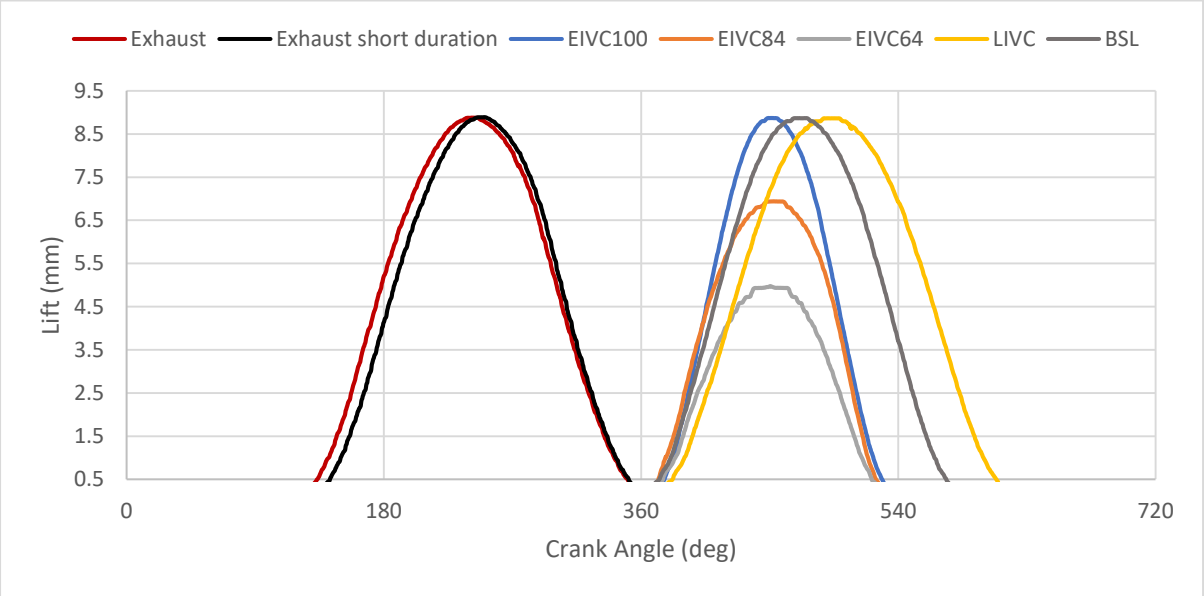

Figure 5.1 Valve profiles

Table 5.1 Valve timings and durations

Valve Profile	Lift (mm)	Duration (CA deg)	IVO/EVO (CA deg)	IVC/EVC (CA deg)
EIVC100	8.9	152	376	528
EIVC84	7	152	372	524
EIVC64	5	146	375	521

LIVC	8.9	226	382	608
Baseline	8.9	200	373	573
Exhaust	8.9	211	133	344
Exhaust short duration	8.9	201	143	344

5.1.2 Operation points

Table 5.2 shows four operation points used for comparison of the test results between single and two valve mode.

Table 5.2 Testing points

Speed (rpm)	**NIMEP (bar)**			
1500	4	6	9	12.6
3000	4	6	9	12.6

5.2 Single vs two valve mode

5.2.1 Test results at 1500rpm

The effect of single valve operation on ECR and throttle angle are shown in Figure 5.2 and Figure 5.3. The highest ECR throughout the whole load range was found from EIVC100 with single valve mode, the two valve mode provided slightly lower ECR. The throttle position for both profiles was almost identical, however the intake pressure was slightly increased for single valve mode (Figure 5.4) which caused higher ECR. Due to lower flow area when only 1 intake valve is open, a higher intake pressure is required to allow the same amount of air into the cylinder as with two intake valves. This is usually achieved by larger throttle opening, however in this case a large pressure drop at IVO caused an increase in intake pressure just before the valves which was enough to trap the required amount of air into the cylinder without altering throttle angle.

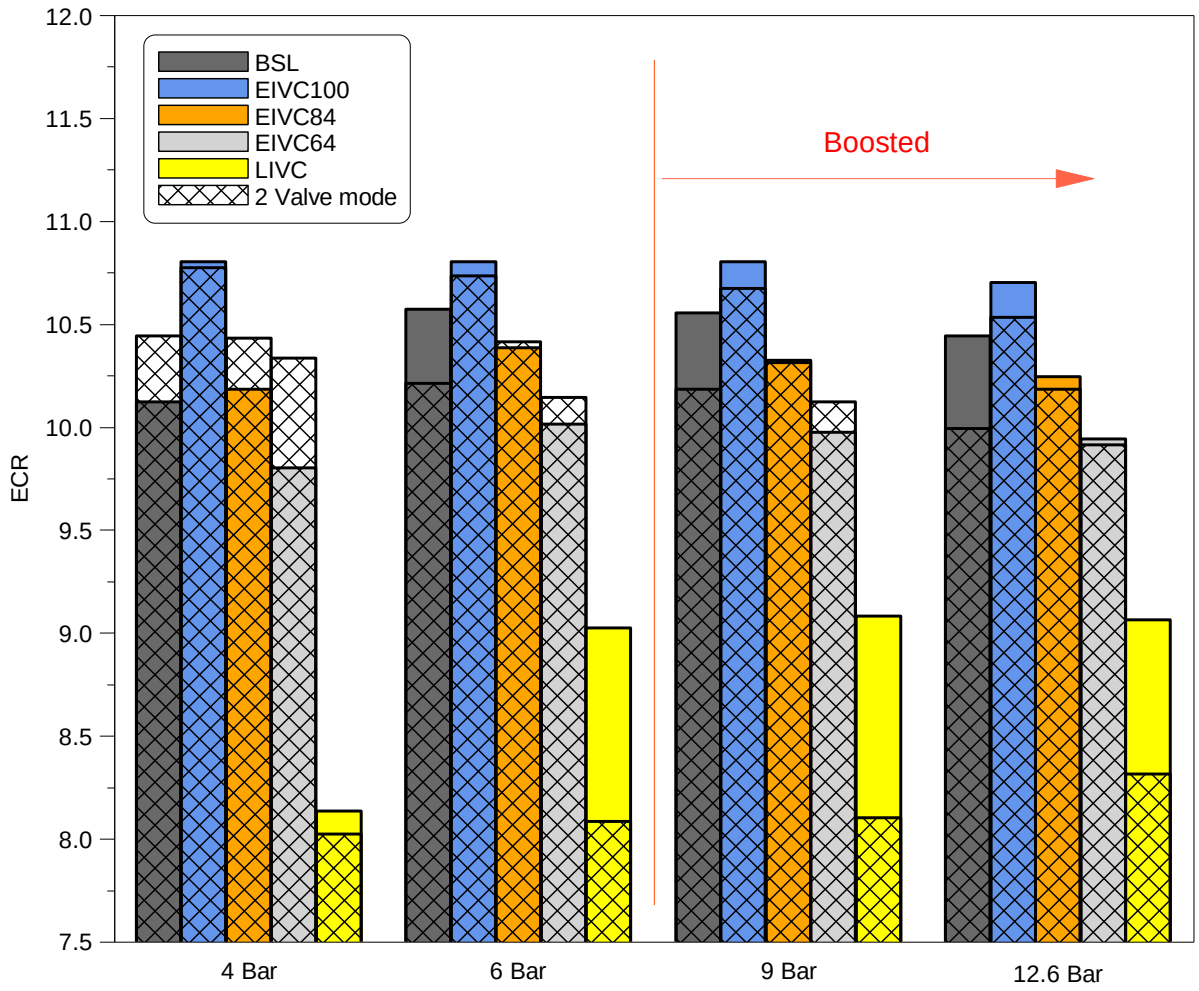

Figure 5.2 ECR comparison between valve modes at various loads at 1500rpm

EIVC84 with single valve achieved slightly lower ECR than two valve mode at all load points except for 12.6bar. The intake pressure was higher than two valve mode across the whole load range and throttle angle was higher only at 12.6bar. The intake pressure was increased due to the same reason as in case with EIVC100, however it was not enough to maintain the same ECR as with 2 valve mode at lower loads. EIVC64 with single valve mode achieved similar results with even lower ECR than two valve mode at lower loads. At 12.6bar EIVC64 with single valve mode required much larger throttle opening than two valve mode as the flow into the cylinder was restricted by the closed valve.

The baseline profile with single valve mode had higher ECR than two valve mode for loads above 4bar net IMEP as less charge was pushed through the single valve after BDC leading to greater amount of air being trapped inside the cylinder. The throttle position and intake pressure was almost the same for both throughout the whole load range.

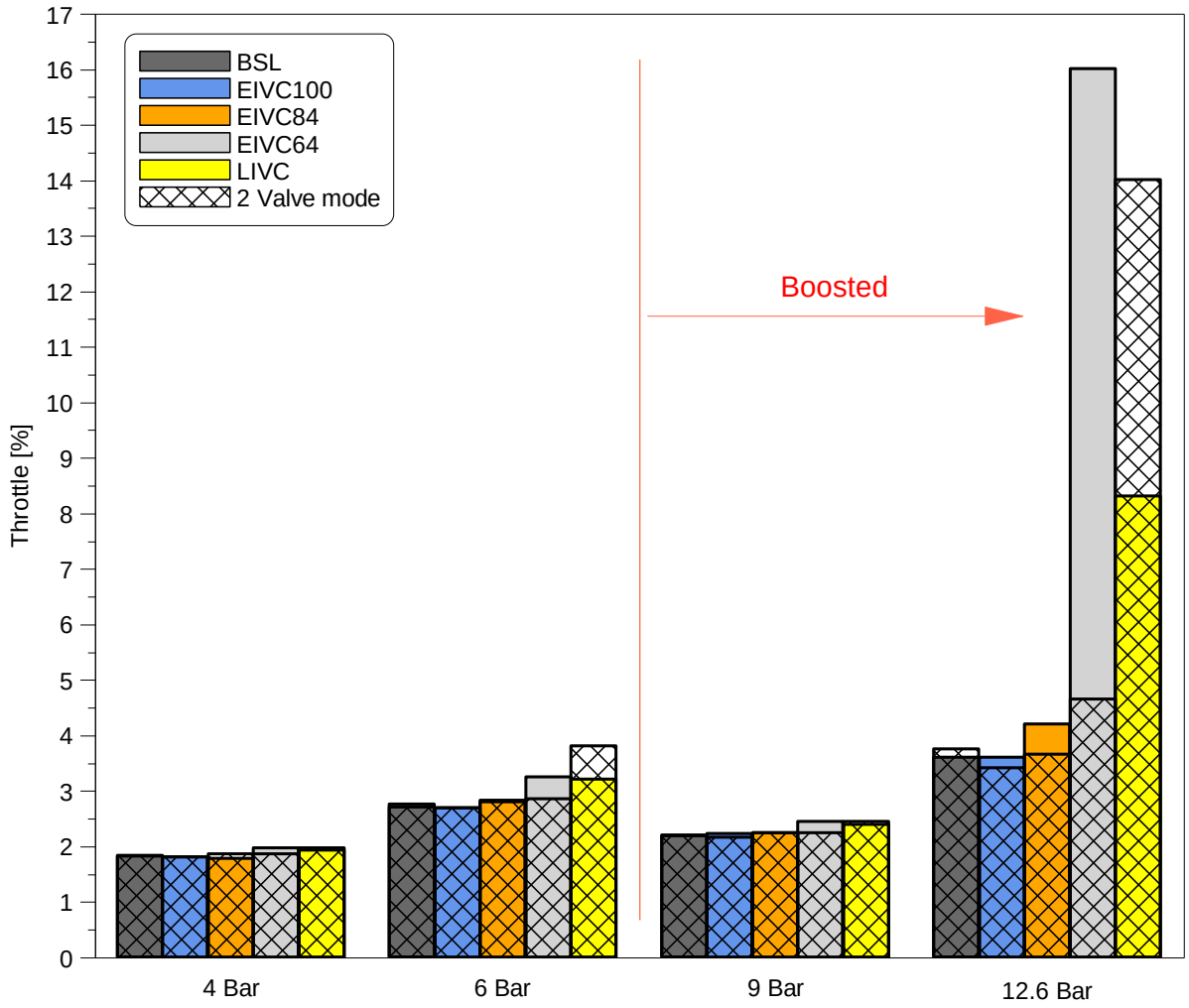

Figure 5.3 Throttle opening comparison between valve modes at various loads at 1500rpm

LIVC produced the lowest effective compression ratio across the whole load range. The single valve mode significantly increased ECR for LIVC almost at all load cases. The throttle angle was less than of two valve mode at 6 and 12.6bar as well as the intake pressure at loads above 4bar net IMEP. This can be explained by the fact that there was less air in the cylinder to be expelled back to the intake between BDC and IVC and smaller amount of charge was able to pass through single valve than two. Thus, the intake pressure decreased but more air was left in the cylinder leading to higher ECR than of the two valve mode.

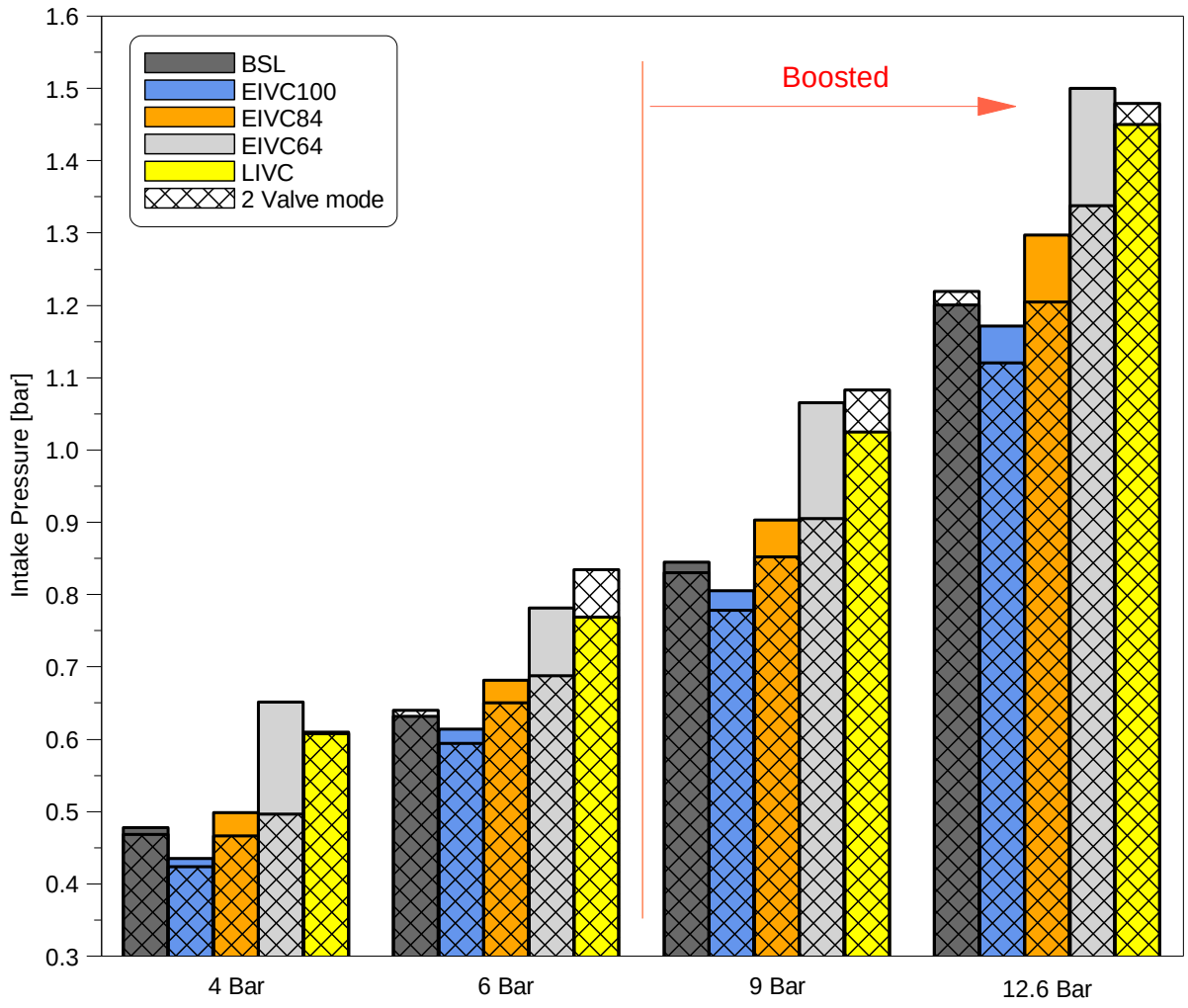

Figure 5.4 Intake pressure comparison between valve modes at various loads at 1500rpm

Comparison of PMEP between single and two valve mode is shown in Figure 5.5. The graph clearly demonstrates that single valve mode has increased pumping losses for all valve profiles across the whole range of load points. It is obvious that LIVC profile with single valve mode had the most negative effect on pumping losses due to reduced intake pressure compared to the one from the two valve mode, BSL profile had a smaller effect but the intake pressure was reduced not at all of the load cases. However, all EIVC profiles with single valve mode had intake pressure greater than that of two valve mode but produced higher pumping losses. This could be due to a decrease in discharge coefficient as the flow speed into the cylinder was increased with single valve mode, a similar effect as with reduction of valve lift for EIVC profiles from previous chapter.

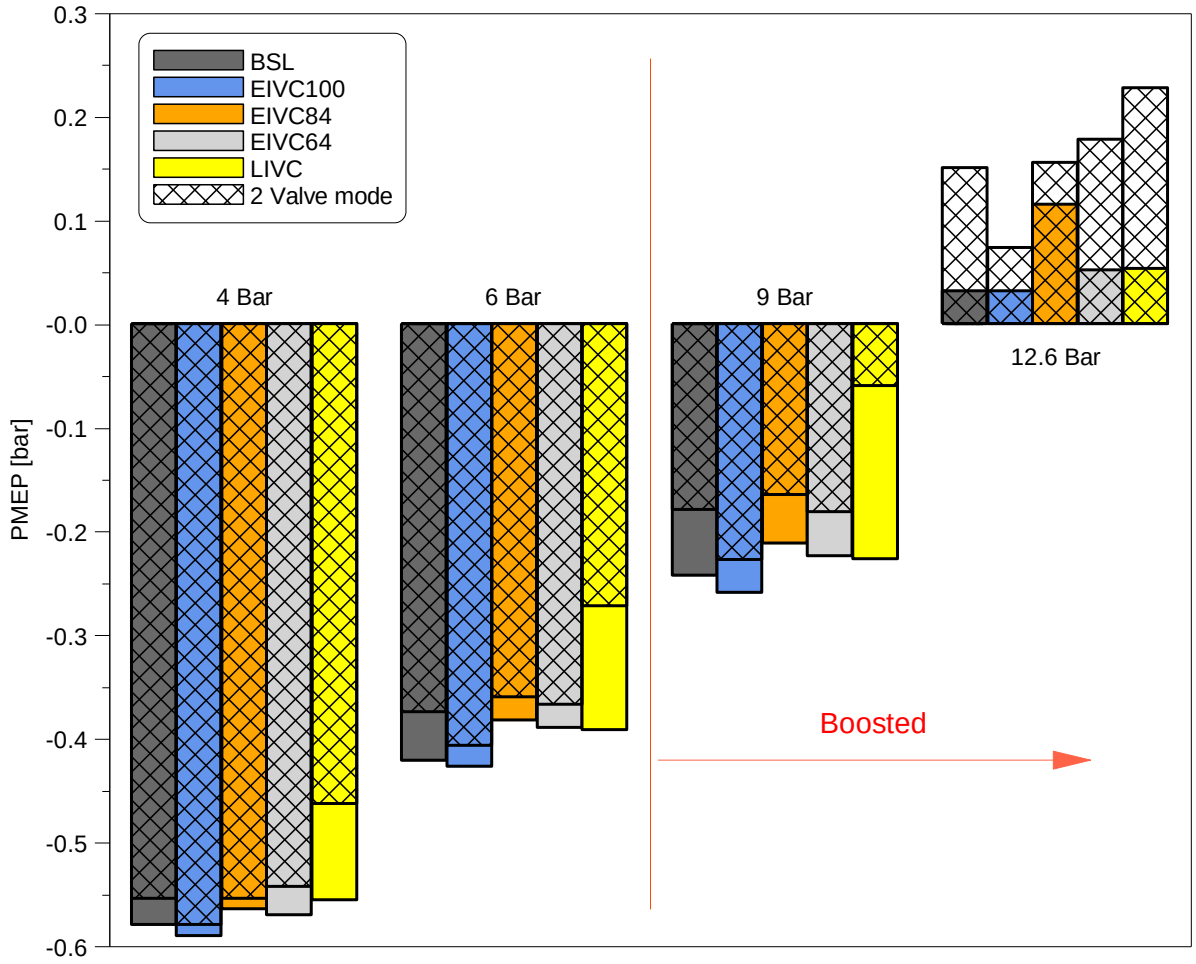

Figure 5.5 PMEP comparison between valve modes at various loads at 1500rpm

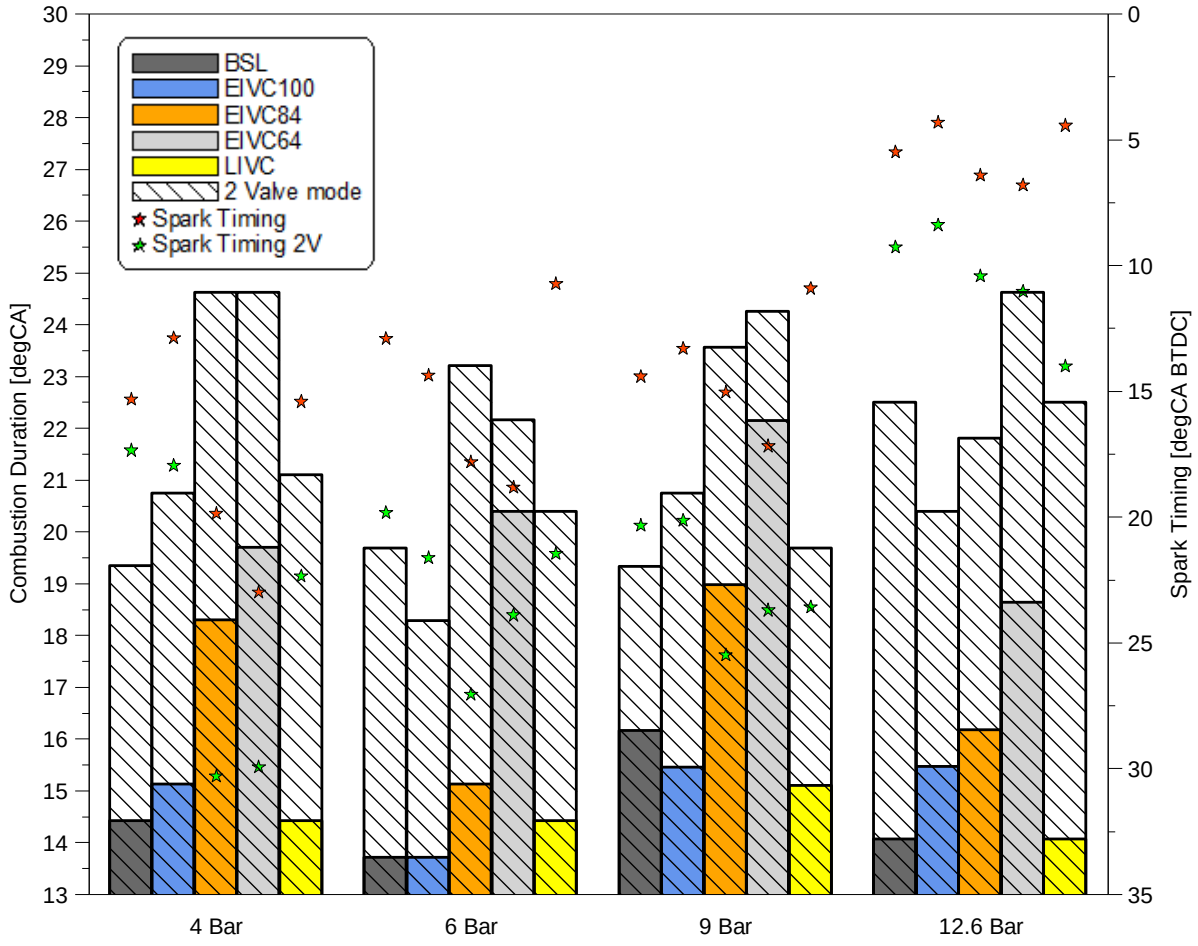

Figure 5.6 Combustion duration and spark timing comparison between valve modes at various loads at 1500rpm

Single valve mode also affected combustion duration and spark timing for each valve profile as can be seen in Figure 5.6. In general single valve mode produced significantly shorter combustion duration than those of the two valve mode. The MBT spark timing was retarded for all profiles with single valve mode due to smaller flame development angle than of two valve mode (Figure 5.7). All of these factors indicate that the single valve mode improved in-cylinder charge motion for all profiles across the whole load range. The shortest combustion durations were achieved mostly by LIVC and BSL profiles, whereas EIVC64 produced the longest durations indicating slower flame speed and reduced turbulence intensity. The MBT spark timing was advanced more for profiles with larger flame development angle except for EIVC100 at 4 and 12.6bar net IMEP. Single valve mode operations were characterised with shorter 10-50% burn duration throughout the load range, similar result was found for 50-90% burn duration except for EIVC64 at 9bar (Figure 5.8 and Figure 5.9). The trends for the first and second part of flame propagation period were similar, however at 9bar the 50-90% burn was significantly increased for BSL and EIVC profiles with short lifts.

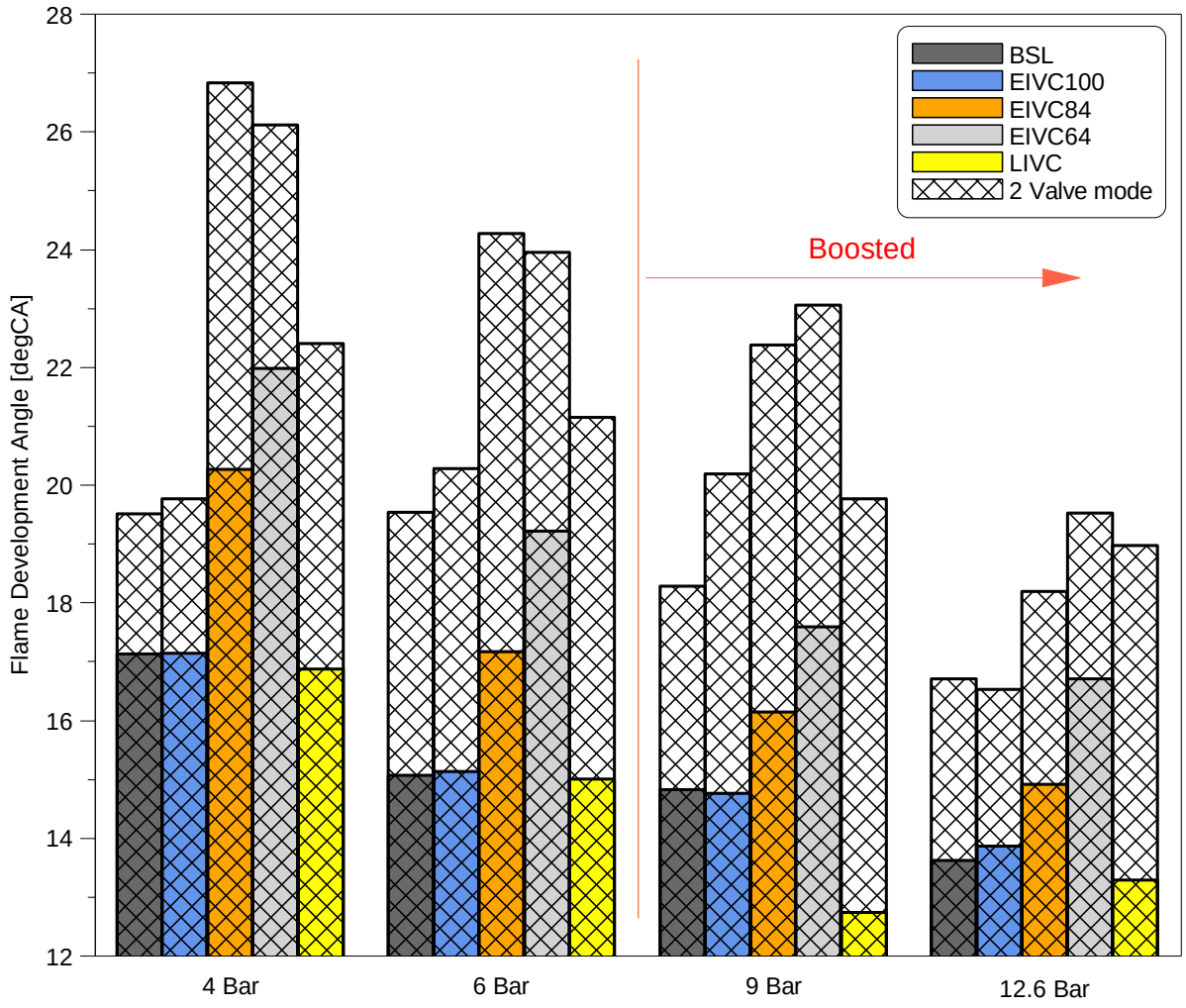

Figure 5.7 Flame development angle comparison between valve modes at various loads at 1500rpm

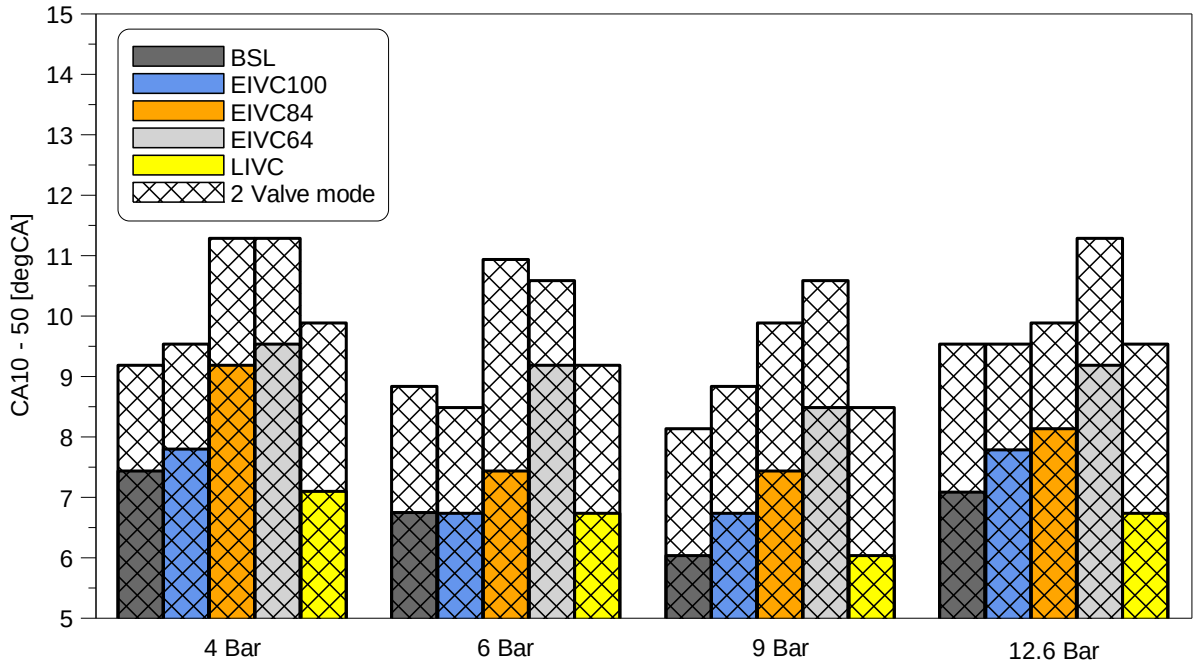

Figure 5.8 CA10-50 comparison between valve modes at various loads at 1500rpm

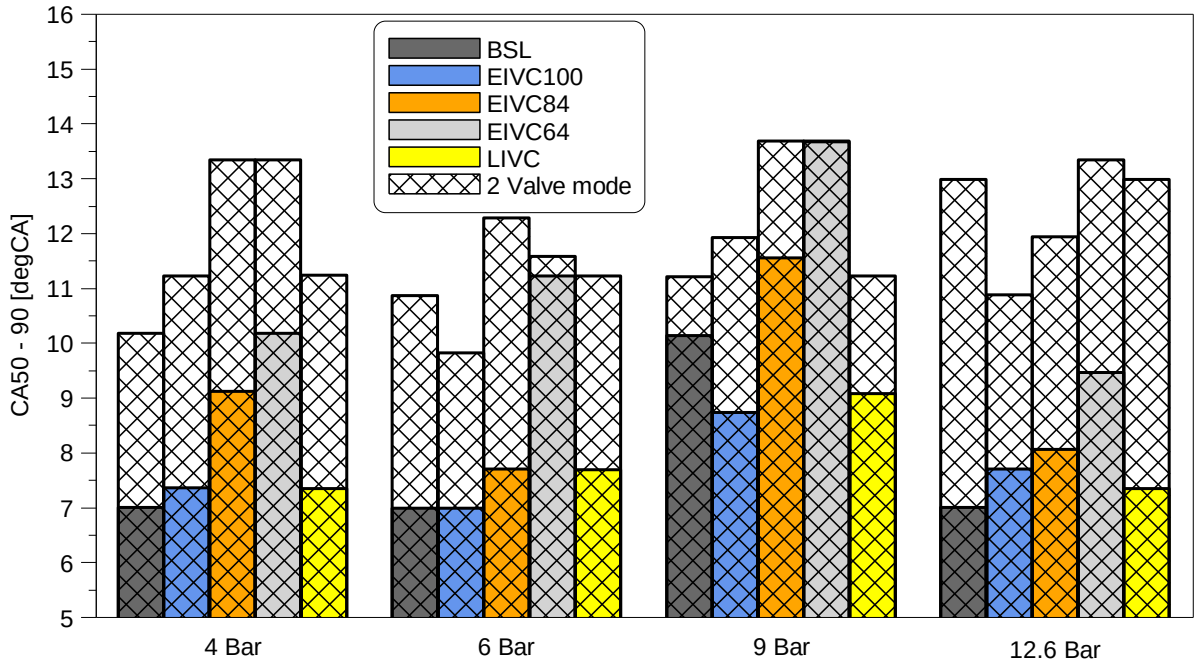

Figure 5.9 CA50-90 comparison between valve modes at various loads at 1500rpm

Single valve mode overall increased in-cylinder lambda for all valve profiles except at 12.6bar net IMEP as seen in Figure 5.10 indicating an improvement of in-cylinder charge mixing compared to 2 valve mode. Indicated specific fuel consumption was also affected by the single valve mode (Figure 5.11). At 4bar net IMEP EIVC profiles achieved lower fuel consumption with single valve mode due to shorter combustion duration and cylinder lambda being closer to stoichiometric. However, single valve baseline and LIVC profiles achieved higher ISFC than

that of 2 valve mode despite faster burning and close to stoichiometric lambda. The increase in PMEP had greater effect on the fuel consumption for these two profiles.

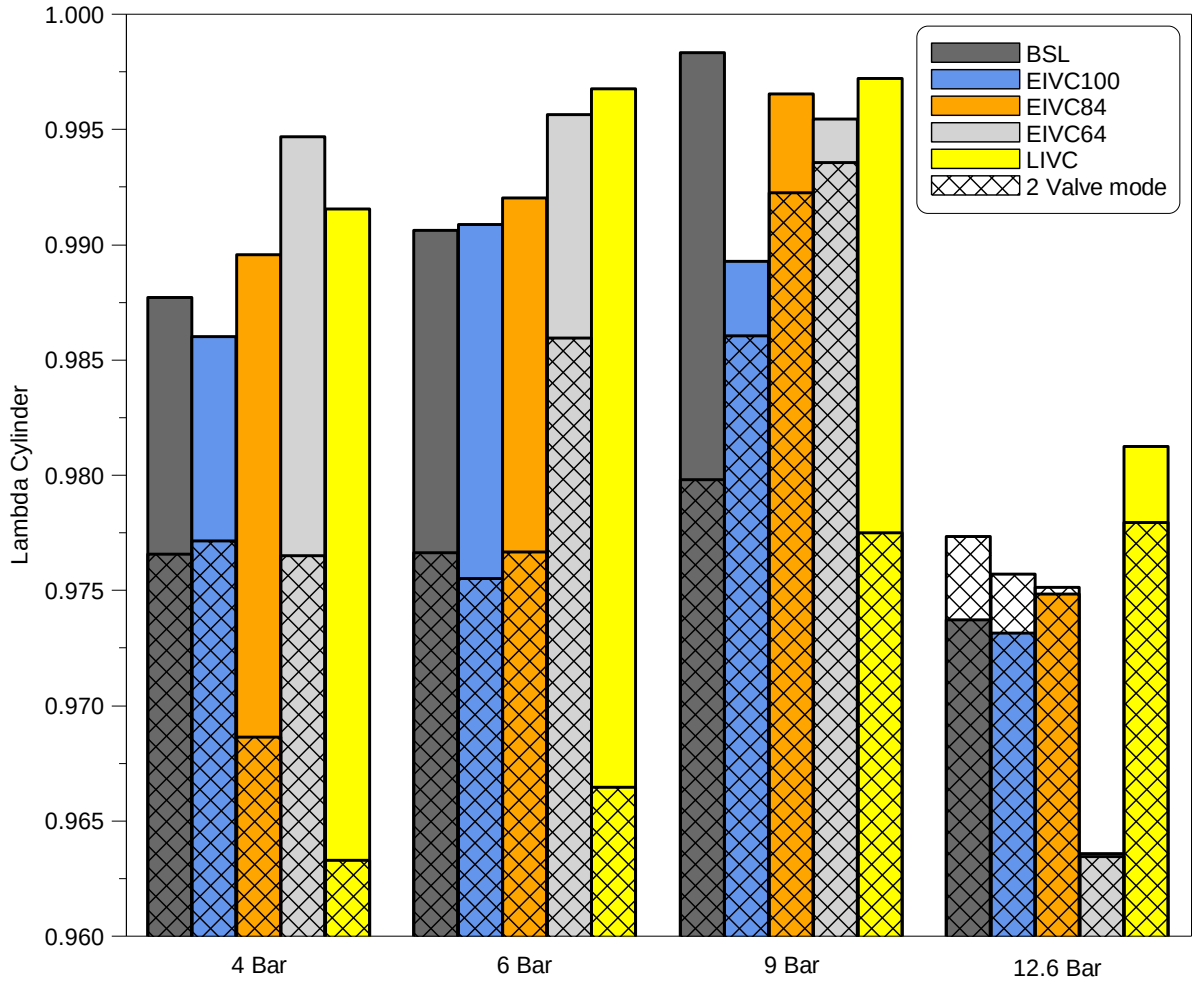

Figure 5.10 In-cylinder lambda comparison between valve modes at various loads at 1500rpm

At 6bar net IMEP all profiles with single valve mode achieved higher ISFC due to increased pumping losses which had greater effect than shorter combustion duration at this load. At 9 bar only BSL and LIVC with single valve mode achieved lower fuel consumption than 2 valve mode due to faster combustion and significantly increased cylinder lambda. At 12.6bar all single valve profiles had higher ISFC than those with 2 valve mode except for the baseline due to shorter combustion.

From the above results it is evident that single valve mode improves in-cylinder turbulence and charge mixing while reducing the combustion duration, however it increases pumping losses. Both of these factors affect fuel consumption and there is a trade off when one of those will be more significant than the other. In case with the above experiments shorter combustion duration allowed to reduce ISFC for single valve EIVC profiles at low load, BSL and LIVC at 9bar and BSL at 12.6 bar.

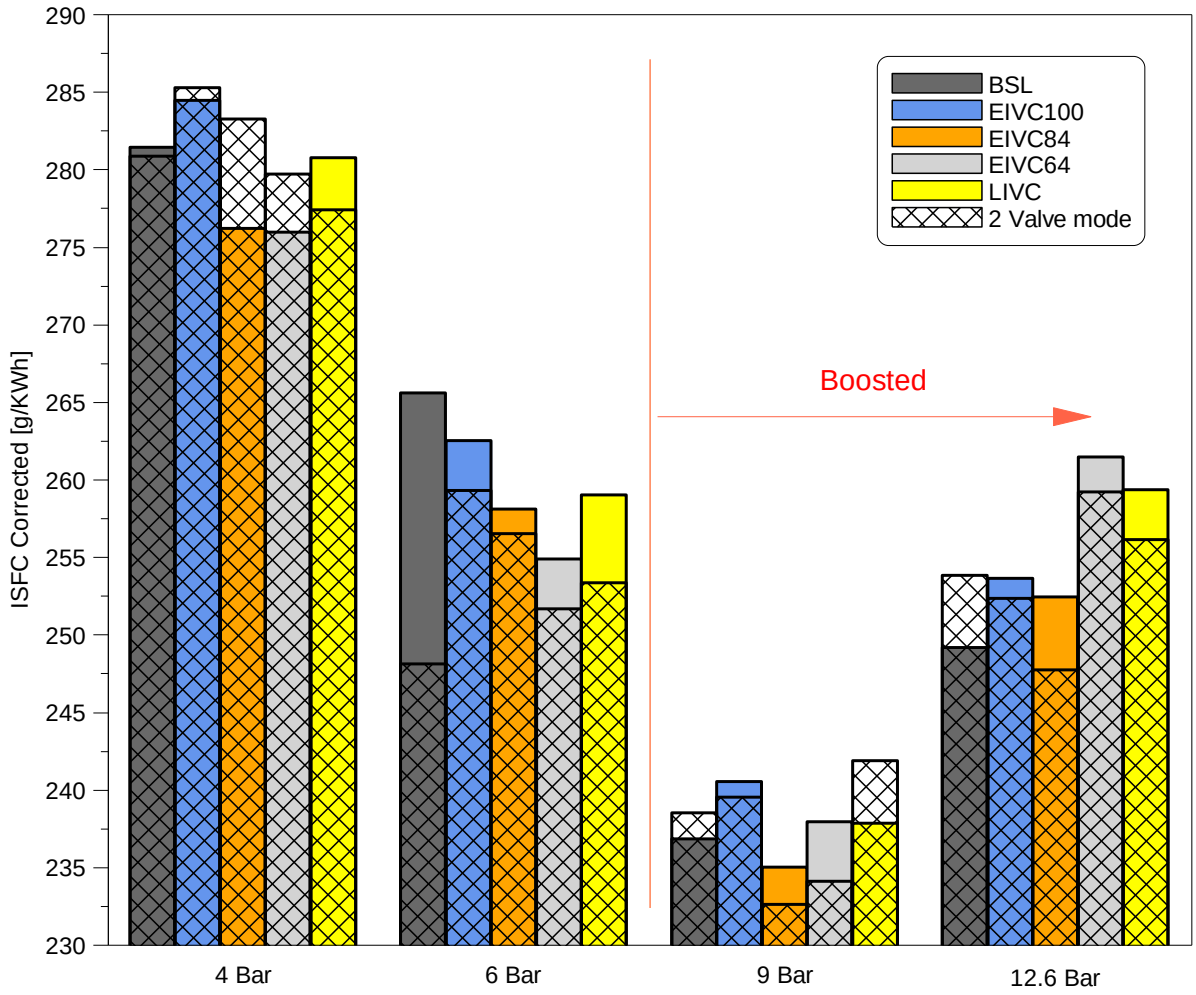

Figure 5.11 ISFC corrected comparison between valve modes at various loads at 1500rpm

Comparison of emissions between single and two valve mode is shown in Figure 5.12, Figure 5.13 and Figure 5.14. Throughout all load cases higher concentration of ISCO was present with lower in-cylinder lambda i.e. combustion of fuel rich mixture. As single valve mode increased cylinder lambda for all profiles from 4 to 9bar net IMEP the CO emissions were lower compared to the two valve mode. At 12.6 bar only LIVC with single valve mode had cylinder lambda increased, thus it was the only profile to achieve lower CO emissions compared to two valve mode. Overall single valve LIVC profile produced lower ISCO emissions among other profiles throughout the whole load range.

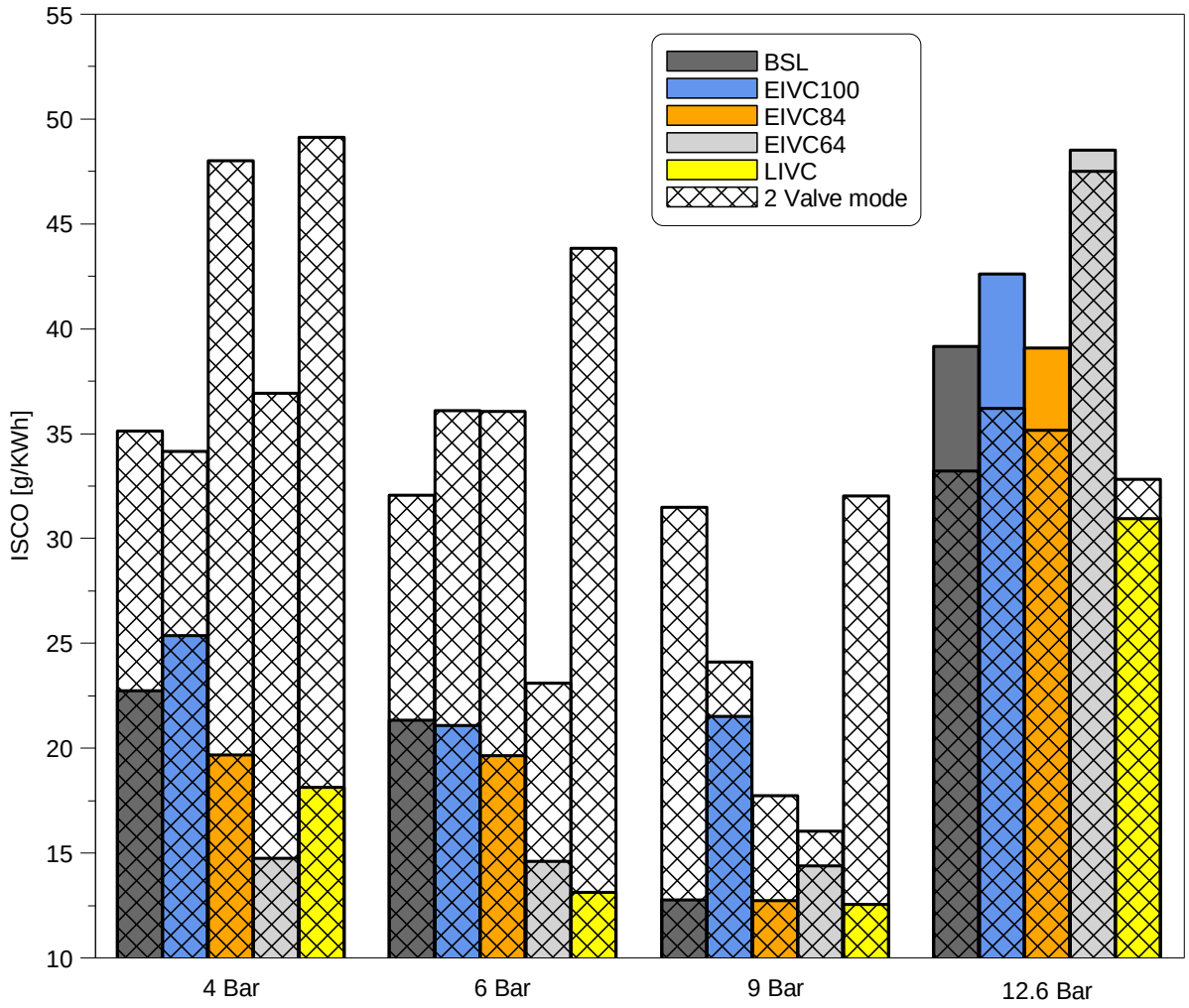

Figure 5.12 ISCO emission comparison between valve modes at various loads at 1500rpm

Overall, single valve mode resulted in lower HC emissions than those of two valve mode operations thanks to faster combustion which reduced bulk quenching at the cylinder wall allowing for more complete combustion. At 4bar net IMEP the lowest level of ISHC among single valve profiles was achieved by the baseline profile due to the shortest combustion duration, the LIVC profile had similar combustion duration but due to the highest in-cylinder pressure during combustion achieved the highest HC emissions. At 6bar net IMEP the lowest ISHC was achieved by single valve LIVC profile due to fast flame speed and the lowest in-cylinder pressure during compression and combustion strokes. At 9bar net IMEP single valve EIVC100 provided lowest ISHC of 4.5 g/KWh due to fast combustion and lower than LIVC and BSL in-cylinder pressure during combustion which reduced quenching at the cylinder wall. At 12.6bar net IMEP lowest HC emissions were achieved by single valve EIVC64 profile due to the lowest in-cylinder pressure during combustion stroke. Overall HC emissions were reduced with load except at 12.6bar where spark timings were significantly retarded due to knocking combustion.

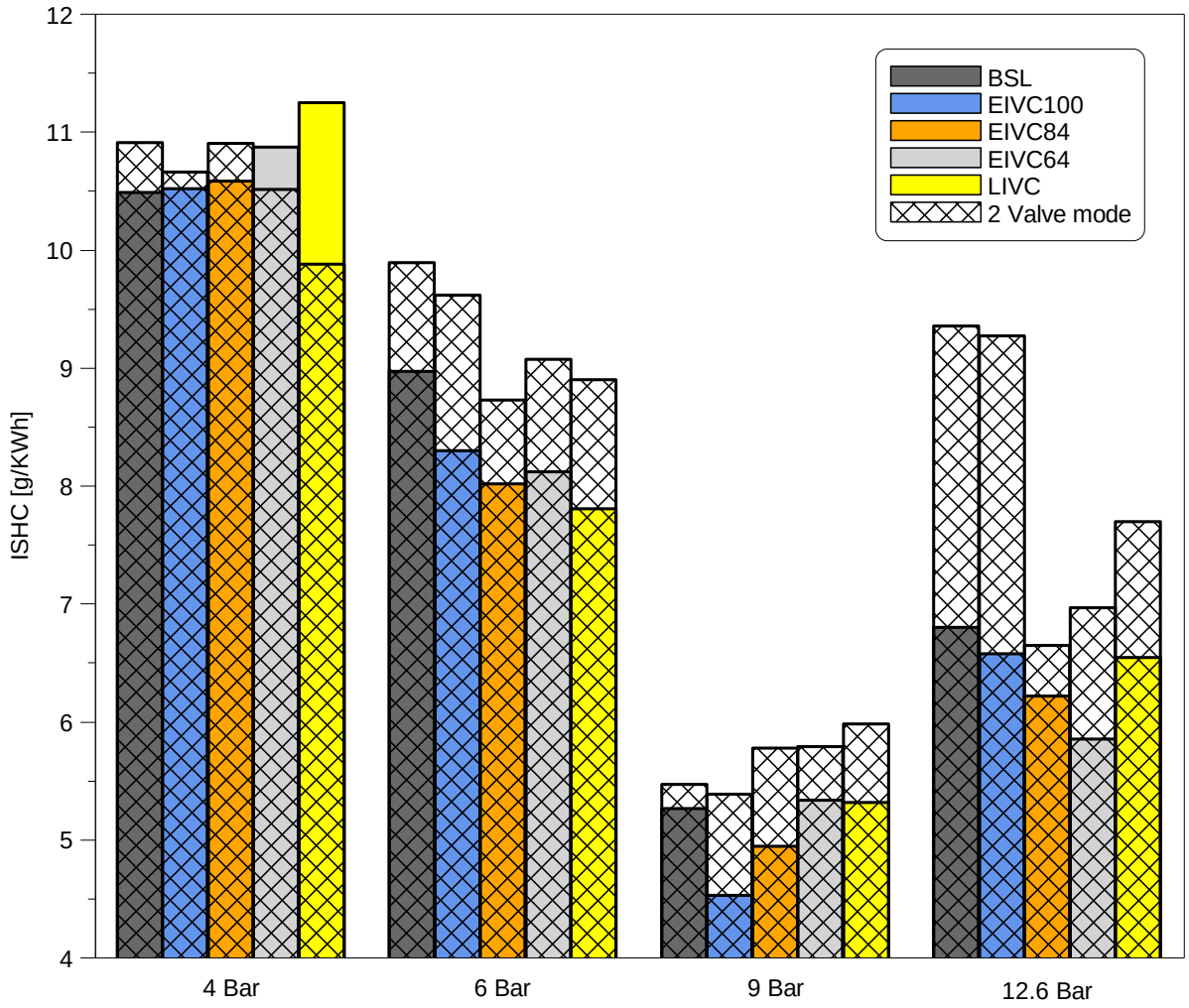

Figure 5.13 ISHC emission comparison between valve modes at various loads at 1500rpm

NO_X emissions were increased with single valve mode throughout the load range due to higher in-cylinder pressure during combustion compared to profiles with two valve mode, which led to the highest peak combustion temperatures. Lowest NO_X level at 4bar net IMEP among single valve profiles were produced by EIVC100 and 84 due to lower in-cylinder pressures during combustion compared to the rest of the single valve profiles. At 6bar net IMEP LIVC achieved the lowest NO_X among other single valve profiles due to the lowest in-cylinder pressure during expansion stroke and the most retarded MBT spark timing which provided lower rate of temperature increase during combustion. Single valve EIVC100 provided the highest in-cylinder pressure, thus the highest $ISNO_X$ concentration. A similar result was achieved at 9bar, where EIVC84 had the lowest in-cylinder pressure during combustion leading to the lowest NO_X among single valve profiles and BSL profile had the highest in-cylinder pressure during combustion which led to the highest NO_X emissions at this load. All of those factors led to very low $ISNO_X$ emissions compared to the other profiles. EIVC64

achieved the lowest NO_X among single valve profiles due to significantly lower in-cylinder peak pressure which led to the lowest temperatures during the expansion stroke.

Overall, single valve mode aided in reduction of ISCO emissions up to 9bar and ISHC after 6bar net IMEP, however it had an adverse effect on $ISNO_X$ concentration throughout the load range.

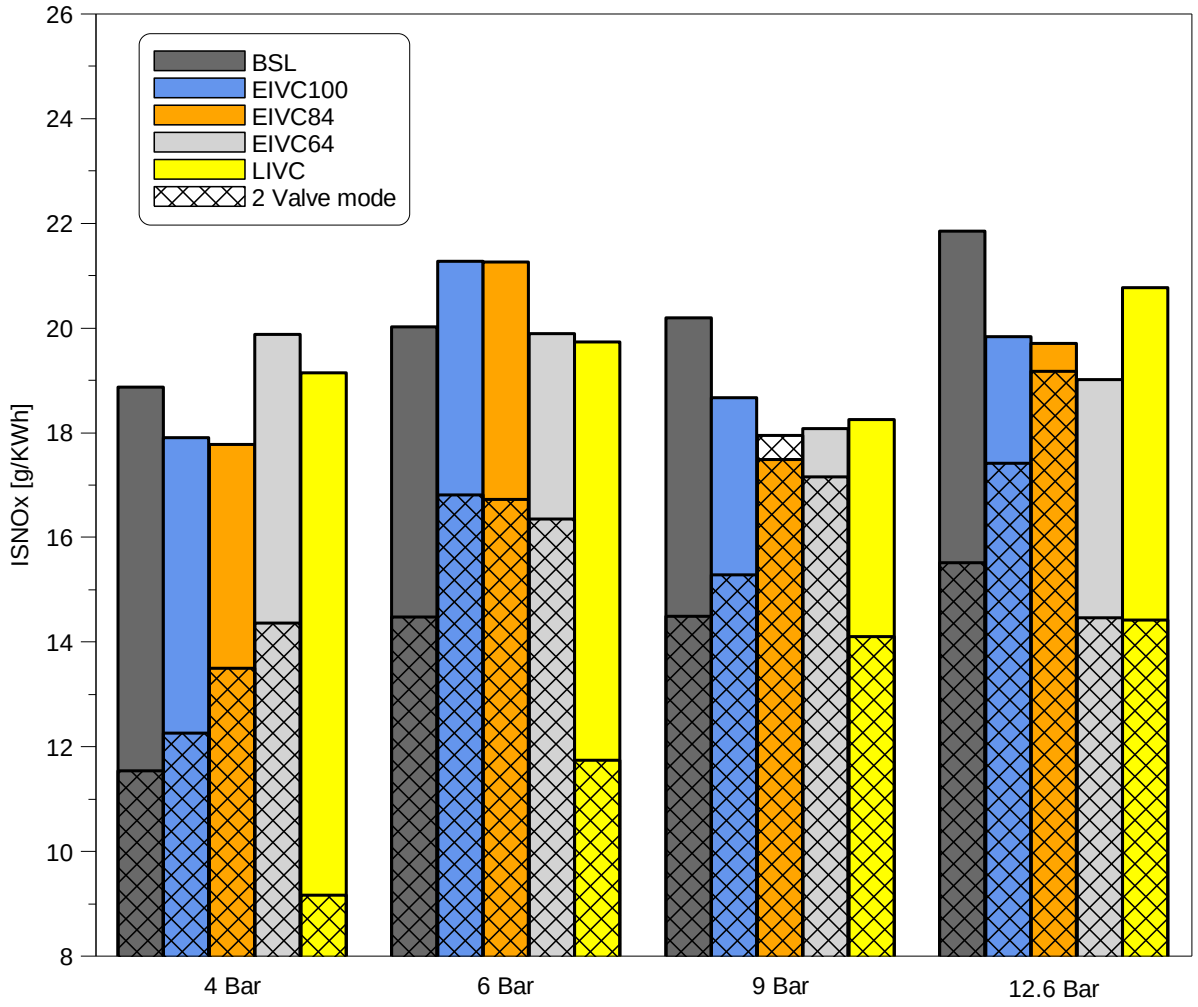

Figure 5.14 $ISNO_X$ emission comparison between valve modes at various loads at 1500rpm

5.2.2 Test results at 3000rpm

The effect of single valve operation on ECR and throttle angle are shown in Figure 5.15 and Figure 5.16. Overall, single valve mode increased effective compression ratio for BSL and LIVC profiles, while reducing it for EIVC64. The highest ECR of 10.8 throughout the whole load range was found from the baseline profile with single valve mode. The throttle position of this profile was almost identical to two valve mode, however the intake pressure was slightly lower for single valve mode (Figure 5.17) indicating that less charge is being pushed out of the cylinder before IVC. This was due to higher inertia which allowed to fill the cylinder with

air even after BDC causing less charger to escape back to the intake manifold resulting in higher ECR than two valve mode. Single valve LIVC profile had a similar effect, where throttle angle was similar to two valve mode (except at 12.6bar) but the intake pressure was lower as smaller amount of charge was able to pass through single valve than two after BDC.

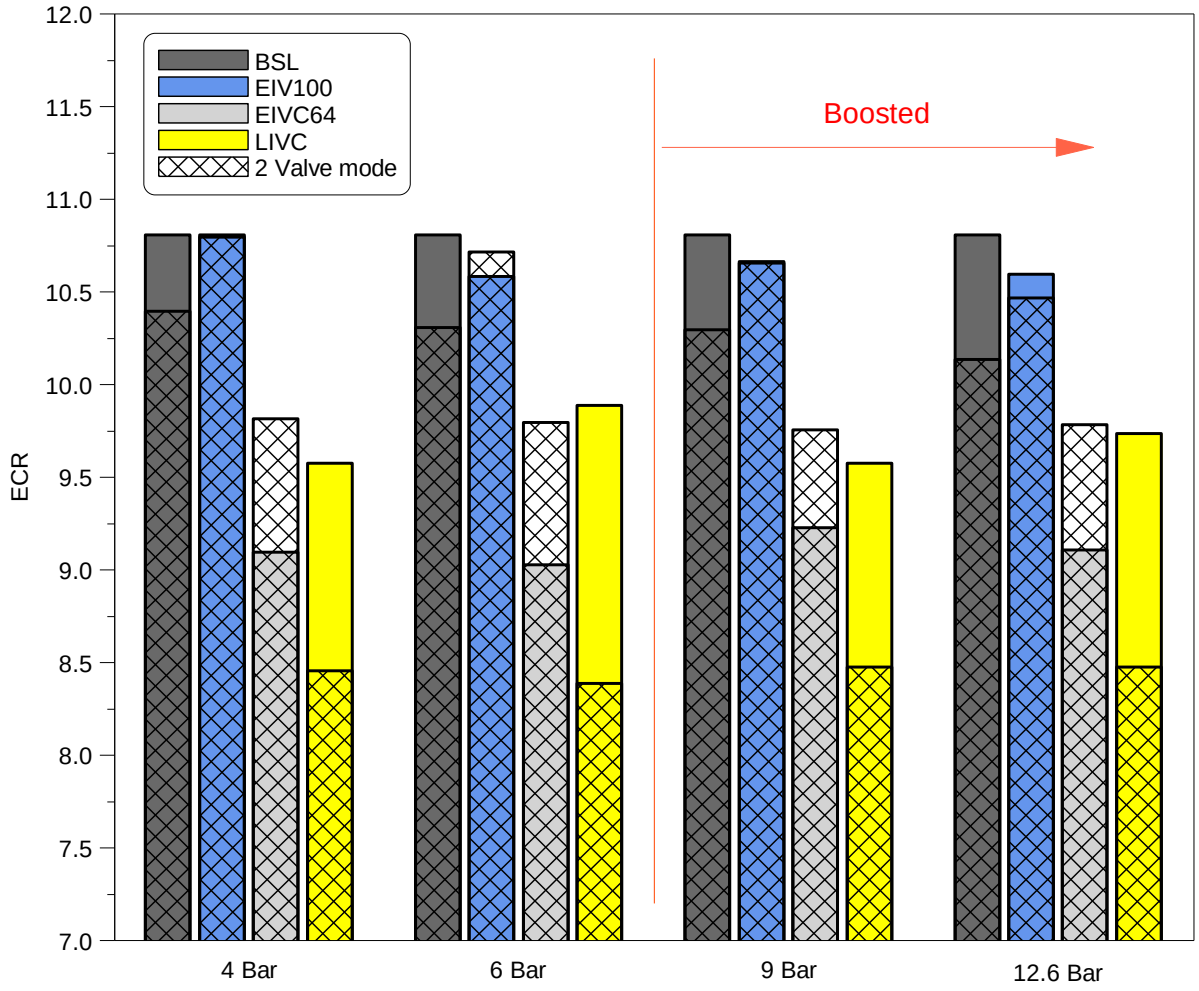

Figure 5.15 ECR comparison between valve modes at various loads at 3000rpm

EIVC64 with single valve achieved lower ECR than two valve mode at all load points. The intake pressure was higher than for two valve mode across the whole load range. Throttle angle was higher at 4bar and 9bar net IMEP, however at 6bar throttle angle was lower as additional boost of 0.6bar was used to achieve this load with single valve mode, at 12.6bar higher boost (1.1bar) was required for single valve mode to achieve the load therefore throttle angle was lower. The intake pressure was increased due to larger throttle angle or higher boost. However, there was not enough time to allow the cylinder to be filled with enough air to maintain the same ECR as with 2 valve mode.

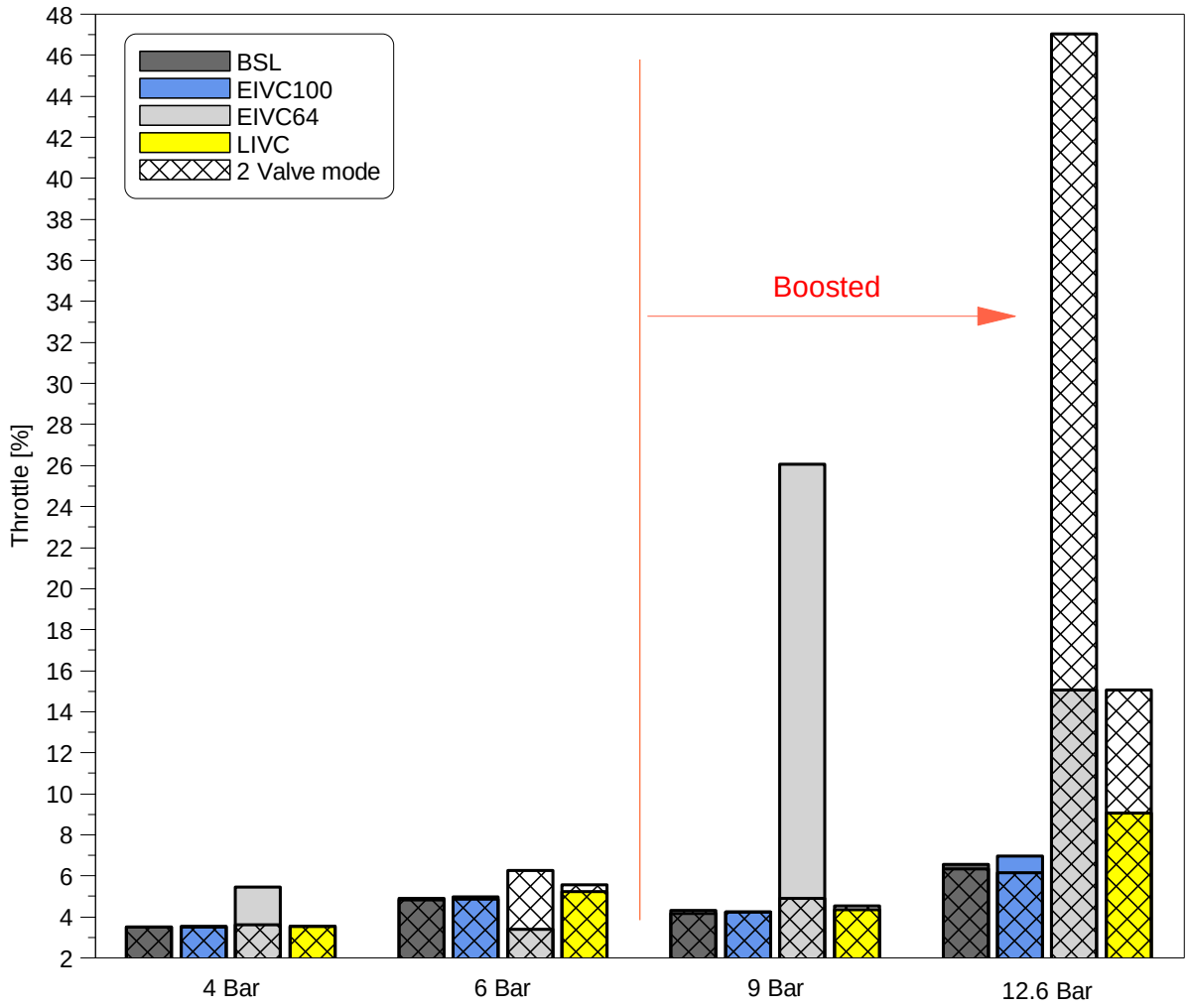

Figure 5.16 Throttle opening comparison between valve modes at various loads at 3000rpm

EIVC100 achieved similar ECRs and throttle angles between the valve modes. The intake pressure was increased for the single mode due to larger pressure drop at IVO.

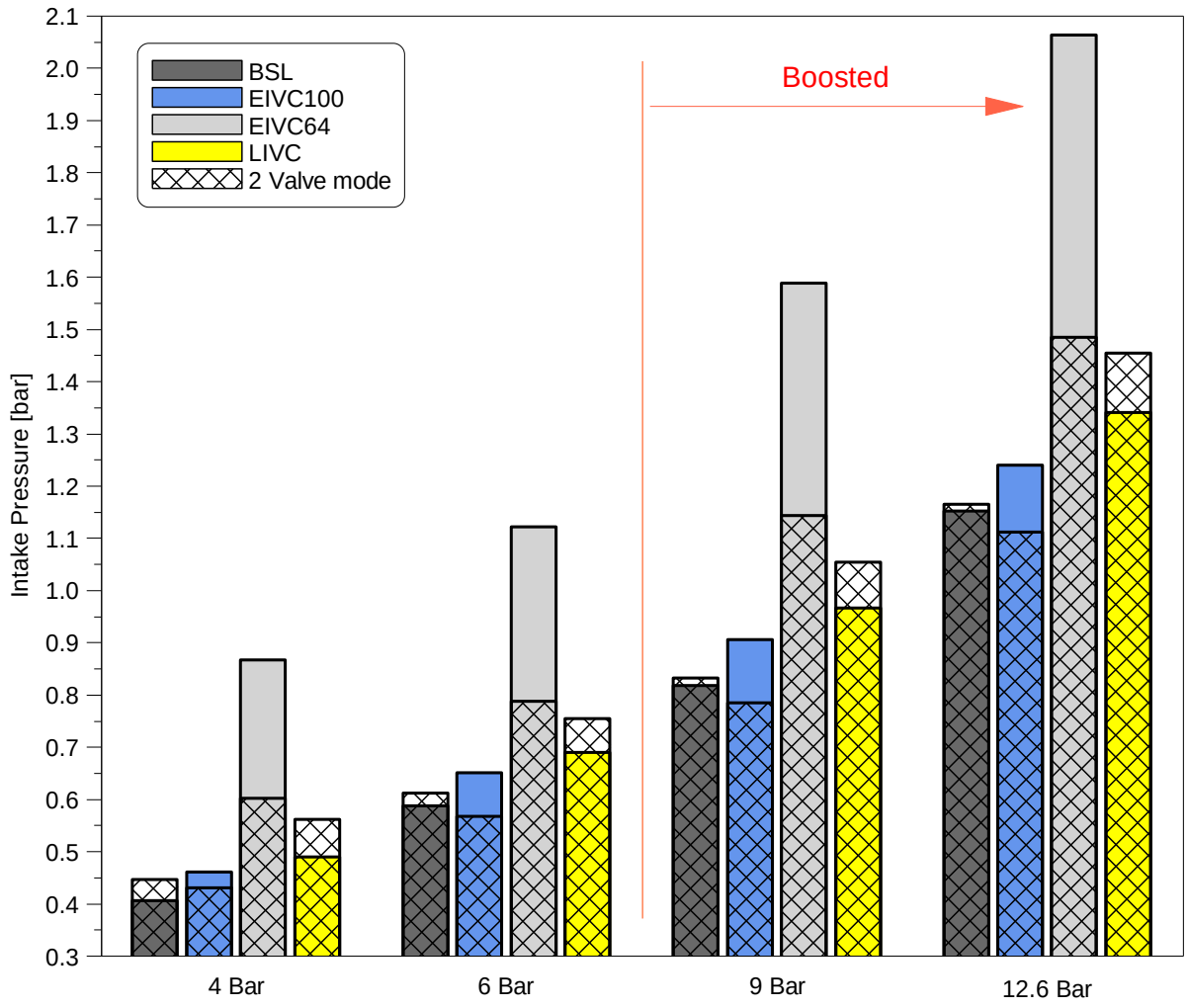

Figure 5.17 Intake pressure comparison between valve modes at various loads at 3000rpm

Comparison of PMEP between single and two valve mode is shown in Figure 5.18. Similarly to results at 1500rpm the single valve mode has increased pumping losses for all valve profiles across the whole range of load points at 3000rpm. LIVC profile with single valve mode had the most negative effect on pumping losses due to reduced intake pressure. BSL profile had a smaller effect as the intake pressure was reduced less than for LIVC. EIVC100 with single valve mode had intake pressure slightly greater than that of two valve mode but achieved higher pumping losses due to a decrease in discharge coefficient. Single valve EIVC64 profile had the least negative effect on PMEP due to largely increased intake pressure, however the decrease in discharge coefficient caused higher pumping losses than those from two valve mode.

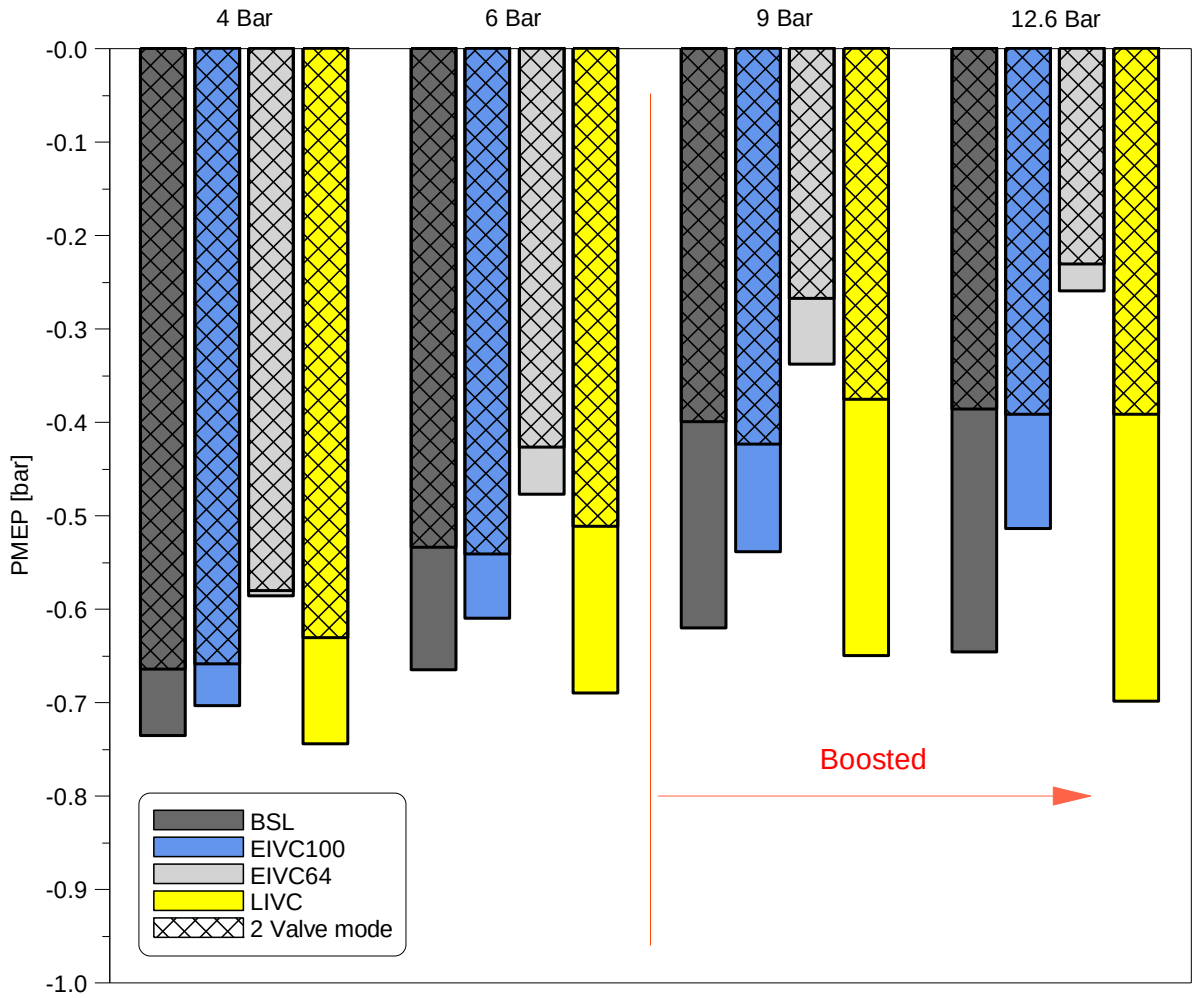

Figure 5.18 PMEP comparison between valve modes at various loads at 3000rpm

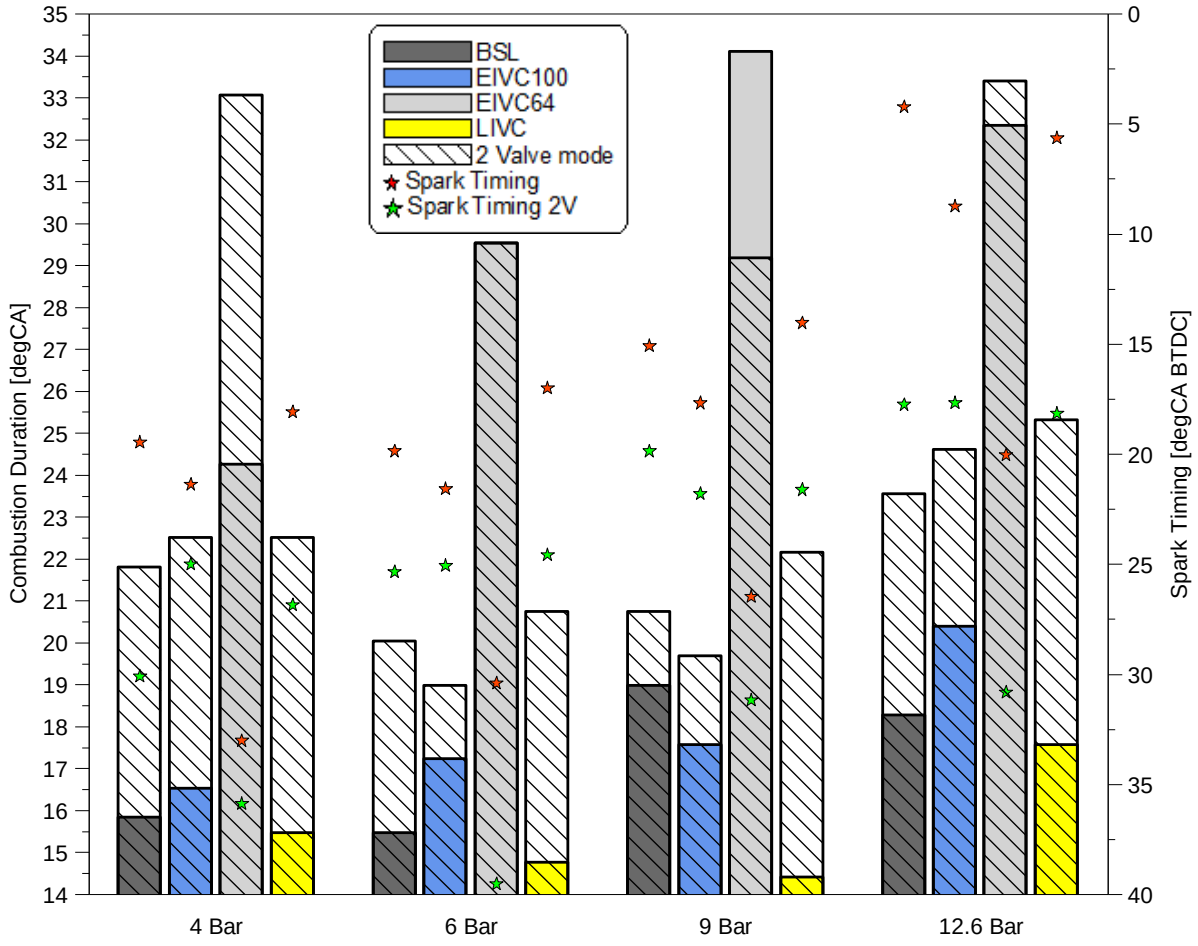

Figure 5.19 Combustion duration and spark timing comparison between valve modes at various loads at 3000rpm

Single valve mode overall reduced combustion duration for each valve profile except for EIVC64 at 6 and 9bar net IMEP as can be seen in Figure 5.19. As well as combustion duration the flame development angle was also reduced for all profiles with single valve mode (Figure 5.20), which led to retarded MBT spark timing. All of these factors indicate that there is an increase of in-cylinder turbulence for all profiles across the whole load range thanks to single valve mode. LIVC profile with single valve mode provided the shortest combustion durations, whereas EIVC64 produced the longest durations indicating slower flame speed and reduced turbulence intensity compared to other single valve modes. The MBT spark timing was advanced more for profiles with larger flame development angle except for BSL at 12.6bar net IMEP where spark timing was knock limited. The 10-50% burn was shorter for profiles with single valve mode throughout the load range as seen in Figure 5.21, similar result was for 50-90% burn except for EIVC64 above 4bar (Figure 5.22). The trends for the first and second part of flame propagation period were similar, however at 6bar and 9bar the 50-90% burn was significantly increased EIVC64 and a slight increase at 9bar for BSL and at 12.6bar for EIVC100.

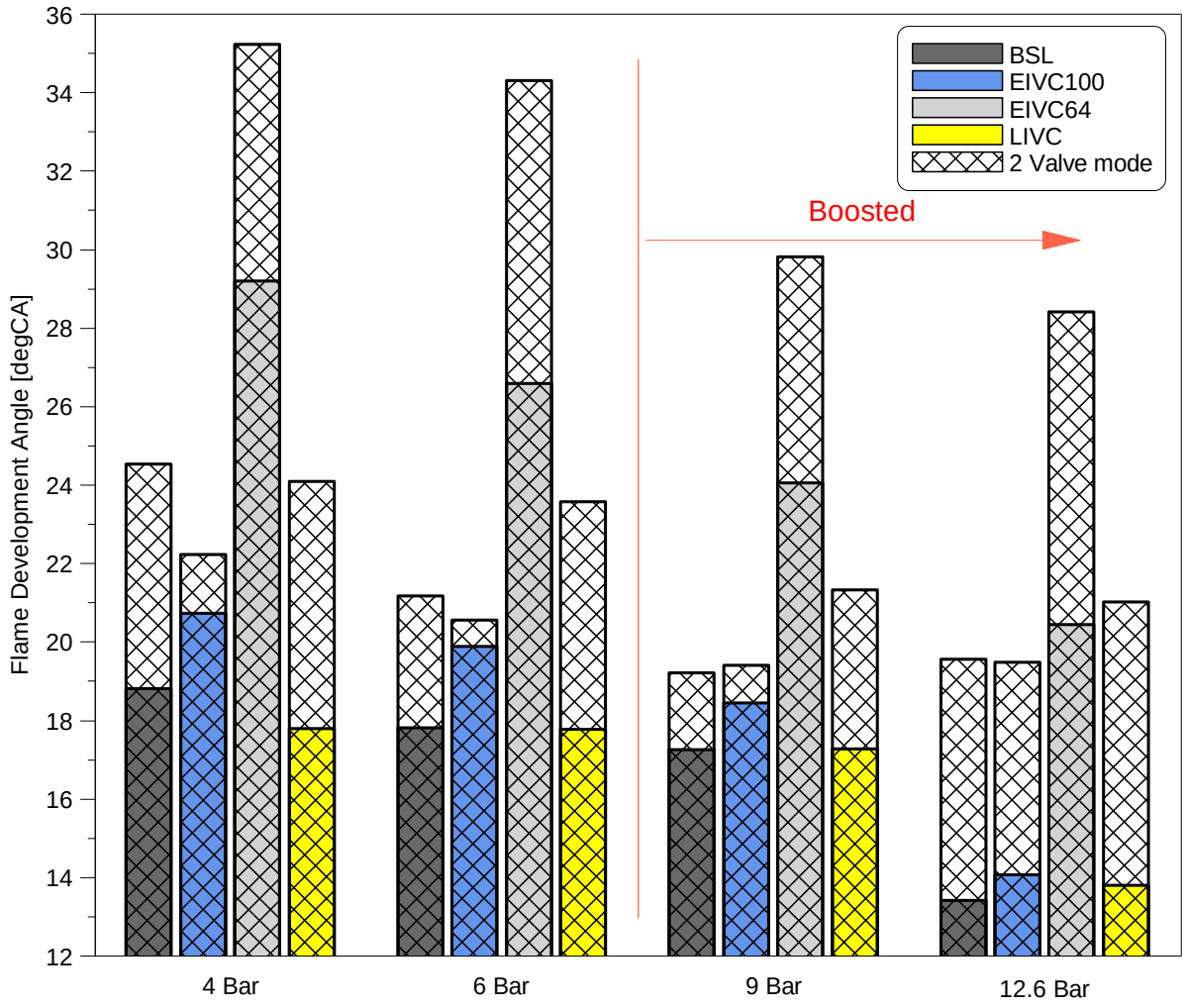

Figure 5.20 Flame development angle comparison between valve modes at various loads at 3000rpm

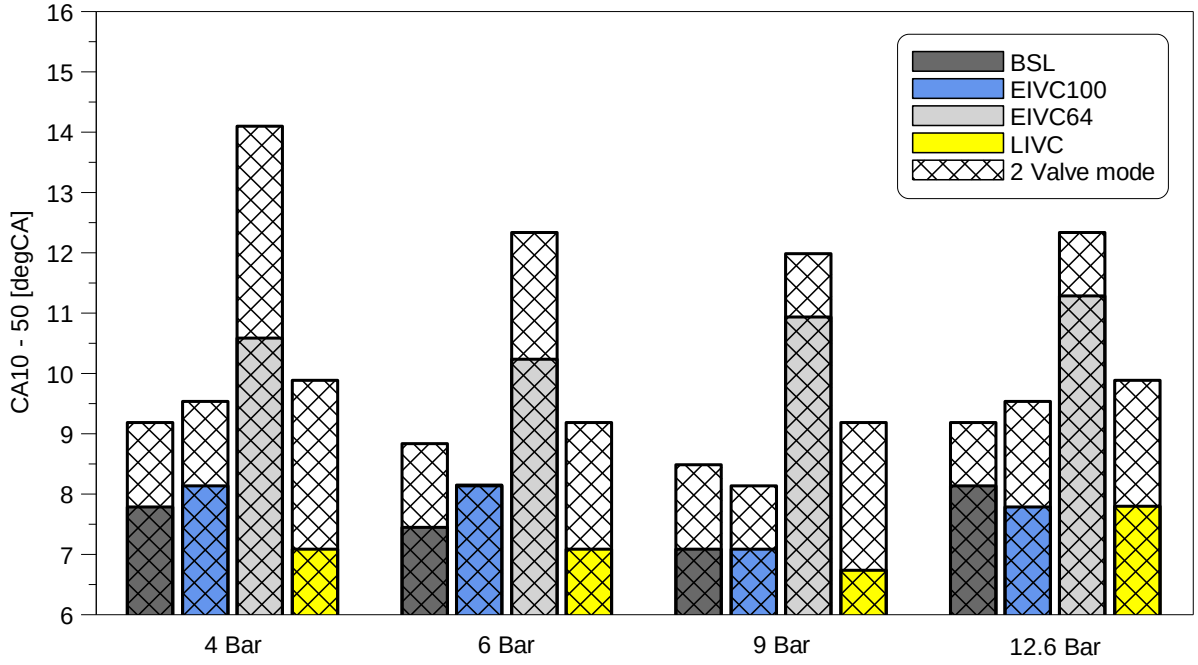

Figure 5.21 CA10-50 comparison between valve modes at various loads at 3000rpm

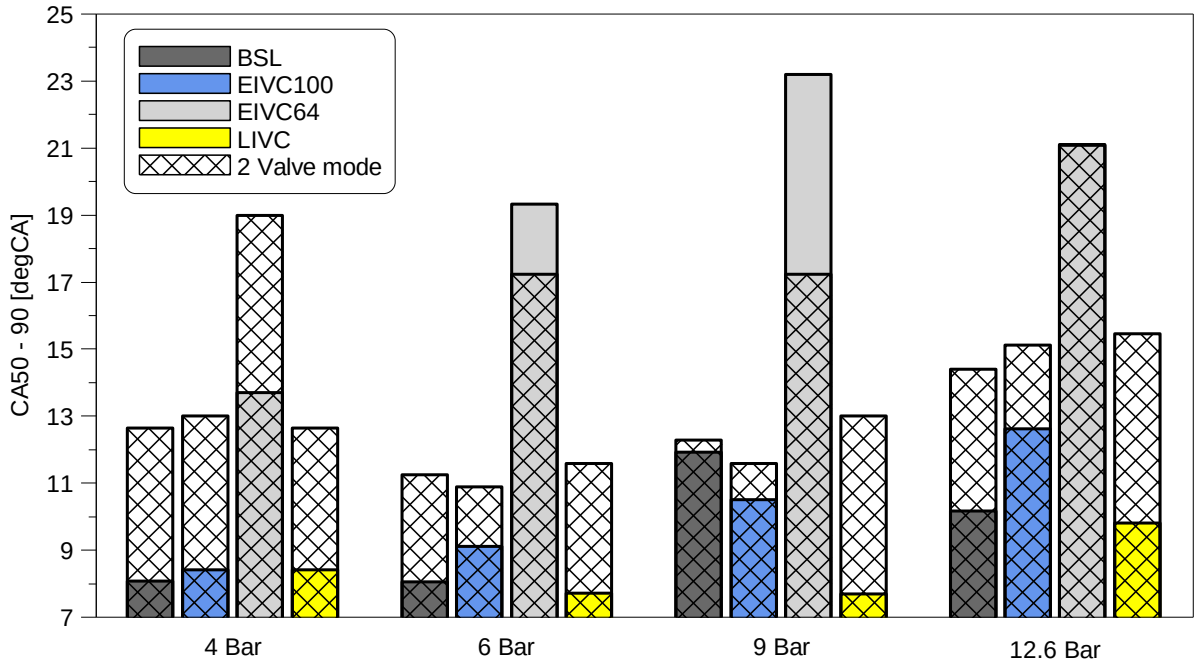

Figure 5.22 CA50-90 comparison between valve modes at various loads at 3000rpm

Like at 1500rpm, single valve mode significantly increased in-cylinder lambda for all profiles across the whole load range, at some load cases lambda was slightly above 1 as seen in Figure 5.23. This indicates that in-cylinder charge mixing was improved compared to 2 valve mode.

Figure 5.24 demonstrates comparison of ISFC between the valve modes taking into account power required for the supercharger. At 4bar net IMEP single valve EIVC64 profile achieved the lowest fuel consumption due to low pumping losses, shorter combustion duration and increased cylinder lambda. Similarly, BSL and EIVC100 had reduced fuel consumption with single valve mode but due to higher pumping losses their ISFC values were greater than EIVC64. Single valve LIVC profile achieved higher ISFC than that of 2 valve mode due to the lowest PMEP value.

At 6bar net IMEP only EIVC100 with single valve mode provided lower ISFC than that of two valve mode due to shorter combustion duration and increased lambda. For other single valve profiles increased pumping losses had greater effect than shorter combustion duration and increased lambda resulting in increased fuel consumption compared to two valve mode.

At 9bar EIVC64 with single valve mode achieved lower fuel consumption than 2 valve mode due to increased cylinder lambda, despite longer combustion duration and greater pumping losses.

At 12.6bar all single valve profiles had lower ISFC than those with 2 valve mode due to shorter combustion and significantly increased cylinder lambda. The lowest fuel consumption was provided by EIVC100 thanks to short combustion duration, low pumping losses and close to stoichiometric cylinder lambda.

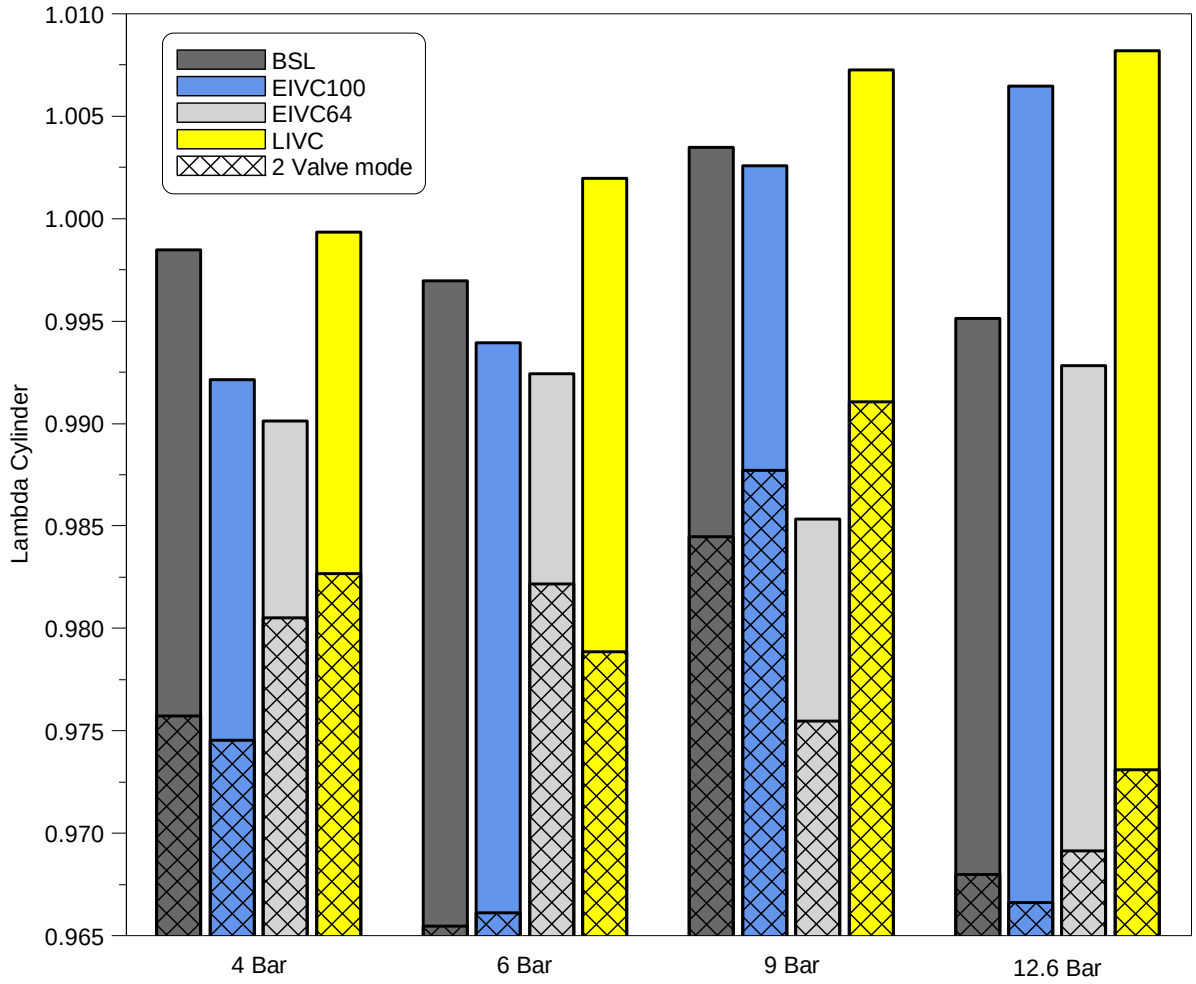

Figure 5.23 In-cylinder lambda comparison between valve modes at various loads at 3000rpm

Similarly to 1500rpm, the above results demonstrate that single valve mode improves in-cylinder turbulence and charge mixing while reducing the combustion duration at a cost of increased pumping losses. Those factors affect fuel consumption and there is a trade off when one of them will be more significant than the other. In case with experiments at 3000rpm shorter combustion duration and increased lambda allowed to reduce ISFC for most of the single valve profiles at 4 and 12.6bar net IMEP.

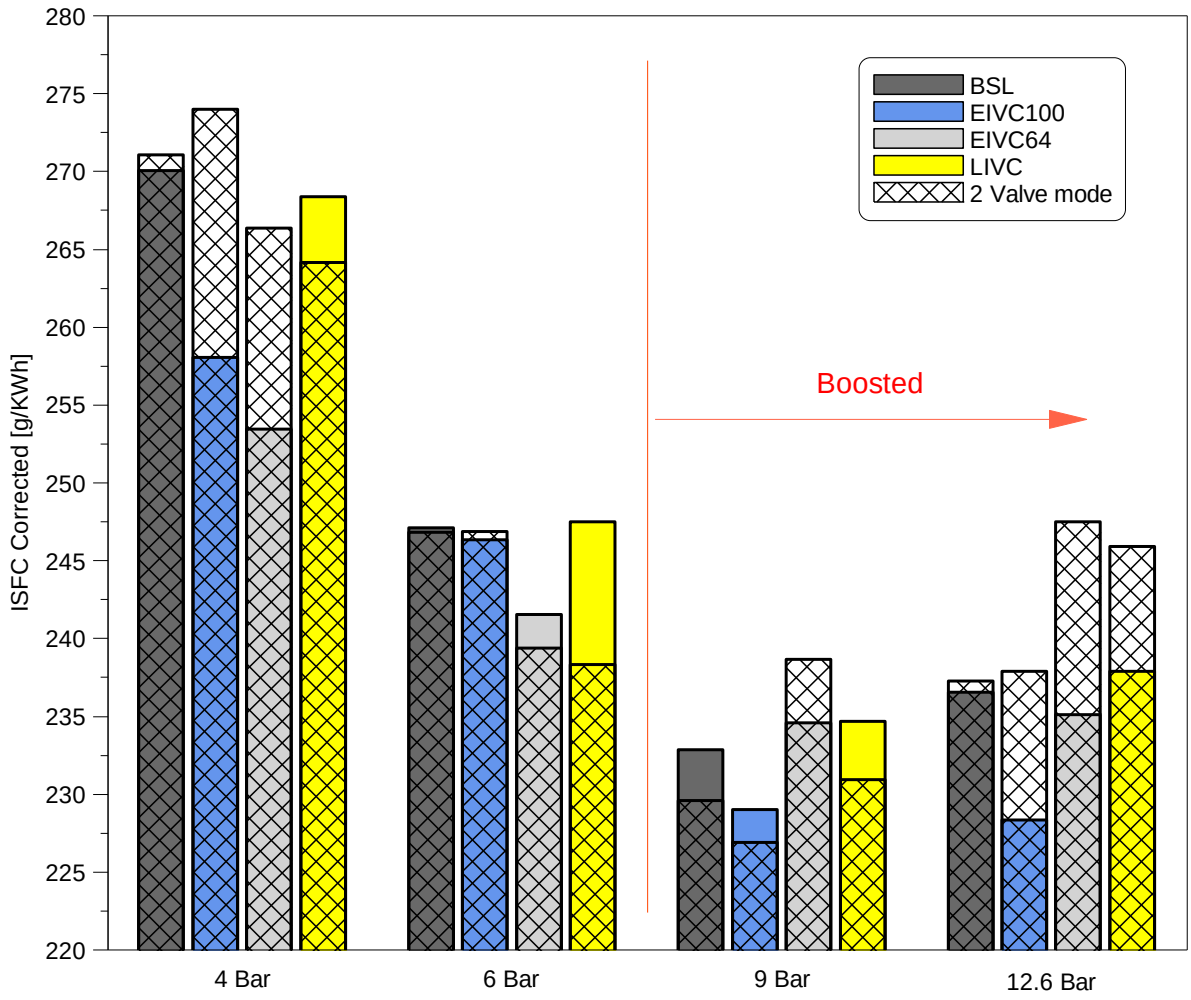

Figure 5.24 ISFC corrected comparison between valve modes at various loads at 3000rpm

Comparison of emissions between single and two valve mode is shown in Figure 5.25, Figure 5.26 and Figure 5.27. Single valve profiles produced lower ISCO than two valve profiles due to increased cylinder lambda throughout the load range. Among single valve profiles, at each load case the highest concentration of ISCO was present with EIVC64 due to the lowest in-cylinder lambda, thus combustion of fuel rich mixture, whereas LIVC provided the lowest CO emissions as in-cylinder lambda was the highest.

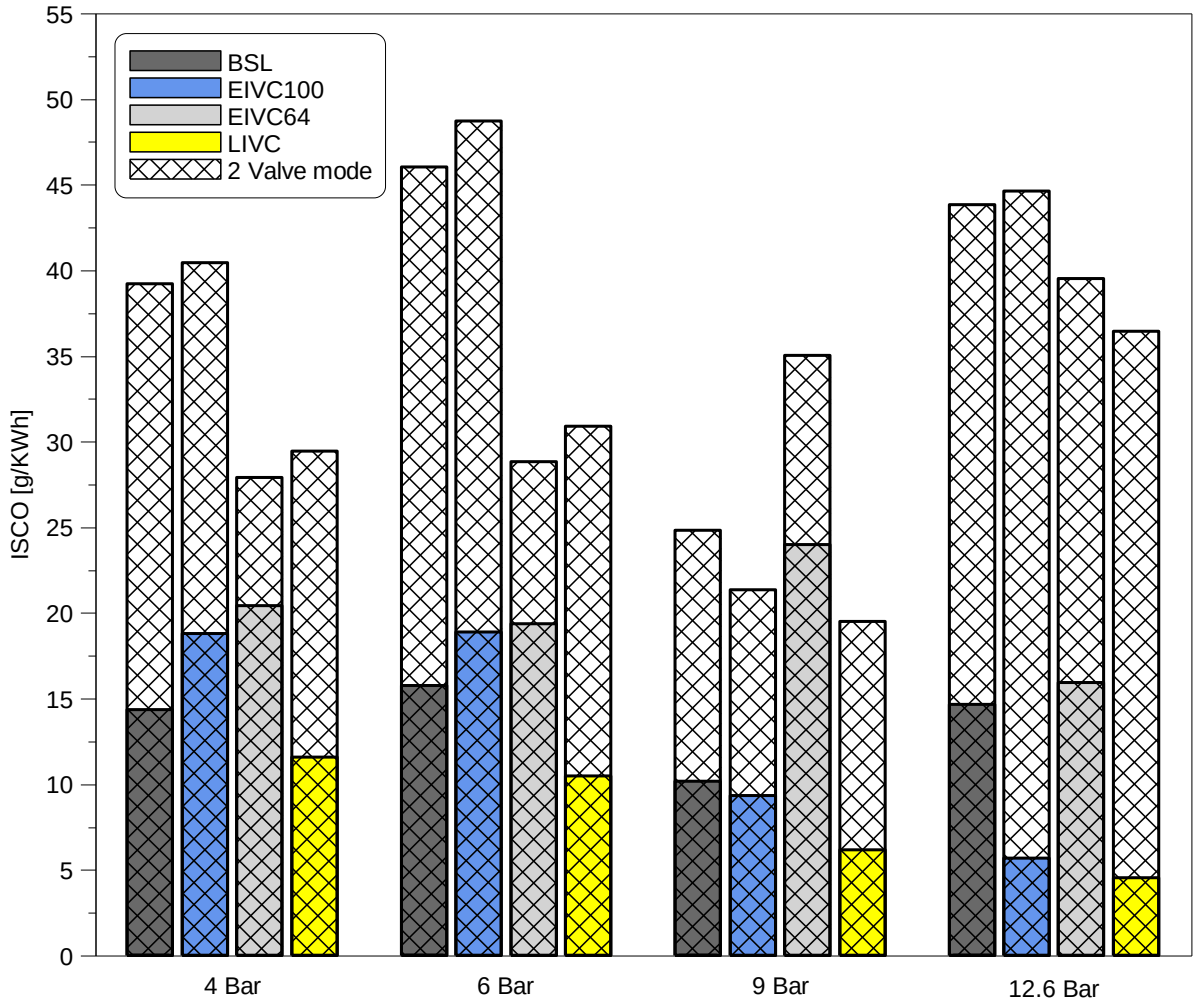

Figure 5.25 ISCO emission comparison between valve modes at various loads at 3000rpm

Single valve mode reduced HC emissions compared to two valve mode for all profiles across the whole load range thanks to faster combustion which reduced bulk quenching at the cylinder wall except for EIVC64 at 9bar net IMEP where combustion duration was higher than with two valve mode. The lowest levels of ISHC across all the load cases were achieved by the single valve LIVC profile due to the shortest combustion durations. The highest HC concentrations among single valve profiles were provided by EIVC64 due to the slowest combustion which resulted in bulk quenching, except for 4bar net IMEP where BSL profile had the highest ISHC due to high in-cylinder pressure during the expansion stroke. Overall HC emissions were reducing with load for single valve profiles and the lowest value recorded was 1.98 g/kWh at 12.6bar with LIVC profile.

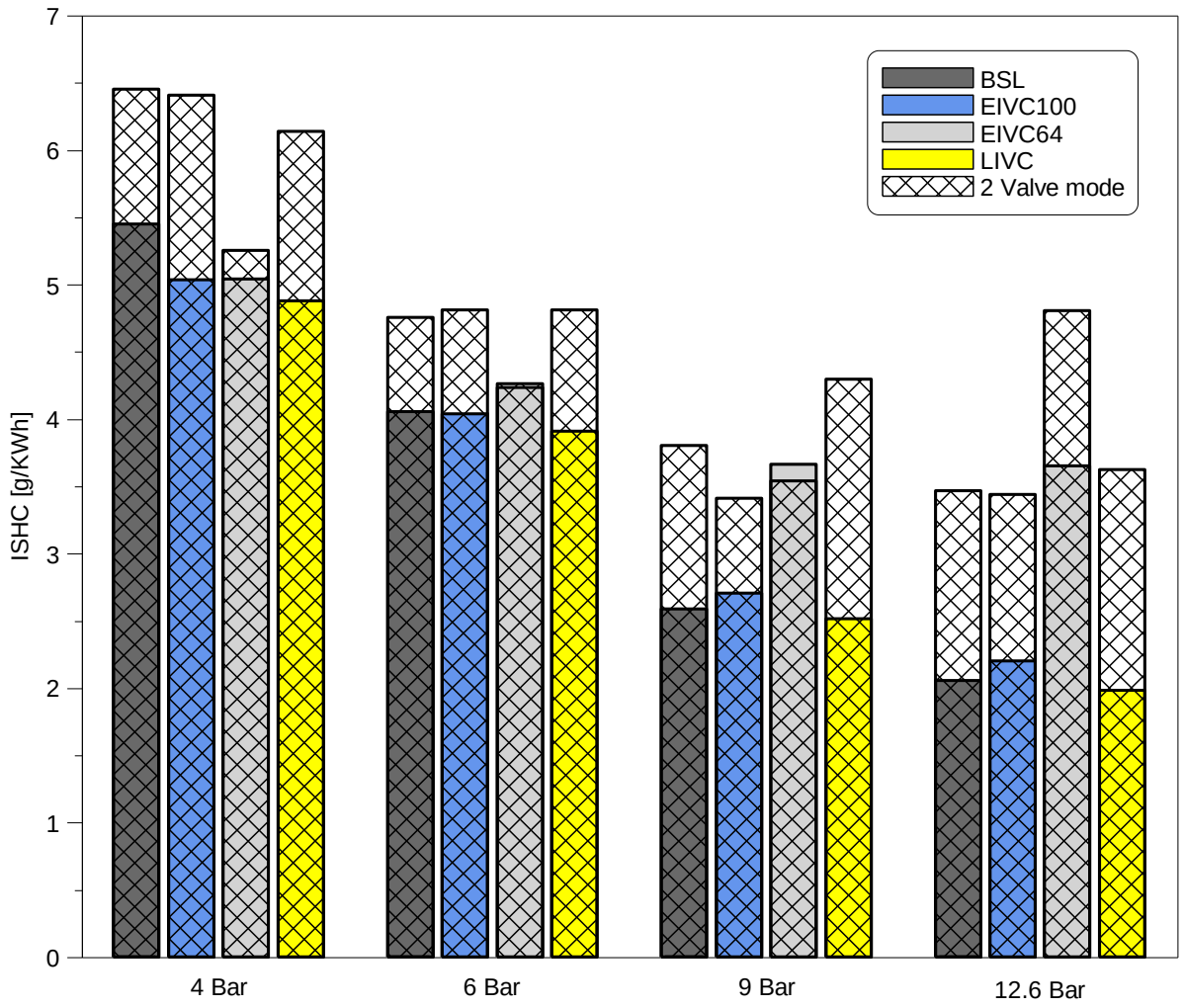

Figure 5.26 ISHC emission comparison between valve modes at various loads at 3000rpm

NO_X emissions were increased with single valve mode throughout the load range (except for EIVC64 at 6bar) due to higher in-cylinder pressure during combustion compared to profiles with two valve mode, which led to the highest peak combustion temperatures. The lowest NO_X level among single valve profiles was produced by EIVC64 due to the lowest in-cylinder pressures during combustion compared to the rest of the single valve profiles, except at 12.6bar where BSL had lower in-cylinder pressure but due to richer cylinder lambda EIVC64 had lower peak temperature. Single valve LIVC and BSL profiles provided high in-cylinder pressures throughout load range which resulted in the highest $ISNO_X$ concentrations.

Overall single valve mode significantly reduced ISCO emissions throughout the load range. ISHC emissions were also reduced for most of the single valve profiles, however $ISNO_X$ concentration was greatly increased throughout the load range.

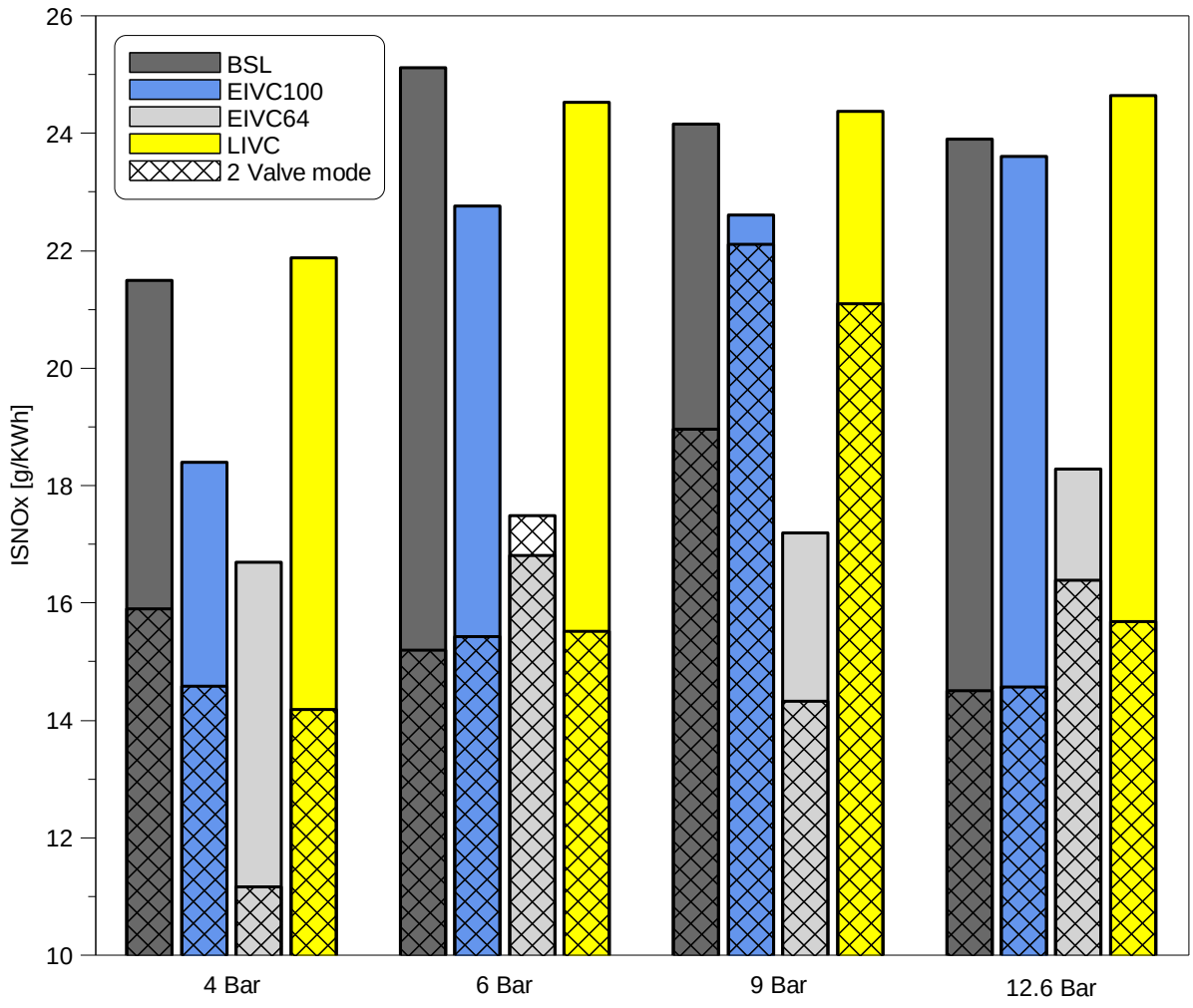

Figure 5.27 ISNO$_X$ emission comparison between valve modes at various loads at 3000rpm

5.3 Summary

In this chapter, single intake valve test results were compared to two valve mode in terms of engine performance and emissions. The tests were performed at 1500rpm and 3000rpm engine speed with a range of loads from 4bar to 12.6bar. The main findings are summarised below:

- LIVC profile with single valve mode achieved higher ECR than with the two valve mode due to smaller amount of charge escaping from the cylinder through single valve. However, ECRs from other profiles were not affected much.
- As the flow of fresh air was restricted to one intake valve, the pumping losses were increased for all profiles with single valve mode.
- On the other hand, single valve operation improved in-cylinder turbulence due to stronger swirl motion leading to faster flame propagation.

- The MBT spark timing was less advanced than for the two valve mode due to faster combustion.
- The lambda values were increased with single valve mode resulting in close to stoichiometric combustion.
- Single valve mode aided in reduction of fuel consumption at low engine load conditions and with some valve profiles at 9bar and 12.6bar NIMEP.
- Valve profiles with single valve mode achieved lower CO and HC emissions, however NO_X concentrations were increased compared to profiles with two valve operation.

Chapter 6 Miller Cycle and Atkinson Cycle Operations with Different Intake Maximum Opening Position (MOP)

6.1 Test conditions

6.1.1 Valve profiles

In this experiment, the best valve profiles in terms of ISFC from chapter 4 were compared to the same profiles with early MOP and the Baseline. However, iVT control system was not able to apply early MOP to valve profiles with partial lift i.e. EIVC84 and EIVC64, thus those profiles were replaced by the next best profile or EIVC100 in case the next best profile was one of them. Figure 6.1 shows the baseline profile and the best profiles selected for each load case from chapter 4 at 1500rpm (MOP50 – maximum opening position is in the middle of the valve event, which results in symmetrical profile shape), where LIVC is used at 4 and 12.6bar, BSL is used at 6bar and EIVC100 at 9bar. Figure 6.2 shows those profiles with MOP being shifted 35% earlier (maximum opening position is at 35% duration of the valve event leading to asymmetrical profile). Table 6.1 shows the valve timings for early MOP profiles at 0.5mm lift.

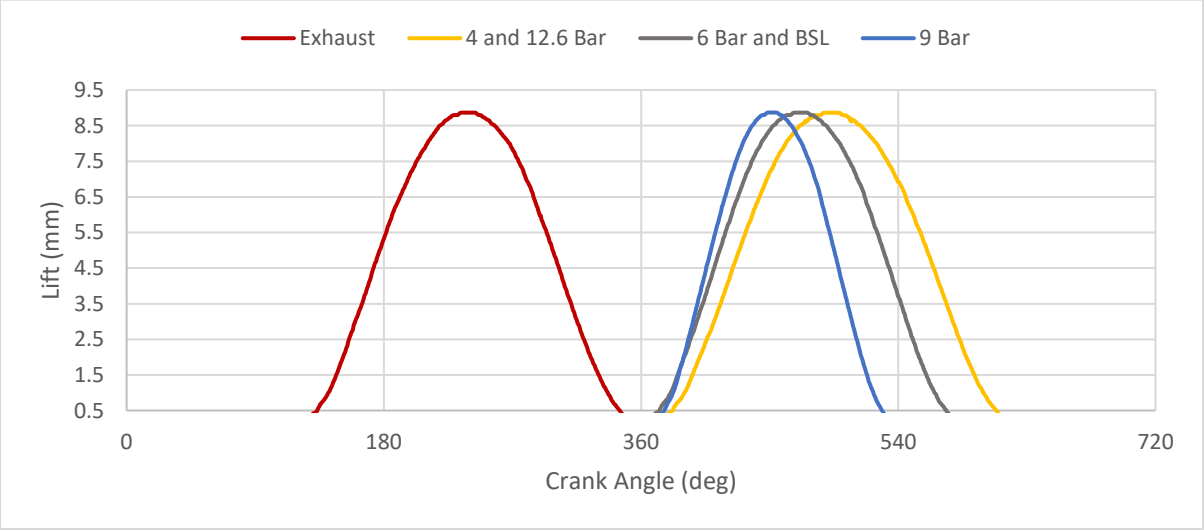

Figure 6.1 MOP50 valve profiles at 1500rpm

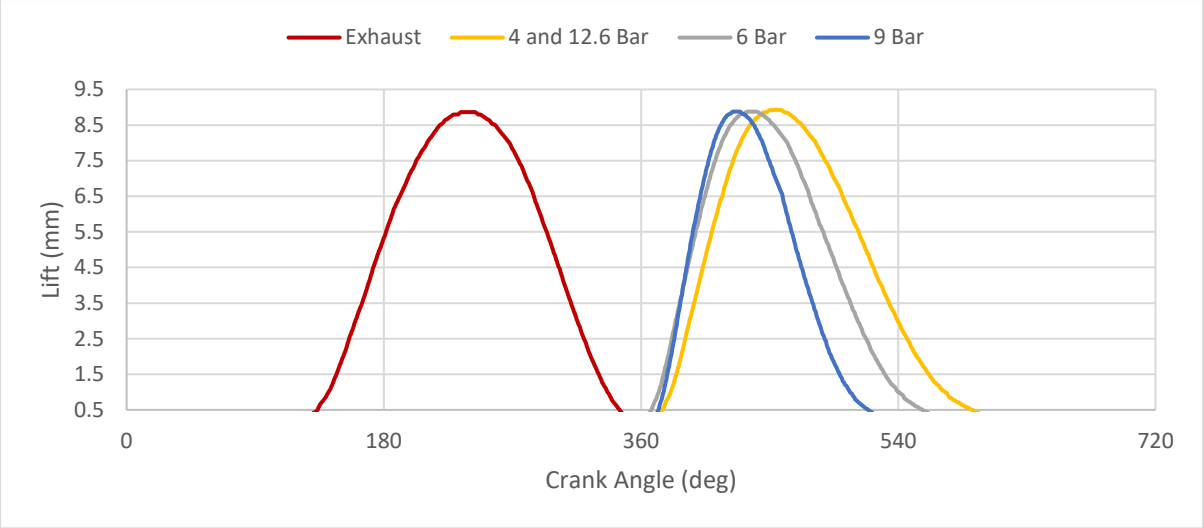

Figure 6.2 MOP35 valve profiles at 1500rpm

The same approach was used to select the best profiles at 3000rpm, however MOP was shifted 40% as at 35% the flow through the valves was not stable at this engine speed. Also at 12.6bar NIMEP the exhaust duration was shortened due to high in-cylinder pressure as was mentioned in previous chapters. Figure 6.3 shows the baseline and MOP50 profiles, where LIVC is used at 4, 6 and 12.6bar, and EIVC100 for 9bar. Figure 6.4 and Table 6.2 shows MOP40 valve profiles and timings at 0.5mm lift.

Table 6.1 Valve timings and durations for MOP35 profiles

Valve Profile	Lift (mm)	Duration (CA deg)	IVO/EVO (CA deg)	IVC/EVC (CA deg)	MOP (CA deg)
4 and 12.6 Bar	8.9	217	375	592	456
6 Bar	8.9	189	367	556	443
9 Bar	8.9	146	372	518	430
Exhaust	8.9	211	133	344	240

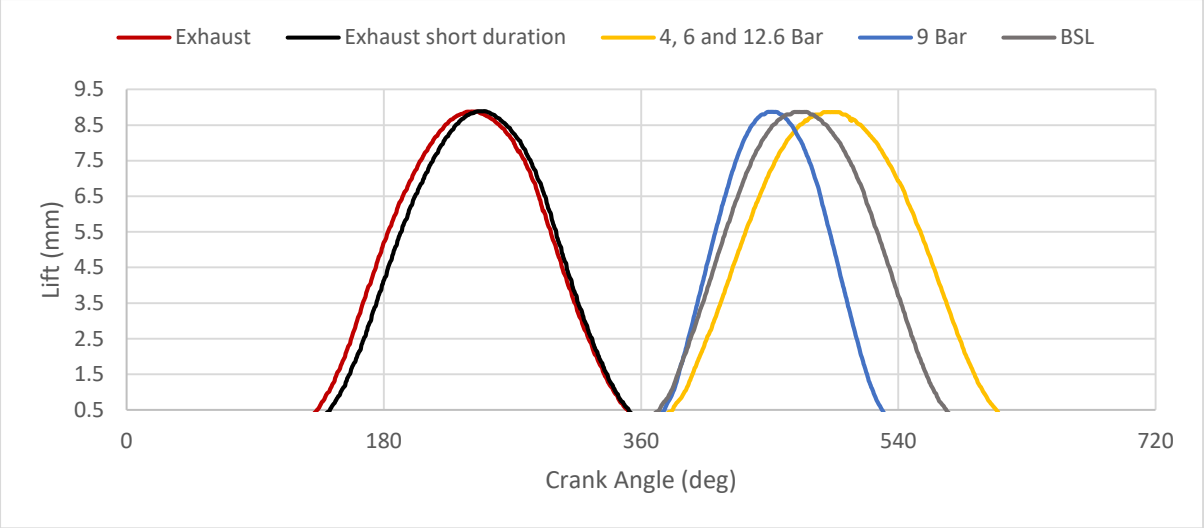

Figure 6.3 MOP50 valve profiles at 3000rpm

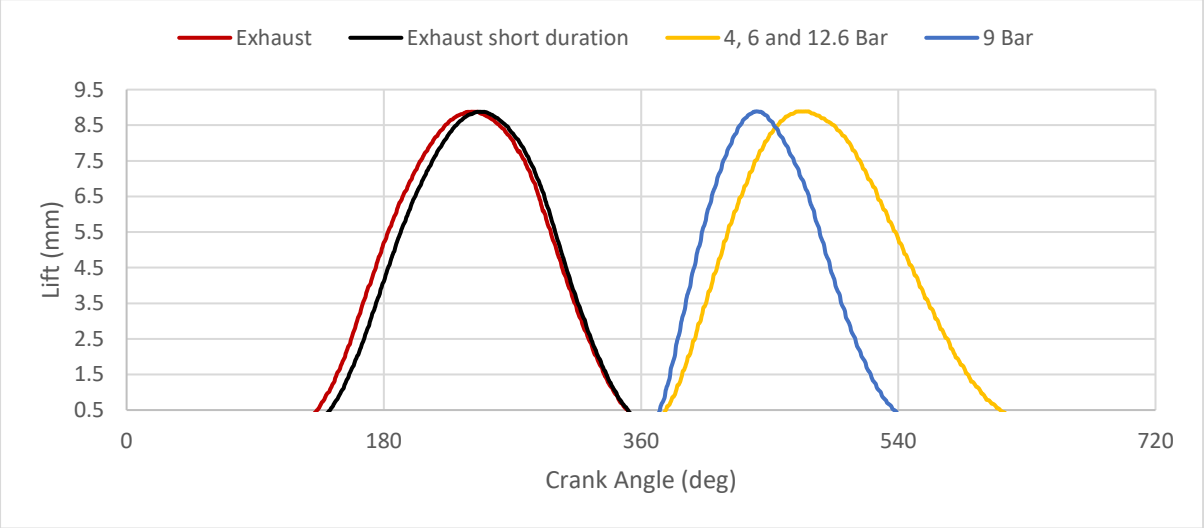

Figure 6.4 MOP40 valve profiles at 3000rpm

Table 6.2 Valve timings and durations for MOP40 profiles

Valve Profile	Lift (mm)	Duration (CA deg)	IVO/EVO (CA deg)	IVC/EVC (CA deg)	MOP (CA deg)
4, 6 and 12.6 Bar	8.9	234	377	611	475
9 Bar	8.9	163	373	536	445
Exhaust	8.9	218	132	350	241
Exhaust short duration	8.9	208	142	350	247

6.1.2 Operation points

Table 6.3 shows four operation points used for comparison of the test results between the baseline, MOP50 and MOP35 at 1500rpm and MOP40 at 3000rpm.

Table 6.3 Testing points

Speed (rpm)	**NIMEP (bar)**			
1500	4	6	9	12.6
3000	4	6	9	12.6

6.2 Early MOP vs MOP50 vs Baseline

6.2.1 Test results at 1500rpm

The effects of early MOP on ECR and throttle angle are shown in Figure 6.5 and Figure 6.6. At 4bar net IMEP baseline had the highest ECR due to earlier IVC compared to the rest of the profiles. MOP35 provided slightly lower ECR than MOP50. The throttle position for MOP35 was only slightly larger than MOP50, however its intake pressure was more than 0.1bar higher as can be seen in Figure 6.7. This indicates that more air is being pushed out of the cylinder during the compression stroke with MOP35 and causing ECR to reduce.

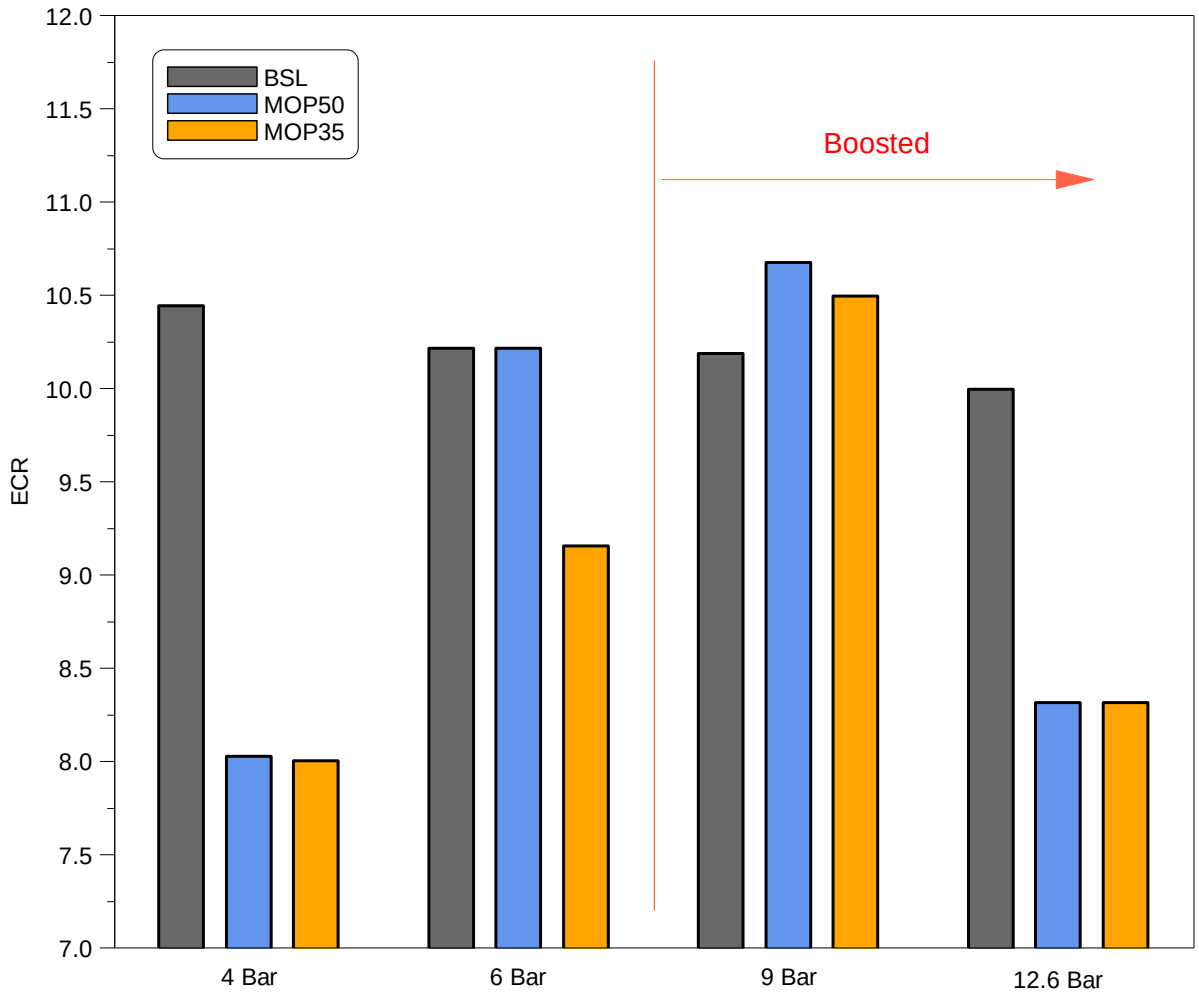

Figure 6.5 ECR comparison at various loads at 1500rpm

At 6bar net IMEP BSL and MOP50 are the same profiles. MOP35 provided lower ECR and higher intake pressure than MOP50 while keeping similar throttle angle. Similarly to previous load case, this indicates that more charge is being expelled into the intake manifold after BDC causing ECR to reduce. At 9bar BSL had the lowest ECR as it had the latest IVC. MOP35 had larger throttle angle and higher intake pressure but lower ECR than MOP50. At 12.6bar MOP35 had the same ECR as MOP50, even though the intake pressure and throttle angle were increased. The baseline profile had the highest ECR due to the earliest IVC.

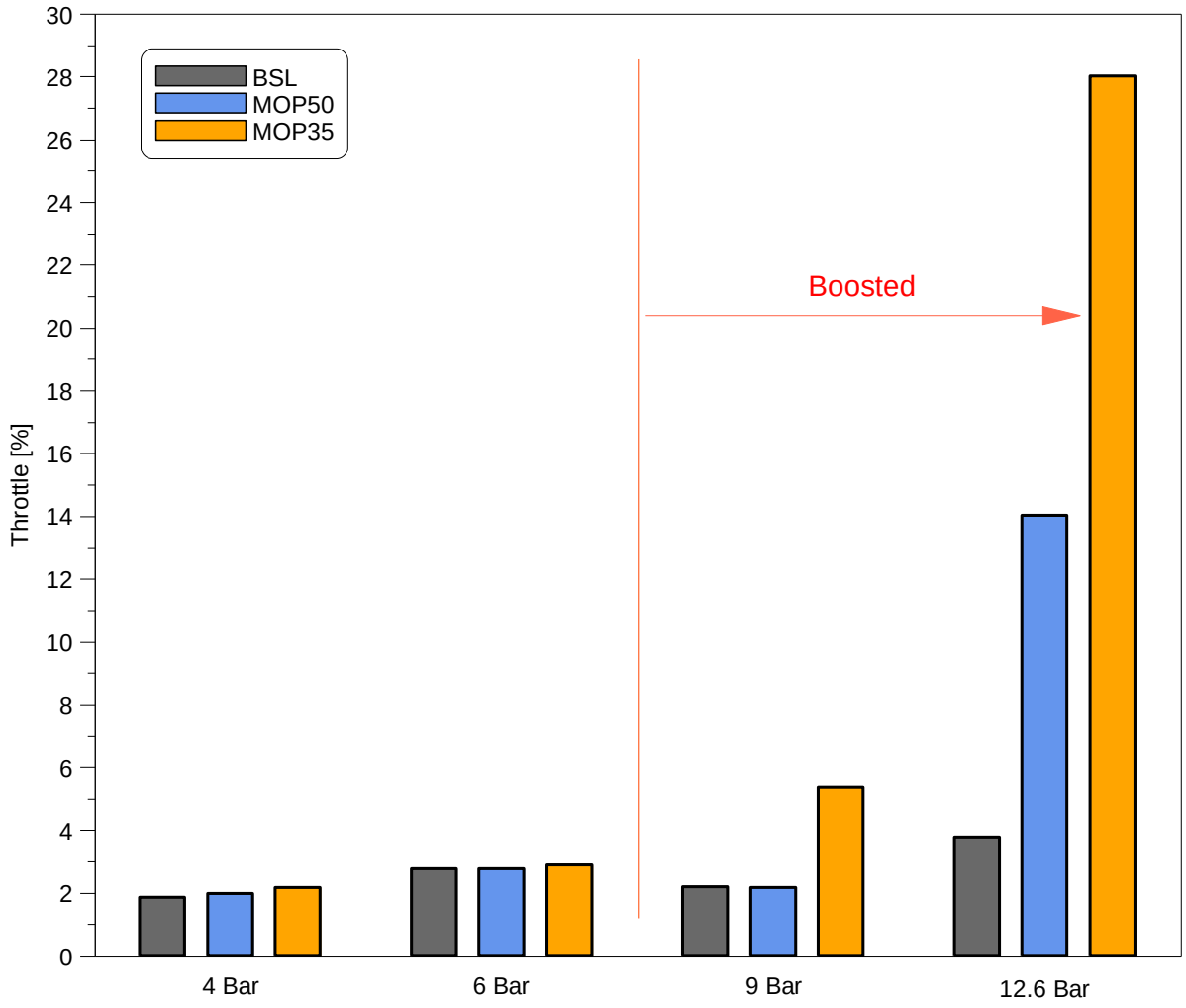

Figure 6.6 Throttle opening comparison at various loads at 1500rpm

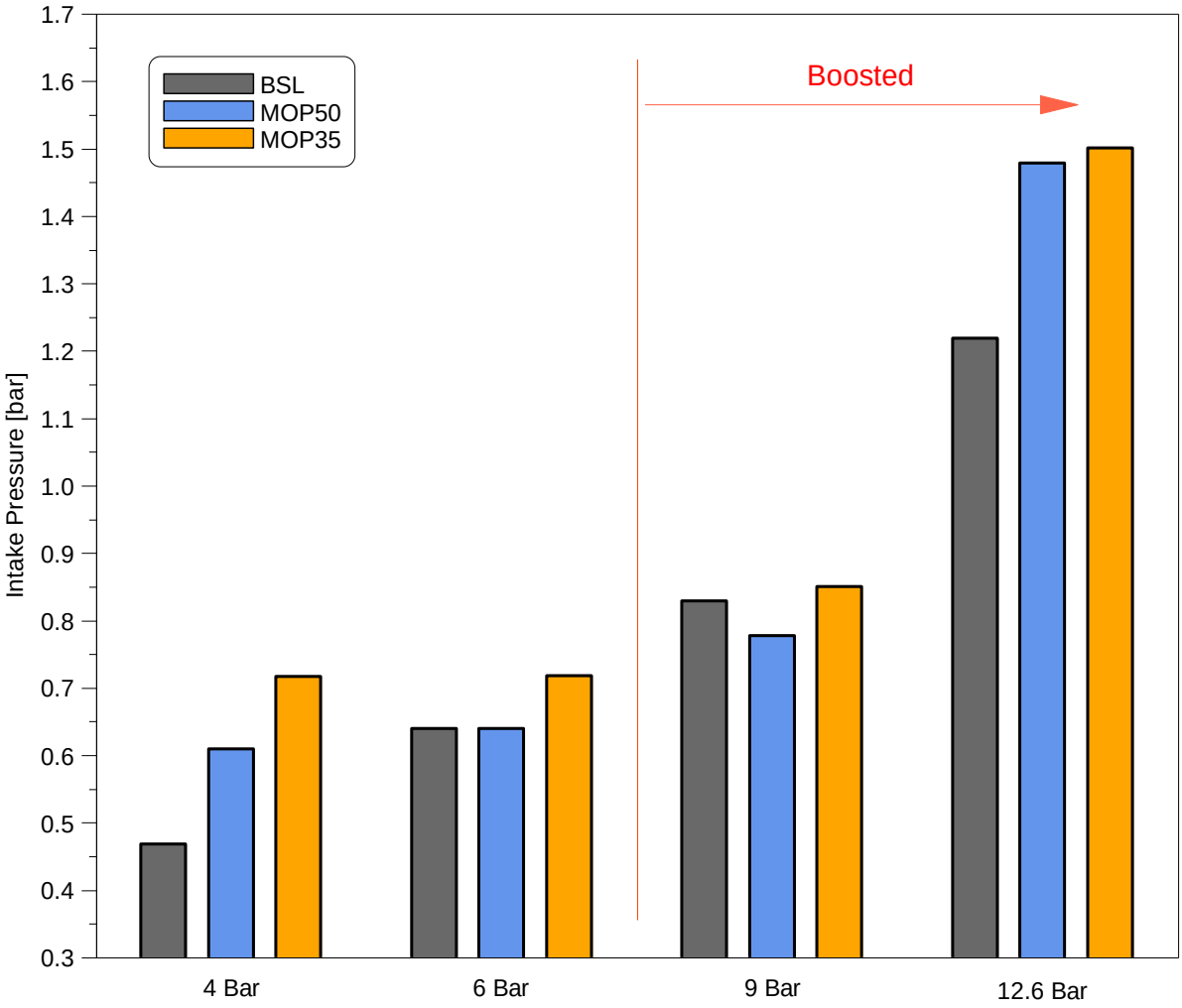

Figure 6.7 Intake pressure comparison at various loads at 1500rpm

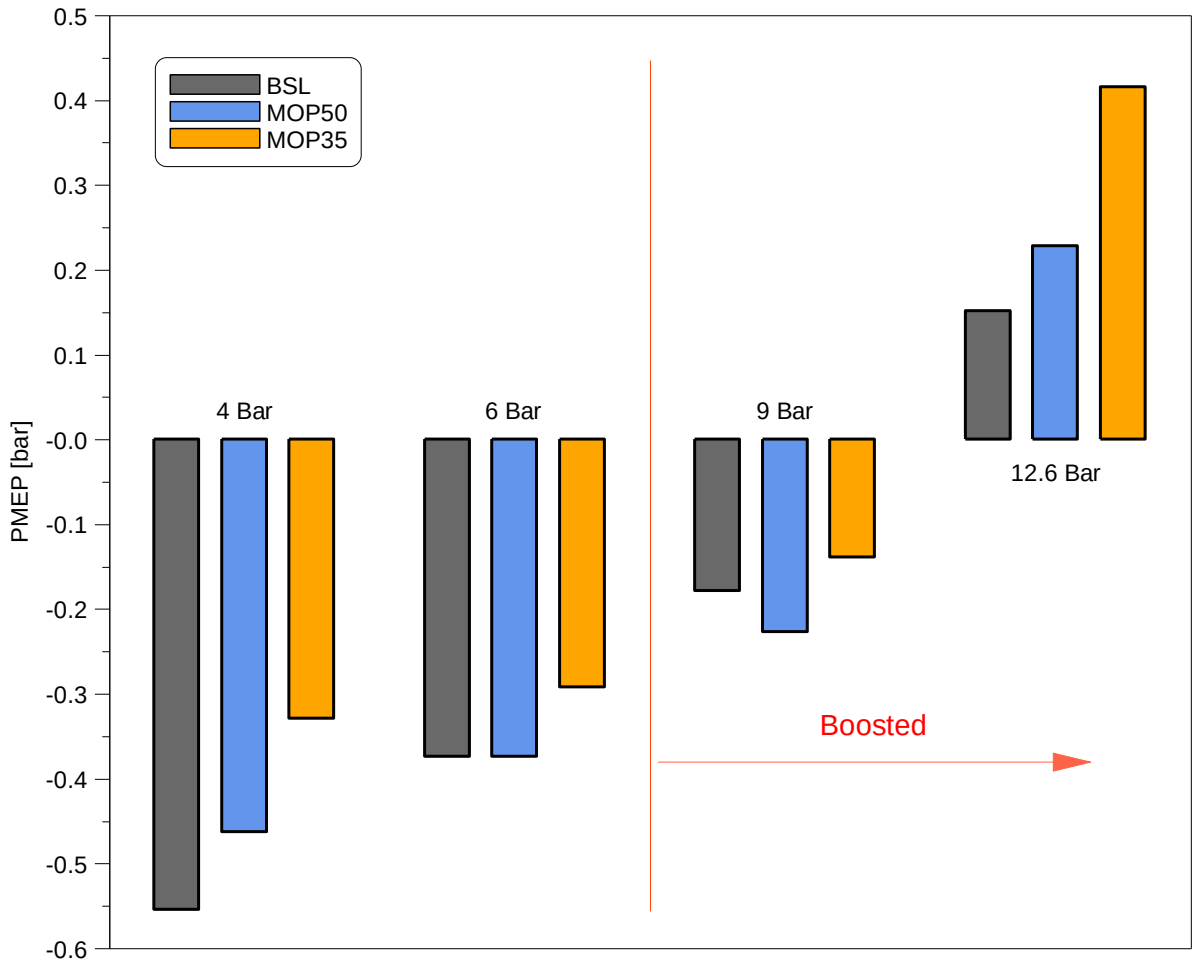

Figure 6.8 PMEP comparison at various loads at 1500rpm

Figure 6.8 shows a comparison of PMEP between BSL, MOP50 and MOP35. Form these results it is clear that the pumping losses are inversely proportional to the intake pressures. In general the baseline profile had the lowest intake pressures throughout the load cases which led to the largest pumping losses. Hence MOP35 had the lowest pumping losses due to the highest intake pressures. Furthermore, MOP35 had larger inflow area just after IVO than MOP50 due to earlier maximum opening which aided in further reduction of pumping losses. An example of this effect can be clearly seen at 12.6bar net IMEP where MOP35 intake pressure is only slightly greater than MOP50 but the difference in PMEP is more pronounced.

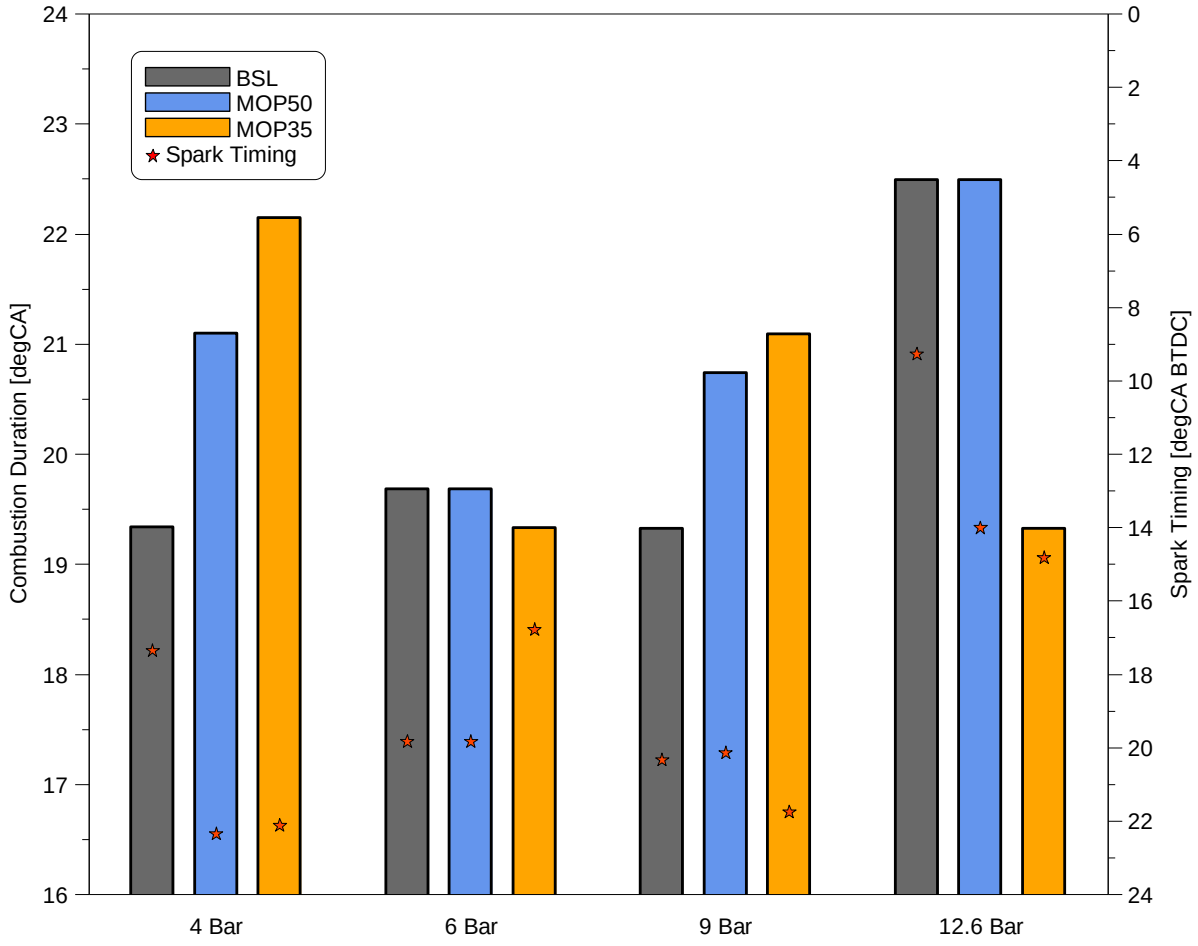

Figure 6.9 Combustion duration and spark timing comparison at various loads at 1500rpm

Comparison of combustion duration and spark timing is demonstrated in Figure 6.9. At 4bar net IMEP the baseline profile provided the shortest combustion duration, whereas early MOP slowed the flame speed due to lower ECR which led to longer combustion duration than MOP50. The MBT spark timing was advanced for MOP35 and MOP50 due to long flame development angle (Figure 6.10). At 6bar net IMEP BSL and MOP50 were characterised with the same and longer combustion duration. Whereas MOP35 had much lower ECR than BSL profile but achieved shorter combustion duration, this indicates that early MOP improved in-cylinder turbulence. The MBT spark timing was retarded for MOP35 due to shorter flame development angle. At 9bar net IMEP BSL profile produced the shortest combustion duration. MOP35 resulted in longer combustion duration than MOP50 due to lower ECR. MBT spark timing was advanced for MOP35 due to the longest flame development angle. At 12.6bar net IMEP the spark timing was knock limited for all profiles. The BSL profile has the most retarded spark timing in order to avoid the knocking combustion due to the higher ECR. The shortest combustion duration was produced by MOP35 even though ECR value was almost identical for MOP50. This indicates that earlier MOP improved in-cylinder turbulence resulting in faster combustion.

As shown in Figure 6.11 CA10-50 was almost identical for all profiles at 4 and 6bar net IMEP. At 9bar net IMEP, BSL produced the shortest CA10-50, whereas at 12.6bar MOP35 produced the shortest 10-50% burn. The trend for 50-90% burn was similar to the combustion duration for all profiles across the load range.

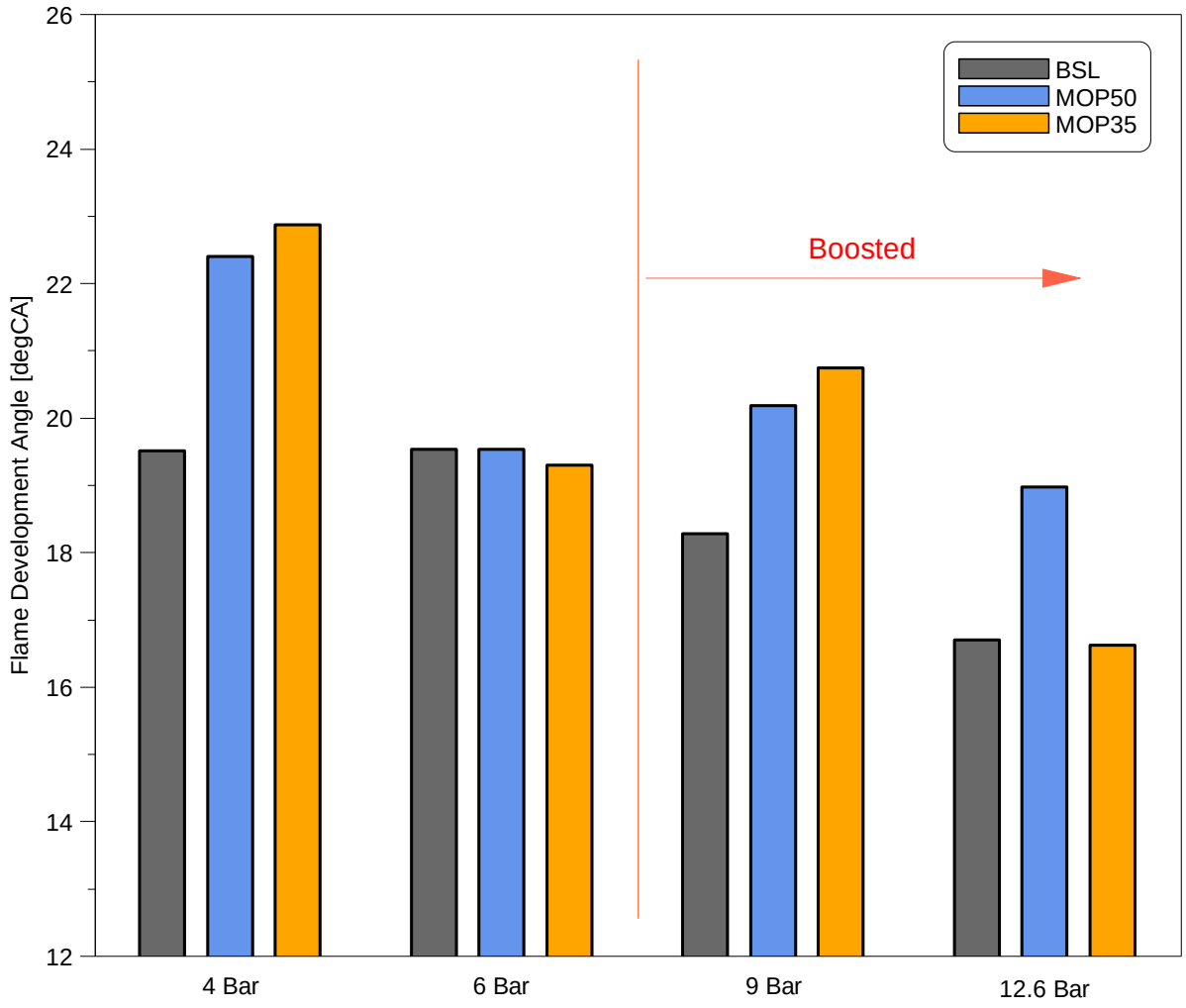

Figure 6.10 Flame development angle comparison at various loads at 1500rpm

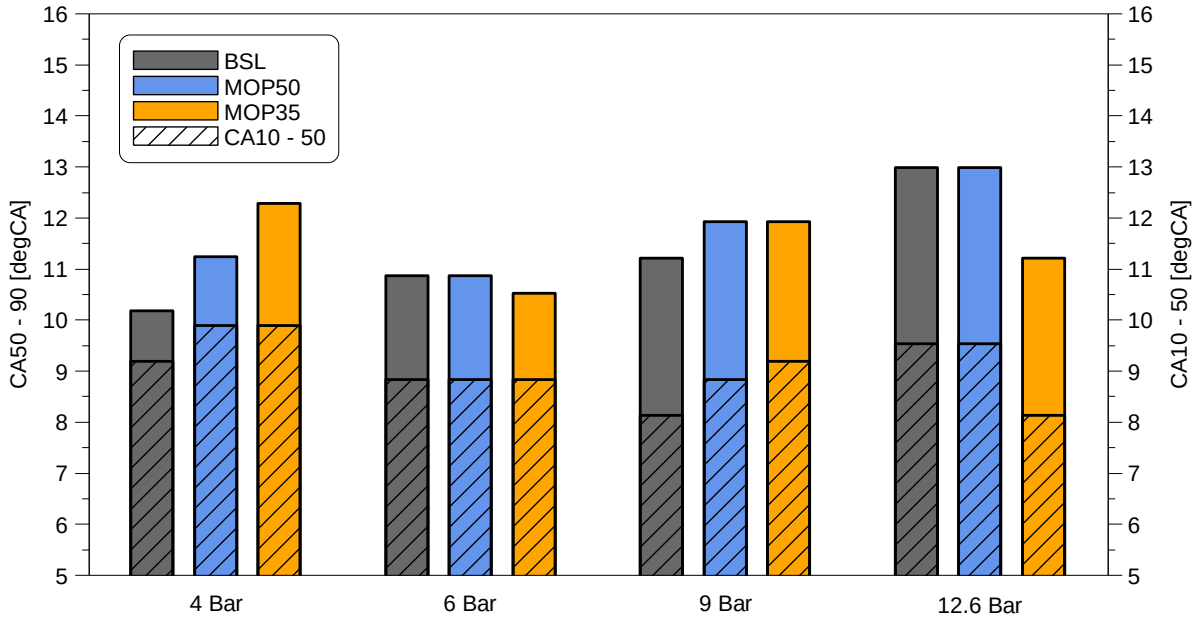

Figure 6.11 CA10-50 and CA50-90 comparison at various loads at 1500rpm

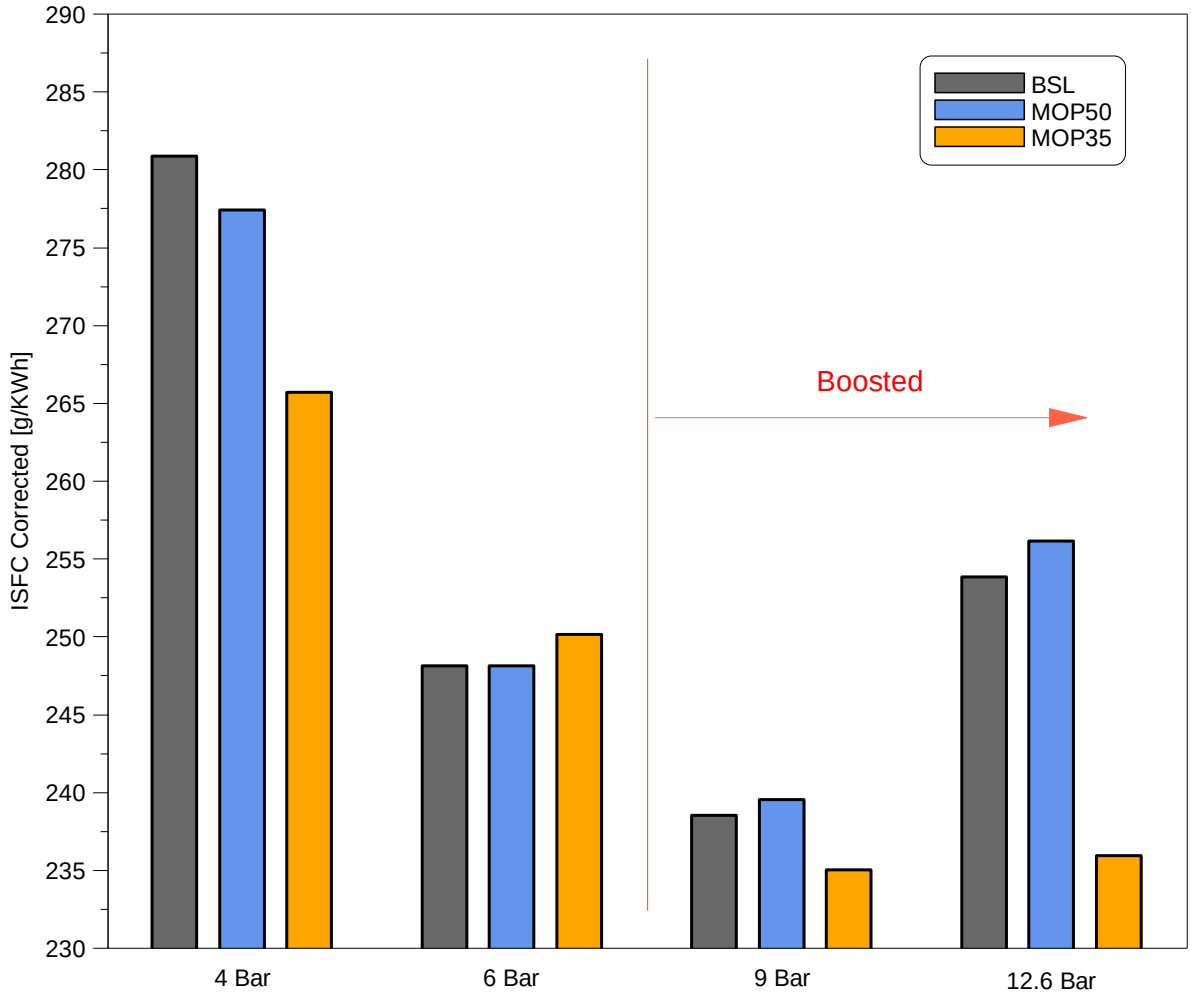

Figure 6.12 ISFC corrected comparison at various loads at 1500rpm

Comparison of indicated specific fuel consumption is shown in Figure 6.12. At 4bar net IMEP MOP35 reduced fuel consumption by 5.4% than the baseline profile due to significantly reduced pumping loss and close to stoichiometric in-cylinder lambda (Figure 6.13). However, at 6bar, MOP35 resulted in the highest fuel consumption due to richer cylinder lambda even though pumping loss and combustion duration was lower than from other profiles. At 9bar net IMEP, MOP50 achieved the highest ISFC due to the largest pumping loss, whereas MOP35 provided the lowest pumping loss, thus shown as the most fuel efficient profile. At 12.6bar, fuel consumption was reduced by almost 20g/KWh with MOP35 compared to BSL profile. This significant improvement was achieved thanks to the higher positive PMEP and shortest combustion duration, as well as close to stoichiometric in-cylinder lambda. Overall MOP35 improved fuel consumption across all the load points except for 6bar.

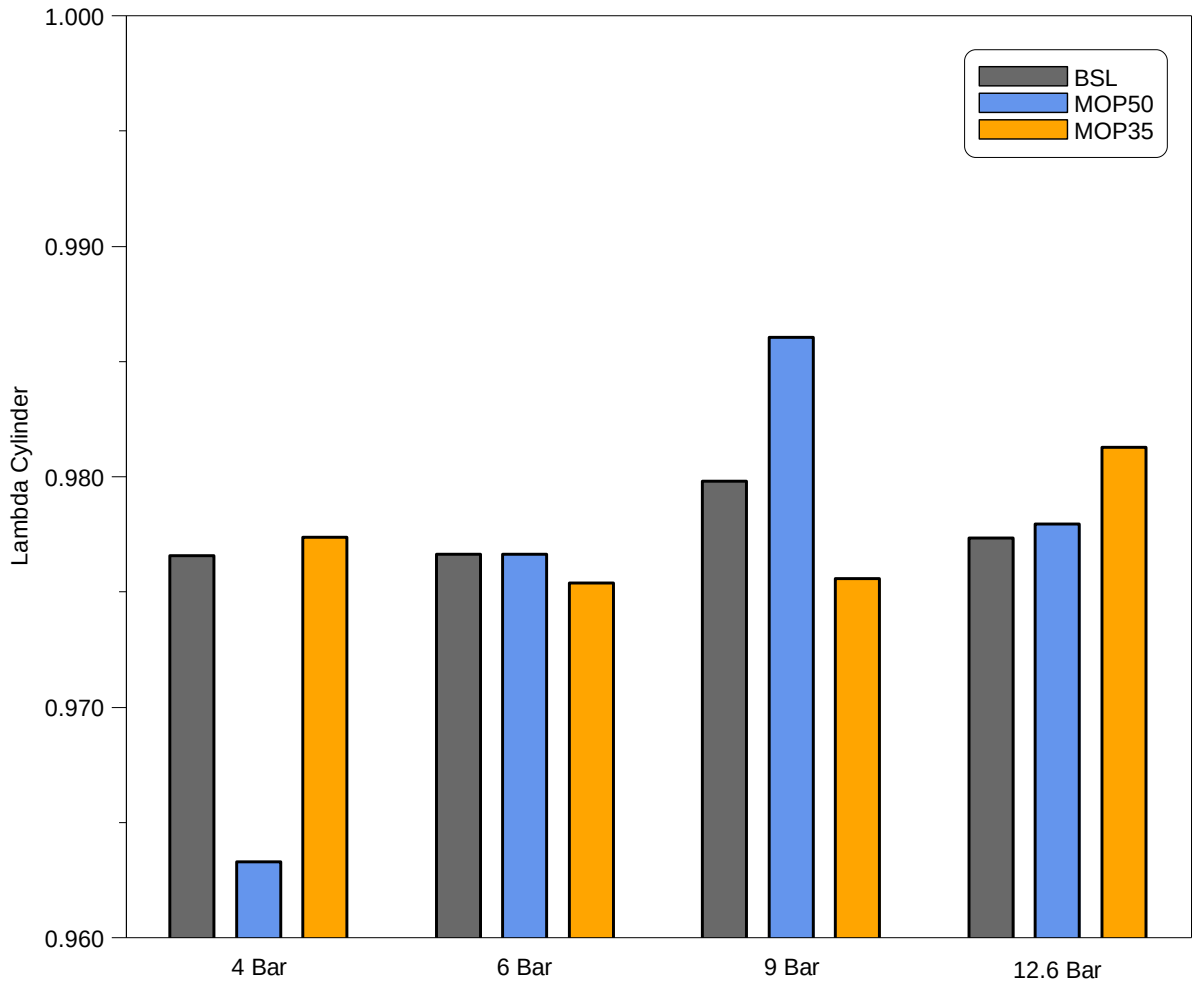

Figure 6.13 In-cylinder lambda comparison at various loads at 1500rpm

Emissions results are shown in Figure 6.14, Figure 6.15 and Figure 6.16. Throughout all load cases ISCO concentration was inversely proportional to in-cylinder lambda, lower in-cylinder lambda resulted in higher CO emissions. MOP35 reduced ISCO at 4 and 12.6bar load, but increased emission at 6 and 9bar due to fuel rich combustion.

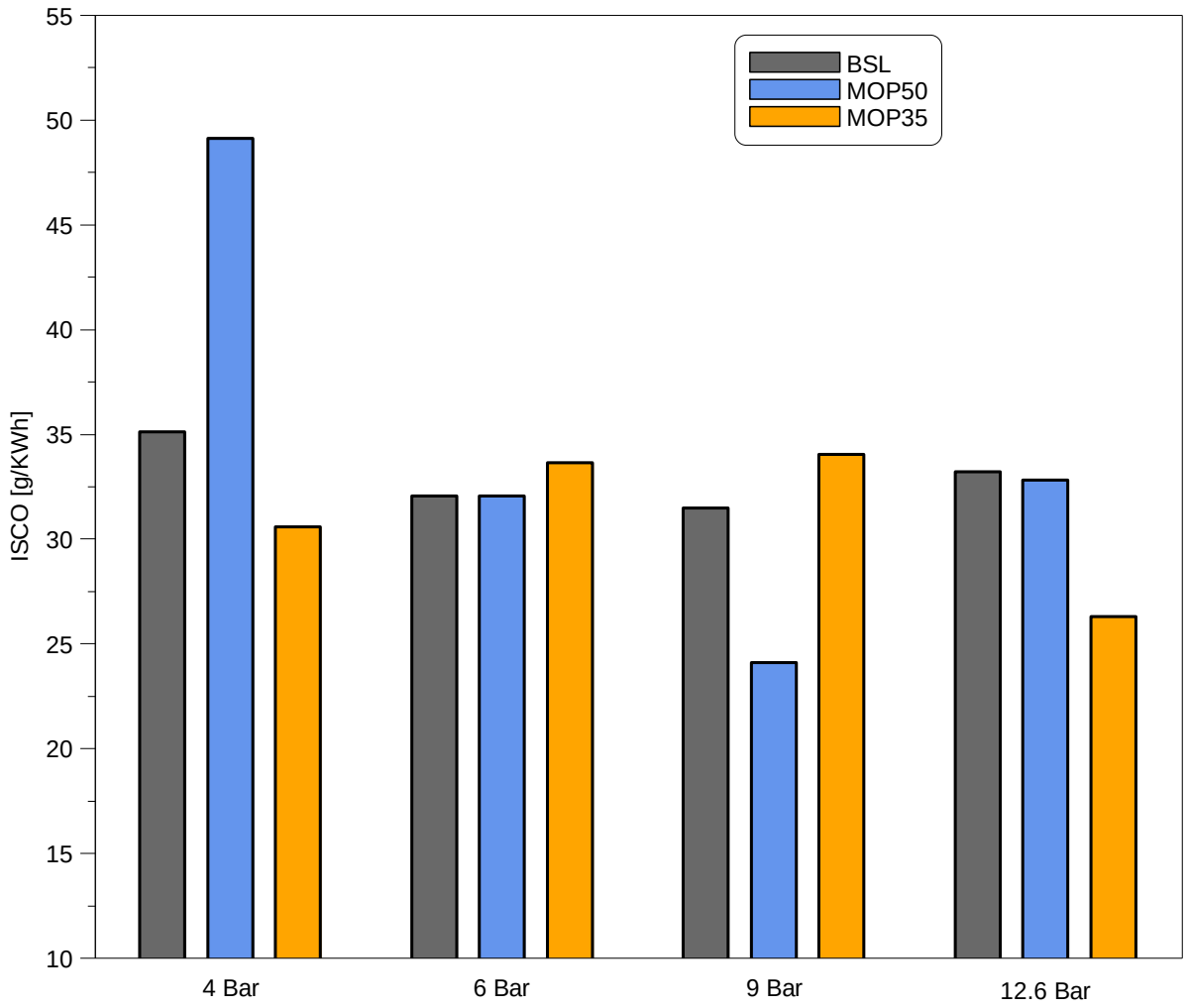

Figure 6.14 ISCO emission comparison at various loads at 1500rpm

At 4bar net IMEP MOP35 achieved the lowest level of HC due to the lowest in-cylinder pressure during compression and expansion strokes. This prevented some of the mixture being forced into crevices and led to more complete combustion compared to BSL and MOP50 profiles. At 6bar net IMEP MOP35 significantly reduced ISHC compared to BSL due to significantly lower in-cylinder pressure and improved combustion speed which allowed to reduce bulk quenching at the cylinder wall as well as forcing mixture into crevices. At 9bar net IMEP HC emissions were similar between all three profiles, however MOP35 achieved the lowest emissions due to lower in-cylinder pressure during compression stroke and combustion. At 12.6bar net IMEP HC emissions were increased dramatically for BSL and MOP50 because of incomplete combustion due to knock limited spark timing. The lowest ISHC value was achieved by MOP35 due to the fastest combustion, which allowed to reduce bulk quenching at the cylinder wall.

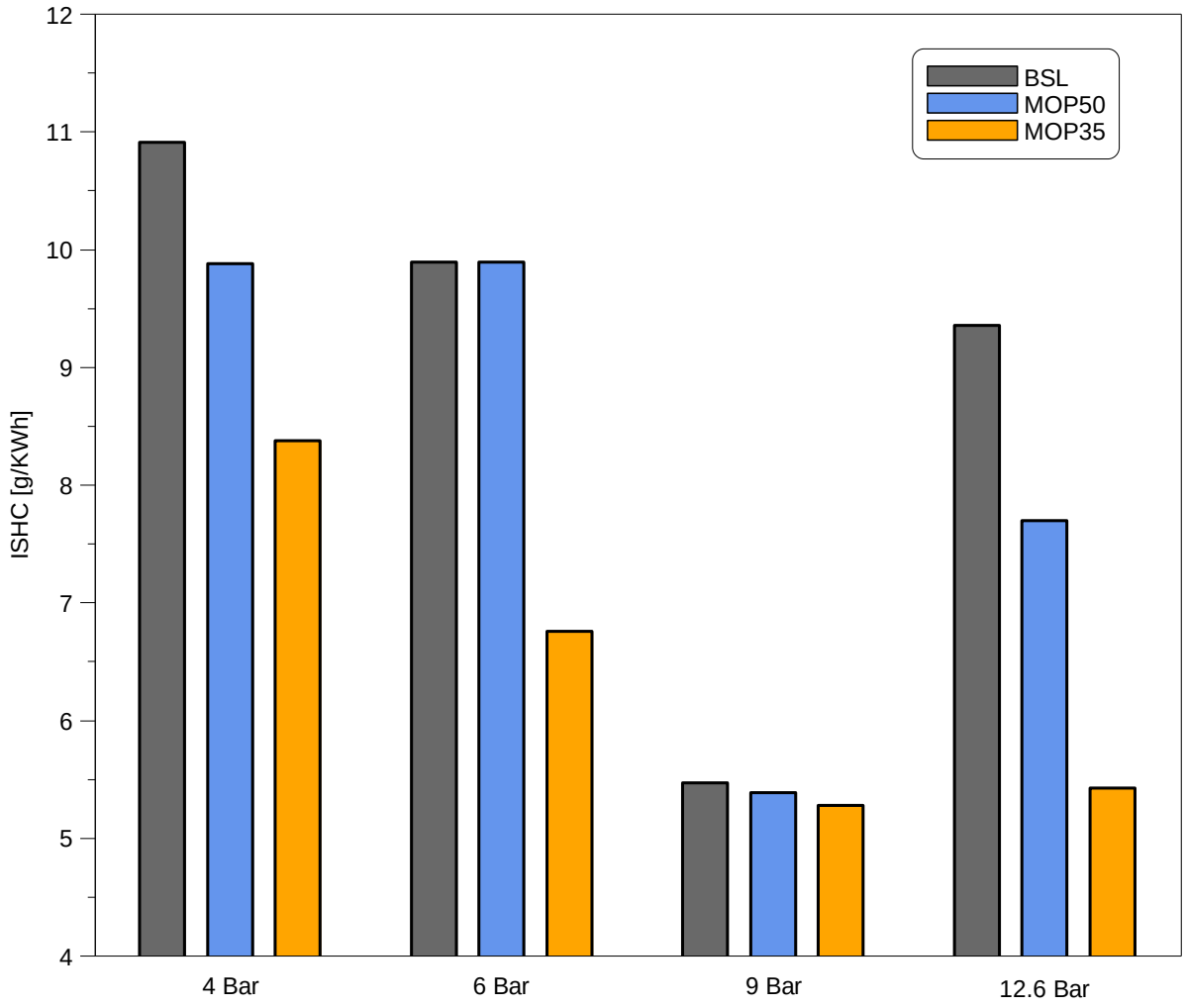

Figure 6.15 ISHC emission comparison at various loads at 1500rpm

The lowest NO_X emissions were achieved by MOP50 profile at 4bar net IMEP due to low temperature combustion of fuel rich mixture. MOP35 achieved slightly higher NO_X due to earlier spark timing which provided higher rate of temperature increase resulting in higher peak temperature during combustion. At 6bar net IMEP MOP35 achieved the lowest $ISNO_X$ due to significantly lower in-cylinder pressure during combustion and later spark timing which led to the lowest peak combustion temperature among other profiles. At 9bar, BSL profile achieved the lowest NO_X emissions due to lower in-cylinder temperature at the end of combustion, indicating faster cooling of the burnt gas and rapid freezing of NO_X formation. At 12.6bar net IMEP MOP35 achieved the highest $ISNO_X$ due to the most advanced spark timing and the highest peak in-cylinder pressure during combustion which led to higher cylinder temperatures throughout the expansion stroke compared to the other profiles. MOP50 achieved the lowest NO_X emissions due to lower cylinder pressure during the compression stroke and at the end of combustion than BSL profile resulting in lower temperatures. $ISNO_X$

was generally increasing with load due to increasing in-cylinder pressure and temperature during compression and combustion.

Overall MOP35 reduced ISCO emissions at 4 and 12.6bar and ISHC emissions across all load cases.

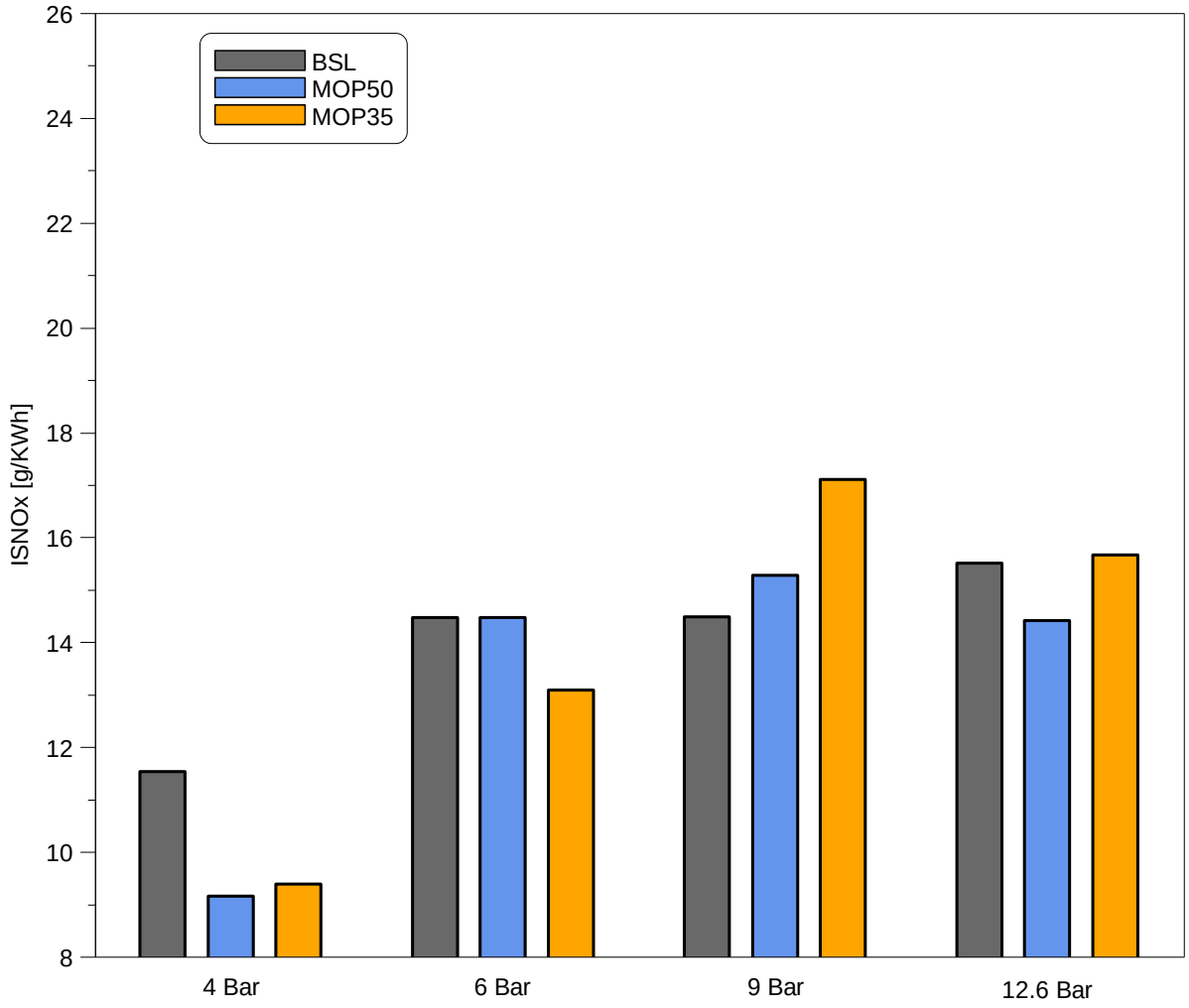

Figure 6.16 $ISNO_X$ emission comparison at various loads at 1500rpm

6.2.2 Test results at 3000rpm

The effects of early MOP on ECR and throttle angle are shown in Figure 6.17 and Figure 6.18. At 4bar net IMEP baseline profile achieved the highest ECR due to earlier IVC compared to the rest of the profiles. MOP40 provided slightly lower ECR than MOP50 due to lower intake pressure as seen in Figure 6.19 because of slightly smaller throttle opening. Therefore less air is being let into the cylinder during the intake stroke with MOP40 which led to lower ECR than MOP50.

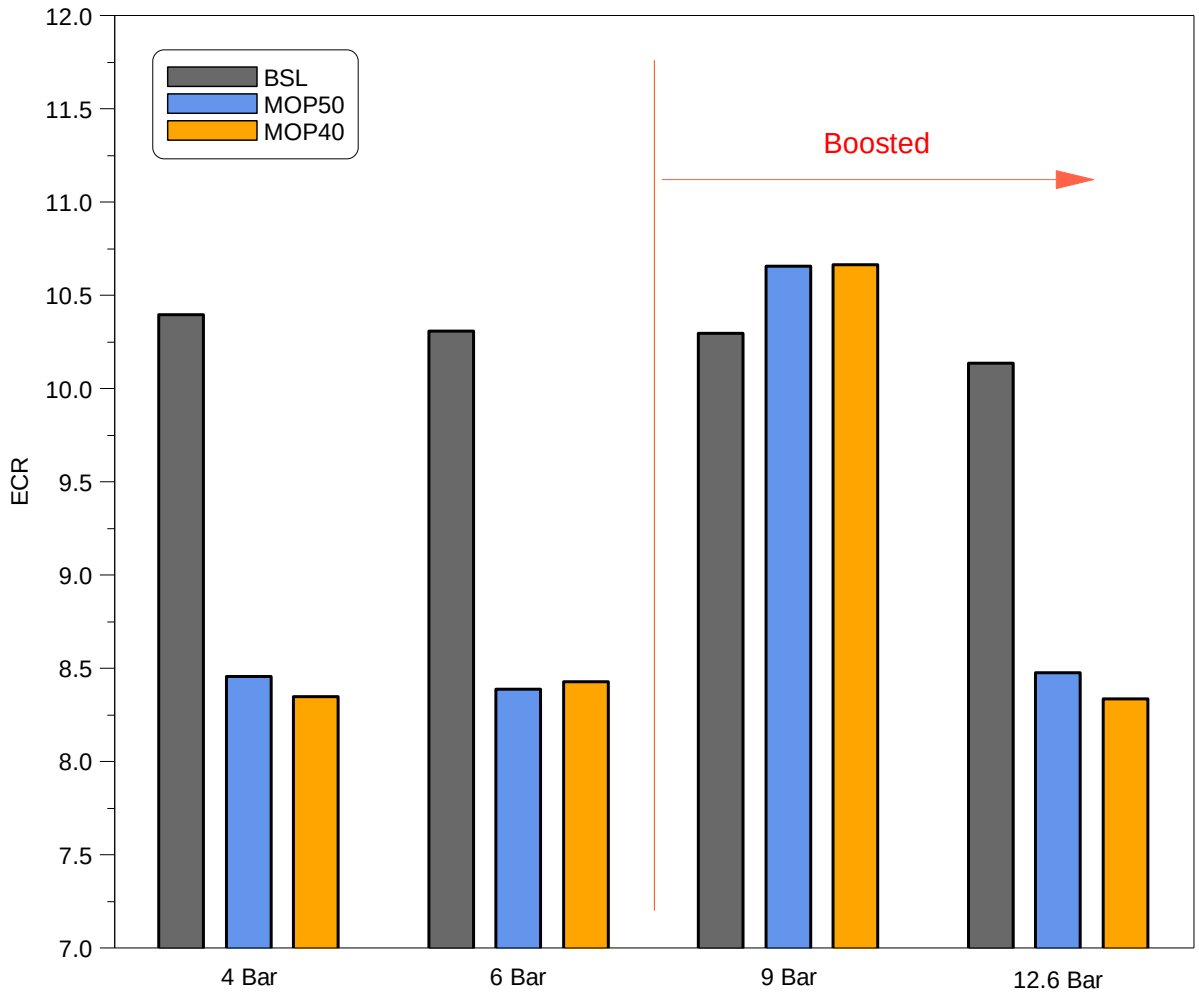

Figure 6.17 ECR comparison at various loads at 3000rpm

At 6bar net IMEP BSL produced the highest ECR due to the earliest IVC. MOP50 and MOP40 provided almost the same ECR with the latter being slightly larger. Both throttle opening and intake pressure were lower for MOP40, indicating that less charge was pushed out of the cylinder during compression stroke, thus resulting in higher ECR than MOP50. At 9bar BSL had the lowest ECR as it had the latest IVC. MOP50 had larger throttle angle and higher intake pressure but slightly lower ECR than MOP40. At 12.6bar BSL had the earliest IVC, thus resulted in the highest ECR. MOP50 had higher ECR than MOP40 due to significantly larger throttle opening and greater intake pressure. Overall difference in ECR between MOP40 and MOP50 is small across all load cases.

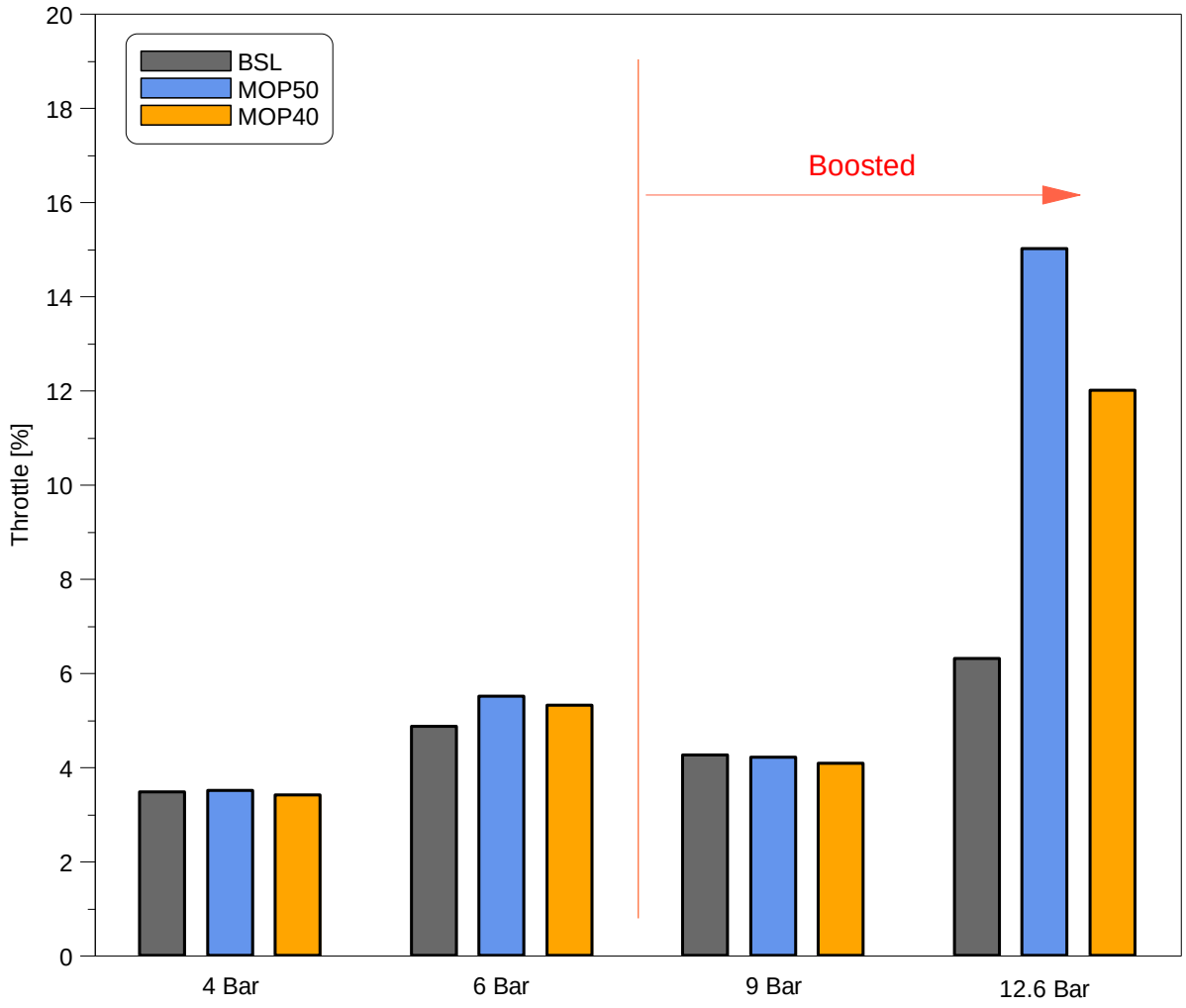

Figure 6.18 Throttle opening comparison at various loads at 3000rpm

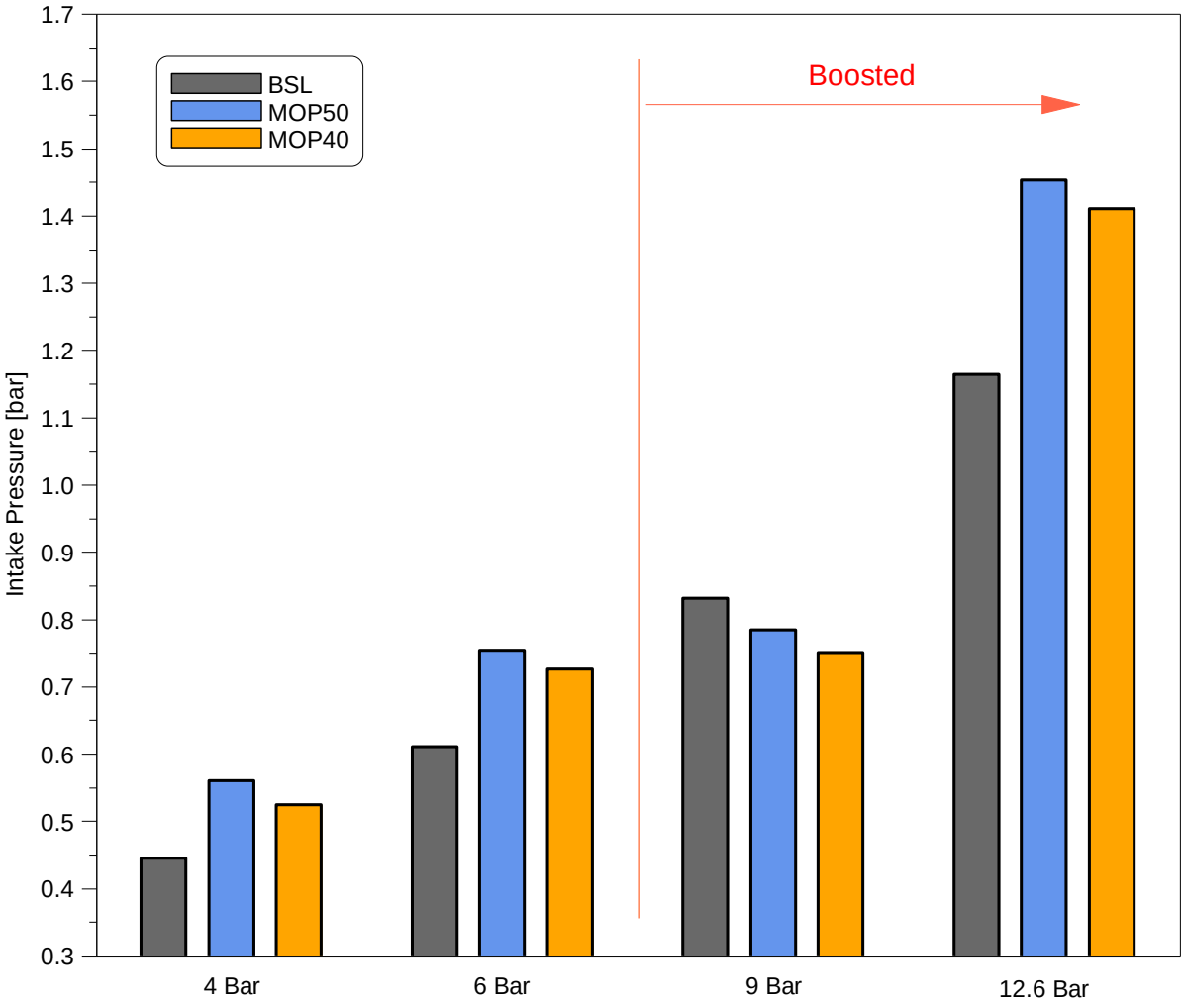

Figure 6.19 Intake pressure comparison at various loads at 3000rpm

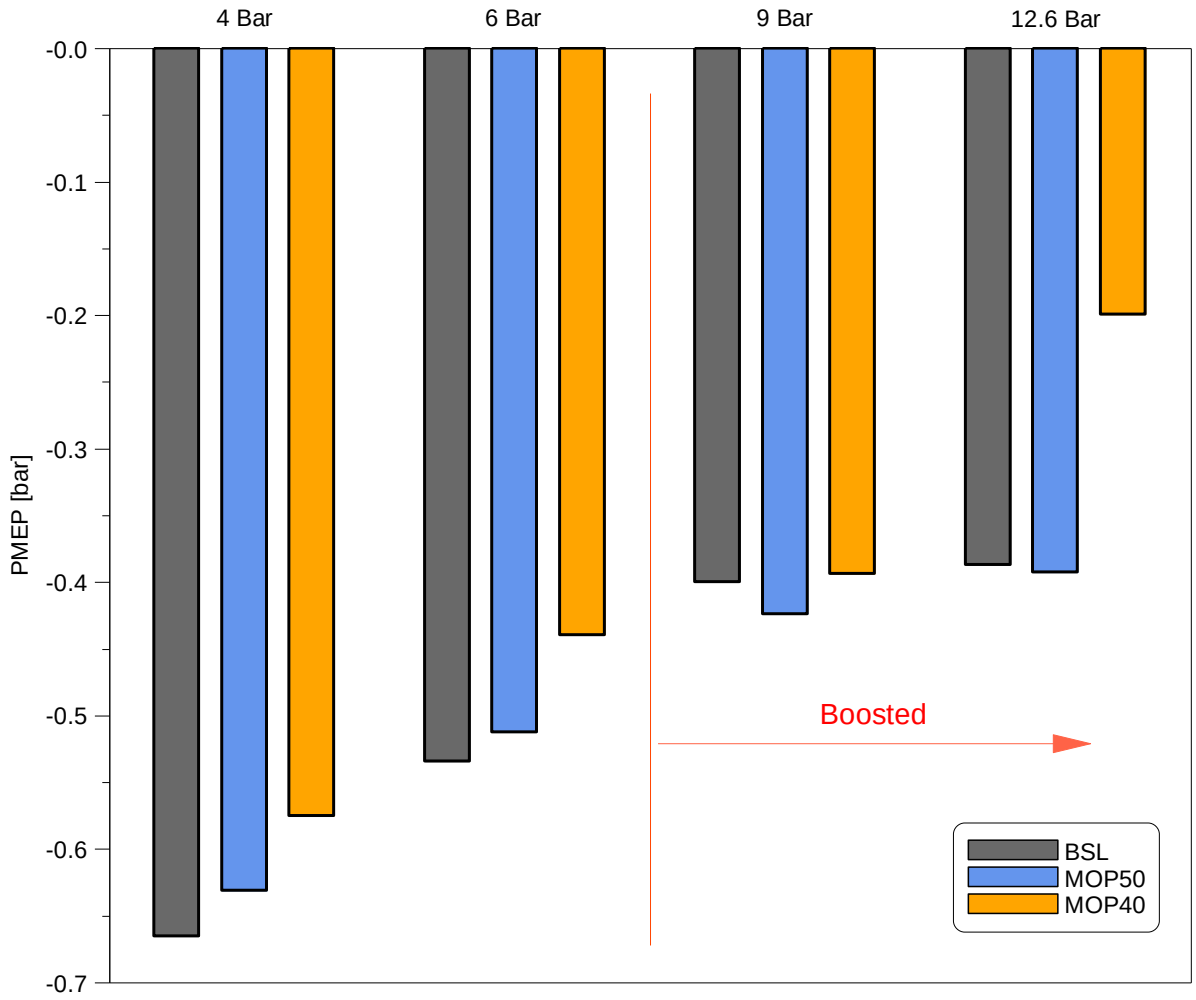

Figure 6.20 PMEP comparison at various loads at 3000rpm

Figure 6.20 demonstrates a comparison of PMEP between BSL, MOP50 and MOP40. Form these results it is clear that MOP40 reduced pumping losses across all the load points. At 4bar net IMEP baseline profile achieved the lowest PMEP value due to the lowest intake pressure. MOP50 had the highest intake pressure but achieved slightly larger pumping loss than MOP40 due to lower inflow area just after IVO. ***Figure 6.21*** demonstrates how difference in valve lift just after IVO affects in-cylinder pressure drop. MOP40 and MOP50 open at the same time, however at 400deg CA MOP40 has 1mm higher lift and in-cylinder pressure does not drop below 0.3bar, whereas MOP50 cylinder pressure continues to drop further. This pressure drop defines the pumping loss, the larger the drop the greater the pumping loss.

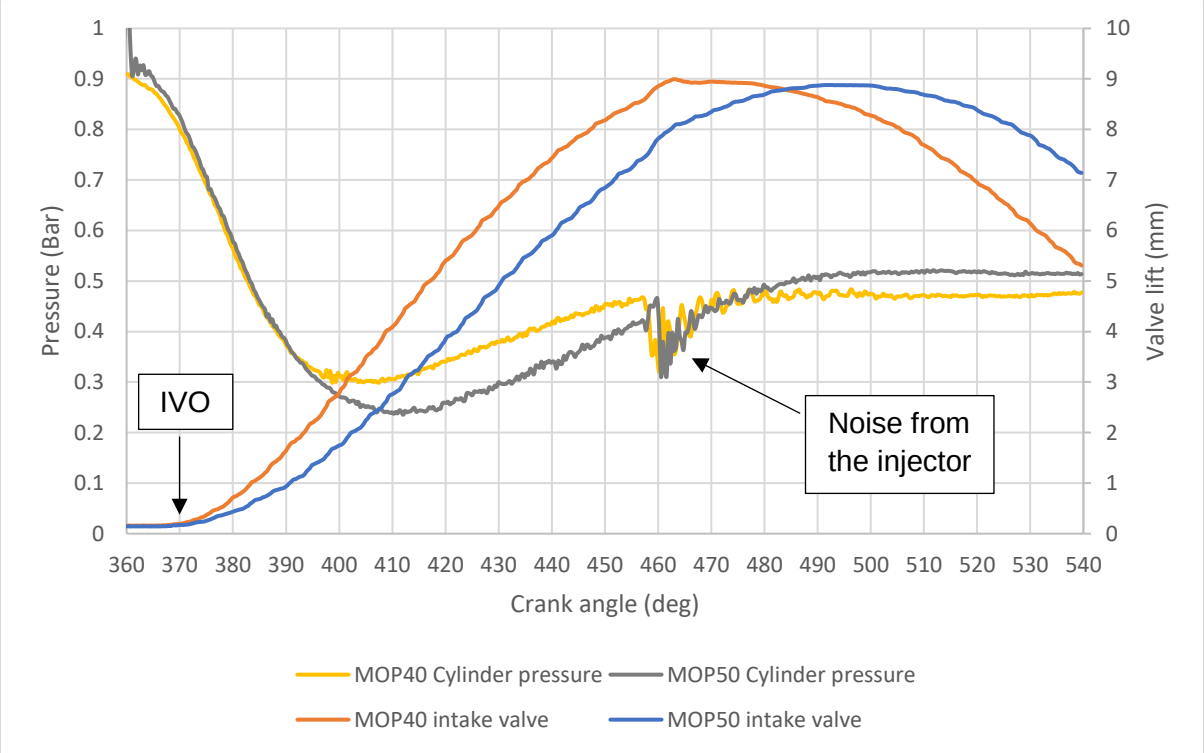

Figure 6.21 Comparison of in-cylinder pressure between MOP40 and MOP50

Similar results were achieved at 6bar, where MOP40 achieved the lowest pumping loss due to relatively high intake pressure and the largest inflow area. At 9bar net IMEP MOP50 produced the highest pumping loss due to the smallest inflow area after IVO, whereas MOP40 had the lowest intake pressure and the largest inflow area which led to the smallest pumping loss. MOP40 significantly reduced pumping loss at 12.6bar due to larger inflow area, whereas MOP50 achieved the largest pumping loss despite the highest intake pressure due to the smallest inflow area. Overall MOP40 reduced pumping losses due to earlier maximum opening which led to larger inflow area after IVO.

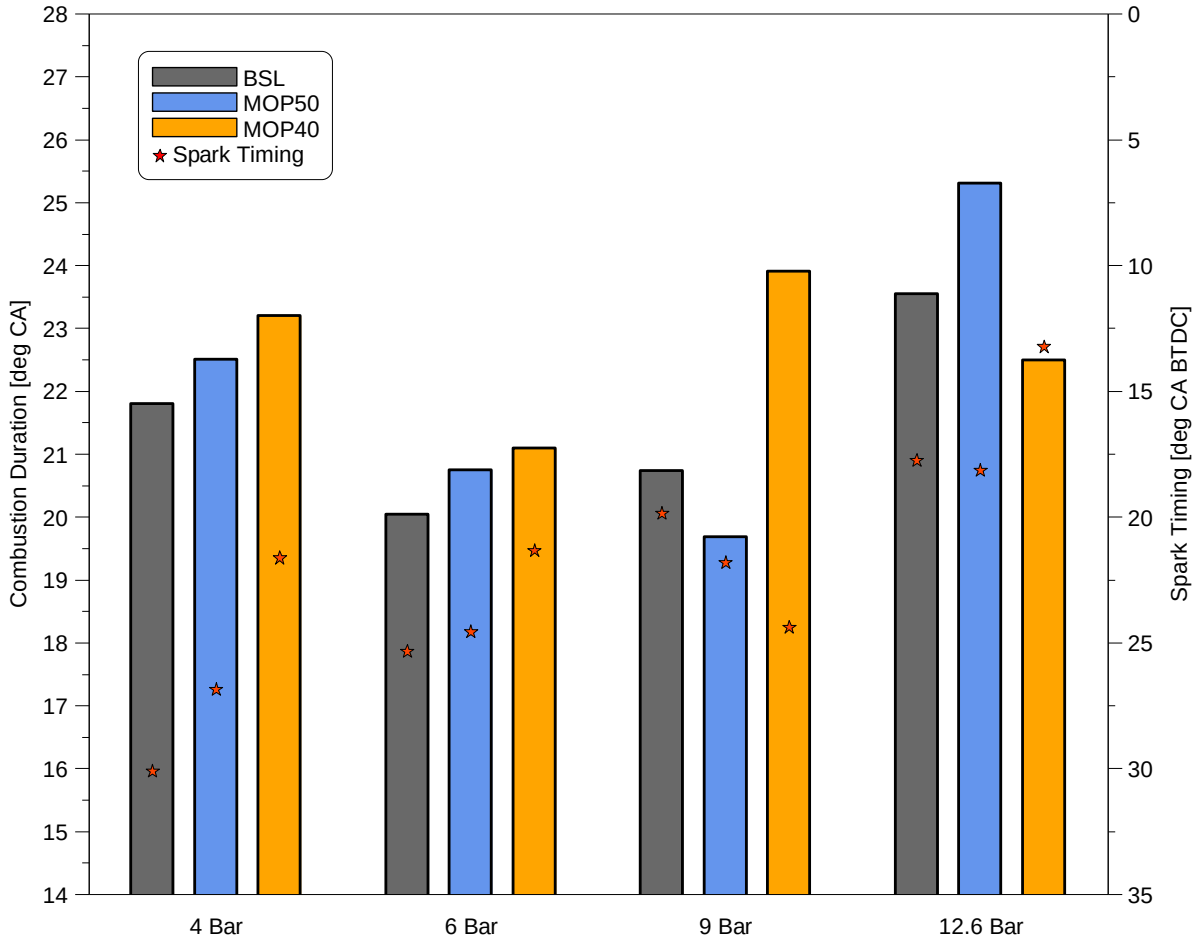

Figure 6.22 Combustion duration and spark timing comparison at various loads at 3000rpm

Comparison of combustion duration and spark timing is shown in Figure 6.22. At 4bar net IMEP baseline profile provided the shortest combustion duration, whereas MOP40 slowed the flame speed due to the lowest ECR which led to longer combustion duration than MOP50. The MBT spark timing was retarded for MOP40 and MOP50 due to shorter flame development angle than baseline profile (Figure 6.23). At 6bar MOP40 achieved the longest combustion duration even though its ECR was larger than MOP50. BSL profile produced the shortest combustion duration due to the highest ECR. The MBT spark timing was retarded for MOP40 due to shorter flame development angle than other profiles. At 9bar net IMEP MOP50 produced the shortest combustion duration whereas MOP40 produced the longest combustion duration with slightly higher ECR. This indicates that early MOP reduced in-cylinder turbulence. MBT spark timing was advanced for MOP40 due to the longest flame development angle. At 12.6bar net IMEP the shortest combustion duration was produced by MOP40 even though ECR value was lower than MOP50. This indicates that early MOP improved in-cylinder turbulence resulting in faster combustion. The spark timing was knock limited for all profiles at this load case, however MOP40 had retarded spark timing due to the shortest flame development angle.

As shown in Figure 6.24, CA10-50 had similar trend as combustion duration for all profiles. CA50-90 was extended significantly for MOP40 at 9bar net IMEP.

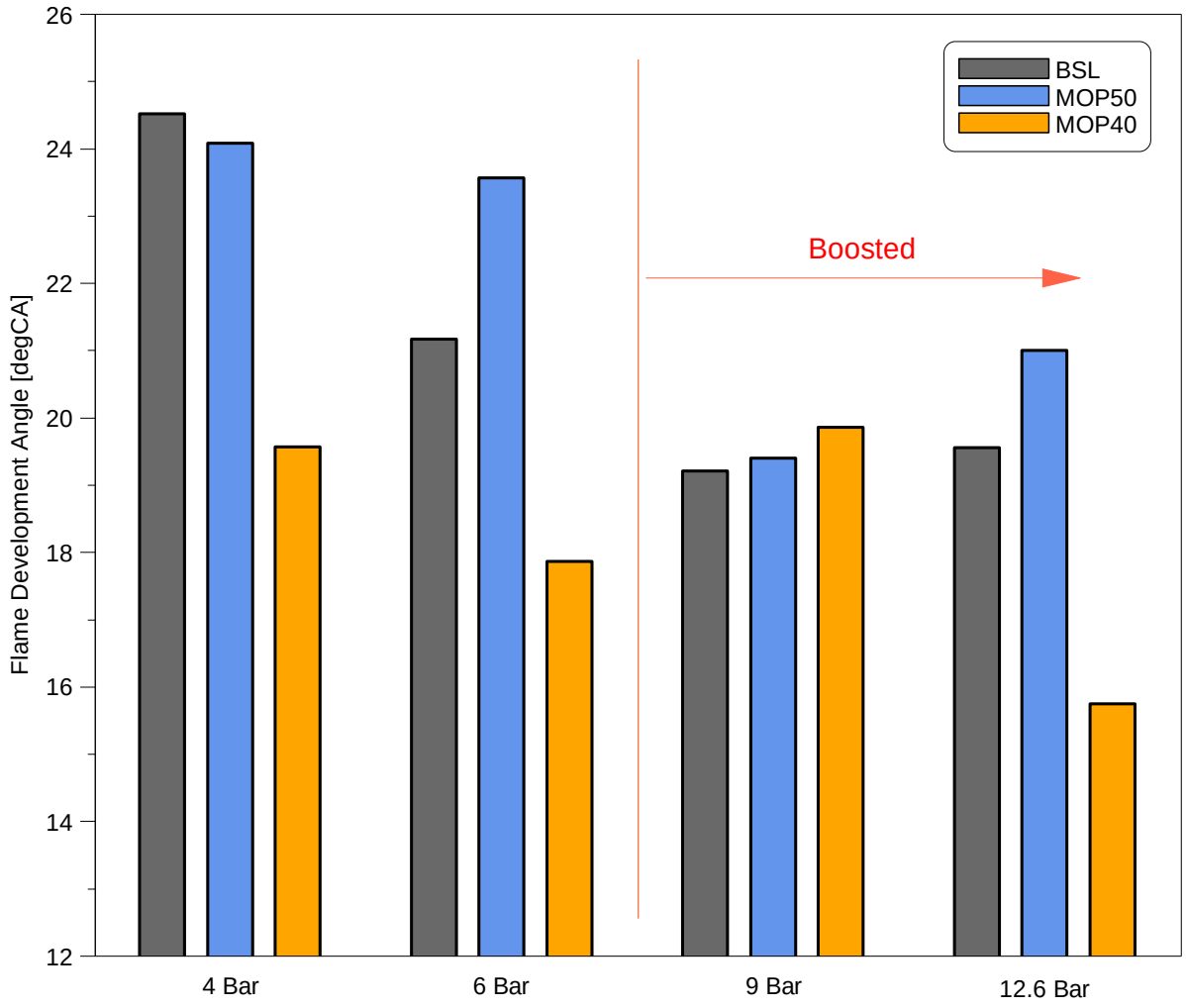

Figure 6.23 Flame development angle comparison at various loads at 3000rpm

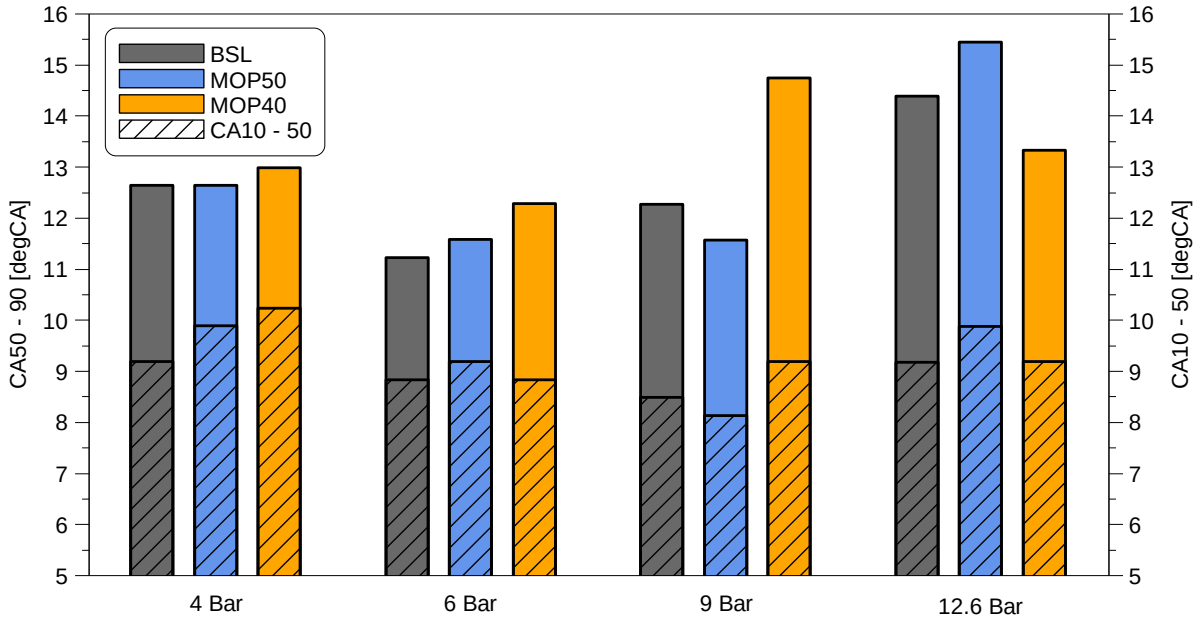

Figure 6.24 CA10-50 and CA50-90 comparison at various loads at 3000rpm

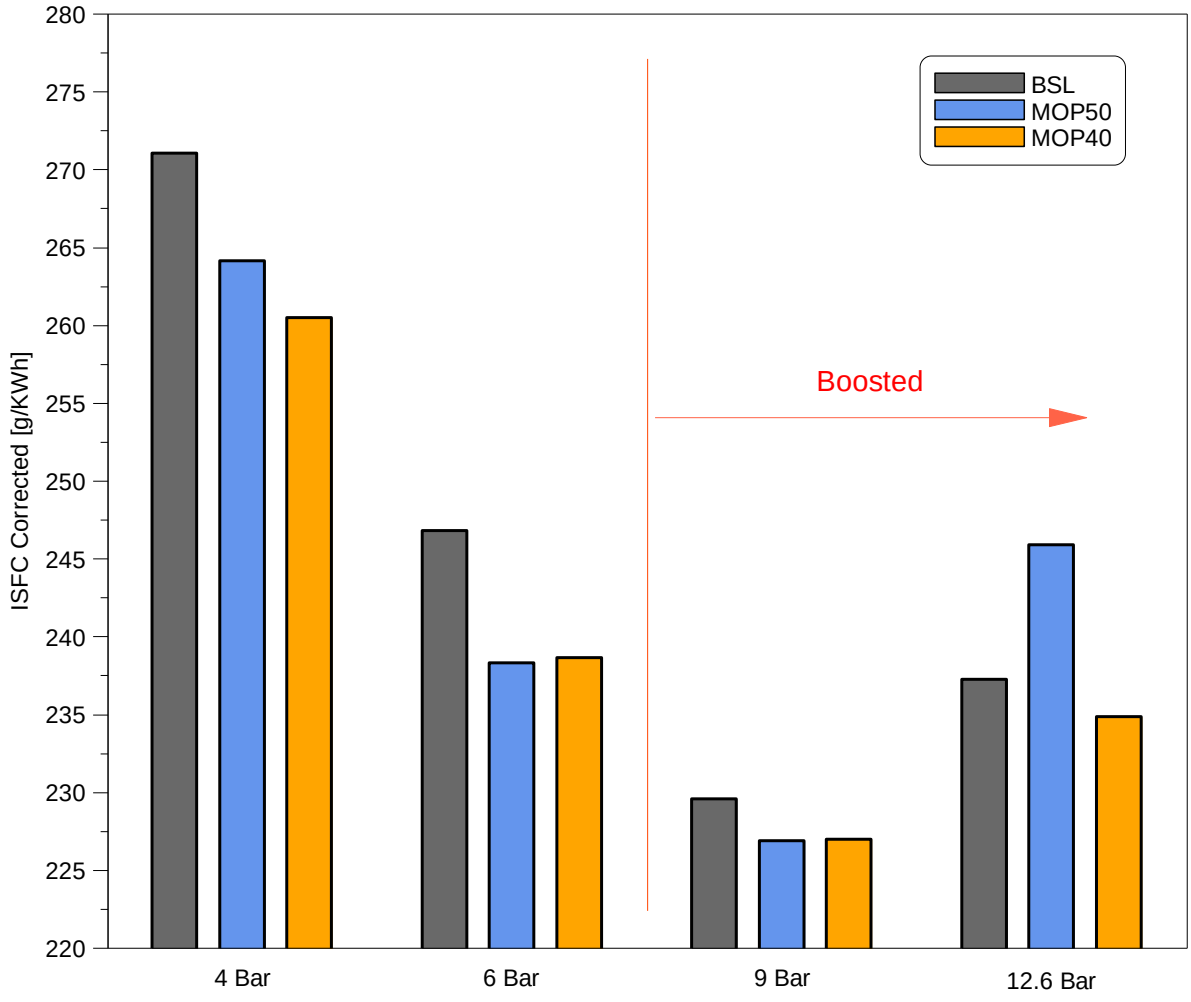

Figure 6.25 ISFC corrected comparison at various loads at 3000rpm

Comparison of indicated specific fuel consumption is shown in Figure 6.25. At 4bar net IMEP MOP40 reduced fuel consumption by 4.4% than the baseline profile due to reduced pumping loss and close to stoichiometric in-cylinder lambda (Figure 6.26). However, at 6bar, MOP40 achieved slightly higher fuel consumption than MOP50 due longer combustion duration even though it had the lowest pumping loss and the closest to stoichiometric AFR. BSL produced the highest ISFC due to large pumping loss and fuel rich in-cylinder mixture. At 9bar net IMEP, MOP50 and MOP40 achieved almost the same, whereas the baseline profile provided the highest fuel consumption due to the richest in-cylinder combustion. At 12.6bar, MOP50 provided the highest ISFC due to the largest pumping loss and the slowest combustion. MOP40 produced significantly lower fuel consumption compared to MOP50 due to the lowest pumping loss, shortest combustion duration and close to stoichiometric in-cylinder AFR. Overall MOP40 improved fuel consumption at low and high load conditions.

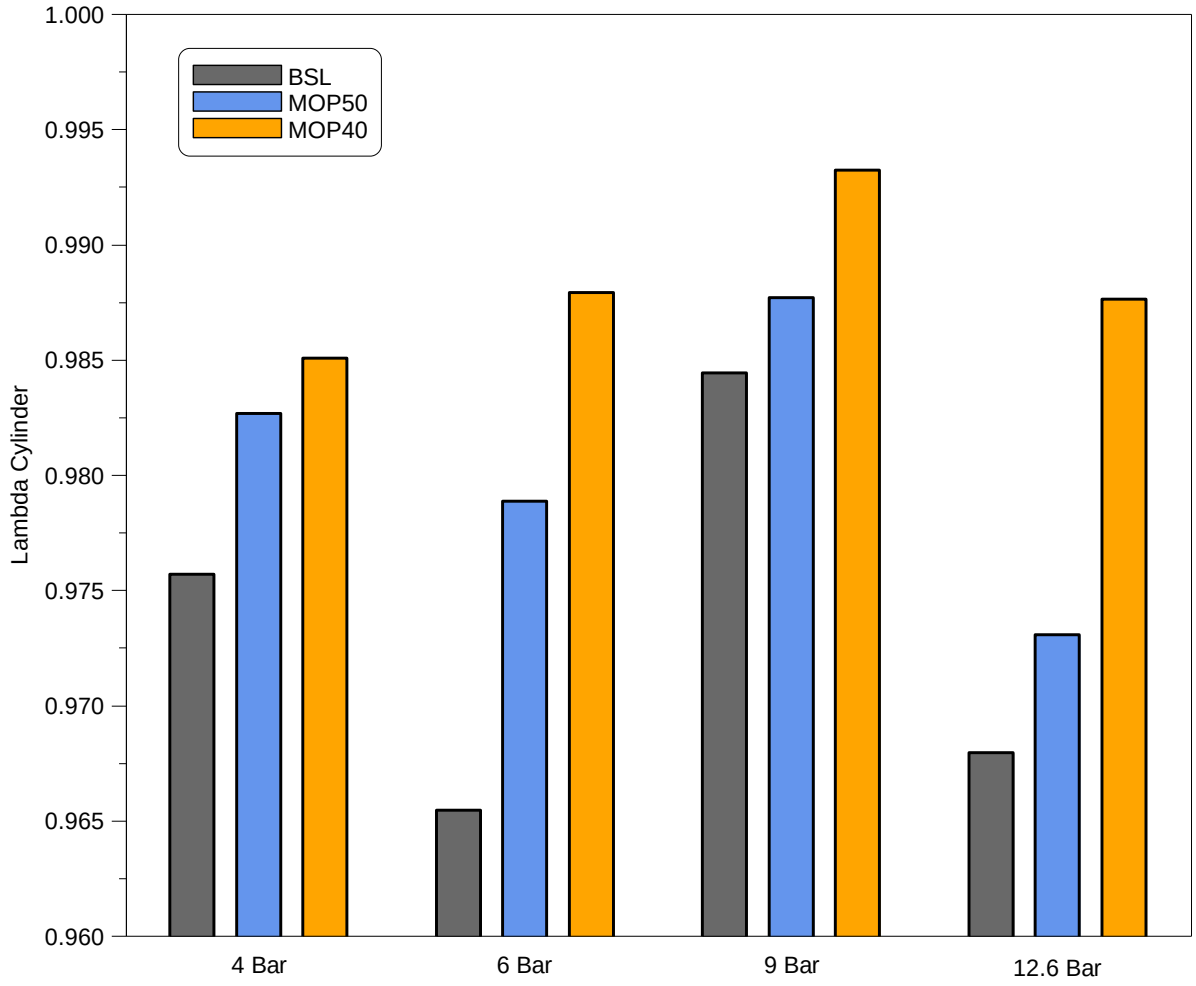

Figure 6.26 In-cylinder lambda comparison at various loads at 3000rpm

Emissions results are shown in Figure 6.27, Figure 6.28 and Figure 6.29. Throughout all load cases ISCO concentration was inversely proportional to the in-cylinder lambda, lower in-

cylinder lambda indicates richer mixture, thus CO emissions are higher. MOP40 reduced ISCO at all load points due to close to stoichiometric in-cylinder lambda.

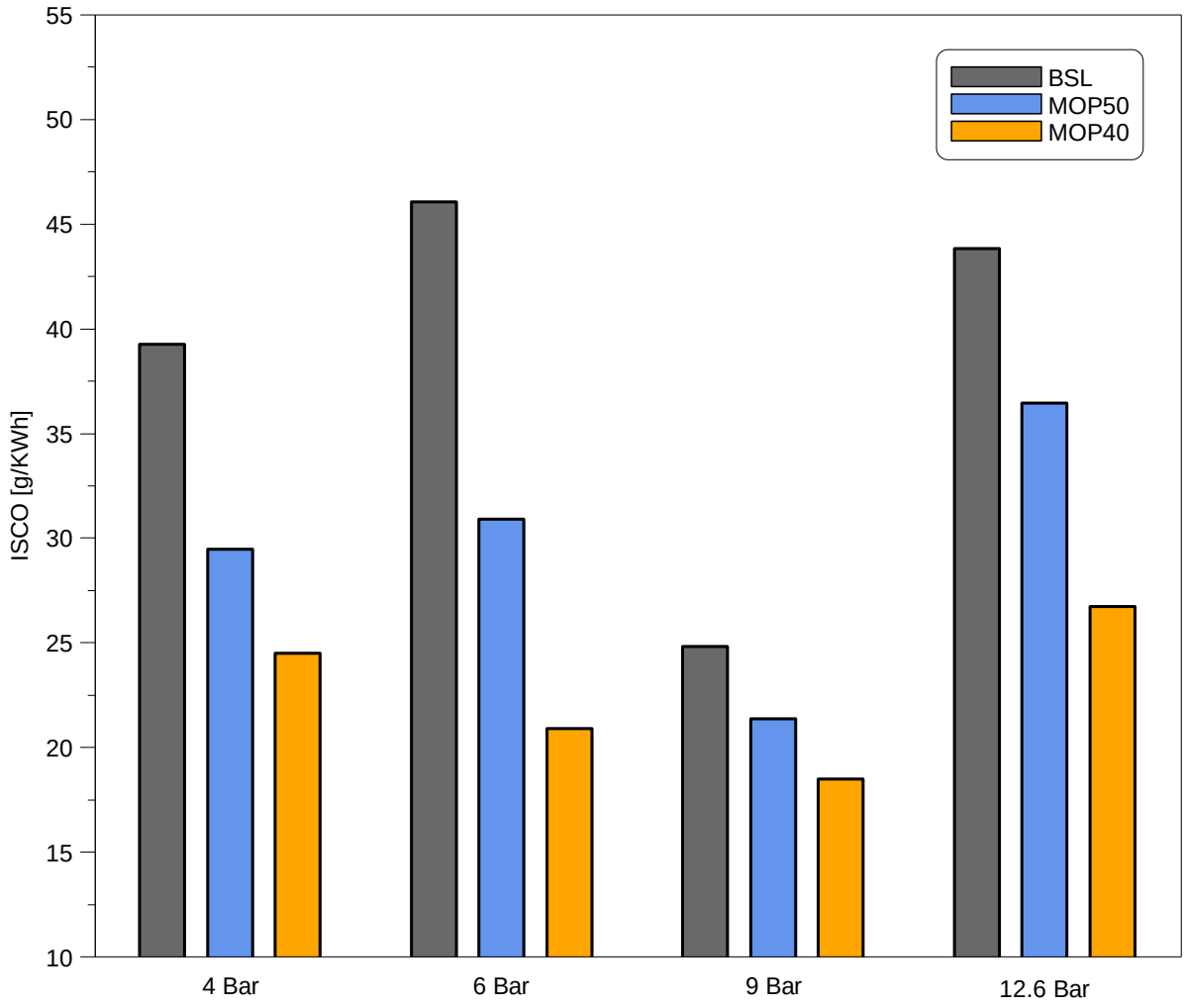

Figure 6.27 ISCO emission comparison at various loads at 3000rpm

At 4bar net IMEP MOP40 achieved the lowest level of HC due to the lowest in-cylinder pressure during compression and expansion strokes. This prevented some of the mixture being forced into crevices and led to more complete combustion compared to BSL and MOP50 profiles. At 6bar net IMEP MOP40 achieved the lowest ISHC due to lower in-cylinder pressure before and at the end of combustion which allowed to reduce quenching at the cylinder wall as well as forcing mixture into crevices. At 9bar net IMEP BSL and MOP40 achieved similar level of HC emissions, however MOP50 achieved the lowest ISHC due to the lowest in-cylinder pressure at the second half of the combustion and the fastest flame speed which prevented bulk quenching at the cylinder wall. At 12.6bar net IMEP HC emission level was similar for all profiles. The lowest ISHC value was achieved by the baseline despite low in-cylinder pressure and fast combustion of MOP40.

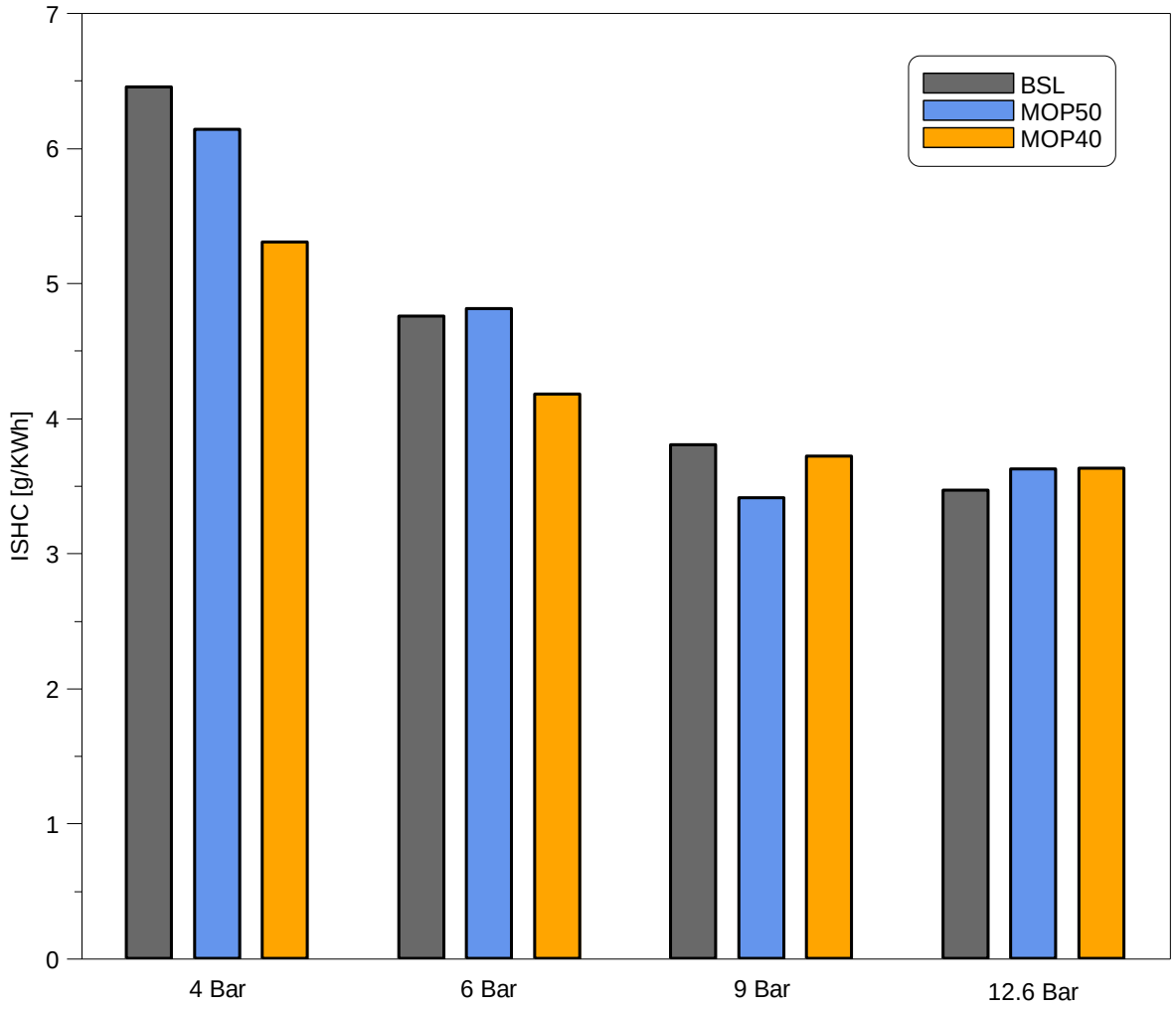

Figure 6.28 ISHC emission comparison at various loads at 3000rpm

The lowest NO_X emissions were achieved by MOP40 profile at 4bar net IMEP due to the lowest in-cylinder pressure during combustion and later spark timing which led to the lowest peak combustion temperature. Baseline achieved the highest NO_X due to significantly higher in-cylinder pressure and the most advanced spark timing. At 6bar net IMEP MOP40 achieved the lowest $ISNO_X$ due to relatively low in-cylinder pressure during combustion and late spark timing which led to the lowest peak combustion temperature among other profiles. At 9bar, BSL profile achieved the lowest NO_X emissions due to the lowest in-cylinder peak temperature as indicated by low pressure and retarded spark timing. At 12.6bar net IMEP BSL profile achieved the lowest $ISNO_X$ despite having the highest in-cylinder temperature throughout compression stroke and majority of combustion as well as advance spark timing.

Overall MOP40 reduced ISCO emissions across all load cases. ISHC and $ISNO_X$ emissions were also reduced at 4 and 6 bar net IMEP compared to the baseline.

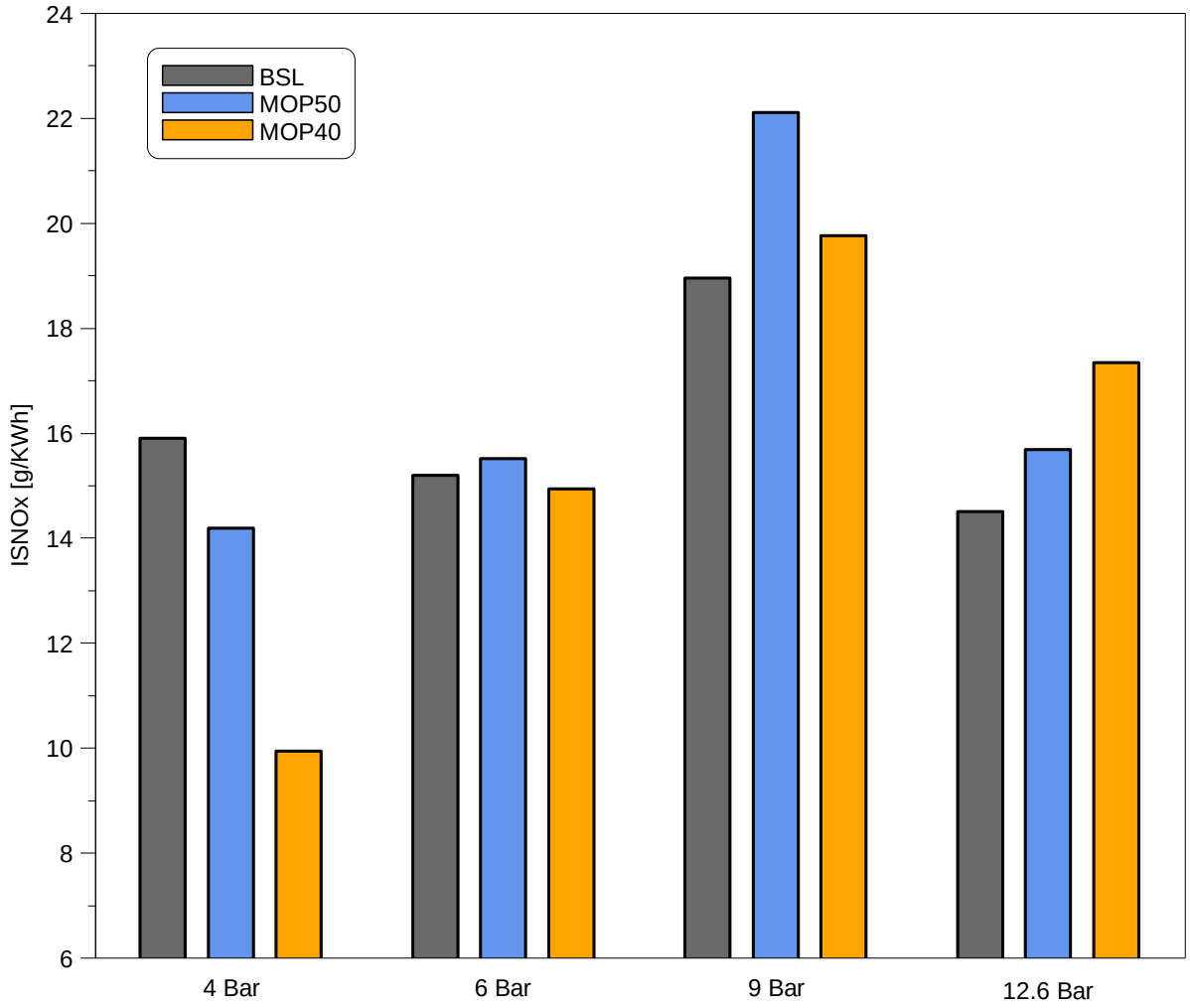

Figure 6.29 ISNO$_X$ emission comparison at various loads at 3000rpm

6.3 Summary

In this chapter, early MOP test results were compared to two valve mode (MOP50) in terms of engine performance and emissions. The tests were performed at 1500rpm and 3000rpm engine speed with a range of loads from 4bar to 12.6bar. The main findings are summarised below:

- Early MOP profiles achieved lower ECRs than MOP50 throughout all testing points.
- At 1500rpm, the pumping losses were reduced for early MOP profiles due to increased intake pressure as throttle angle was larger than for MOP50 profiles. However, at 3000rpm, early MOP profiles achieved lower pumping losses than MOP50 due to larger inflow area just after IVO even with lower intake pressure.
- At both engine speeds early MOP profiles achieved shorter combustion duration at 12.6bar NIMEP.

- Overall early MOP aided in further reduction of ISFC, especially at low and high load conditions.
- CO and HC emissions were reduced with early MOP profiles, NO_X emissions were reduced only at low engine load compared to the baseline.

Chapter 7 Conclusions and Suggestions for Future Work

7.1 Summary and conclusions

In this research the iVT system was employed to investigate the effects of Miller and Atkinson cycle operations on the performance, combustion and emissions of a single cylinder direct injection spark ignition engine at different engine loads at 1500rpm and 3000rpm using five intake valve profiles. The two valve mode was used to compare the effects of LIVC and EICV profiles with three lift variations to the baseline. The single valve mode was used to induce swirl motion inside the cylinder to improve fuel economy. The early MOP profiles were implemented to reduce pumping loss and further improve fuel efficiency.

During the two valve mode operation, LIVC and EIVC profiles with low lifts achieved lowest pumping losses across all of the test points thanks to the highest intake pressures required for lower effective compression ratio provided by Miller and Atkinson cycle. However, very low ECRs would require additional boost pressure to maintain the same NIMEP which would impact the fuel efficiency and total cost of the powertrain. With both EIVC84 and EIVC64 the difference in required intake pressures was not significant compared to the baseline profile at 1500rpm. It was found that at 6 and 9bar net IMEP EIVC84 had lower intake pressure than EIVC64 and lower pumping losses, this could be due to the discharge coefficient which is changing with lift or intake pressure. At high load operations lower ECR allowed to advance spark timing when combustion was knock limited due to reduced temperature at the end of compression allowing for higher compression ratio to improve fuel efficiency. However, at part load EIVC and LIVC profiles produced slower flame speed than the baseline. It was noted that lower valve lift had a great effect in reducing the flame speed than lower ECR, leading to longer combustion. Valve profiles also affected in-cylinder lambda even though exhaust lambda was kept at 1 which also affected fuel economy. Overall EIVC with short lifts and LIVC profiles were successful in reducing fuel consumption. At 1500rpm LIVC reduced NO_X emissions overall but increased CO emissions. However, EIVC profiles lowered CO and HC emissions but increased NO_X almost at all load cases. At 3000rpm LIVC and EIVC64 achieved overall lower CO emissions whereas EIVC64 reduced HC emissions at part load.

During the single valve mode operation, the ECR for LIVC profile became higher than the two valve mode as less charge was able to escape from the cylinder, though ECRs from other profiles were not affected much. The pumping loss became larger than the two valve mode due to the restriction of the flow imposed by the closed intake valve. However, the single valve operation led to stronger swirl motion resulting in improved mixing of air and fuel and

turbulence, thus faster flame propagation. As a result the MBT spark timing was less advanced than for the two valve mode. The lambda values were also increased with single valve mode resulting in close to stoichiometric combustion. ISFC was mostly reduced at low load conditions. EIVC64 improved fuel economy even at 9 and 12.6bar NIMEP at 3000rpm, compared to EIVC64 with two valve mode. Overall single valve mode aided in reduction of CO and HC emissions, however it had an adverse effect on NO_X concentrations due to higher in-cylinder pressure during combustion.

Early MOP reduced ECR for all test points compared to MOP50. It also reduced pumping losses even though the intake pressure was lower than MOP50, this is due to larger inflow area just after IVO thanks to rapid intake valve opening. Combustion duration was shorter for early MOP profiles at 12.6bar NIMEP at both engine speeds. Overall early MOP was successful in further reduction of ISFC, especially at low and high load conditions. In general early MOP reduced CO and HC emissions.

From the above observations it is clear that Miller and Atkinson cycles can improve fuel economy and reduce emissions of a SI engine, but there is a trade-off between the optimum efficiency, lowest emissions and cost of the powertrain.

7.2 Suggestions for future work

To get the full benefit of Miller and Atkinson cycles the following could be done in addition to this research:

Introduce variations of IVC timings for EIVC and LIVC profile to find optimum ECR for each engine condition.

Confirm the effect of valve lift and intake pressure on the discharge coefficient via CFD simulations or laser anemometry.

Implement additional valve lifts for EIVC profiles to study the effect of discharge coefficient and various ECRs.

Apply valve overlap for all profiles to investigate its effect with Miller and Atkinson cycles.

Optimise iVT control for early MOP operation with short lift profiles and test all profiles with early MOP to identify the optimum for maximum fuel efficiency.

Produce a map of optimum valve profiles for the range of engine speeds and loads and conduct a transient test for WLTP cycle on a production IC engine with iVT system, compare the results with the baseline engine.

Investigate the synergy of iVT and increased compression ratio for better fuel economy.

References

[1] NASA GLOBAL CLIMATE CHANGE (2021) *The Causes of Climate change*. Available at: https://climate.nasa.gov/causes/ (Accessed: 4 July 2021).

[2] Betts, R. (2021) *Met Office: Atmospheric CO_2 now hitting 50% higher than pre-industrial levels.* Available at: https://www.carbonbrief.org/met-office-atmospheric-co2-now-hitting-50-higher-than-pre-industrial-levels (Accessed: 4 July 2021).

[3] International Council on Clean Transtportation (2020) *ANNUAL REPORT 2018.* Available at: https://theicct.org/sites/default/files/ICCT-AnnualReport-2018.pdf (Accessed: 5 July 2021).

[4] European Commission (no date) *CO_2 emission performance standards for cars and vans.* Available at: https://ec.europa.eu/clima/policies/transport/vehicles/regulation_en (Accessed: 5 July 2021).

[5] Holst, F. and Solbreck, M. (2014) *Numerical and Experimental Investigation of the Atkinson Cycle on a 2.0 liter 4-cylinder Turbocharged SI-engine.* Master's thesis. Chalmers University of Technology. Available at: https://publications.lib.chalmers.se/records/fulltext/209156/209156.pdf (Accessed: 4 February 2022).

[6] Ebrahimi, R (2011) 'Thermodynamic modeling of performance of a Miller cycle with engine speed and variable specific heat ratio of working fluid', *Computers & Mathematics with Applications*, 62(5), pp. 2169-2176.

[7] Kutlar, O.A., Arslan, H. and Calik, A.T. (2005) 'Methods to improve efficiency of four stroke, spark ignition engines at part load', *Energy Conversion Management*, 46(20), pp. 3202-3220. doi:10.1016/j.enconman.2005.03.008.

[8] ACEA DRIVING MOBILITY FOR EUROPE (2021) *Fuel types of new passenger cars in the EU.* Available at: https://www.acea.auto/figure/fuel-types-of-new-passenger-cars-in-eu/ (Accessed: 5 July 2021).

[9] AA (2017) *Car choice impacts your green score and your cash*. Available at:

https://www.theaa.com/driving-advice/fuels-environment/emissions (Accessed: 8 October 2018).

[10] DieselNet (2021) *EU: Cars and Light Trucks.* Available at: https://dieselnet.com/standards/eu/ld.php#stds (Accessed: 7 July 2021).

[11] McGrath, M. (2016) *Four major cities move to ban diesel vehicles by 2025.* Available at: https://www.bbc.co.uk/news/science-environment-38170794 (Accessed: 7 July 2021).

[12] COMMISSION DELEGATED REGULATION (EU) (2021) *Regulation (EU) 2019/631 of the European Parliament and of the Council of 17 April 2019 setting CO_2 emission performance standards for new passenger cars and for new light commercial vehicles, and repealing Regulations (EC) No 443/2009 and (EU) No 510/2011 (recast)*. Official Journal of the European Union.

[13] Goodall, O. (2021) *BIK rates and company car tax.* Available at: https://www.nextgreencar.com/company-car-tax/bik-rates/ (Accessed: 8 July 2021).

[14] Garret (2019) *Turbo Tech 101 | Basic: Understanding the Parts of the Turbocharger.* Available at: https://www.garrettmotion.com/wp-content/uploads/2019/10/GAM_Turbo-Tech-101_BASIC.pdf (Accessed: 10 July 2021).

[15] Tharad, V. (2018) *6 DIFFRENT TYPES OF TURBOCHARGER*. Available at: https://www.linkedin.com/pulse/6-diffrent-types-turbocharger-vijay-tharad (Accessed: 15 January 2018).

[16] Minasyan, A. (2017) 'Development of an Advanced Axial Inflow Turbocharger Turbine'. Assignment for *ME5308, MEng Motorsport Engineering*, Brunel University. Unpublished.

[17] Ganesan, V. (2008) *Internal Combustion Engines.* McGraw-Hill Education.

[18] Johnson, J. and Braven, K. R. (2008) *Comparison of Homogeneous, Stratified and High-Squish Stratified Combustion in a Direct-Injected Two-Stroke Engine*. SAE International. doi:10.4271/2008-32-0030.

[19] Zhao, H. (2007) *HCCI and CAI engines for the automotive industry*. Cambridge: Woodhead Publishing.

[20] Kulzer, A., Kufferath, A., Christ, A., Hathout, J. P., Knopf, M. and Benninger, K. (2007) 'Controlled auto-ignition', *AutoTechnology,* 7(4), pp. 56-59.

[21] Cairns, A. and Blaxill, H. (2005) *The Effects of Combined Internal and External Exhaust Gas Recirculation on Gasoline Controlled Auto-Ignition.* SAE International. doi:10.4271/2005-01-0133.

[22] Chen, T., Xie, H., Li, L., Zhang, L., Wang, H. and Zhao, H.(2014) 'Methods to achieve HCCI/CAI combustion at idle operation in a 4VVAS gasoline engine', *Applied Energy,* 16, pp. 41-51.

[23] Benajes, J., Molina, S., Novella, R. and Lima, D. (2014) 'Implementation of the Partially Premixed Combustion concept in a 2-stroke HSDI diesel engine fuelled with gasoline', *Applied Energy,* 122, pp. 94–111.

[24] Wang, Z., Wang, J. X., Shuai, S. J. and Ma, Q. J. (2005) *Effects of Spark Ignition and Stratified Charge on Gasoline HCCI Combustion With Direct Injection*. SAE International. doi:10.4271/2005-01-0137.

[25] Splitter, D. and Reitz, R. D. (2014) 'Fuel reactivity effects on the efficiency and operational window of dual-fuel compression ignition engines', *Fuel,* 118, pp. 163-75.

[26] Govardhan, O. M. (2017) 'Fundamentals and Classification of Hybrid Electric Vehicles', *International Journal of Engineering and Techniques,* 3(5), pp. 194-198. Available at: http://oaji.net/articles/2017/1992-1515159589.pdf (Accessed: 18 August 2021).

[27] Greenwood, S. (2017) *Hybrid Vehicles – a simple guide.* Available at: https://www.aathornton.com/hybrid-vehicles-simple-guide/ (Accessed: 18 August 2021).

[28] Ricardo (2020) *Ricardo Dedicated Hybrid Engines: Design Innovation for Reducing Emissions Weight and Cost.* Available at: https://ricardo.com/news-and-media/webinars/electrification/ricardo-dedicated-hybrid-engines (Accessed: 19 August 2021).

[29] Bao, R. and Stobart, R. (2013) *Using Pneumatic Hybrid Technology to Reduce Fuel Consumption and Eliminate Turbo-Lag*. SAE International. doi:10.4271/2013-01-1452

[30] Tai, C., Tsao, T., Levin, M., Barta, G. and Schechter, M. M. (2003) *Using Camless Valvetrain for Air Hybrid Optimization*. SAE International. doi:10.4271/2003-01-0038.

[31] Dönitz, C., Vasile, I., Onder, C., and Guzzella, L. (2009) *Realizing a Concept for High Efficiency and Excellent Driveability: The Downsized and Supercharged Hybrid Pneumatic Engine.* SAE International. doi:10.4271/2009-01-1326.

[32] Lee, C., Zhao, H., and Ma, T. (2009) Analysis *of a Cost Effective Air Hybrid Concept.* SAE International. doi:10.4271/2009-01-1111.

[33] Trajkovic, S., Tunestål, P., and Johansson, B. (2008*) Investigation of Different Valve Geometries and Vavle Timing Strategies and their Effect on Regenerative Efficiency for a Pneumatic Hybrid with Variable Valve Actuation*. SAE International. doi:10.4271/2008-01-1715.

[34] Kreuter, P., Heuser, P. and Schebitz, M. (1992) *Strategies to Improve SI-Engine Performance by Means of Variable Intake Lift, Timing and Duration*. SAE International. doi:10.4271/920449.

[35] Satyanarayana, P., Loganathan, B., Lakshminarasimhan, V., Ramesh, A. and Sujatha, S. (2014) *Development of a Cam Phaser System to Improve the Performance of a Small Engine.* SAE International. doi:10.4271/2014-32-0110.

[36] Wan, M. (2011) *Department of Engine.* Available at: http://www.autozine.org/technical_school/engine/Index.html (Accessed: 10 September 2018).

[37] Luttermann, C., Schünemann, E., and Klauer, N. (2006) *Enhanced VALVETRONIC Technology for Meeting SULEV Emission Requirements*. SAE International. doi:10.4271/2006-01-0849.

[38] Unger, H., Schneider, C., Schwarz, K., Koch, F., (2008), *Valvetronic: Experience from 7 years of series production and a look into the future*. BMW Group.

[39] Fujita, T., Onogawa, K., Kiga, S., Mae, Y. et al. (2008) *Development of Innovative Variable Valve Event and Lift (VVEL) System*. SAE International. doi:10.4271/2008-01-1349.

[40] ADPTraining (2013) *Toyota Valvematic Valve Timing*. Available at: https://www.youtube.com/watch?v=HOqGWg1YJh4 (Accessed: 23 September 2018).

[41] Wong, K. (2005) *New VTEC Implementation: SOHC i-VTEC on the R18A.* Available at: http://krzp.w.interiowo.pl/honda/instrukcja/inne/silnik.18.html (Accessed: 2 October 2018).

[42] Akima, K., Seko, K., Taga, W., Torii, K. and Nakamura, S. (2006) *Development of New Low Fuel Consumption 1.8L i-VTEC Gasoline Engine with Delayed Intake Valve Closing.* SAE International. doi:10.4271/2006-01-0192.

[43] Lou, Z., Wen, S., Qian, J., Xu, H., Zhu, G. and Sun, M. (2015) *Camless Variable Valve Actuator with Two Discrete Lifts.* SAE International. doi:10.4271/2015-01-0324.

[44] Picron, V., Postel, Y., Nicot, E. and Durrieu, D. (2008) *Electro-Magnetic Valve Actuation System: First Steps toward Mass Production.* SAE International. doi:10.4271/2008-01-1360.

[45] Frederic, A., Picron, V., Hobraiche, J., Gelez, N. and Valeo, S. (2010) *Electro Magnetic Valve Actuation System e-Valve: Convergence Point between Requirements of Fuel Economy and Cost Reduction.* SAE International. doi:10.4271/2010-01-1197.

[46] *FREEVALVE* (no date) Available at: http://www.freevalve.com (Accessed: 5 October 2018).

[47] Andersen, J., Nilsson, P., Karlsson, J., Gundersen, O. (2011) *Optimized Flex-fuel Engine with fully Variable Valve Timing*. Available at: http://www.freevalve.com/wp-content/uploads/2015/11/Optimized-Flexfuel-Engine-with-FVVT_20111130.pdf (Accessed: 5 October 2018).

[48] Evans, P. (2009) *Camless combustion engine may improve ICE efficiency*. Available at: http://www.gizmag.com/camless-combustion-engine-cargine-engineering/12200 (Accessed: 5 October 2018).

[49] Atkinson, J. (1886) *GAS ENGINE.* United States Patent Office Patent no. 336,505. Available at: https://patents.google.com/patent/US336505A/en (Accessed: 15 April 2020).

[50] Atkinson, J. (1887) *GAS ENGINE.* United States Patent Office Patent no. 337,496. Available at: https://patents.google.com/patent/US367496A/en (Accessed: 15 April 2020).

[51] Miller, R. (1954) *HIGH-PRESSURE SUPERCHARGING SYSTEM.* United States Patent Office Patent no. 2,670,595. Available at: https://patents.google.com/patent/US2670595A/en (Accessed: 15 April 2020).

[52] Miller, R. (1956) *HIGH EXPANSION, SPARK IGNITED, GAS BURNING, INTERNAL COMBUSTION ENGINES.* United States Patent Office Patent no. 2,773,490. Available at: https://patents.google.com/patent/US2773490A/en (Accessed: 15 April 2020).

[53] Cleary, D. and Silvas, G. (2007) *Unthrottled Engine Operation with Variable Intake Valve Lift, Duration, and Timing.* SAE International. doi:10.4271/2007-01-1282.

[54] Constensou, C. and Collee, V. (2016) *VCR-VVA-High Expansion Ratio, a Very Effective Way to Miller-Atkinson Cycle.* SAE International. doi:10.4271/2016-01-0681.

[55] Osborne, R., Downes, T., O'Brien, S., Pendlebury, K. et al. (2017) *A Miller Cycle Engine without Compromise - The Magma Concept.* SAE International. doi:10.4271/2017-01-0642.

[56] Garcia, E., Triantopoulos, V., Boehman, A., Taylor, M. et al. (2020) *Impact of Miller Cycle Strategies on Combustion Characteristics, Emissions and Efficiency in Heavy-Duty Diesel Engines.* SAE Intternational. doi:10.4271/2020-01-1127.

[57] Visnic, B. (2017) *Volkswagen's new 'B-Cycle' engine: potential diesel surrogate. Available at:* https://www.sae.org/news/2017/06/volkswagens-new-b-cycle-engine-potential-diesel-surrogate (Accessed: 26 June 2021).

[58] Macklini, D. N. (2015) *EXPERIMENTAL AND NUMERICAL STUDY OF A TWO-STROKE POPPET VALVE ENGINE FUELLED WITH GASOLINE AND ETHANOL.* PhD thesis. Brunel University.

[59] Stone, R., Kelly, D., Geddes, J. and Jenkinson, S. (2017) 'Intelligent Valve Actuation – A Radical New Electro-Magnetic Poppet Valve Arrangement', *Aachen Colloquium Automobile and Engine Technology,* 26, pp. 445-467.

[60] Takeda, K. and Koike, H. (1995) 'Motor Exhaust Gas Analyzer MEXA-7000 Series 2. Downsizing and Modular Configuration of Analyzers', *Readout,* 11, pp. 7-13.

[61] Douglas R. (1990) *AFR and Emissions Calculations for Two-Stroke Cycle Engines*. SAE International. doi:10.4271/901599.

[62] Zhao, H. and Ladommatos, N. (2001) *Engine Combustion Instrumentation and Diagnostics.* SAE International.

[63] Kocher, L. E., Koeberlein, E., Van Alstine, D. G., Stricker, K. and Shaver, G. (2012) 'Physically-based volumetric efficiency model for diesel engines utilizing variable intake valve actuation', *International Journal of Engine Research*, 13(2), pp. 169-184. doi:10.1177/1468087411424378.

[64] Heywood, J. B. (2018) *Internal Combustion Engine Fundamentals, Second Edition*. McGraw-Hill Education.

[65] Zhang, Y. (2014) *Experimental investigation of CAI combustion in a two-stroke poppet valve DI engine.* PhD thesis. Brunel University.